Monitoring of Saint Louis coast (Senegal) using multi-sensor remote sensing techniques

Adelaide Taveneau

THÈSE

En vue de l'obtention du

DOCTORAT DE L'UNIVERSITÉ DE TOULOUSE

Délivré par : *l'Université Toulouse 3 Paul Sabatier (UT3 Paul Sabatier)*

Présentée et soutenue le *10/03/2023* **par :**

Adélaïde TAVENEAU

Télédétection multi-capteurs du littoral à Saint Louis (Sénégal)

JURY

Nicolas Robin	Maître de conférence (CEFREM, Perpignan)	Rapporteur
Bertrand Lubac	Enseignant Chercheur (EPOC, Bordeaux)	Rapporteur
Anouk De Bakker	Ingénieure (Deltares, Delft)	Examinatrice
Patrick Marchesiello	Directeur de recherche (IRD, Toulouse)	Examinateur
Thierry Garlan	Scientifique senior (SHOM, Brest)	Examinateur
Rafaël Amar	Directeur de recherche (IRD, Toulouse)	Directeur de thèse
Erwin Bergsma	Ingénieur (CNES, Toulouse)	Co-endadrant
Yann Balouin	Ingénieur (BRGM, Montpellier)	Invité
Abdoulaye Ndour	Chercheur (UCAD, Dakar)	Invité

École doctorale et spécialité :
SDU2E : Océan, Atmosphère, Climat

Unité de Recherche :
LEGOS (UMR 5566)

Directeur de Thèse :
Rafaël ALMAR

Rapporteurs :
Nicolas ROBIN et *Bertrand LUBAC*

Résumé — La ville historique de Saint Louis au Sénégal est située sur la flèche sableuse appelée la Langue de Barbarie, et est particulièrement exposée à l'érosion et à la submersion marine : des bâtiments se sont effondrés et la population a été relogée. A Saint Louis, la compréhension de la morphodynamique de la plage est plus qu'ailleurs d'une importance capitale pour améliorer les décisions de gestion basées sur la science. Ce doctorat teste la faisabilité de l'utilisation de la télédétection par satellite dans le suivi de la morphologie côtière, à la fois la topographie et la bathymétrie. Les techniques de télédétection s'appuyant sur des satellites à la demande à très haute résolution (sub-métrique) tels que la constellation Pléiades offrent désormais de nouvelles perspectives permettant l'estimation de la topographie de la partie émergée de la plage par (tri-)stéréogrammétrie, et l'inversion de la bathymétrie par la cinématique des vagues. Les missions régulières telles que Landsat et Sentinel-2 sont plus adaptées pour capturer à l'échelle régionale l'évolution de la flèche littorale sur un jeu de données de 37 ans, avec le littoral et les barres sableuses. Ici, ces observations ont permis de comprendre le lien étroit entre la plage urbaine locale et l'évolution intrinsèque de la flèche sableuse régionale, ainsi qu'avec la plage subaquatique. Malgré les limites actuelles, cette thèse montre l'intérêt (croissant) de l'utilisation de la surveillance par satellite pour comprendre la dynamique des sablières avec des besoins pratiques en ingénierie côtière.

Mots clés : Management des zones côtières, Satellites, Topographie, Bathymétrie, Flèches sableuses, Morphodynamique, Transport sédimentaire.

Abstract — The historical city of Saint Louis in Senegal is situated on the *Langue de Barbarie* sand spit and is particularly prone to erosion and ocean flooding: buildings have collapsed and population relocated. At Saint Louis understanding the beach-morphodynamics is more than elsewhere of paramount importance to improve science based management decision. Here this PhD tests the feasibility of using satellite remote sensing in monitoring coastal morphology, both topography and bathymetry. Remote sensing techniques relying on very high resolution (sub-metric) on-demand satellites such as the Pleiades constellation now offer new perspectives allowing for the estimation of the topography of the emerged part of the beach using (tri-)stereogrammetry, and bathymetry inversion through wave kinematics. Regular missions such as Landsat and Sentinel-2 are more suited to capture on a regional scale the sand spit evolution over a 37 years data-set, with shoreline and sandbars. Here, these observations allowed to understand the close link between the local urban beach with the regional sand spit intrinsic self-evolving evolution, and with the subaqueous beach. Despite current limitations, this PhD shows the (growing) interest of using satellite monitoring to understand the dynamics of sandpits with practical coastal engineering needs.

Keywords: Coastal Management, Satellites, Topography, Bathymetry, Sand spit, Morphodynamics, Sediment transport.

Citation

"Dans un voyage ce n'est pas la destination qui compte mais toujours le chemin parcouru, et les détours surtout."

Philippe Pollet-Villard

Remerciements

Après trois années il est enfin temps d'écrire les remerciements de cette thèse. Trois années qui ont été riche de rencontres, de discussions, de voyages et de rires. Mon aventure dans la recherche a commencé en 2018 à Galway en Irlande. J'ai eu l'occasion de travailler dans un laboratoire et je me suis jurée en rentrant en France que jamais je ne travaillerai dans la recherche. Puis en terminant mon école d'ingénieur une année plus tard, j'ai retenté ma chance avec Yann et Clément à Montpellier, et j'ai compris que finalement, j'allais sûrement poursuivre en thèse. C'est là que, logiquement, s'ensuit la longue liste de remerciements.

Je remercie dans un premier temps mes encadrants de thèse, Rafael et Erwin. Rafael pour avoir poussé mon esprit à se poser toujours plus de questions, et m'avoir fait développé une grande curiosité scientifique. Erwin pour ta pédagogie et ta grande capacité d'écoute. Je tiens à remercier tous mes collègues au Sénégal Abdoulaye Ndour, Boubou Sy, Papa Sagne qui m'ont très bien accueillie à chacune de mes visites, les travaux réalisés en communs ont porté leurs fruits. Avec un merci tout particulier à Cheikh Omar Tidjani Cissé avec qui j'espère que la collaboration perdurera.

Je ne peux décemment pas oublier toutes les heures passées dans mon petit bureau, dos à la baie vitrée, où nous avons partagé des moments studieux mais surtout de rire avec Julia et Hanh. Du sirop, du thé, des canards, des bonbons, des chansons ... A cela s'ajoute tous les autres rencontrés dans le labyrinthe des couloirs : Pierre avec qui on s'est beaucoup soutenu pendant le confinement, en faisant du télé-crapette et des apéros quand nous ne pouvions plus travailler, Lisa qui a toujours été là pour les bons moments comme durant les crises existentielles, Gabriela qui est toujours de super conseil. A toutes ces soirées jeux passées chez Manon et Flo (sans oublier la chorale, les discussions pour se remonter le moral, les pauses thé et j'en passe), à tous ces hoquets partagés avec Romain, les palets avec Antonin, la pétanque avec Alex, les discussions à ne plus en voir le temps passer avec Juliette. A Elisa (ma voisine espionne) pour ces petits repas le midi, à Lise partie trop tôt aus USA mais dont j'espère sincèrement le retour en France, à Simon qui m'a accompagné au Sénégal (et à la mosquée), à Arne et pour tous les petits mots appris "schadenfreude". A Nolwenn qui a fait un passage d'un an au LEGOS mais que je connais de l'école d'ingénieur, merci pour ton sourire, ton optimisme, ton rire et ton soutien. Et à tous les petits nouveaux à qui je souhaite plein de courage pour la suite : Amélie, Camille, Gaëlle, Marcan, Marie...

A Alisée qui a également vécu 3 ans de thèse en même temps, pour tous ces cafés, ces bars, ce fronton, ces crêpes et sorties dans Toulouse sans lesquels on ne serait pas allée au bout. Je ne pensais pas que ses deux filles aux t-shirt assortis de *La Boulette* en serait là aujourd'hui... Plein de courage pour ta carrière de chercheuse Dr. Aliso. Maxime pour toutes ces discussions sans fins, ces concerts, ces ballades au bord de la Garonne. Tony pour toutes tes histoires "améliorées" et jamais exagérées, Momo pour ta bonne humeur.

Merci à ma famille qui a toujours été là pour moi, depuis le tout début. A mes parents, et à mes trois frères et soeurs.

Et enfin merci à Aurélie, de m'avoir supportée dans les périodes difficiles, d'avoir toujours été là pour moi dans les bons moments et dans les moins bons. J'espère que l'on en partagera plein d'autres ensemble.

Contents

List of Figures

List of Tables

Acronyms

LST	*Longshore Sediment Transport*
ASP	*Ames Stereo Pipelines*
DEM	*Digital Elevation Model*
RTK	*Real Time Kinematic*
LiDAR	*Light Detection And Ranging*
NDWI	*Normalized Difference Water Index*
MNDWI	*Modified Normalized Difference Water Index*
RMSE	*Root Mean Square Error*
RPC	*Rational Polynomial Coefficient*
GCP	*Ground Control Point*
RT	*Radon Transform*
FFT	*Fast Fourier Transform*

General introduction

General context

With more than 600 million people living in areas less than 10 metres above sea level (Mas-suanganhe and Arnberg, 2008), the coast is a zone of permanent conflict between natural phenomena and human intervention (Small and Nicholls, 2003). Often exploited for agricultural, industrial or tourist purposes, and constantly exposed to the action of marine processes, the coastline today faces unprecedented environmental and economic pressures. In the context of global warming, and in particular the rise in sea levels, the protection of the coastline is a major socio-economic issue.

Sandy beaches are very dynamic systems and are shaped by many external factors such as waves, tides and wind. Today, 1/4 of the world's sandy beaches show alarming erosion rates of more than -0.5 m/year (Luijendijk et al., 2018). Faced with this situation, the strategic retreat of populations is often difficult to consider and it is therefore essential to develop coastal protection strategies to ensure the sustainability of these beaches. Improving the understanding of the dynamics of such environments, with the aim of integrating means of protection, seems to be a major social challenge in order to propose sustainable solutions.

Knowledge of the natural dynamics of a beach is the first step in the development of a strategy for the protection of these environments (Benavente et al., 2002): structures that take into account the complexity of sediment exchange on a beach will be more effective and sustainable. Coastal management is a complex problem and there is never a simple solution (Christie, 2005). The coastal strip, between the land and the sea, is an environment with complex morphodynamics and it evolves strongly according to the spatial and temporal scales. One of the most commonly used means to characterise the dynamics of a beach is to monitor the position of the shoreline (here characterised as the physical interface between land and sea) over time (Dolan et al., 1978; Stive et al., 2002b; Yates et al., 2009; Splinter et al., 2014). Fixing the latter to a stable position has become a major socio-economic issue, but studies have sometimes ignored the complexity of natural beach dynamics. For many years, coastal engineering has focused on the construction of man-made structures (ports, sea walls, jetties, etc.). The challenge now is to integrate these structures into the natural dynamics of their environment, taking into account the natural mobility of the shoreline.

The exchange of sediment on a beach takes place at different spatial scales - from a metre to hundreds of kilometres. They are driven by different processes that significantly affect the morphology of the shoreline over different time periods (Masselink and Kroon, 2009). Several tools allow the monitoring of beach dynamics at different spatial scales and thus the understanding of their specific mechanisms (Baily and Nowell, 1996).

Problematics and objectives of the PhD

Cited in several newspapers around the world, Saint Louis (Senegal) is a city whose erosion rates are of international concern. Built on a particularly dynamic sand spit, it is located between the mouth of the Senegal River and the Atlantic Ocean, making it a city particularly exposed to sea hazards and flooding (Sadio et al., 2017; Anthony, 2015). The fishing district, Guet Ndar (figure 1.a), is constantly hit by powerful waves that destroy buildings (figure 1.b) and gradually erode the beach (Bergsma et al., 2020). As Guet Ndar is the most densely populated area of Saint Louis, it has become imperative to find a solution to this socio-economic disaster. Initially, emergency solutions were put in place to deal with this social disaster: a strategic relocation plan was launched in 2018 by moving houses 20 metres back for 10,000 people, as well as the construction of a short-term protection structure in front of the most vulnerable area (AFD, 2018). The protective structure is 3.6 km long and 20 m wide and is funded by the French Development Agency (AFD) and the Municipal Development Agency (ADM). One of the objectives of this thesis was to quantify the impact of this structure on the Saint Louis coast. The construction of this breakwater to protect the most vulnerable populations was scheduled to begin in 2019, but work did not start until December 2020.

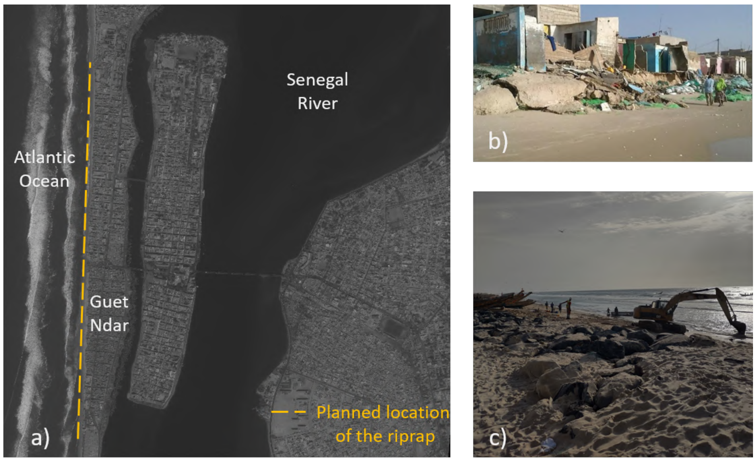

Figure 1: **(a)** Satellite view of the city of Saint Louis with location of the Guet Ndar District. **(b)** Photo showing the damage caused by the sea on the district of Guet Ndar. **(c)** Photo of the construction of the rockfill.

The massive erosion trend in the northern part of the *Langue de Barbarie* sand spit is directly linked to the urgent decision of the 2003 breach (October) (Rodríguez et al., 2014; Bergsma et al., 2020; Taveneau et al., 2021). In fact, a major flood from the Senegal River paralysed the city of Saint Louis for several days. The water level in the streets was so high that a breach was made in the *Langue de Barbarie* with the idea that the water would drain more quickly to the sea (the mouth of the river was tens of kilometres south of the city). However, the breach, which was originally 4 m wide, quickly widened and over time became the new mouth of the river, causing the almost complete erosion of the downdrift part of the spit, as well as an erosive pattern in the northern updrift part.

The main objective of this thesis is to monitor the beach evolution from the local scale (metres) to the regional scale (about ten kilometres) using a multi-sensor approach. The figure below (Figure 2) summarises the means used and the various studies carried out on the available data.

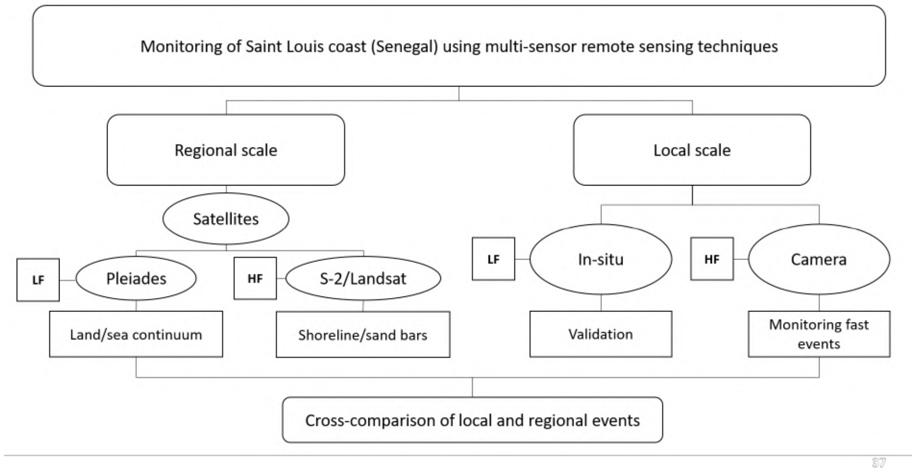

Figure 2: Summary of the tools used to conduct the thesis work. (LF - low-frequency ; HF - high frequency)

The Pleiades satellite tool provides very high precision images and allows a regional area to be covered at low frequency - in the case of our study (LF ; Figure 2). The Sentinel-2 and Landsat missions, which have a lower resolution, have the advantage of providing high-frequency data over a long period of time (from 1984 to the present). Their combined use made it possible to understand the volume of sand exchanged between the lower beach and the shallow water, the dynamics of the nearshore sandbars and the southward extension of the spit. The in situ topo-bathymetric data have validated the various analyses carried out and, finally, the camera installed in January 2021 allows a high-frequency (HF; Figure 2) monitoring of the local impact of the rip-rap by monitoring the position of the shoreline, its response to fast events (storms) and the bathymetry very close to the shore.

Organization of the manuscript

The manuscript is divided into 5 chapters, followed by an overall conclusion.

After a state of the art on how coastal management is carried out around the world – presented in chapter 1, chapter 2 describes the data used in this thesis, as well as the methodology used to carry out the various analyses of the exposed (topography) and submerged (bathymetry) coast of the city of Saint Louis. The main study site (Saint Louis, Senegal, West Africa) is also described in this chapter. Satellite tools and their contribution and advantages in the field of long-term coastal monitoring at large spatial scales are examined throughout this thesis. These tools - although mostly applied to Senegal - can be used on a global scale and an extension of the results to other countries is presented in this thesis.

Chapter 3 focuses on the long-term morphodynamics of the emergent part of the study area. This study is mainly based on the very high resolution acquisitions of the Pleiades satellites, scheduled every 6 months from March 2019. Part of this work has been published in the MDPI journal *Remote Sensing* and presented at conferences at the *Journées Nationales Génie Côtier - Génie Civil* (Taveneau et al., 2020) and *Coastal Dynamics*. It is there that the analysis of the dynamics of the coast is carried out with a view to the installation of a sea wall in the most vulnerable area.

Chapter 4 presents the land-sea continuum of Saint Louis, with bathymetry estimates derived from Pleiades satellites and the fusion of these data with topographic estimates to understand the sand volume exchange between the lower beach and the nearshore submerged area. The nearshore sandbank dynamics derived from Sentinel-2, coupled with the shoreline dynamics, are presented to provide part of the answer to the effectiveness of the protective rip-rap.

Finally, chapter 5 presents the creation of a conceptual model based on the hypothesis of an intrinsic and cyclic elongation of the *Langue de Barbarie* sand spit. This model is extended to three other wave-dominated spits with similar characteristics around the world, and the results are discussed.

Introduction générale

Contexte général

Avec plus de 600 millions de personnes résidant à moins de 10 mètres au-dessus du niveau moyen de la mer (Massuanganhe and Arnberg, 2008), le littoral est une zone de conflits permanents entre les phénomènes naturels et les interventions humaines (Small and Nicholls, 2003). Souvent exploitée à des fins agricoles, industrielles ou touristiques, et sans cesse soumise à l'action des processus marins, la bande littorale est aujourd'hui exposée à des pressions environnementales et économiques sans précédent. Dans un contexte de réchauffement climatique, et plus particulièrement avec la montée du niveau de la mer, la protection des littoraux représente donc en enjeu socio-économique majeur.

Les littoraux sableux sont des systèmes très dynamiques et façonnés par de nombreux facteurs extérieurs tels que la houle, la marée ou le vent. De nos jours, 1/4 des plages sableuses de par le monde présentent des taux d'érosion alarmants supérieurs à -0.5 m/an (Luijendijk et al., 2018). Face à ce constat, le repli stratégique des populations est souvent difficilement envisageable et il devient donc indispensable de mettre en place des dispositifs de protection à la côte afin d'assurer la pérennité de ces plages. L'amélioration de la compréhension de la dynamique de tels environnements dans le but d'y intégrer des moyens de protection apparaît donc comme un enjeu sociétal majeur afin de pouvoir proposer des solutions durables.

La compréhension de la dynamique naturelle d'une plage est la première étape dans le développement d'une stratégie de protection de ces environnements (Benavente et al., 2002) : les ouvrages prenant en compte la complexité des échanges sédimentaires d'une plage seront d'une part plus efficace, et d'une autre plus durable. La gestion et le management des littoraux sont une problématique à facettes multiples, et il n'existe jamais une solution simple (Christie, 2005). La bande littorale, entre terre et mer, est un environnement dont la morphodynamique est complexe, et elle évolue grandement selon les échelles spatiales et temporelles. Un des moyens les plus utilisés pour caractériser la dynamique d'une plage est par l'observation de la position du trait de côte (ici caractérisé comme étant l'interface physique entre la terre et la mer) au cours du temps (Dolan et al., 1978; Stive et al., 2002b; Yates et al., 2009; Splinter et al., 2014). La fixation de ce dernier autour d'une position stable est devenue un enjeu socio-économique majeur, faisant parfois fi de la complexité de la dynamique naturelle de la plage. Durant de nombreuses années, le génie côtier s'est principalement tourné vers la construction d'ouvrages émergés (ports, digues, jetés ...). L'enjeu réside désormais dans la problématique d'intégrer ces ouvrages dans la dynamique naturelle de son environnement, en tenant compte de la mobilité naturelle du trait de côte.

Les échanges sédimentaires d'une plage se produisent à des échelles spatiales variant du mètre jusqu'à plusieurs centaines de kilomètres. Ils sont régis par différents processus qui impactent significativement la morphologie des côtes sur des périodes temporelles variées (Masselink and Kroon, 2009). Un panel d'outils rend possible le suivi de la dynamique d'une plage sur différentes échelles, permettant ainsi d'en comprendre les mécanismes qui lui sont propres (Baily and Nowell, 1996).

Problématiques et objectifs de la thèse

Citée dans plusieurs journaux de par le monde, Saint Louis du Sénégal est une ville dont la tendance à l'érosion inquiète à l'internationale. Construite sur une flèche de sable particulièrement dynamique, elle se situe entre l'embouchure du Fleuve Sénégal et l'océan Atlantique, ce qui fait d'elle une ville particulièrement exposée aux aléas de la mer et aux phénomènes de crues (Sadio et al., 2017; Anthony, 2015). Le quartier des pêcheurs, Guet Ndar (Figure 1.a), subit constamment des assauts de la mer qui emporte des bâtiments (Figure 1.b) et gagne petit à petit du terrain sur la plage (Bergsma et al., 2020). Guet Ndar étant le quartier le plus densément peuplé de Saint Louis, il est devenu vital de trouver une solution face à cette catastrophe socio-économique. Dans un premier temps, des solutions d'urgence ont été mises en place face à cette catastrophe sociale : un plan de relogement stratégique par un recul de 20 m des habitations pour 10000 personnes a été initié en 2018, ainsi que la construction d'un mur de protection court terme sur la zone littorale la plus à risque (AFD, 2018). L'ouvrage prévu par l'Agence Française de Développement (AFD) et l'Agence de Développement Municipal (ADM) devait mesurer 3.6 km de long pour une largeur de 20 m. Un des objectifs de cette thèse consistait à quantifier l'impact de cet ouvrage sur la côte de Saint Louis. La construction de cet enrochement visant à protéger les populations les plus à risque devait commencer en 2019, les travaux n'ont finalement démarré qu'en décembre 2020.

La tendance massive à l'érosion de la partie nord de la Langue de Barbarie a été mise en relation avec la prise de décision urgente de réaliser une brèche dans la flèche sableuse en octobre 2003 (Rodríguez et al., 2014; Bergsma et al., 2020; Taveneau et al., 2021). En effet, des inondations majeures dues à la crue du Fleuve Sénégal ont immobilisé la ville de Saint Louis pendant plusieurs jours. Le niveau d'eau dans les rues de la ville était tel qu'une brèche a été réalisée dans la Langue de Barbarie afin que l'eau s'évacue plus rapidement vers la mer ; l'embouchure du fleuve se trouvant à plusieurs dizaines de kilomètres au sud de la ville. Cependant, la brèche qui faisait originalement 4 m de large s'est très vite élargie, devenant avec le temps la nouvelle embouchure du fleuve et entraînant l'érosion presque complète de la partie sud de la flèche sableuse, ainsi qu'un schéma érosif dans la partie nord de celle-ci.

L'objectif principal de cette thèse est le suivi multicapteurs de l'évolution de la plage, à l'échelle locale de l'ouvrage de construction, jusqu'à l'échelle régionale de la flèche sableuse. La figure ci-dessous (Figure 2) récapitule les moyens mis en place ainsi que les différentes études réalisées à partir des données mises à disposition.

L'outil satellitaire Pleiades fournit une imagerie haute-résolution, et permet de couvrir une zone régionale à basse fréquence dans notre étude (BF ; Figure 2). Les missions Sentinel-2 et Landsat, moins haute résolution, offrent l'avantage de fournir des données haute fréquence sur une longue période temporelle (depuis 1984 à nos jours). Leur utilisation jointe déverrouille la compréhension des volumes de sable échangés entre le bas de plage et les zones en eau peu profonde, de la dynamique des barres sableuses, ainsi que le procédé d'allongement de la flèche sableuse. Les données topo bathymétriques in situ acquises sur le terrain ont permis de valider les différentes analyses réalisées, et enfin la caméra installée en janvier 2021 permet de réaliser un suivi haute fréquence (HF ; Figure 2) de l'impact de l'ouvrage sur la position du trait de côte, ainsi que la réponse de ce dernier à l'échelle événementielle (tempêtes), et finalement fournir des informations sur la bathymétrie proche côte.

Organisation du manuscrit

Le manuscrit s'articule autour de 5 chapitres suivis d'une conclusion générale.

Après un état de l'art de la science sur la gestion des littoraux de par le monde présenté chapitre 1, le chapitre 2 s'emploie à décrire les données utilisées dans cette thèse, ainsi que la méthodologie utilisée pour réaliser les différentes analyses de la côte émergée (topographie) et immergée (bathymétrie) de la ville de Saint Louis. Le site d'étude principal (Saint Louis du Sénégal en Afrique de l'Ouest) y est décrit. Les outils satellitaires, leur contribution et leurs avantages dans le domaine de la surveillance côtière long terme à grande échelle spatiale sont étudiés tout au long de ce travail de thèse. Ces outils - bien que principalement appliqués au Sénégal - peuvent être utilisés à l'échelle mondiale, et une extension de ces outils à d'autres pays est présentée dans cette thèse.

Le chapitre 3 se focalise sur la morphodynamique long terme de la partie émergée du site d'étude. Cette étude se base principalement sur les acquisitions très haute résolution des satellites Pleiades qui ont été programmés tous les 6 mois à compter de la date de mars 2019. Une partie de ce travail a été publié dans la revue *remote sensing* de MDPI (Taveneau et al., 2021) et présenté dans des conférences aux *Journées Nationales Génie Côtier - Génie Civil* (Taveneau et al., 2020), et à *Coastal Dynamics*. L'analyse de la dynamique du littoral, en regard de l'installation d'un enrochement sur la partie de plage la plus sensible à l'érosion, y est réalisée.

Le chapitre 4 présente le continuum terre/mer de Saint Louis, avec les estimations bathymétriques Pleiades ainsi que la fusion de ces données avec celles topographiques dans le but de comprendre les échanges de volume de sable entre le bas de plage et la zone proche côte immergée. La dynamique des barres de sableuses dérivée de Sentinel-2, couplée à la dynamique du trait de côte, est introduite afin d'apporter des premiers éléments de réponse quant à l'efficacité de l'enrochement.

Enfin, le chapitre 5 présente la création d'un modèle conceptuel basée sur l'hypothèse d'un développement intrinsèque et cyclique de la *Langue de Barbarie*. Ce modèle est ensuite étendu à trois autres flèches sableuses (régies par les vagues) à caractéristiques similaires dans le monde, et les résultats seront discutés.

Chapter 1

State of the art

Contents

1.1 Introduction

Historically, coastal areas have always been a zone of intense human activity due to their socio-economic and environmental importance, such as tourism and business (e.g. fishing, ports). They are therefore often densely populated (Small and Nicholls, 2003; Hallegatte et al., 2013; Hinkel et al., 2013). Coastal areas often develop because of the wide variety of socio-economic resources they offer; originally trade, fishing... (Duhamel and Knafou, 2003). However, the presence of numerous megacities means that they are highly vulnerable to flooding and human-induced changes in natural processes (Turner et al., 1996; Pernetta and Milliman, 1995). It has been commonly stated that "50% of the world's population lives within 60 to 100 km of a coastline". In the work of (Small and Nicholls, 2003), they quantified this figure as "the coastal population within 100 km of a coastline and 100 m of sea level, with an average density that is almost 3 times higher than the global average density" (Small and Nicholls, 2003).

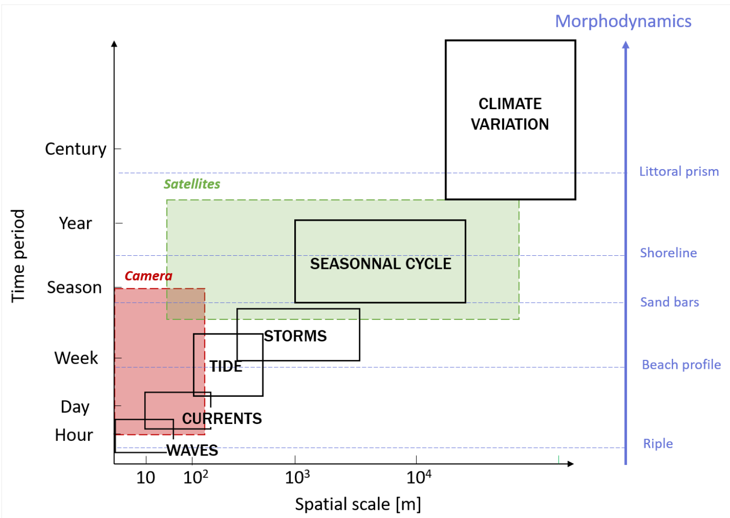

Figure 1.1: Temporal scale of coastal sediment dynamics processes. The green and red areas indicate the tools used in the PhD work and their footprint on a spatiotemporal scale.

Sandy coasts make up more than 31% of the world's coastline (Luijendijk et al., 2018). By definition, sandy coasts are characterised by a sandy profile from the point where the waves reach the sedimentary bed to the dune line. Sandy beaches generally result from the combined action of waves and other metocean processes such as wind and tides (Figure 1.2). Nearshore – within the first few hundred metres seaward of the shore – submerged sandbars may be part of the beach bathymetry (O'Hare and Davies, 1993; Dulou et al., 2000; Hancock, 2005). These submerged features act as a natural barrier as some of the wave energy is dissipated over the sandbars as the waves break. This reduces the potential erosive force of a wave as it reaches the shore. With this in mind, one can imagine that sandbars, or the lack of them, are important components of beach morphodynamics and the resulting hydrodynamics.

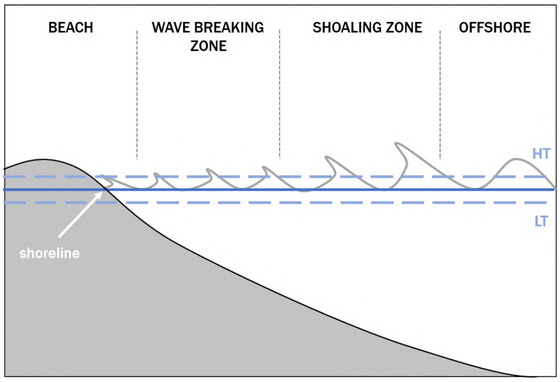

Figure 1.2: Evolution of the surface wave with characterization of different hydrodynamics areas. With high and low-tide levels (respectively HT and LT) as horizontal dashed line. The horizontal line is the mean sea level.

1.2 Hydro-sedimentary beach-processes

1.2.1 Nearshore wave dynamics

Ocean wind waves are gravity waves and can be described as the sum of a series of sinusoidal waves in the open ocean. Each wave component can be characterised by a wavelength L (or a wave number $k = 2\pi/L$), a height H, a period T (or an angular frequency $\omega = 2\pi/T$), and propagates at a phase velocity $C = L/T$ (figure 1.3).

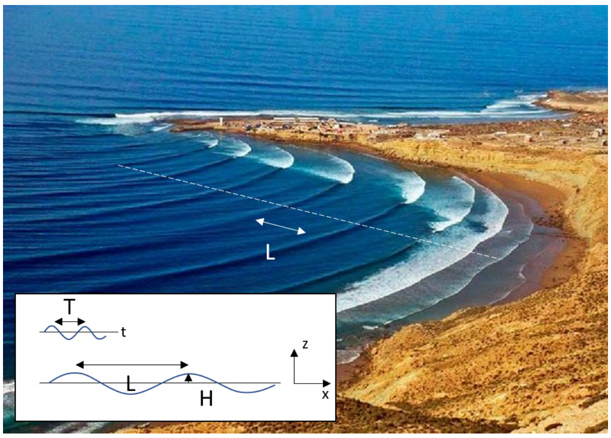

Figure 1.3: Wave parameters represented on Iroise sea photography (picture source (Previmer)).

Wave propagation can be simplified using various hypotheses, e.g. incompressible and non-viscous flow, irrotational fluid with constant density, sinusoidal wave on flat bottom, so that the momentum equations can be linearised (Airy, 1841). The equation describing the wave dynamics from deep to shallow water (although with limited validity) is called the *linear dispersion relation* (equation 1.1) and relates the wave speed to the water depth.

$$\omega^2 = gk \tanh(kh) \tag{1.1}$$

Where g is the gravitational constant and h is the depth. The equation 1.1 states that long waves travel faster than shorter waves. As the wave approaches the shore, its speed decreases with depth and wavelength, while its period remains constant. To maintain the energy flow, the wave amplitude increases: this phenomenon is called shoaling. The degree of shoaling depends on the local bathymetry and wave conditions (Thornton and Guza, 1983; Elgar and Guza, 1985). Similarly, as the depth of the water decreases, the speed at which the wave propagates decreases. As a result, the crest lines of the wave are deformed and become parallel to the isobaths: this is refraction. In the absence of near-shore currents, refraction can be observed when $h < \lambda/2$.

- **Dissipation**

In shallow water, bottom friction increases, creating an instability that develops on a wave crest. As the waves propagate landward, the bathymetry decreases and the wave propagation speed decreases. When the particle velocity associated with the wave motion becomes greater than the phase velocity, the wave crest reaches a threshold and the wave breaks. Wave breaking can be differentiated according to the slope of the beach and can be quantified by the Irribaren numbers ξ_b (equation 1.2 ; (Iribarren and Nogales, 1954; Fredsoe and Deigaard, 1992)).

$$\xi_b = \frac{tan(\beta)}{\sqrt{\frac{H_b}{L_o}}} \tag{1.2}$$

where β = beach slope
H_b = swell amplitude at its breaking point
L_o = offshore wavelength

After breaking, and in the case of a low beach slope, the wave continues to propagate with an amplitude that decreases with depth (Dulou et al., 2000). This parameter is defined by the equation 1.3.

$$H = \gamma h \tag{1.3}$$

γ, the wave breaking parameter, is about 0.8 (Fredsoe and Deigaard, 1992) and can be considered constant. Being able to characterise the swell after it has broken makes it possible to calculate shore currents.

1.2.2 Sediment transport in open beaches and associated currents

Sandy shorelines are dynamic natural systems that are sensitive to a variety of natural processes: swell, tide, storm surge, sea level and the coastal sediment budget (Komar, 2018). These processes together influence the position of the coastline, the morphology of the littoral zone (beaches, dunes, cliffs) and the variation of sediment availability on different time scales (Figure 1.1). Bruun's rule states that there is a long-term equilibrium in the movement of sedimentary material between the coast and the open sea, and thus a sedimentary equilibrium for each sandy area. The rapid succession of unfavourable climatic events, such as storms, can lead to a sedimentary imbalance, causing a permanent (de-)structuring of the beach and eventually leading to an erosive pattern. The term erosion can be used when there is a shortage of sediment: erosion is a natural process that shapes coastlines all over the world. However, its magnitude is influenced by human impact and increases tenfold with the anthropisation of coastlines (Pilkey et al., 2009; Prasad and Kumar, 2014). It is therefore crucial to know its own dynamics in order to adapt decision-making for a sustainable protection strategy (Ruggiero et al., 2000). The knowledge of the morphodynamics of a beach allows to face many problems, such as the anticipation and the prevention of the damages that can be induced by storms (Benavente et al., 2002), or the stabilisation of the coastal position (Corral and Schling, 2017).

In the long term, the natural development of sandy shores depends on the balance between the net supply of sediment and the demand caused by sea-level rise and subsidence. The figure 1.1 describes the occurrence and spatial impact of different phenomena on beach morphology. High energy drivers such as tides, waves and winds are dominant on a time scale of up to one year. Over longer timescales, other drivers such as sea level rise take over (Masselink and Kroon, 2009). These drivers also vary spatially. Coastal behaviour is the combination of a large number of processes acting and interacting on both spatial and time scales (de Vriend et al., 1993). Estimating the evolution of the coast can be done through two different approaches (De Vriend, 1991):

– A "medium term" approach: use of available significant wave data or those calculated with numerical models. The sediment volume conservation equation is fully solved, as the sediment transport is known, by assuming that the beach profile is in equilibrium (Bruun's profile (Bruun, 1988)).

– A "long term" approach: for periods where swell and bathymetry data are not available, but where the coastline can be mapped over several decades using either satellite imagery or aerial photographs.

In a comprehensive analysis using decades of coastline data, most sandy coastlines show that 48% of these coasts have a stable shoreline, 28% are accreting, while only 24% of sandy coasts are eroding at alarming rates ($\simeq -0.5m/yr$ of beach loss) (Luijendijk et al., 2018). The coastal retreat trend is a global phenomenon that affects all parts of the world with spatial inequalities and is the result of a complex interaction of several physical processes, namely swell, tides, storm surges, sea level and the coastal sediment budget (Komar, 2018). In the context of global warming, and in particular with sea-level rise, combined with strong demographic growth in coastal areas, the degradation of coastal zones is exacerbated (Feagin et al., 2005; Lacroix et al., 2019).

1.2.3 Currents in the nearshore area

Ocean currents have different origins and can be divided into four categories:

- Tidal currents: they are periodic in intensity and direction. They are mostly dependent on the location.
- Wind-generated currents: by their nature, they are strong at the surface and their intensity decreases rapidly with depth.
- Seasonal/permanent currents (major ocean currents, balancing currents). They depend on the location.
- Coastal currents induced by ocean swell.

Only coastal currents will be discussed further in this thesis, as the others are irrelevant in the case of our study. There are three types of currents in coastal areas generated by wave action: rip currents, drift currents and undertow currents (Figure 1.4). Considering several wavelengths, these currents can be considered as quasi-stationary. Their intensity depends strongly on the wave climate of the site and the tidal level (Castelle et al., 2006).

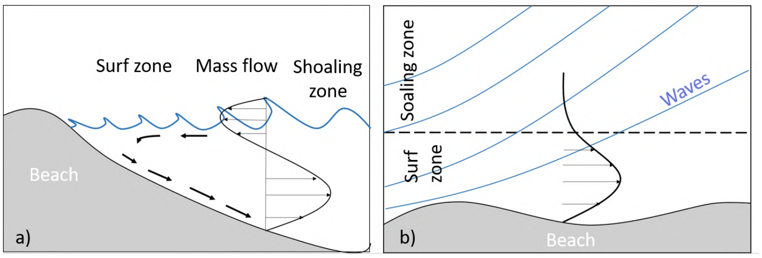

Figure 1.4: Blueprint of **(a)** undertow current and **(b)** longshore drift currents adapted from (Dubarbier, 2014).

In coastal areas, the variable waves breaking over a sandy bed lead to a local imbalance between the buoyancy forces (mass flow) associated with the breaking waves and the excess motion gradient. This imbalance can generate two-dimensional currents with very high velocities (Figure 1.4). This phenomenon can be particularly violent and is one of the leading causes of drowning worldwide (Castelle et al., 2016). The intensity of these currents can last for several hours with velocities greater than 0.5 m/s and are amplified during energetic events such as storms (Thornton et al., 2007; Loureiro et al., 2012). They are called rip currents.

The undertow is a circulation that occurs in the vertical plane (Figure 1.4.a). It represents the compensation of the landward mass flow associated with the excess momentum induced by surface waves by an offshore displacement of water masses in the near-bottom zone. This compensation is greater in the surf zone. For low energy areas, the velocities of this current are about 0.1 to 0.3 m/s for the surf zone. But they can reach 0.5 m/s for very energetic areas (Masselink and Black, 1995). The higher values of this current are usually found on the inside of sandbars (Faria et al., 2000).

Drift currents (Figure 1.4.b) occur for obliquely propagating waves (sites with longshore sediment transport). According to the results of (Keulegan, 1951), the surface drift current is not affected by water depth except at very low wind speeds. During energetic swells, the mean drift current is higher in the surf zone with velocities greater than 1 m/s (Thornton et al., 1996).

These currents allow to describe a large part of the sediment transport, but they are not the only mechanism responsible for the development of sandy bottoms. Turbulence (induced for example by wave breaking) favours the re-suspension of sediment (Grasso et al., 2012). The orbital velocity associated with the asymmetric movement of fluid particles is also part of the sediment transport processes: by re-suspension of the particles in the water column, or by a net induced landward transport (Dubarbier et al., 2017). The latter process is responsible for the phenomenon of beach accretion under low energy wave conditions (Hoefel and Elgar, 2003).

1.2.4 Beach morphodynamics

Sandy beaches have numerous shapes and positions of sandbars, depending on environmental conditions (waves, currents, winds) and sediment characteristics (grain size, porosity). The first classifications of these coastal areas were based on simple observations of a number of individual sand-bar beaches (Wright and Short, 1984; Sunamura, 1988; Lippmann and Holman, 1990). A simple relationship allows the classification of any sandy beach worldwide according to (Wright and Short, 1984) (equation 1.4).

$$\Omega = \frac{H_b}{w_S T_P} \tag{1.4}$$

Where w_S is the particle fall velocity, H_b is the wave height at the breaking point. Some sandy beaches have a fairly stable profile, but in a natural environment sediment fluxes are never in equilibrium. The classification of sandy beaches is as follows:

If $\Omega < 1.5$, the beach is reflective. It is characterised by a very steep upper beach. The surf zone is narrow and limited to the upper beach. In general, these beaches are exposed to long swells of low amplitude and coarse grain size (Figure 1.5).

If $\Omega > 5.5$, the beach is dissipative. These beaches are relatively flat and sandbars can be observed. Wave breaking may occur in several places. Unlike reflective beaches, they are exposed to short and energetic swells and consist of fine-grained sediment (Figure 1.5).

When $1.5 < \Omega < 5.5$, you can find the intermediate beaches. They are the most dynamic and the most common worldwide. The response time of intermediate beaches is often much shorter than that of dissipative beaches, which corresponds to a more stable range state. They also have a large grain size and swell panel. Intermediate beaches are characterised by the presence of one or more three-dimensional sandbars: the breaking zone parallel to the shoreline is non-linear, inducing circulation cells of varying intensity and rip currents. Four sub-classes of beaches can be distinguished, as the morphology of the bar(s) varies considerably: when the bar(s) can be separated from the berm ("LBT" and "RBB"), or partially connected to it ("LTT" and "TBR").

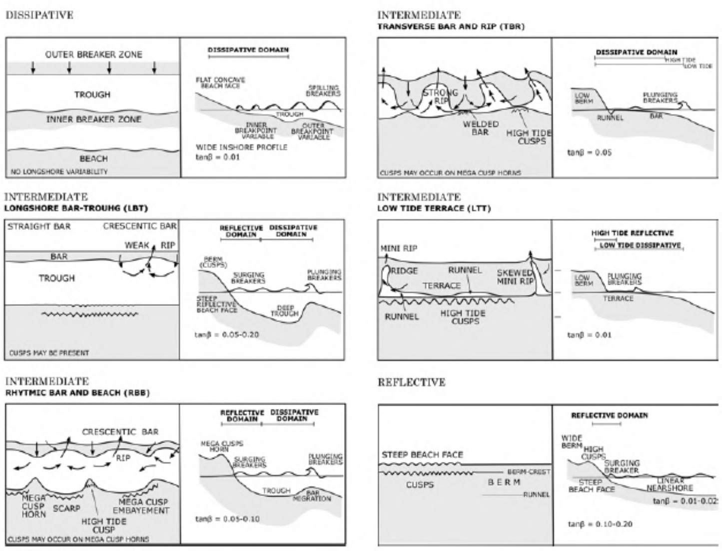

Figure 1.5: Beach classification according to (Wright and Short, 1984). Figure adapted from *Short, 1999.*

Depending on the beach classification (dissipative, reflective or intermediate) evaluated by the Ω parameter, the shape of the submarine sand bar(s) is different.

1.2.5 Morphological evolution of beaches and submerged sand bars

Sandbars play a key role in the sustainability of coastal environments because they reduce the energy of incoming waves: as they approach the shore, waves break against these structures and some of their energy is dissipated. When they reach the shore, they are less energetic and therefore less erosive. Their dynamics are highly correlated with those of the upper beach (Ruessink et al., 2007; Castelle et al., 2010).

In natural environments, sediment fluxes never reach equilibrium because the morphological response of the sandbar(s) is generally longer than the time scales associated with changes in wave regime: this leads to a landward or seaward shift of existing sandy structures. The morphological evolution associated with the dynamics of the sandbars is the main source of profile variability on short (sub-seasonal), medium (seasonal) and long (inter-annual) time scales. On the same intermediate beach, it is then possible to observe numerous sand bar(s) morphologies (Lippmann and Holman, 1989, 1990).

In the cross-shore direction, the short-term dynamics of the sandbars depend on the wave conditions. During very energetic episodes (e.g. storms) the sandbars migrate rapidly seawards with velocities up to 10 m/day (Ruessink et al., 2009). This is due to the feedback between the bottom and the seaward sediment fluxes induced by the undertow (Figure 1.4). Conversely, under low to medium wave conditions, the sandbars migrate slowly shoreward at a rate of about 1 m/day (Van Enckevort and Ruessink, 2003). This dynamic is due to the feedback between the bottom and the seaward sediment flows induced by the orbital velocity non-linearities(Dubarbier et al., 2015). The position of a sandbar - given the seasonal variability of the swell climate - is further from the shore with energetic wave conditions in moderate conditions. Some beaches also have a double bar system which shows a cyclic behaviour on inter-annual scales: net offshore migration of the whole bar system (see in (Ruessink et al., 2009; Almar et al., 2010; Aleman et al., 2017; Shand, 2003; Bouvier et al., 2019)). When the outer beam reaches a *limit depth*, it begins a degeneration phase that leads to the inner beam becoming the new outer beam. At the same time, a new (inner) bar is formed near the coastline.

Figure 1.6: Aerial photography of the coupled morphologies between the intertidal and subtidal areas. Shoreline oscillations are coupled to the sand bars geometry. Illustration adapted from (Price et al., 2013).

The geometry of alongshore sandbars is variable and depends on several parameters such as the wave climate. Previous studies have shown that oblique energetic waves resulting in a strong drift current lead to linearisation of the sandbars (Price et al., 2011; Garnier et al., 2013). In other cases, the drift current can also cause the bar sinuosities to migrate by tens of metres within a day (Aagaard, 1988; Van Enckevort and Ruessink, 2003; Van Enckevort et al., 2004). On the other hand, waves propagating perpendicular to the shore tend to favour the three-dimensional development of a bar (Splinter et al., 2011; Dubarbier et al., 2017). When a beach presents a system of several sandbars, a link is often observed between the morphology of the inner bar and that of the outer bar: the bar closest to the shore has a symmetrical geometry with the more offshore bar, with an extremely rapid reaction time (Price and Ruessink, 2011). Due to its depth, the outer bar is inactive for low energy waves. It is essential to understand the morphodynamics of the sandbar(s) as it is closely linked to the shoreline variations (see Figure 1.6).

1.3 Sand spit systems

1.3.1 Sand spit formation

Sandy beaches are distinguished from spit systems. Spits form under conditions of strong oblique waves that carry sediment into an elongated feature extending away from the eroding headland (Dean and Dalrymple, 2001) (Figure 1.7). These coastal areas present a complex morphodynamics characterised by significant changes (Fitzgerald et al., 1984; Hicks et al., 1999; Fenster and Dolan, 1996). Three mechanisms explaining a sand spit formation are generally documented in the existing literature: spit elongation by sediment accumulation at its tip introduced by longshore transport, accretion at the end of a barrier spit bordering a tidal inlet – usually associated with erosion patterns on the opposite side of the inlet – and the less common, the self-generating spit (a spit that does not require external sediment availability to elongate) (Aubrey and Gaines, 1982). The most commonly cited feature in the literature is the wave-dominated one - corresponding to the first mechanism described. These sand spits are formed by dominant waves or currents transporting sediments that are gradually deposited on an elongated feature (Aubrey and Gaines, 1982; Stive et al., 2002b).

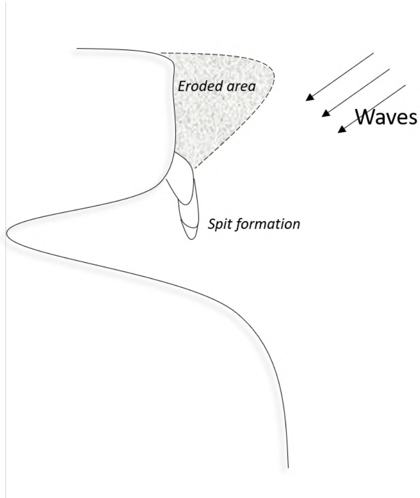

Figure 1.7: Formation of a simple spit, adapted from (Dean and Dalrymple, 2001).

A spit progressively elongates - towards the direction of LST - as sand accumulates at its end, and its growth rate is directly related to the LST and the depth of water into which the spit grows (Dean and Dalrymple, 2001; Evans, 1942; Allard et al., 2008). Its morphological changes depend on many parameters such as the interactions between wave transformation (Ashton et al., 2016; Allard et al., 2008), tidal exchange (Powell et al., 2006; Robin et al., 2007), LST (Evans, 1942; Schwartz, 1982), river discharge (Chaumillon et al., 2014; Adams et al., 2016), sediment availability (Hequette and Ruz, 1991; Aubrey and Gaines, 1982), winds and tides, sea level rise (Hequette and Ruz, 1991), and human interactions (Allard et al., 2008; Lorenzo et al., 2007; Nahon et al., 2019). Previous studies have shown that wave-induced current processes (Allard et al., 2008) and LST variability (Duc Anh et al., 2020) are the processes most responsible for morphological changes in spits. Two general phases for spit development are highlighted in the literature (Aubrey and Gaines, 1982): first, spit accretion by the LST, and second, tidal inlet migration.

1.3.2 Inlets dynamics

The dynamics of the inlet spit – which is directly linked to the spit morphology – is important to consider as its migration or closure causes many societal problems: changes in shipping channels, saltwater intrusion (Pradhan et al., 2015; Dada et al., 2021), or increased risk of coastal flooding (Duc Anh et al., 2020; Anthony, 2015). The geometry and evolution of the mouth is influenced by several parameters on different time scales: the length of the spit, the width of the spit, the rate of elongation... (Kraus, 1999). Intrinsically, the opening of the estuary occurs during strong flow (Anthony and A.B.Blivi, 1999; Cooper, 2001), and its closure during the period of energetic waves and thus highest LST (Rice, 1974). In several cases around the world, sediment accumulation at the end of the spit had caused it to elongate to such an extent that its mouth was several kilometres away from the river mouth. In these cases, rapid breach intervention may be necessary to protect coastal infrastructure or vulnerable ecosystems. However, small breaches can easily become large inlets that either cause significant economic and social losses(Schmeltz et al., 1982; Wamsley and Kraus, 2005; Laïbi et al., 2014) or initiate erosion trends on the up-drift part of the spit (Zăinescu et al., 2019; Taveneau et al., 2021). The *Langue de Barbarie* sand spit in Senegal is such an example: the inlet was so far down-drift from the river mouth that an artificial breach was urgently made in the sand spit to lower the water level in the up-drift town during strong floods (Bergsma et al., 2020; Sadio et al., 2017; Anthony, 2015; Ndour et al., 2018). This breach quickly became the new mouth of the river: the natural cycle of the spit (sediment accumulation at its tip) was re-initiated (Taveneau et al., 2021; Sadio et al., 2017) and an up-drift erosion pattern was detected (Bergsma et al., 2020; Taveneau et al., 2021) (Figure 1.8).

Figure 1.8: Satellite images from Google Earth, pre-and post-2003 breach to illustrate the breaching process. The stars indicate the river mouth location.

Breaching is in fact one of the mechanisms that drives spit migration and, along with other parameters, controls its width (Pierce, 1969; Leatherman, 1979; Zaremba and Leatherman, 1984; Boothroyd, 1985). Natural breaches occur during natural disasters such as earthquakes, hurricanes or severe cyclones (Zăinescu et al., 2019; Villagran et al., 2011), but mostly during strong storm events (Schoonees et al., 1999; Zăinescu et al., 2019). Moreover, the narrower the spit, the more likely the breach (Masselink and van Heteren, 2014). Several analytical models - for wave-dominated spits - have been implemented to predict their growth rate (Kraus, 1999; Palalane et al., 2014; Duc Anh et al., 2020) and the inlet migration pattern(s) (Kraus, 1999; Tung et al., 2009). The spit width, on the other hand, is inversely proportional to the spit growth rate (Kraus, 1999; Duc Anh et al., 2020): for an inlet that has largely migrated down-drift, the sand spit is more likely to be naturally breached (Masselink and van Heteren, 2014). Our present study focuses on the most commonly observed sand spits, i.e. those elongated by down-drift sediment accumulation.

1.4 Beach management and engineering

By definition, a 'coastal structure' is a structure that has a direct impact on the morphology of a coast and locally modifies hydro-sedimentary processes. These structures are initially designed to fix the position of the shoreline, reduce wave crossing or dissipate wave energy.

Other types of structures, such as ports, can also have an impact on the coastal zone without addressing the risks associated with the sea. The construction of such structures dates back to the time when the coasts were settled (Charlier et al., 2005). Since the middle of the 20th century, marine structures for coastal management have flourished on the European and American coasts (Dean and Dalrymple, 2004), and even more so in Japan (Seiji et al., 1987).

1.4.1 Lessons from deployed protective structures

The methods of protecting a beach against erosion can be divided into two categories: the so-called "hard" or "rigid" methods, which aim to fix the coastline (groins, dikes, rip-rap...), and the "soft" or "flexible" methods, which are easily reversible techniques (replenishment of the beach with sediment, work on the vegetation...) and which are integrated into the environment in which they are installed (Figure 1.9). The distinction between "soft" and "hard" methods is essentially made according to the criteria of impact on the natural sediment dynamics of the site and according to the reversibility of the protection structure (ANCORIM, 2017). These two methods – to limit coastal erosion and to protect the coasts from flooding – have been widely implemented worldwide (Ranasinghe et al., 2006). However, the study of "soft" methods has received little attention in the literature (Black and Mead, 2001).

In the past, coastal development has often involved several measures to fix the position of the shoreline: construction of sea walls, dikes, jetties... The impact of these structures can sometimes have a negative feedback on the coast, as in many cases large financial resources have to be invested to alleviate the problems (blocking of sediment transport, erosion on adjacent coasts) caused by old constructions that did not take into account the complexity of coastal dynamics (Inman and Brush, 1973). In Tunisia, breakwaters caused severe erosion patterns (Marzougui and Oueslati, 2017), and 13 projects suffered negative environmental reactions due to rapid and uncontrolled coastal development in Egypt (Frihy, 2001). It is therefore essential to carry out long-term monitoring and mapping of a coastline in order to understand its morphodynamics so that a coastal protection strategy can be in line with the natural dynamics of the coast (Le Xuan et al., 2022). Access to high resolution parameters such as topography and bathymetry over a large area allows the understanding of the natural behaviour and variability of the beach (Gesch et al., 2016). In this context, remote sensing observations are well suited to better adapt coastal management because they can cover a regional area with high frequency acquisitions (Cazenave et al., 2017; Almeida et al., 2019; Bergsma et al., 2020; Taveneau et al., 2021; Turner et al., 2021).

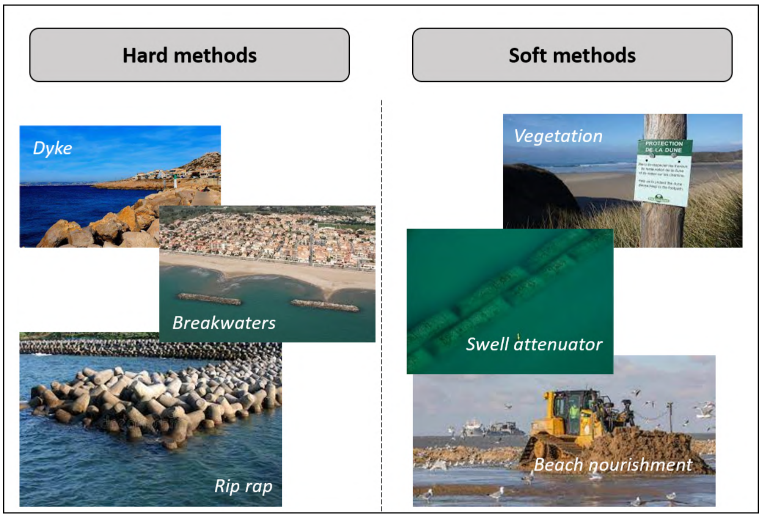

Figure 1.9: Summary of some coastal protective structures (soft or hard methods).

Whereas in the past "hard" methods were preferred, today the trend is towards the use of "soft" methods that have a lower environmental impact. The aim of these methods is no longer to fix the position of the shoreline definitively, but to achieve a more continuous management by integrating the natural dynamics of the beach (De la Torre et al., 2014). Beach nourishment, in which a large amount of compatible sediment is placed on a beach to move the shoreline seaward (Dean, 2018), offers the benefits of reducing storm damage and restoring environmental improvement (Dean, 2002). However, only 11% of studies monitoring the impact of beach nourishment have controlled for both natural spatial and temporal variation (Peterson and Bishop, 2005). Submerged breakwaters, when properly implemented, allow better control of shoreline and sandbar dynamics (Bouvier et al., 2017), but can also severely damage a beach if all its complexity is not properly considered (Jackson et al., 2003; Ranasinghe et al., 2010). The latest innovation in coastal protection is the 'sand motor'. This method provides natural beach nourishment by concentrating and redistributing sediments across the coastal system, both spatially and temporally. The Sand Motor system has shown positive results in a multi-year analysis in the Netherlands (Brière et al., 2018).

1.4.2 Coastal monitoring using remote technologies

The current state-of-the-art methods for coastal monitoring, which are limited to the local scale, are: in-situ measurements, which are very expensive and therefore often carried out at intervals of several months, but provide a high degree of accuracy; fixed cameras implanted on the coast - a low-cost solution - which provide a wealth of data, but are less accurate (Bergsma et al., 2019d; Holman et al., 2013; Bergsma et al., 2019e; Bergsma and Almar, 2018a; Angnuureng et al., 2020a). Both methods are reliable, but their spatial coverage is limited to the local scale. To accurately estimate coastal erosion processes, it is essential to understand the overall morphodynamics of an area at a regional scale. Digital Elevation Models (DEMs) derived from airborne remote sensing techniques such as LiDAR (Light Detection and Ranging) are one of the solutions to obtain these data with accuracy at larger spatial scales (Kidner et al., 2004; Le Mauff et al., 2018). However, airborne LiDAR remains extremely expensive. A tool that combines the advantages of each of these methods is the satellite: it is inexpensive (or freely available), covers regional areas and provides very high resolution (sub)metric images with a high acquisition frequency - such as Pleiades (CNES/Airbus) or WorldView-3, to name but two examples. These types of satellites are of interest for monitoring the evolution of rapid events, such as the impact of a storm on beach erosion on a regional scale (Benveniste et al., 2019; Melet et al., 2020a; Eustáquio Amaro et al., 2015). These agile satellites also offer the unprecedented opportunity to obtain topography and bathymetry DEMs in a single pass only (Collin et al., 2018; Eustáquio Amaro et al., 2015; Almeida et al., 2019) with a vertical precision and accuracy for topography similar to the state-of-the-art methods for coastal monitoring (0.35 m $\leq$ RMSE $\leq$ 0.48 m (Almeida et al., 2019)).

1.4.3 West African sand spits and the case of Saint Louis city on the Langue de Barbarie

The main area of study in this thesis focuses on the coasts of West Africa, and in particular the Senegalese coast of the historic city of Saint Louis. This city has the peculiarity of being built on a very dynamic sand spit called the *Langue de Barbarie* (presented in chapter 3). The central zone of this area is severely affected by coastal erosion: several metres per year Ndour et al. (2018). Whole areas of the *Langue de Barbarie* have already been eaten away. The massive construction and urbanisation of this natural coastline is accelerating the phenomenon by limiting the natural resilience of the coast. Moreover, the spit is located in a very hydrodynamic area. The aim of this thesis was to set up a complete monitoring of the area, using a multi-scale approach, in order to quantify the effectiveness and impact of a protective rip-rap that will be constructed at the end of 2020 (local scale) and to understand the natural morphodynamics at a regional scale (spit scale).

1.5 Positioning of the thesis work in the field studied

This chapter has introduced the phenomena that drive the morphodynamics of a beach, the different methods that can be used to protect the coastline from marine hazards, and the different technologies/tools that can be used to monitor the coastline on both a spatial and temporal scale. Beach morphology is complex and there is no simple answer for coastal management and decision making. It has been highlighted that satellite observations could bring a new dimension to coastal monitoring, given the numerous advantages that this remote sensing method offers compared to others.

This thesis focuses on several objectives: to quantify the exchange between the large and small scales - linking local erosion to regional processes and capturing the missed processes using the regional scale high resolution but sparse time data from the Pleiades satellites and the lower resolution but more frequent revisit of Sentinel-2.

To accurately estimate wave and sea level induced coastal erosion, a good knowledge of coastal topography and bathymetry is key (Toimil et al., 2022). Today, regional morphological information on coastal dynamics and global knowledge of coastal morphodynamics face an observational gap from local to regional scales. The use of both satellites – addressing the regional scale issue – and in situ and camera data (Figure 2) for the local scale, unlocks the observational issues in this work. It opens up the possibility of having a spatio-temporal evolution of coastal parameters from the local to the regional scale, and to further investigate a longer time scale. This work will allow the contribution of coastal processes from sea level to the coast to be properly assessed, and therefore its vulnerability. This thesis is mainly based on the use of satellite techniques: for the assessment of the topography of the study site (Chapter 3), for the estimation of the bathymetry and the location of the sandbars (Chapter 4), and for the extension of the results from the study site to other similar spits worldwide (Chapter 5). The next chapter describes the different satellite missions used for the studies and the methodology applied.

In summary, the three main questions that this thesis seeks to answer are as follows:

- What is the sediment exchange between the submerged and exposed parts of the beach?
- What are the links between local and regional scales?
- Can satellites answer the previous questions to support coastal engineering issues?

Chapter 2

Study site and Material

Contents

2.1 Introduction

Coastal monitoring is essential to assess the vulnerability of a beach and to quantify the changes in sand volume between the lower beach and the shallow water areas. This intertidal zone, located at the land-sea interface, is the most challenging area for coastal engineering to understand, as it is the shoreline dynamics that it seeks to influence. In coastal studies, topography and bathymetry are the parameters that allow the understanding of the morphodynamics of a beach and can be obtained using a variety of techniques. The most accurate are in-situ field measurements; these data allow the (in)validation of studies using other techniques (remote sensing, models for example). For the in-situ acquisition of topography, Real Time Kinematic GPS (RTK-GPS), which has a centimetre accuracy, is the most commonly used instrument. Bathymetry is more difficult to acquire because its quality is highly dependent on wave conditions: the more energetic the waves, the worse the bathymetry. Multi-beam (or mono-beam) echosounders are a common tool for bathymetric measurements. However, traditional topo-bathymetric surveys cannot always cover all spatio-temporal scales, as they are very expensive and dependent on the environmental conditions in which they are collected (Lippmann and Smith, 2009). As the tools that can be used for coastal monitoring are better described in the chapter 1, the focus of this chapter will be on the advantages of satellites.

Remote sensing techniques allow a regional understanding of coastal areas by providing images that can cover hundreds of kilometres, as the images are taken from space. Depending on the satellite mission - whether on-demand or open access - the frequency of acquisition can be very high (a few seconds (δT) between images for Pleiades images, regular revisits every 5 to 8 days of the same site for Sentinel-2). The cost of these techniques is much lower, if not free, than for in-situ missions, and the resolution of the satellite products can be submetric (0.5 m for panchromatic images, 2 m for multispectral images; Pleiades). The satellite tool seems to combine the advantages sought for coastal engineering issues and seems well indicated to answer the needs of the PPCS project in Saint Louis (Almar et al., 2022c).

This chapter introduces the main study site of this thesis, and describes the satellite missions used, which are Pleiades, Sentinel-2 and Landsat, along with their accuracy, and the pertinence of these tools for coastal monitoring matters. The impact of some satellite-inherent parameters, depending on the methodology used, is also presented.

2.2 The study site: Saint Louis city (Senegal, West Africa)

2.2.1 The Senegalese coastline

In Africa, 67% of beaches are sandy (Luijendijk et al., 2018), making this continent particularly vulnerable to the risks associated with sea-level rise due to global warming (Melet et al., 2020a), to marine hazards, to the increasing risks of coastal flooding (Kupfer et al., 2022; Alves et al., 2022) and to the phenomenon of coastal erosion (Melet et al., 2018). According to the IPCC report, a 0.5m rise in sea level would lead to a 10 to 100-fold increase in the frequency of marine flooding (Pachauri et al., 2014). In West Africa, the coastal zone is densely populated and concentrates about 51% of the urban population (a percentage that could increase in the coming years (Goussard, 2014)). It is also home to several megacities and major infrastructures: this area and its population must benefit from increased protection against growing risks (Alves et al., 2020; Dada et al., 2021). Ensuring the sustainability of these coastal environments is a major social issue.

Focusing on Senegal alone, the country's coastline stretches for 700 km. Its low topography and sandy sedimentary deposits make it particularly vulnerable to coastal erosion (Weissenberger et al., 2016). Its coasts can be divided into two areas: the *Petite Côte* to the south of Dakar – the capital – where protective structures (breakwaters, groins, rip-rap...) flourish, and the *Grande Côte* to the north, which is more natural and where the main study site of this thesis, the city of Saint Louis, is located.

2.2.2 Saint Louis Senegal: a site undergoing severe erosion

The city of Saint Louis has the peculiarity of being built on a very dynamic sand spit, the *Langue de Barbarie*, which separates the Senegal River from the Atlantic Ocean (Figure 2.1). Dominated by a strong oblique swell (north-west) leading to one of the strongest coastal drifts in the world towards the south, the spit is a very dynamic structure (Sadio et al., 2017; Almar et al., 2019b; Taveneau et al., 2021). Over the last century, the length of the spit has varied between 10 km and 30 km, always moving southwards - the same direction as the longshore drift (Sadio et al., 2017; Taveneau et al., 2021). Thus, the coastline around Saint Louis and the *Langue de Barbarie* are subject to sediment transport to the south, resulting in significant morphological changes and eventually an erosive pattern (Anthony, 2015; Sadio et al., 2017). The tidal regime of this site is semidiurnal and microtidal: 0.5m at neap tide and 1.6m at spring tide. In October 2003, a major flood in Saint Louis required an urgent decision to relieve the city of extreme water levels in the streets – an artificial breach was opened in the *Langue de Barbarie*. The breach, initially 4m wide, quickly widened to become the new mouth of the river. By October 2006, the mouth had widened to nearly 2 km, and the old mouth further downstream had naturally closed (Anthony, 2015; Sadio et al., 2017). In the post-breach period (after 2003), the width of the river mouth has stabilised between 0.5 km and 1 km. This stabilisation is related to a balance between the hydraulic efficiency of the river, including tidal flow, and the energy of incident waves and sediment bypass (Sadio et al., 2017; Anthony and Aagaard, 2020). At the same time (after the 2003 breach), the spit began to show trends of transverse erosion – at a rate of -4.2 m/yr (Ndour et al., 2018) – which appeared to be a direct effect of the 2003 artificial breach (Rodríguez et al., 2014; Anthony, 2015; Bergsma et al., 2020; Taveneau et al., 2021).

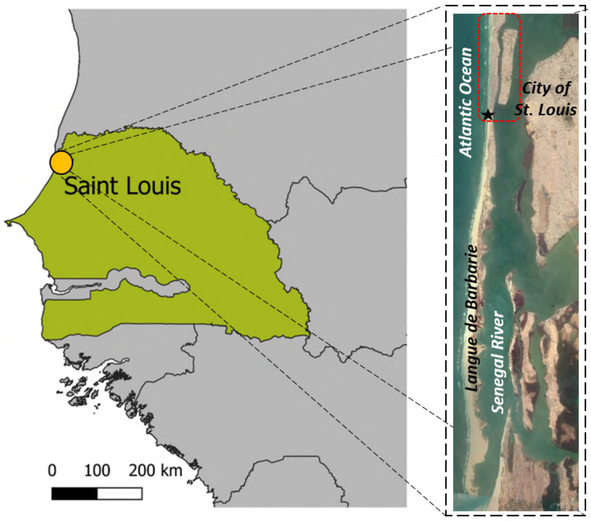

Figure 2.1: Senegal location (green) and of the study site region Saint Louis (yellow) and Pleiades satellite image of the sand spit (Langue de Barbarie) with location of the urbanized area (in red). The black star indicates the location of the camera installed in January 2021.

In this context, the ADM (Agence de Développement Municipal) has been entrusted with the management of several projects for the protection of Saint Louis. Among these, the project financed by the World Bank aims at modelling the long-term morphological evolution of the *Langue de Barbarie* and river modelling together with the socio-economic aspects and costs, and is coordinated by EGIS/Deltares. This thesis is part of an AFD (Agence Française de Développement) project aimed at finding an urgent short-term solution to combat the erosive trend and protect the local population. These two projects are complementary and the solutions will be implemented sequentially. First to address the emergency, and then to implement long-term sustainable solutions (Alves et al., 2020; Dada et al., 2021).

The AFD-funded project brings together researchers from three different institutes: UCAD (Université Cheikh Anta Diop) in Dakar and UGB (Université Gaston Berger) in Saint Louis (Senegal) and the IRD (Institut de Recherche et de Développement) in Toulouse (France). The common theme of this collaboration was the implementation of a long-term scientific monitoring of the littoral and the impact of the *Langue de Barbarie* protective riprap (Ndour et al., 2020). The urgency of the situation in several neighbourhoods due to a major retreat of the coastline made it possible to obtain financial assistance from the AFD to launch the PPCS project (Coastal Protection Project in Saint Louis), the main objectives of which were to

- Emergency protection of the *Langue de Barbarie* coastline, centred on the construction of a 2,150 metre-long sea wall to halt the retreat of the coastline (Figure 2.2).
- Communication, education and scientific monitoring.
- Project Management, Monitoring and Evaluation, which is responsible for activities

related to the management, coordination, monitoring and evaluation of the project.

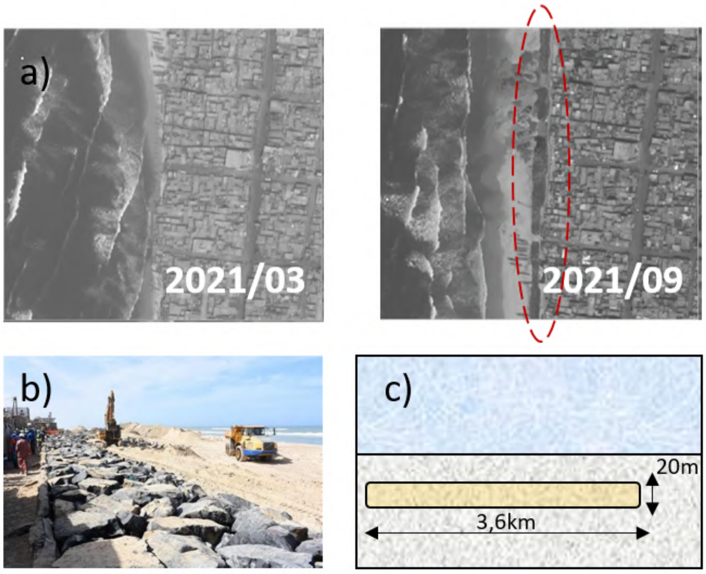

Figure 2.2: **(a)** Pleiades panchromatic images of the beach to monitor the progress of the construction of the riprap (red ellipse). **(b)** Construction of the riprap. **(c)** Riprap characteristics as defined in the (AFD, 2018) report.

Figure 2.3: **(a)** Team during the 03/2020 bathymetry acquisition in Saint Louis. **(b)** Camera that was set up in 01/2021 facing the protective riprap. **(c)** Topography acquisition in 12/2021. **(d)** Installation of the echosounder on the dugout for bathymetric acquisition. **(e)** Presentation of inter-university work (03/2022) and course on the use of the satellite tools.

The main scientific axes of the project, as defined, were the monitoring of the sediments (bathymetry, topography) by means of ground truth (in situ) data, the monitoring of the impact of the protection structure by means of a video camera, and the satellite monitoring of the Pleiades (bathy-topo) with the realisation of a morphological continuum (IRD-UCAD-UGB, 2019). This thesis intervenes on these last two axes. Indeed, satellites such as the Pleiades constellation are well suited to meet these challenges: topography can be derived from (tri-)stereogrammetric techniques (cf. chapter 3) and bathymetry from depth inversion by wave kinematics (cf. chapter 4). A continuum can then be derived from these two analyses. As for the in-situ data set, it allows the comparison of the satellite derived products with the ground truth to validate their accuracy and relevance for coastal engineering issues. Within this framework, scientific exchanges, training, academic exchanges and field data collection have been established during these three years (Figure 2.3). However, due to delays in the construction of the rip-rap, the focus on the morphological response of the beach using a video camera could not be fully addressed.

2.3 Satellite material and in-situ acquisitions

2.3.1 On-demand very high resolution Pleiades images

Launched in 2011 and 2012 respectively, the Pleiades 1A and 1B satellites orbit out of phase at an altitude of 694 km. Developed by the CNES (Centre National d'Études Spatiales) and commercialised by Airbus, these very high-resolution satellites are capable of taking images of any point on the planet in less than 24 hours for civil and military users. Their product can be obtained on demand, in particular through the DINAMIS (*Dispositif Institutionnel National d'Approvisionnement Mutualisé en Imagerie Satellitaire*) programme of the CNES, a French academic partner (`https://dinamis.data-terra.org`), which provides simplified access to spatial imagery. In addition to single or (tri)stereo images, the Pleiades constellation is capable of acquiring a burst of up to 12 images in a single pass. The acquired images are delivered as two products: panchromatic images with a resolution of 0.5 m ground pixel and multispectral images (red, green, blue, infrared bands) with a resolution of 2 m. They are accompanied by a RPC (Rational Polynomial Coefficient) file, which is used to correct systematic errors in each image due to surface relief, camera orientation, nadir, camera tilt and geometric errors.

Date	H_S [m]	T_P [s]	Dir [°]	$Tide$ [m]
2019/03/21	2.3	17	280	0.8
2019/09/17	1.3	9	275	1.65
2020/03/17	1.8	8	350	0.8
2020/09/30	1.3	11	275	1.2
2021/03/31	1.6	12	285	1.6
2021/09/29	1.4	13	200	1.1
2022/03/15	2.7	8	350	0.7
2022/09/15	1.6	11	350	1.4

Table 2.1: Wave parameters during the Pleiades acquisition (with H_S the significative wave height, T_P the wave period, Dir the wave direction and the $Tide$.

At Saint Louis, such burst and tri-stereo images (>3 to 12 images) will be collected every two years from March 2019 to March 2022, and the corresponding wave parameters on the day of acquisition are given in Table 2.1. Such a data set does not exist except for Saint Louis. The tri-stereo Pleiades images were acquired at the cross-orbit angles 25°, −17°, −17°, 19°, 19°, 19°, and −17°. The time difference between each frame is set to $\delta T \simeq 9.5$ seconds. This gives a base to height ratio of $B/H = 0.12$. In general, for flat areas, a low B/H value gives a better height accuracy of the stereoscopy (Jacobsen and Topan, 2015).

2.3.2 Regular-revisit long-term Landsat and Sentinel-2 images

Two other satellite missions with higher acquisition frequency but lower resolution were used to complete the study: Landsat 5-7-8 and Sentinel-2. Their characteristics are described below:

- The Landsat optical satellites were launched by the National Aeronautics and Space Administration (NASA) in 1984 for Landsat 5 (L5), in 1999 for Landsat 7 (L7) and in 2013 for Landsat 8 (L8). They orbit at an altitude of 705 km and have a cycle of about 16 days. They provide multi-spectral imagery with a resolution of 30 m pixels. The time coverage of the first L5 satellite was from 1984 to 2013, while the other two are still acquiring data.

- Sentinel-2A and 2B, launched in 2013 and 2015 respectively, are part of the European Copernicus programme. They orbit at an altitude of 786 km, the resolution of their images is 10 m and they can revisit the same site every 5 days. The characteristics of each mission are summarised in the table 2.2.

Satellite mission	Time coverage	Revisit period	Pixel size
L5	1984-2013	16 days	30m R, G, B, NIR, SWIR1
L7	1999-present	16 days	30m R, G, B, NIR, SWIR1, 15m panchromatic
L8	2013-present	16 days	30m R, G, B, NIR, SWIR1, 15m panchromatic
S2	2015-present	5-8 days	10m R, G, B, NIR, 20m SWIR1

Table 2.2: Summary of the different used data set of satellite imagery.

Landsat and Sentinel images are freely available and their regular visits to the same location provide a wealth of data (Bergsma and Almar, 2020; Vos et al., 2019). These satellites make it possible to monitor specific areas with good resolution on a regional scale and to follow events with rapid morphological evolution, such as storms. The *Langue de Barbarie* images have been collected from 1984 to the present day, with gaps between 1991 and 1999 (Bergsma et al., 2020). With the introduction of the Sentinel-2 constellation in 2015, the number of images collected has increased exponentially.

For the study period (from 1984 to December 2022), the number of satellite images at Saint Louis is given in the table below 2.3:

Satellite mission	Time period 1984-2022
Landsat 5	108 images
Landsat 7	356 images
Landsat 8	188 images
Sentinel 2	462 images

Table 2.3: Number of images available for each satellite missions over the period 1984-2022.

Because Landsat 5-7-8 and Sentinel-2 are optical satellites, images taken under heavy cloud cover cannot be used for coastal monitoring: a certain percentage of the 1,114 images taken for Saint Louis are therefore unusable.

2.3.3 In-situ bathymetric and topographic acquisitions

In this project, in-situ measurements are essential to (in)validate the satellite derived estimates (topography and bathymetry). Several field campaigns were carried out during the thesis in collaboration with SHOM (Service Hydrographique et Océanographique de la Marine), Deltares, IRD and the Senegalese universities UGB and UCAD. The topographic survey was carried out using RTK-GPS (Real Time Kinematics) with centimetre accuracy. Bathymetric data were more difficult to acquire and were collected using a single-beam echosounder mounted on a dugout. Here is a summary of the existing in-situ data set over the PhD period.

- **(2019)** A topographic survey of the whole spit was carried out in March (SHOM-IRD-UGB-UCAD) and a bathymetric survey in January (Deltares).
- **(2020)** A topographic survey of the whole spit (SHOM-IRD-UGB-UCAD) and a bathymetric survey (IRD) were carried out in March.
- **(2021)** A transect survey to georectify a transect to the camera field of view was carried out in December (IRD-UGB-UCAD).
- **(2022)** A topographic survey of the whole spit was carried out in March (SHOM).

2.4 Chapter conclusion

The originality of our approach is to combine satellite observations to be validated with in-situ measurements. Remote sensing techniques are indeed well suited to meet the challenges of the PPCS project and its specific needs. These techniques allow studies at high temporal frequency (S2), accurate (Pleiades; 0.5 to 2 m), at regional scale (tens of kilometres). These tools make it possible to obtain a series of indicators such as the temporal position of the coastline or the height of the land (topography), to mention just two examples. Recent studies have used tri-stereogrammetric techniques (Collin et al., 2018; Almeida et al., 2019; Turner et al., 2021) using Pleiades satellites to estimate the topography on regional areas through the computation of Digital Elevation Models. Within the framework of this thesis, the tri-stereo technique was carried out at Saint Louis (Senegal) to derive a DEM every 6 months. For the first time, the regional morphological changes have been carried out on a regional scale using Pleiades satellites in order to assess the sand volume changes - both spatially and temporally - to help decision makers to manage this coastline. The next chapter presents the morphodynamics of the *Langue de Barbarie* sand spit, from a local point of view – the urban area most affected by coastal erosion – to regional changes. The advantages and limitations of the use of satellites are discussed.

Chapter 3

Monitoring the morphological evolution of the sand spit through satellite Digital Elevation Model (DEM): local to regional beach evolution

Contents

3.1 Introduction

Coastal erosion in Saint Louis, Senegal, is threatening the housing and access to the sea of the local population, which consists mainly of fishing communities. This chapter aims to quantify beach erosion in the urban area of Saint Louis, which is located at the northern end of the 13 km long *Langue de Barbarie* sand spit (see chapter 2). The coastal evolution at Saint Louis is monitored over a 3-year period using Pleiades sub-metric satellite imagery, which allows stereogrammetry to derive Digital Elevation Models (DEMs). Comparison with ground truth data shows sub-metric differences from the satellite DEMs. The accuracy of the satellite derived topography using satellite stereogrammetry is of the same order of magnitude as the coastal change itself, highlighting its limitations. Therefore, the DEM data are combined with decades of coastline derived from Landsat and Sentinel-2 imagery. It is these long-term observations that show that the spit is stretching, narrowing in its northern part and lengthening downdrift to the south.

The first part of this chapter provides a preview of the regional scale topographic evolution - carried out with the DEMs derived from the Pleiades dataset. The analysis ranges from local cross-shore transect analysis, used to validate a stereogrammetry method, to the quantification of sand volume (ex)changes between the northern and southern parts of the spit.

The second part of this chapter describes the spit elongation process, highlighted by the shoreline evolution from 2015 to 2020, and compared to the 2003 break position that initiated the erosion/elongation trends. Finally, the advantages and limitations of the use of satellites in coastal monitoring for topographic issues are discussed.

The results of this chapter are partly based on the published article (Taveneau et al., 2021).

3.2 Methodology

3.2.1 Pleiades-derived topography using stereogrammetry

The coastal DEMs (Digital Elevation Models) are derived from the sensor-level panchromatic Pleiades images (0.5 m resolution) using a stereogrammetric method: the AMES Stereo Pipeline (ASP) software (Shean et al.). This software produces a 2 m resolution DEM of the coastal zone from the city of Saint Louis to about 20 km south. In this case we have 3 input images, effectively performing a tri-stereo analysis to reconstruct the DEMS. Tri-stereogrammetry was preferred to stereogrammetry because the use of three images instead of two significantly improves the derived topography (Collin et al., 2018; Almeida et al., 2019; Taveneau et al., 2021; James et al., 2022). Another robust open access tool - the CNES Algorithms to Reconstruct Surface (CARS) - was used to produce DEMs of the study site (Youssefi et al., 2020; Michel et al., 2020). In both ASP and CARS software, three panchromatic images are taken as input, correlated between pairs, and then a final correlation between the two correlated pairs gives the output DEM. At each correlation step, a coefficient q – which is used as an indicator of how good the correlation is between two pixel locations – is calculated. The higher q is for a pair of images, the better the probability that the evaluated pixel is at the same location for image 1 and image 2.

Both methods use the RPC files – which are part of the satellite delivered product – that provide an idealised geometry and hence the relationship between the sensor level satellite image coordinates and the ground coordinates. A co-registration algorithm is applied that removes DEM offsets, checks for altitude-dependent biases, and checks for sensor-specific and higher-order altitude-dependent biases (as the Pleiades satellites are not part of the referenced sensors in this algorithm, this last step is ignored). This algorithm (McNabb) was developed based on the method of (Nuth and Kääb, 2011) and is a robust analytical solution based on the residuals of the pairwise elevation difference and the aspect and slope of the study site to correct for biases and errors between the DEMs. Finally, all the resulting DEMs are vertically fixed using a set of ground control points (GCPs) collected during the in-situ acquisitions in March 2019. Only after this post-processing sequence, the DEMs are compared to derive a spatio-temporal evolution of the *Langue de Barbarie* (Tahoun et al., 2015).

The AMES Stereo Pipeline software has a function that ortho-rectifies a satellite image at sensor level by projecting the image onto the DEM it generates (Shean et al.). The method is as follows: a DEM is calculated from three raw satellite images (panchromatic or multi-spectral) using the tri-stereogrammetry method described above. This DEM is automatically orthorectified and then the satellite images are projected onto the DEM at the sensor so that the output images are fully orthorectified.

To validate the satellite DEMs, ground surveys carried out a few days apart from the satellite acquisitions (in March 2019, March 2020 and March 2022) will allow the satellite-derived results - both for topography and bathymetry - to be compared with the in-situ data.

3.2.2 The impact of the satellite geometry on DEM accuracy

The accuracy of DEMs derived from stereo images depends on several parameters that have to be determined before ordering a Pleiades image set, the base-to-height ratio being 1 (Hasegawa et al., 2000; Jacobsen and Topan, 2015; Letortu et al., 2020). In March 2019, a set of 10 images was acquired, allowing the influence of two input parameters on the reliability of the DEM to be investigated. The RMSE between the DEMs and the in-situ dataset has been calculated for two regions of interest: over the whole Pleiades DEM and over the urban area highlighted in Figure 2.1. As the angle along the satellite orbit varies between the seven Pleiades acquisitions, a study of the impact of the acquisition angle along the orbit was carried out to ensure that the comparison of different data sets (seven Pleiades acquisitions) – using the same methodology – is consistent (Figure 3.1). It was found that its impact can be considered negligible (about 10^{-2} cm) and thus the along angle, which varies greatly between the different Pleiades images, is not an issue.

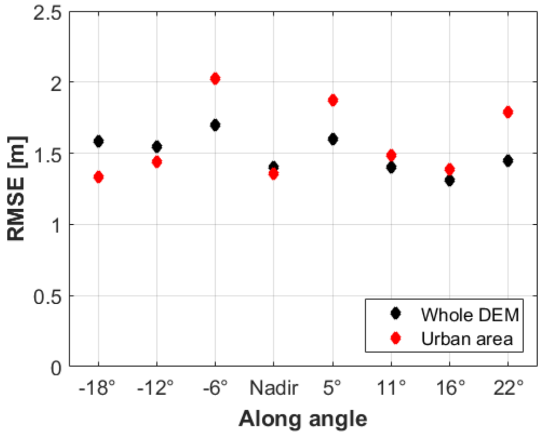

Figure 3.1: Impact of the along angle on the DEM accuracy - study made over the Pleiades sequence acquired in March 2019 and compared with in-situ survey.

For the 2019 Pleiades sequence, the RMSE standard deviation for the B/H ratio is 0.08 for the whole satellite image and 0.05 for the urban area. This highlights the fact that the B/H ratio has a strong influence on the accuracy of the DEM. However, as the Along Orbit Angle parameter does not show a trend when considering the whole DEM, it shows a greater variability within the urban area with a value of 0.27 standard deviation. The accuracy of the DEMs is better in two cases: when the stereo estimate is built from very near nadir along-orbit angles, or when the stereo estimate is built from large alongshore angles $\in [-18°, -12°, 11°, 16°]$.

When the terrain has more irregularities in the topography - such as in the urban area with the presence of buildings - the stereo method works better and the resulting DEM is more accurate if high orbital angles are used between the satellite pairs used (Letortu et al., 2020; Loghin et al., 2020). However, as the topography of the study area is very low over most of the inland part, it is concluded that neither the B/H ratio nor the along-orbit angle parameter has a major impact on the accuracy of our method. However, considering the results and the limitations of the method, the ideal conditions for a Pleiades acquisition would be at low tide and during the summer (i.e. wet season) to avoid the heavy swell conditions.

3.2.3 Shoreline extraction methodology

3.2.3.1 Sentinel-2 and Landsat

The CoastSat open-access toolkit (Vos et al., 2019) provides multi-year time series of any sandy coast in the world, using imagery from the L5, L7, L8 and S2 satellites of Google Earth Engine. As the African coasts are mainly sandy (Luijendijk et al., 2018) and with limited data availability (Almar et al., 2022c), this tool comes in very handy for Saint Louis. The sand/water interface is automatically mapped using a robust sub-pixel resolution shoreline detection technique through the calculation of the Modified Normalised Difference Water Index (MNDWI). The MNDWI is commonly used in remotely sensed imagery to distinguish land from open water features: in urbanized coastal areas, the MNDWI is more appropriate than the NDWI because it reduces the noise of built-up areas (Xu, 2006).

$$MNDWI = \frac{Green_{band} - SWIR}{Green_{band} + SWIR} \tag{3.1}$$

where $Green_{band}$ = pixel values from the satellite green band
$SWIR$ = pixel values from the short-wave infrared band

This Python toolkit - using both Landsat and Sentinel-2 imagery - provides multi-year time series of any sandy coastline in the world. Cropping these images around any study site allows easy retrieval of shorelines and peak positions of sand spits.

3.2.3.2 Pleiades

Water lines are detected from the ortho-rectified satellite imagery using the Normalised Difference Water Index (NDWI) in Chapter 3. The NDWI is a ratio between the green and near infrared bands.

$$NDWI = \frac{Green_{band} - InfraRed_{band}}{Green_{band} + InfraRed_{band}} \tag{3.2}$$

As water bodies absorb most light in the visible to infrared part of the electromagnetic spectrum, NDWI uses the green and near infrared bands, $Green_{band}$ and $InfraRed_{band}$ respectively, in equation 3.2 to identify water bodies (McFeeters, 1996). Once the water bodies have been identified, the shoreline is determined as the intersection of these water bodies. The calculated NDWI range values $\in [-1; 0]$ represent light areas without vegetation or water.

3.3 Comparison with ground truth

To validate the satellite-based topography method, an inter-comparison between in-situ data and Pleiades-derived topographies was performed. The two DEMs used - those from March 2019 and March 2020 - were individually median filtered in two dimensions (over 10 m longshore and 5 m cross-shore). The resulting beach profiles were averaged, and the vertical offset between the Pleiades data and the in-situ data was removed from the Pleiades data.

Three cross-shore transects (TA, TB and TC; Figure 3.2.a) were selected on the *Langue de Barbarie* sand spit to illustrate the performance of the satellite derived topography in comparison to the field data. These cross-shore transects are in the same location for the 2019 and 2020 datasets. For the inter-comparison, the DEMs used are those produced by ASP (Shean et al.), as the RMSE is higher than 3 m for the DEMs produced by CARS (Youssefi et al., 2020; Michel et al., 2020). This validation was only performed on these two Pleiades acquisitions, as the in-situ field measurements were performed in March of each year. There are no data available for March 2021, and the data for March 2022 are still being processed.

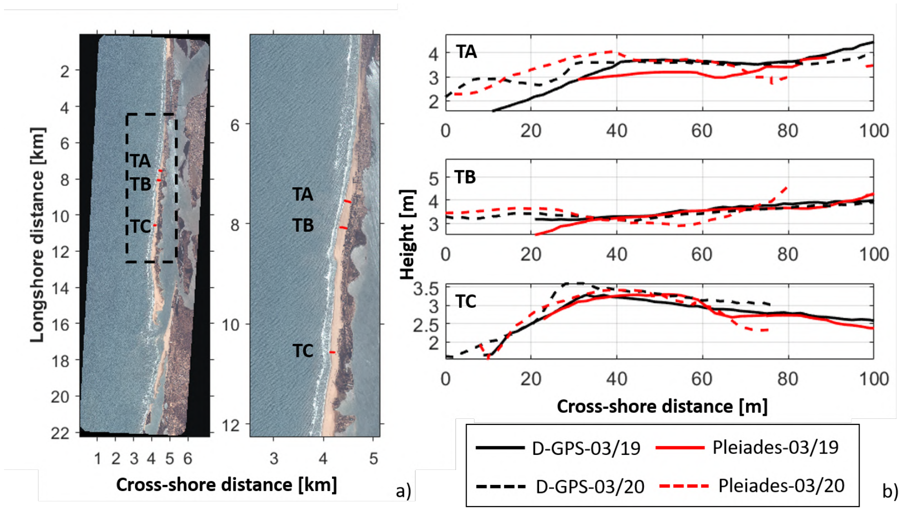

Figure 3.2: **a**) Satellite image superposed from 03/2019 with chosen transects for inter-comparison and zoom onto the chosen transects. (**b**) Inter-comparison (Pleiades - dashed lines, and D-GPS - continuous lines) over the chosen transects in March 2019 and March 2020 (Shean et al.) *(from (Taveneau et al., 2021)).*

The beach profiles are generally well captured by the Pleiades-derived topography (Figure 3.2.a), considering a root mean square error between 0.72 m $\leqslant$ RMSE $\leqslant$ 1.19 m in March 2019 and 0.97 m $\leqslant$ RMSE $\leqslant$ 1.07 m in March 2020 (Table 3.1). The total RMS errors for 2019 and 2020 are $RMSE_{2019} = 1.31$ m and $RMSE_{2020} = 1.15$ m respectively. Considering that the in-situ surveys and the Pleiades acquisitions were separated by only a few days, small morphological changes in the lower beach zone may have occurred during this period, resulting in minor differences. It is also apparent that the stereoscopic method underperforms on the lower beach in 2019, as no topography could be derived for 0 m to 30 m cross-shore (Figure 3.2.b).

Transects	RMSE [m] 03/19	RMSE [m] 03/20
T1	1.19	0.92
T2	1.01	0.97
T3	0.72	1.07

Table 3.1: Difference between satellite-based DEM and RTK-GPS survey (RMS error) for each cross-shore transect.

The annual change in topography can be observed on the beach cross-shore transects (Figure 3.2.b). Accretion is observed on the northern transect, which is closer to the urban area according to Figure 2.1, and the beach seems relatively stable for the other two (TB and TC; Figure 3.2.b). TA shows a greater discrepancy with in-situ measurements than the other two transects. This can be explained by the particularly energetic wave climate during the 2019 survey (Table 2.1), which can affect the lower beach (Dail et al., 2000).

To estimate the magnitude of uncertainty associated with the lower beach swash zone, the horizontal swash excursion was calculated using an empirical parameterisation (equation 3.4) and ocean forcing (Table 2.1) with a constant beach slope $\beta \simeq 4\%$. The beach slope was estimated from the isotopography position (Figure 3.3). The horizontal tidal excursion is estimated to be $\simeq$ 31 m in 2019 and $\simeq$ 12.9 m in 2020. The projected horizontal tidal excursion for both acquisitions is $\simeq$ 20 m. This width seems to correspond to the lack of Pleiades data in 2019, as highlighted in Figure 3.2.b.

The most dynamic part of the beach is the lower beach, which is the most challenging section for stereoscopy due to the hydrodynamics (swash) between images, the tide level at the moment of acquisition (time of acquisition not flexible) and the lack of textures. The DEMs are validated punctually at control points to estimate the uncertainty/error in the waterline estimates (horizontal displacement of an iso level) – affecting the calculated erosion rate Figure 3.3 – and volume change (vertical evolution), so the validation of these parameters applies to the latter two and no assessment can be drawn from the Pleiades DEMs. It should also be noted that the TA transect shows a greater difference between the D-GPS transects and the Pleiades estimates than TB and TC: the beach profile trend is still found by the satellite, but despite the correction applied to the DEMs data, the lower beach relief morphology (0 m $\simeq$ cross-shore $\simeq$ 40 m ; Figure 3.2.b) does not match between the in-situ data and the satellite-derived topography. It is particularly noticeable in the 2019 data that there is no estimate of the topography for cross-shore values $\in [0, 30]$ m (Figure 3.2.b). This is related to the fact that the wave conditions during the Pleiades acquisition in March 2019 were particularly energetic ($H_S = 2.3$ m, and $T = 17$ s ; Table 2.1), inducing a significant run-up on the beach. As the tri-stereo method is not the most suitable for the topography of the lower beach, the study of the bathymetry of the nearshore and intertidal zone would provide more accurate results.

3.4 Local beach dynamics within the urban area

Figure 3.3.a, shoreline changes were calculated from the difference between the 2019 and 2020 waterline positions. Two cross-shore transects with the largest rates of shoreline change were selected (100 m $\leq$ *distance* $\leq$ 400 m corresponding to T3, and 1400 m $\leq$ *distance* $\leq$ 1500 m corresponding to T1, Figure 3.3.a).

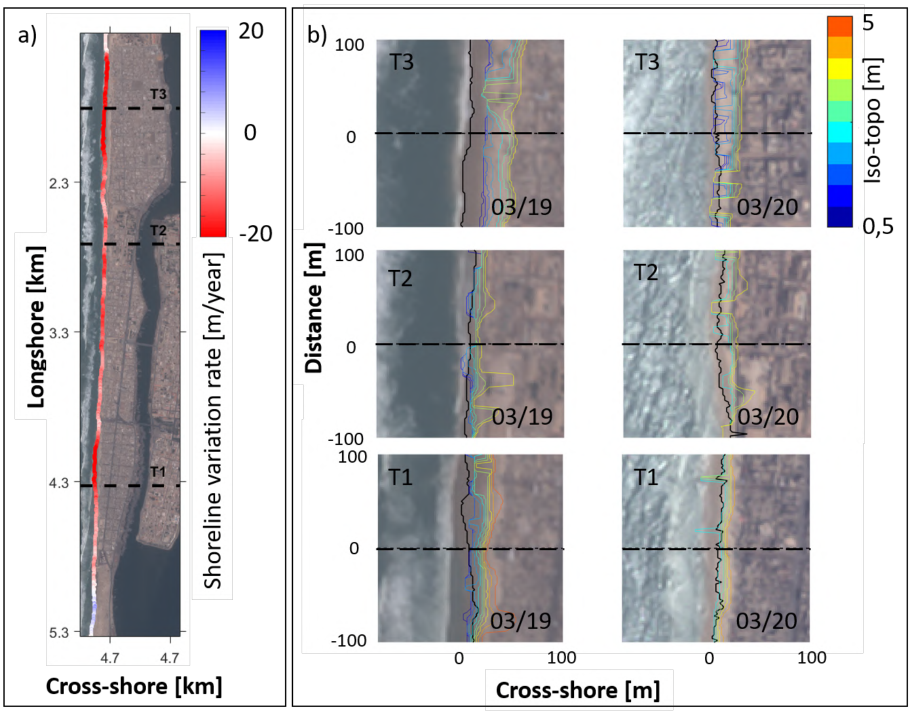

Figure 3.3: (**a**) Erosion rate within a year derived from Pleiades images in the urban area - calculated from the difference between the waterlines position of 2019 and 2020. (**b**) Iso-topography derived from Pleiades onto the chosen transects which height ranging from 0.5 m to 5 m (colour lines), and associated waterline position (black lines) *(from (Taveneau et al., 2021))*.

The isotopo position (Figure 3.3.b) allows the average slope of the beach to be estimated at $\simeq$ 4%, and shows a narrowing of the beach that is also visible in the zoomed satellite images (Figure 3.3.b). This narrowing is particularly noticeable for transects T1 and T3, where the rates of shoreline change are highest: $\simeq$-20 m/year for both (Figure 3.3.a). The beach at T2 appears to be stable and its rate of shoreline change is lower ($\simeq$-5 m). However, the wave conditions were different between the two Pleiades acquisitions: as the tide was the same (0.8 m - low tide conditions; Table 2.1), the swell was more energetic in 2019, resulting in a more pronounced beach run-up.

A previous study explained the observed erosion trends in the urban area from 2004 to 2020 (north side of Saint Louis - corresponding to transect T1 ; Figure 3.3.b) as a response to the 2003 *Langue de Barbarie* breach. Not only was an erosion trend identified, but the erosion rate has accelerated over the last two decades (from 2000 to 2020) in the vicinity of the fish market (Bergsma et al., 2020). The erosion trend is still visible in the urban area in the Pleiades satellite images (Figure 3.3).

However, as the first results from 2019 to 2020 emphasised an erosion trend on the urban area's coastal strip, the latest results show that the beach - in this defined urban area - is finally accreting. In fact, in early 2021, a camera was installed on a lighthouse at the southern boundary of the urban area (its position is indicated in Figure 2.1) and the two snapshots taken about 5 months apart in 2021 leave no doubt that the beach has widened (Figure 3.4).

Figure 3.4: Images acquired with the camera (see Figure 2.1 for location) on the indicated time. A small picture (bottom panel, on the left) shows the ongoing construction of the riprap *(from (Taveneau et al., 2022))*.

Zoom 1 (Figure 3.5), which shows the difference between the topography of 03/2022 and that of 03/2019, confirms the accretion trend observed in the camera footage in 2021 (blue band). However, this accretion trend was already reversed before, as mentioned above: both the local population feedback and the satellite results (Figure 3.5.a) emphasised the severe erosion of the beach in the fishermen's neighbourhood.

In December 2021, work began on the construction of a sea wall in this area. This structure, financed by the AFD (Agence Française de Développement) and managed by the ADM (Agence de Développement Municipal), will be 20 metres wide and 3.6 kilometres long. Its location – shown in yellow on the figure 1 – has been chosen to protect the most vulnerable populations from erosion.

3.5 Evolution of the *Langue de Barbarie* sand spit

The *Langue de Barbarie* sand spit has a length that has fluctuated enormously (between 10 and 30 km) over the last decades (Sadio et al., 2017) (Figure 3.6). Over the data availability of Pleiades, the length of the sand spit has been increasing, extending southwards (zoom 2 ; Figure 3.5) in the same direction as the LST with an average migration rate of about 710 m/year (between 2019 and 2022). The inland spit remained stable and the southern part of the spit gained a large volume within one year (Figure 3.5.a).

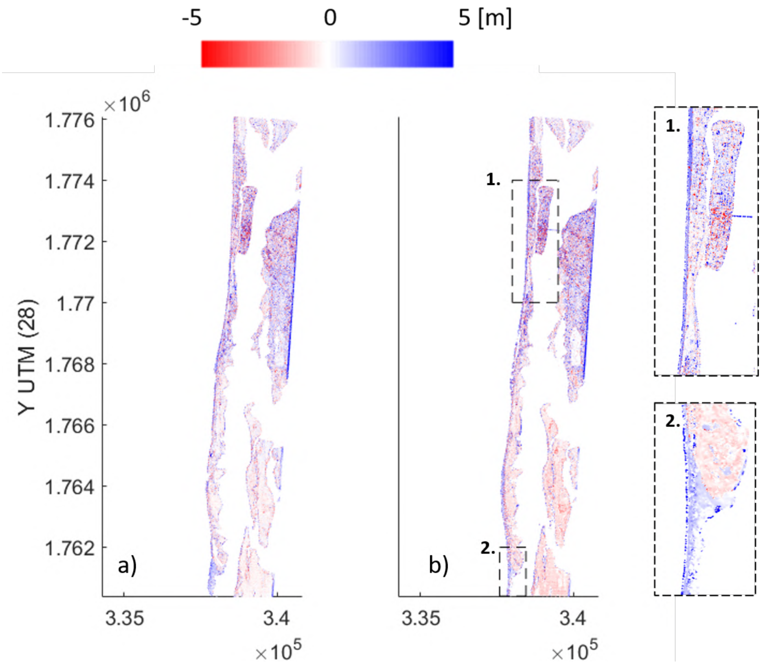

Figure 3.5: **(a)** Difference between the 2019 and 2020 (March) DEMs. **(b)** Difference between the 2019 and 2022 (March) DEMs. **(1. and 2.)** Zooms respectively on the urban area and the sand spit tip: difference of the topography evaluated with Pleiades satellite on the whole data set (2022-2019).

The longshore sediment transport rates provided by SOGREAH (1994) (SOGREAH, 1994) give a north-south drift volume of between 600 and 700 × $10^3 m^3/year$, and appear to be the direct cause of the southward extension and narrowing of the spit in the northern part (Figure 3.5.a,b). This accretion at the southern tip of the spit is particularly noticeable in this DEM difference (Figure 3.5), represented by the blue colours, even in a few years. A large part of the inland spit remained stable with a vertical change of less than 1 m. It can be seen that the major morphological changes occurred at the southern tip of the *Langue de Barbarie* and at several points along the Atlantic side of the spit, including the urban area at zoom 1.

The coastlines shown in Figure 3.6.a are derived from Sentinel-2 satellite imagery using the CoastSat tool (Vos et al., 2019) and highlight the southward accretion trend of the *Langue de Barbarie* over the last 5 years. Since 2015, the position of the tip of the spit has shifted increasingly southwards, with migration rates ranging from 160 m/year to 870 m/year (Table 3.2).

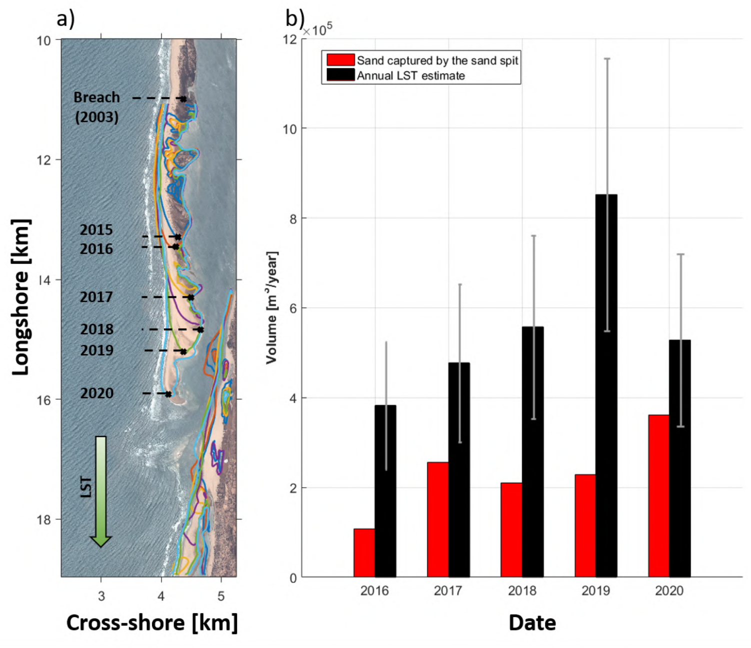

Figure 3.6: (**a**) Sand spit tip position and shorelines derived from S2-satellite over time using CoastSat Open-Access tool (Vos et al., 2019). (**b**) Volume of sand annually captured by the sand spit (red) compared to the annual LST estimates obtained from ERA5 data (black) with its standard deviation (gray) *(from (Taveneau et al., 2021))*.

The longshore sediment transport rates are related to the volume of sand captured by the spit (Figure 3.6.b). This captured volume was calculated as $V_S = H_{average}A_S$, where $H_{average}$ is the average topography height and A_S is the area gained by the spit each year.A_S was estimated by the shorelines by taking the difference between the area at year N and the area at year N-1. To properly understand the magnitudes obtained on the sand volumes of the tip of the *Langue de Barbarie*, the annual LST was calculated from the ERA5 data by annually averaging the results of Kaczmarek (Kaczmarek et al., 2005), Kamphuis (Kamphuis, 1991) and Bayram's formula (Bayram et al., 2007).

Over the region of interest – that is, the spit area shown in Figure 3.6.a – the mean topography elevation is estimated to be H_{mean} = 1.07 m thanks to the March 2019 to 2022 Pleiades DEMs. The migration rates of the sand spit vary greatly over the last 5 years (Table 3.2), as does the volume of sand dragged from north to south by the LST and captured by the sand spit, which shows great variability (Figure 3.6.b).

From 2015 to 2020, the average alongshore migration of the sand spit is about $230 \times 10^3 m^3/year$. This represents 35% of the north-south drift volume (Sadio et al., 2017; Almar et al., 2019b), meaning that the spit extension has the potential to capture a large amount of the alongshore sand drift.

In order to fully understand the stretching mechanism of the *Langue de Barbarie*, the spit growth rates derived from the S2 images and those derived from the LST are presented in

Figure 3.6.b. The rates derived from the LST values have been calculated as follows, from the assumption of the sand conservation equation based on the work of (Duc Anh et al., 2020):

$$R_S = \frac{Q}{B_S(D_B + D_C)} \tag{3.3}$$

Wherein Q is the LST, B_S the constant spit width, D_B the berm height, and D_C the depth of closure.

The presented equation has been developed for wave-dominated sand-spits whose morphology is mainly determined by the LST variation. In the literature, the morphodynamics of *Langue de Barbarie* meet these criteria (Anthony, 2015; Sadio et al., 2017; Ndour et al., 2018). The results between the satellite observations and the LST estimates are presented in Table 3.2.

Date	Migration rate S2 [m/year]	Migration rate estimates (Equation 3.3) [m/year]
2015/2016	160	210
2016/2017	870	250
2017/2018	550	280
2018/2019	460	350
2019/2020	740	270

Table 3.2: Migration rates over the years derived from satellite measurements and Equation 3.3

The calculated migration rates based on a sand conservation equation 3.3, and thus the LST (Table 3.2), show here a large difference with the satellite-derived observations. Such a difference in these estimates raised a question: what if the southward extension of the *Langue de Barbarie* is not only determined by climatic control on the wave regime, but has an intrinsic dynamic?

3.6 Satellite-based coastal monitoring for coastal engineering: potential strengths and limitations

This work demonstrates the potential of using very high resolution satellites for coastal monitoring, and in particular for monitoring sediment dynamics (reviewed in (Salameh et al., 2019)) and quantifying spatial and temporal volumetric beach evolution (Eamer and Walker, 2013; Turner et al., 2021). Satellites cover larger regions than traditional survey methods, provide a comprehensive understanding of beach morphodynamics, allow access to remote data sources, and open the possibility for future improvements in precision. In developing countries, satellites can provide a large database over a long period of time. The erosion rate and shoreline position derived from the Pleiades and Sentinel-2 time series allow the identification of the most vulnerable hotspots along this coastal stretch, and emphasise the role of large-scale dynamics in studying small-scale beach dynamics. This is highlighted by the erosion trend in the urban area (northern *Langue de Barbarie*) and the extension of the spit towards the south, while the northern part is narrowing. This erosion is probably a combined result of the trapping of part of the sand load transported by the LST in the post-2003 breach - which is now the new estuary - and an enhanced tidal prism through this new estuary (Niang and Kane, 2014; Anthony, 2015).

The potential of very high resolution satellites, such as Pleiades, for coastal monitoring has been highlighted in our study, and the study of changes to the Saint Louis coastline will continue. From December 2020, a protective structure will be built to protect the urban area in the northern part of the spit (Ndour et al., 2016) and the most vulnerable inhabitants. After assessing the beach variability prior to construction in order to design the structure, satellite monitoring will continue to monitor the effectiveness of this protection and its impact downstream.

DEMs derived from tri-stereogrammetric methods to obtain topography estimation show promising results and represent a new way to estimate morphological changes of a coastal area. However, they have limitations that need to be taken into account (Amante, 2018), such as the difficulties encountered by Pleiades in analysing water surfaces and areas without texture (Loghin et al., 2020). The global RMSE between in-situ measurements and Pleiades estimates is 1.15 m $\leq RMSE \leq$ 1.31 m and these results are not as good as those found in (Almeida et al., 2019). The difference between the two studies can be explained by the flatness of the *Langue de Barbarie* topography ($\simeq$ 2.56 m above sea level). The flatness of a site has an indirect effect on DEM accuracy (Yamazaki et al., 2017) - Low reflectance and texture of the raw optical satellite image result from specific ground characteristics and alter the calculation of the disparity that is converted to ground elevation. The signal - metric changes induced by a storm or on a seasonal scale - is of about the same order as the noise: this study shows the potential of the method, but highlights the need for greater accuracy and further development. However, as the slopes in our beach/dune system are weak ($\simeq$ 4%), the tri-stereo method does not produce large errors and does not depend on visual monitoring as is the case for cliff 3D reconstitution (Letortu et al., 2020). Our study site has a limited number of GCPs. Increasing the number of GCPs would improve the correction of the DEMs and reduce the overall RMSE.

The uncertainty of the method at the lower beach related to high frequency unresolved hydrodynamics is estimated using the swash excursion length, calculated as follows:

$$swash = \frac{1.1}{2}(1.56T^2 H_S(0.5625\beta^2 + 0.004))^{\frac{1}{2}} \quad (3.4)$$

Wherein T is the wave period, H_S the significant wave height, and β the beach slope. The beach slope was derived from Pleiades imagery. This equation is the up-to-date reference formulation relevant for a wide range of conditions (Stockdon et al., 2006; Melet et al., 2018).

A large uncertainty arises from the satellite derived DEM. Other open access tools can generate a surface model using a stereo method, such as MicMac (Rupnik et al., 2017). In previous studies, the mean vertical error of the surface models was as follows 0.35 m $\leq$ ASP $\leq$ 0.48 m (Almeida et al., 2019), and 0.17 m $\leq$ MicMac $\leq$ 0.34 m (Rupnik et al., 2018). In our work we used ASP and CARS to perform a tri-stereo, but the RMSE between the in-situ data and the CARS produced DEMs were not satisfactory enough to use them in our beach morphology study. These values compete with the centimetre errors obtained with the LiDAR method for assessing coastal processes (Sallenger et al., 2003; Chen et al., 2018; Rotnicka et al., 2020), whose vertical accuracy ranged from 0.05 m to 0.15 m (Nelson et al., 2009).

3.7 Chapter conclusion

In this chapter, 2m Digital Elevation Models (DEMs) derived from sub-metric Pleiades optical satellites have been used to monitor both local and regional coastal changes around Saint Louis (Senegal, West Africa) along the *Langue de Barbarie* sand spit over a year. The tri-stereo method used here to compute the DEMs gives a metric root mean square difference compared to RTK GPS surveys. By bringing together local erosion in the urban area with the larger scale extension of the *Langue de Barbarie* spit, this work offers a new vision of regional morphodynamics and how scales are intertwined. Even if a stand-alone use for coastal studies is not yet conceivable at this stage, given the accuracy limitations encountered, satellite-based topography monitoring appears to be a breakthrough in the decades-old technological barriers of linking coastal spatio-temporal scales, which is crucial for understanding coastal behaviour and for coastal engineering.

However, this study has highlighted the usefulness of the satellite tool for understanding regional phenomena such as the spit elongation process, which is described in more detail in chapter 5. To complete this topographic study and to understand the mechanisms responsible for beach evolution at Saint Louis, the work in the next chapter focuses on regional bathymetry to establish a land-sea continuum and to understand the control of submerged sandbars on the beach.

Chapter 4

Satellite-derived land/sea morphology continuum: toward a better quantification of sediment exchanges to understand beach evolution

Contents

4.1 Introduction

To complement the work presented in the previous chapter on aerial topography, this chapter introduces the extension with nearshore bathymetry. This knowledge of land-sea continuum exchange is essential for coastal engineering issues and more generally for understanding aerial beach evolution (Anthony and Aagaard, 2020). To estimate the bathymetry over a large spatial scale, very high resolution Pleiades imagery will be used in combination with regular revisit Sentinel-2 imagery to track the shoreline and sandbar position to provide answers to the natural beach variability and the impact of the protective nourishment currently being implemented.

4.1.1 Introduction to the coupled nearshore sand bar-shoreline system

Nearshore sandbars are morphological features that commonly characterise sandy and wave-dominated shores (Van Enckevort and Ruessink, 2003; Van Enckevort et al., 2004; Castelle et al., 2007). Located in the surf zone, they are the result of a combination of sediment transport induced in the cross-shore and longshore directions (Ribas et al., 2017). Their shape – which depends on environmental conditions and sediment characteristics – varies widely from linear to three-dimensional features and was first classified by (Wright and Short, 1984). This classification was established on the basis of observations of a large panel of individual sandbars in micro-tidal coastal areas and allows a beach to be defined as reflective, dissipative or intermediate. It is even possible to observe numerous bar morphologies on the same intermediate beach (Lippmann and Holman, 1989, 1990). In natural environments, sediment fluxes never reach equilibrium because the morphological response of the sandbar(s) is generally longer than the time scales associated with changes in wave regime: this leads to a landward or seaward shift of the existing sandy structures. This morphological evolution of a littoral system associated with sandbar dynamics is the main source of profile variability on short (sub-seasonal scale), medium (seasonal scale) and long (inter-annual scale) time scales.

The sandbar system plays a key role in the sustainability of the coastal environment, as it reduces the energy of the incoming wave: as the waves approach the shore, they break against these structures and some of their energy is dissipated, so that when they reach the shore they are less energetic and therefore less erosive. Their longshore dynamics have been shown to be highly correlated with the upper beach ruessink07, castelle10, bouvier19, and wave conditions are the main driver responsible for their short-term cross-shore dynamics. During very energetic episodes (e.g. storms), the sand bars migrate rapidly seawards with migration rates of up to 10 m/day due to the feedback between the bottom and the seaward sediment fluxes induced by the undertow (Ruessink et al., 2009; Almar et al., 2010). Conversely, sand bars migrate slowly shoreward under low to medium energy wave conditions with velocities of about 1 m/day (Van Enckevort and Ruessink, 2003) due to the feedback between the bottom and the seaward sediment fluxes induced by the orbital velocity non-linearities (Dubarbier et al., 2015). The position of a sandbar - given the seasonal variability of the swell climate - is further from the shore under energetic wave conditions than under moderate conditions.

Some sandy beaches also have a double bar system which shows a cyclic behaviour on inter-annual scales: net offshore migration of the whole bar system (see in (Ruessink et al., 2009; Aleman et al., 2017; Shand, 2003; Bouvier et al., 2019)). When the outer bar reaches a *limit depth*, it begins a degeneration phase that leads to the inner bar becoming the new outer bar. At the same time, a new (inner) bar is formed near the coastline. Recent studies have used satellite imagery to follow the morphodynamics of sandbars on a regional scale. SPOT satellite (*Satellite Pour l'Observation de la Terre*) images, coupled with in-situ wave measurements, have been used to follow the migration of sand bars between 1986 and 2000 (Lafon et al., 2004).

This chapter describes two different types of work. Firstly, the regional bathymetry study carried out with the Pleiades satellites highlights the difficulties encountered in obtaining a product that can be used for coastal engineering purposes. On the other hand, the dynamics of the sandbars obtained with the Sentinel-2 satellites – which have a higher temporal frequency of acquisition than the Pleiades constellation – allow conclusions to be drawn about the effectiveness of the protection structure being built in Saint Louis.

4.1.2 Strategies and techniques of bathymetry collection

In a large number of coastal areas, bathymetric information is unavailable or, in most cases, decades old. However, bathymetric information is extremely useful for constraining coastal sea state models (Melet et al., 2020a). Observations from space are an important complement to existing terrestrial and airborne observing systems, with the advantage of systematic monitoring (Benveniste et al., 2019; Salameh et al., 2019): satellites provide unparalleled spatial coverage of every coastline in the world with high spatial resolution (Melet et al., 2020b; Bergsma et al., 2020). Data are collected regularly, with unrestricted access to any coastline in the world (no natural or administrative access restrictions), allowing monitoring over time, unlike highly demanding field observations which are necessarily limited in space and time.

Types of survey approaches Traditionally, near-shore bathymetry data are collected using a boat-mounted echosounder, which provides spatially dense but temporally sparse data. Acoustic altimetry is another way of obtaining bathymetry information, and provides data that are temporally dense but spatially poor because these instruments have a fixed implementation (Moulton et al., 2014; Brodie et al., 2018). However, the cost of surveys is significant and the acquisition and processing times are several weeks for an echosounder survey of a few tens of square kilometres. To overcome this problem, new techniques have recently been developed to access bathymetric data at a higher temporal frequency with a large spatial coverage at a lower cost. Video is one of the solutions and is used worldwide to monitor sandy beaches in underwater areas: Africa (Abessolo et al., 2022), Europe (Bouvier et al., 2020; Valentini et al., 2017; Bergsma et al., 2019d), Australia (Splinter et al., 2018) and the pioneering Duck site in the USA (Holman and Bergsma, 2021) to name but a few. For many years, cameras were the only means of obtaining depth estimates in coastal areas where the wave climate was too dangerous to collect in situ data (Lippmann and Smith, 2009). However, as cameras are fixed features, bathymetry estimates can only be made at a very local scale. UAVs or drones are also emerging as interesting tools to derive coastal bathymetry at such a local scale, more agile but with more sparse temporal acquisition than fixed video systems (Bergsma et al., 2019a; Tsukada et al., 2020; Angnuureng et al., 2020b). More recently, satellite imagery has been used to estimate bathymetry on a regional scale (Traganos et al., 2018; Sagawa et al., 2019; Almar et al., 2019a; Ashphaq et al., 2021; Salameh et al., 2019).

The Angnuureng et al. (2022) study reviews different remote sensing techniques compared to ground truth to monitor the beach evolution of an engineered stretch of coast, and presents the advantages and disadvantages of each platform. Morphological changes in a beach profile cover a wide range of spatio-temporal scales, ranging from a few hours (storm) to several weeks (climatic swell variations), see Figure 1.1. It is essential to fully understand these processes that drive the morphodynamics of a beach in order to better adapt and design a sustainable solution for these environments. In coastal management, decision making is based on an understanding of sediment volume changes in a beach system (submerged and emergent) over time and space (Davidson et al., 2007; Turner et al., 2021). In addition, accurate estimates of bathymetry are essential for modelling work.

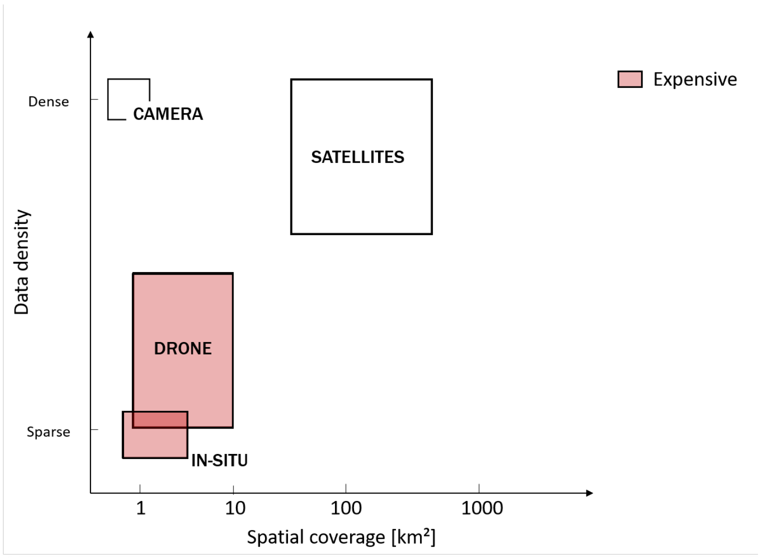

Figure 4.1: List of the used device to obtain bathymetry information with their respective spatial coverage and frequency density. The red squares indicate the high cost of the method.

From optical signals (i.e. drone, video camera or satellite), several methods allow the derivation of water depth (Figure 4.1). Colour-based methods, developed from the pioneering work of (Lyzenga et al., 2006; Caballero and Stumpf, 2019), are limited to non-turbid waters and could therefore not be the preferred solution for deriving bathymetry at the Saint Louis site. Wave kinematics methods work well in conditions where colour-based methods would fail, i.e. in turbid or optically deep waters, which is the case for most open coasts around the world (Bergsma and Almar, 2020). Wave characteristics change at different depths, making depth accessible to remote sensing methods that aim to track wave evolution (Holman et al., 2013). As a wave travels landward, its wavelength and speed decrease until it breaks – its period remains quasi-constant. Using the linear dispersion equation (equation 1.1) introduced earlier and the wave parameters, it is possible to evaluate a local depth H. This method is commonly called "bathymetric inversion". In terms of the control of the water column on the wave kinematics, three zones can be distinguished: from deep water with almost no influence, to incremental control in the intermediate water, to shallow water. The boundary between these zones is a wave dependent rule of thumb.

– Deep water: $H > L/2$

– Intermediate water: $L/2 > H > L/20$

– Shallow water: $H < L/20$

In coastal management, only the intermediate and shallow waters are of interest. Intermediate water is where the bottom begins to affect wave propagation: the waves slow down as they approach the shore due to bottom friction, and the wave direction changes to parallel to the shore. The only parameter that does not change is the wave period. Thus, as the waves slow down as they enter shallower water, both the wavelength and the speed decrease.

Several approaches are generally used to estimate bathymetry from optical measurements of waves, including spatial and temporal processing of the information through spectral or correlation approaches. They all have in common to capture the wave kinematics: wavelength or period with celerity (Stockdon and Holman, 2000) to inverse the bathymetry from the wave dispersion.

The spectral method estimates velocity by computing the Fourier transform (or discrete Fourier transform, or wavelet (Santos et al., 2022)) of a spatio-temporal wave signal – at a given frequency – and the best correlation with predefined wavelengths. *cBathy* is a well-known algorithm that uses the spectral method for depth estimation (Holman et al., 2013; Holman and Bergsma, 2021). Originally developed for shore-based video systems, it became the basis for the development of satellite spectral methods (Bergsma et al., 2019b), which are now widely used within the S2Shores programme (IRD/SHOM/CNES agreement) – (Almar et al., 2021b; Daly et al., 2022). While spectral methods are efficient with dense and large computational windows (multiple wavelengths or periods), they have intrinsic resolution limitations, particularly in shallow coastal waters where improving coastal resolution down to one wavelength (i.e. from about 50 to 300 m) is of paramount importance.

Correlation methods are used to overcome this limitation. The temporal method (Almar et al., 2009; Birrien et al., 2013) is based on calculating the phase shift between adjacent time series. A temporal phase shift Δt below the wave period is chosen and a light signal is associated with each cross-shore position (Almar et al., 2021a). This light signal is correlated with its neighbours to find the best correlation between two signals for the Δt phase shift. This maximum correlation corresponds to the distance that the observed wave travels in δt. This process is then repeated for each position to obtain a maximum averaged correlation and thus a dominant velocity for each point. This method reaches its limits when the data set used is noisy: in (Almar et al., 2009), the maximum errors are found around the breaking point of the sandbars for the *Truc Vert* beach in Aquitaine (France). The temporal method also requires long time series, which are not always available from satellites. In (Almar et al., 2022a), a sensitivity analysis shows that the use of a spatial approach becomes advantageous over a temporal approach when the duration is less than one wave period. A spatial correlation is based on spatial cross-correlation between frames and is compared to spectral approaches. It has the advantage of not requiring more than one wavelength to calculate the wave velocity.

More details on correlation approaches are given below.

4.2 Regional bathymetry from very high resolution Pleiades images

4.2.1 The wave-based S2Shores temporal and spatial correlation methods

In order to obtain a regional-scale bathymetry estimate for the study area – Saint Louis – the Pleiades images, taken every 6 months, which cover a large area both onshore and offshore, are well suited. The multispectral imagery – which has a resolution of 2m ground/pixel – is used to resolve the wave pattern parameters. From each multispectral image, only the blue band was retained for analysis. The choice of the blue band was made because using only one satellite band significantly reduces the processing time of the algorithm, and the blue band is sufficient to detect the wave pattern as the sea largely absorbs the blue colour. As a trio of images are acquired for each dataset, three images are used as inputs in the wave pattern detection method. These images are taken at a known δt of 9.5 s apart. Two methods can then be used to determine the wave parameters: the spatial or the temporal.

The temporal method gives an estimate of the wave velocity and period, and the spatial method gives access to the wave velocity and wavelength. To solve the linear dispersion equation (Equation 1.1) to access the local depth, only two of the three wave parameters needed (wavelength, velocity and period) are required, as there is a relationship between them ($c = L/T$). Once two of the wave parameters are known, the local depth can be estimated. The spatial method has been the focus of this work and will be described in more detail.

4.2.2 The cut-out of the raw images into sub-images

To speed up the execution of the spatial method script, the raw satellite images (2m resolution) are sliced into sub-images for which the minimum length has been examined. The smaller the sub-image size, the faster the algorithm. A cross-shore transect was chosen and a sensitivity study was carried out to select the most appropriate sub-image length (Figure 4.2). This sensitivity test was conducted based on the 03/2019 dataset, where the wave climate was very energetic (Table 2.1). As seen in Figure 4.2, the wavelength and celerity over the cross-shore transect have similar values for the sub-image length from 300 m to 800 m. When deriving the bathymetry from these parameters, one can see the inconsistency of the 100 m sub-image length parameters - the curve trend is completely flat. For the 03/2019 acquisition date, which has particularly long wavelengths, the sub-image length reaches a resolution limit when smaller than 300 m. As the execution time grows exponentially with the sub-image length (Figure 4.2 ; left panel) – it is necessary to find a compromise between the quality of the estimate and the execution time of the method. According to this sensitivity study, the sub-image length was set to 300 m.

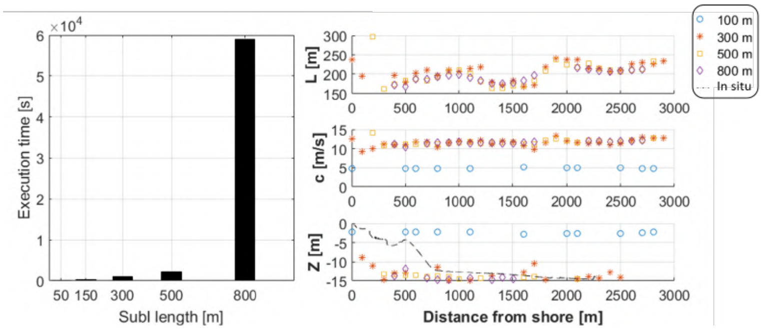

Figure 4.2: **(Left)** Execution time for one cross-shore transect depending on the sub-image length.**(Right)** Sensitivity study on the sub-image length to assess the quality of wave parameters estimates over a cross-shore transect, and depth comparison.

4.2.3 Detection of the wave pattern

An offshore sub-image is used as an example to describe the spatial method used and how the wave parameters are estimated. At the same location, the analysis is performed on the three sub-images taken at $\delta t = 0$ s, $\delta t = 9.5$ s and $\delta t = 19$ s by the Pleiades tri-stereo.

A wave pattern can be observed directly from space using satellite images due to sunlight reflected from the sea surface (sun glitter). Wave parameters can be derived from satellite sun glitter images, which contain information such as the wave height, its period, and finally its direction (Kudryavtsev et al., 2017; Yurovskaya et al., 2019). To project a 2D domain into polar space, the RT (Radon Transform) is applied to each sub-image of the same location (but at different δt)). The Radon transform allows the identification of oblique linear signals – such as waves – and can be identified by intensity peaks (see right panel ; Figure 4.3). The RT highlights linear features in an image by integrating the image intensity along lines defined by angle θ and offset ρ (equation 4.1) (Radon, 1917; Bergsma et al., 2019c). Compared to a 2D Fast Fourier Transform (FFT), the RT provides better angular resolution (Bergsma et al., 2019b) and is therefore preferred. The output of the RT sub-image is called a sinogram, and the wavelength can be directly derived from it as it is spatially the distance between two maxima (e.g. two minima) of the detected signal (see L right panel; Figure 4.3). To get rid of the noise and get a better wavelength estimate, the signal where L can be measured is autocorrelated.

$$R_I(\theta, \rho) = \oiint_D I(x, y)\delta(\rho - x\cos\theta - y\sin\theta)\, dx\, dy \tag{4.1}$$

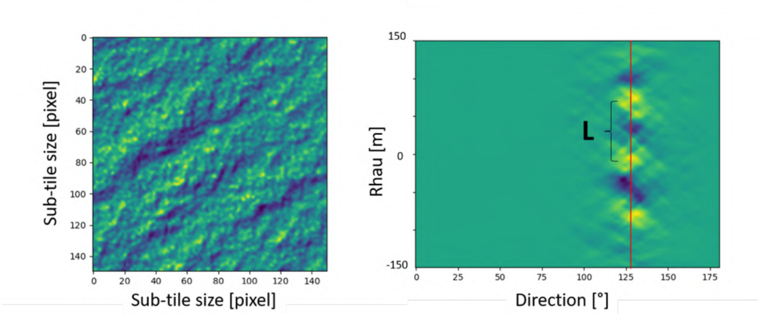

Figure 4.3: Raw offshore subtile from 03/2020 Pleiades imagery (2 m resolution pixel) **(left)** and its associated sinogram calculated with Radon Transform **(right)**. The signal picked to estimate the waves parameters along the forced direction is in red, and the wavelength **L** corresponds to the distance between two intensity peaks.

However, if the raw satellite image is very noisy, is it possible for multiple signals to appear on the sinogram? The two strongest signals detected on the sinogram correspond to the wind waves and the swell, respectively (Holman et al., 2013; Almar et al., 2021a). In this case, the signal with the greater numerical weight is considered to be the swell. In fact, the camber line of the swell is more important than that of the wind waves: it is then expected that the sunlight reflected on the swell will be more intense and therefore the strongest signal in amplitude. In this work, the chosen signal (corresponding to the swell) is always the one where the mean variance over ρ is maximum (vertical red line; right panel figure 4.3). These signals are then extracted for the three consecutive sub-images and used to find the celerity. To estimate the wave celerity, the extracted signals are correlated for each time-sequential image pair as shown in Figure 4.4 to estimate the celerity. The median of the celerities found is then calculated and taken as the dominant celerity of the wave field.

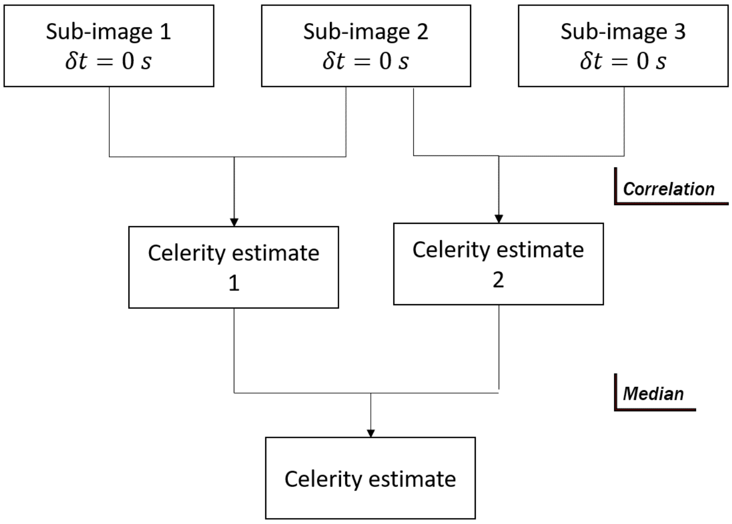

Figure 4.4: Blueprint of how the celerity is estimated on one sub-image for the spatial method.

Here the case of correlation between the first image extracted signal $\delta t1 = 0$ s and the second at $\delta t2 = 9.5$ s is taken as an example (Figure 4.5). The two previously selected signals are correlated between them, giving the signal in the lower panel. During $dt = \delta t2 - \delta t1$ the wave has travelled a certain distance d. This distance d is obtained by measuring the distance between the centre of the signal and the first peak (left or right) with the largest amplitude. Three cases can be distinguished:

- Wave period $T < dt$.

  The same wave can be observed in successive satellite images. The correlation of the signals finds a maximum peak in the green area (Figure 4.5).

- Wave period $T > dt$.

  The wave has no time to propagate between two successive frames. Looking at partial images at the same location, the correlation is maximum for the wave (at $\delta t = 0$ s) that is correlated with the propagating wave (at $\delta t = 9.5$ s). This corresponds to the blue region (Figure 4.5).

- Wave period $T = dt$

  No propagation can be seen because the satellite period δt is identical to the wave period. The velocity is not calculable and therefore no depth inversion can be performed.

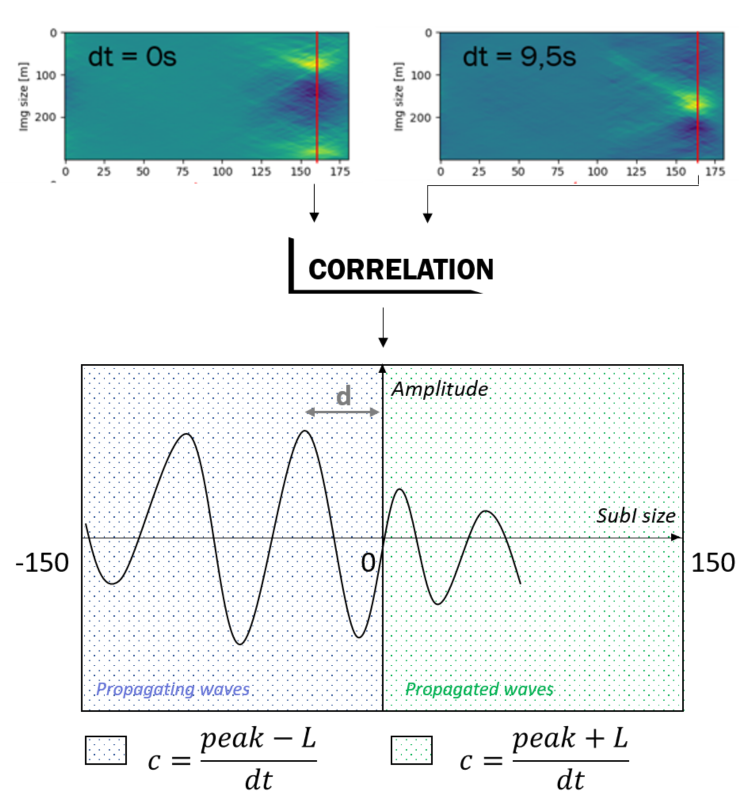

Figure 4.5: Blueprint resuming how to find the celerity parameter on one sub-image. The wave signal (red) is found on two temporally successive images and correlated to each other. The correlated signal allows calculating the distance d travelled by the wave in dt and thus estimate the local celerity with the given formula.

However, the very nearshore area is still a challenge to resolve with this method: wave harmonics are generated in a very shallow area (Sénéchal et al., 2002), making the detection of a wave pattern almost impossible: distortions are introduced by optical reflection of the waves (Almar et al., 2009). (this will be further developed when studying the very nearshore zone). In these very shallow waters, the linear dispersion used for inverse bathymetry also becomes inappropriate with increasing amplitude dispersion effects (Tissier et al., 2011; Bergsma and Almar, 2018b).

4.2.4 Results on satellite-derived bathymetry and land-sea continuum

Here, while the Pleiades satellites revisit a location on Earth every day, the Saint Louis location is acquired every 6 months (see chapter 3) (set on the French inter-institute programme DINAMIS). Using the spatial method described above, it is possible to obtain a regional estimate of the bathymetry for each acquisition date. We can see that each year the results show some differences between the September acquisitions (corresponding to the rainy season) and those of March (dry season): the wave climate varies enormously between the dry season, when the waves come mainly from the NW, and the wet season, when their direction changes (Figure 4.6).

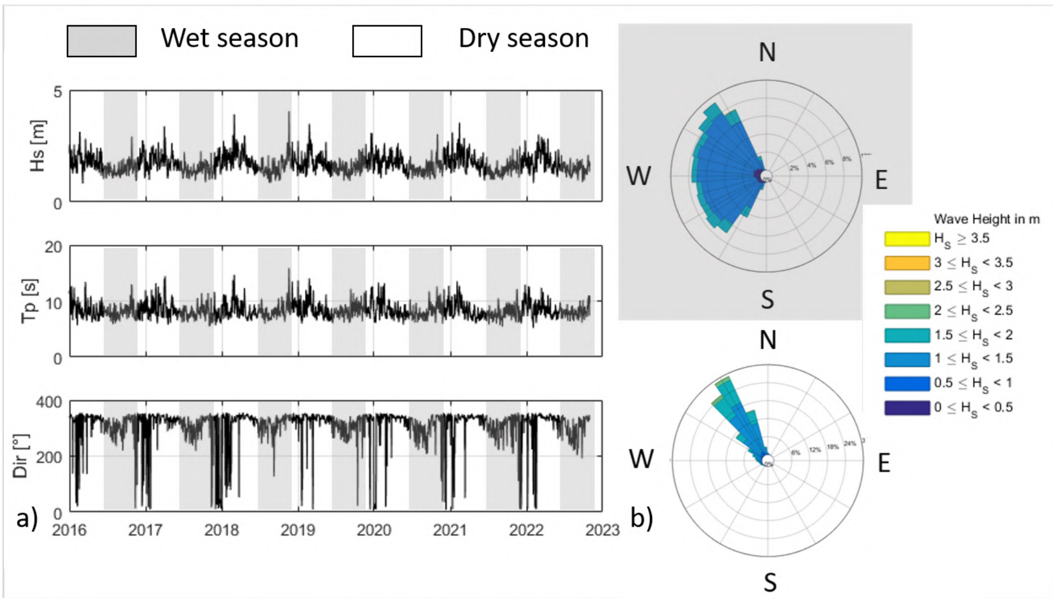

Figure 4.6: **(a)** Wave parameters time series over the time period of interest and their **(b)** associated wave spectra (Pereira). The data come from the reanalysis model ERA5 (Hersbach et al., 2018).

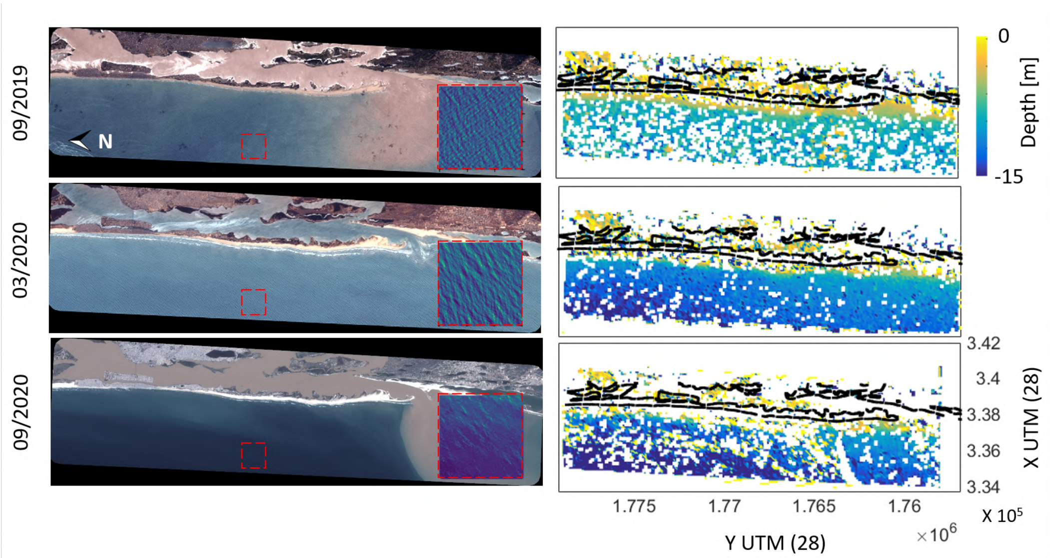

Figure 4.7: From 03/2019 to 09/2020, raw satellite imagery on the left with the associated bathymetry estimate on the right (the shoreline is represented as a black line). The red squares are zooms on the same offshore location to show the wave pattern.

Therefore, it can be expected that the satellite bathymetry estimates between the dry season acquisitions and the wet season acquisitions will be affected by this changing wave climate, as the estimate relies only on wave propagation observations (as described above). Figure 4.7, focusing on the raw satellite images, shows that there is an intense turbidity in the September acquisitions (the 03/2019 acquisition is not part of this study, as it falls in the case where $T = dt$). The submarine Saint Louis is located on a continental shelf and its depth does not exceed -15 m for the first few kilometres. The bathymetric trends (Figure 4.7) show consistent values that decrease as one approaches the coast (black line). However, it is noticeable that the September estimates seem to be less accurate than those of March: in 09/2019 the offshore values are too high, in 09/2020 the river plume strongly influences the bathymetry estimate.

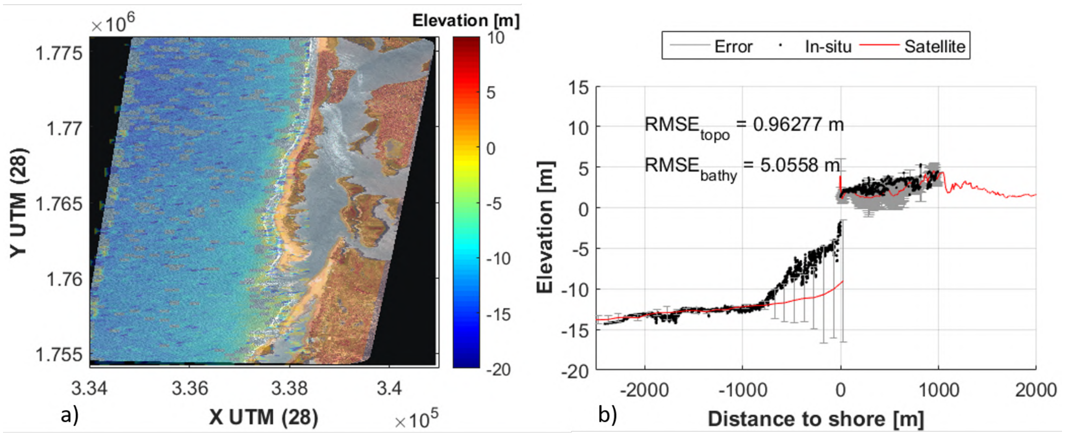

Figure 4.8: **(a)** Spatial land/sea continuum derived from Pleiades 03/2020 acquisition, the vertical height (in metre) is represented with the colour shades. **(b)** Comparison of in situ (black) and satellite-derived data (red) on a longshore median transect. The alongshore error between in-situ measurements and satellite estimate is represented as error bars (gray) (from (Taveneau et al., 2022)).

To ensure the consistency of the bathymetry estimates, both the bathymetry and topography estimates from the 03/2020 acquisition are merged and compared with the in-situ data (those from 01/2019 for the bathymetry and those from 03/2020 for the topography). This satellite-derived land/sea continuum at a regional scale is presented in Figure 4.8.a. On the one hand, the topography is correctly estimated (cf. chapter 3). On the other hand, the bathymetry is correctly estimated offshore, but the nearshore depth is largely overestimated by the satellite (as already observed in (Daly et al., 2022)) due to optical problems with breaking waves. However, unlike shelf issues (Cesbron et al., 2021), the area of interest for coastal engineering is precisely the area that the satellite fails to estimate: there is a clear need to improve the nearshore estimate to meet the needs of the PPCS project.

To improve the method on this very complex nearshore area, the next test case focuses on a 1 km by 1 km nearshore zone to see if the spatial method is robust enough to resolve the bathymetry in a nearshore area (see also (Gawehn et al., 2022)). The sub-image size is reduced from 300 m (used to perform the bathymetry on the whole image) to 100 m. This sub-image limit is chosen in the knowledge that at least half a wavelength would be found in a sub-image (i.e. that which is allowed by the correlation-based method compared to the spectral approaches). The position of the sandbar can be inferred from this new estimate, but three major problems with this resolution of the nearshore bathymetry are identified and indicated by numbers on Figure 4.9. Seaward unresolved "patches" are listed with the number **(1.)**. Biases inherent in the use of optical imagery can cause what we call a *non-resolved "patch"*: the wave pattern is detected optically thanks to sky or sunlight reflected from the sea surface (Holman et al., 2017; Almar et al., 2021a; Kudryavtsev et al., 2017). Depending on the angle at which the satellite is acquired, this reflection is not optimal for each wave and can introduce bias. However, this limitation is not the only problem encountered. In the area between the sandbar and the shore, shown as number (**(2.)** Figure 4.9), there is a harmonic generation due to the reflection of the swell on the shore. In this case, the set of images provided by Pleiades with a $\delta T \simeq 9.5$ s is not sufficient to estimate any parameters in this very dynamic area. The last point, number **(3.)**, is the overestimation of the bathymetry, which is expected to be deeper on and after the sandbar. Looking back at the normalised image, it can be seen that the wind waves are particularly visible in the overestimated depth areas. Wave parameter detection using the spatial method shows that wind waves optically have more weight than swell (k^2 law with energy (Cox and Munk, 1954; Stilwell Jr, 1969)). Without pre-processing, the algorithm mainly detects wave parameters that are shorter and steeper than swell waves. This affects the performance of the bathymetric inversion method, which was found to be optimal for longer waves.

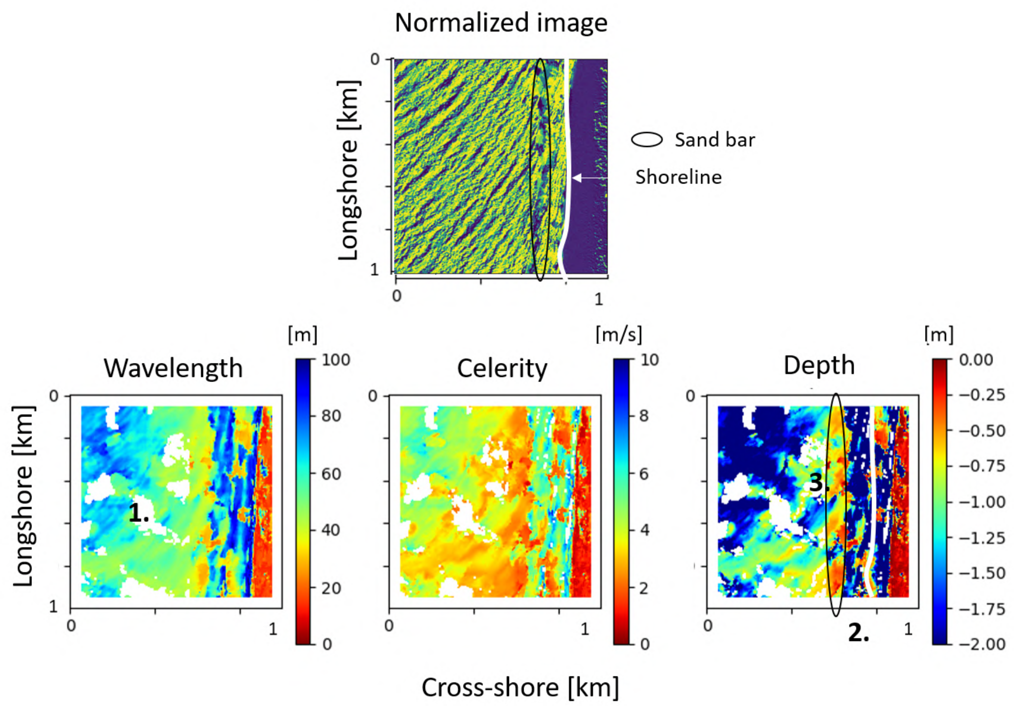

Figure 4.9: Wave parameters (wavelength, celerity) enabling the depth inversion derived from the normalized image (Top panel). The sand bar location has been circled in black, the shoreline retraced in white. The **1., 2., 3.** numbers indicate the limitations discussed in the text.

In summary, the use of the Pleiades satellites allows the location of sandbars to be determined every 6 months and a reasonable estimate of regional bathymetry to be obtained. However, both results are not useful for the PPCS project: sandbars are very dynamic features (Van Enckevort and Ruessink, 2003; Van Enckevort et al., 2004; Castelle et al., 2007) and having their location every two years is not enough to determine their dynamics. Also, the bathymetry of the offshore shelf varies only slightly below the closure depth (Bergsma et al., 2020; Anthony and Aagaard, 2020). The dynamics of the sandbar(s) are needed in this work to fully understand the morphodynamics of the Saint Louis beach, so another higher frequency approach was developed.

4.3 Nearshore sand bars detection

4.3.1 Sand bars and shoreline location

In the literature, no previous work has identified the existence of nearshore sand bar(s) on the Saint Louis coast. This study focuses on the morphodynamics of the sandbars (tracked by Sentinel-2 satellites) and the possible link of their dynamics with those of the coastline and the sand spit.

As described in chapter 2, the Sentinel-2 mission regularly revisits the same location, providing a wealth of data. The location of the sandbar(s) can be inferred from satellite imagery thanks to the foam generated by the wave breaking on it. This method was first used by (Lippmann and Holman, 1989): the location of natural sandbars can be remotely inferred from the dissipation of wind waves and swell over the crest of the bar. Indeed, if the wave climate is energetic enough, the waves will break on the inner bar and the foam generated will be visible in the images (Figure 4.10 ; top panel). If the wave climate is stronger, the waves will also break on the outer bar. Detecting the maximum intensity signature of waves breaking on sandbars is a method widely used in coastal video monitoring (Van Enckevort and Ruessink, 2003; Bouvier et al., 2019; Almar et al., 2010), among others.

Similarly, the coastline is detected by the transitions of pixel intensity in several spectral bands and is a common technique in video monitoring of the coast (Almar et al., 2012; Valentini et al., 2017; Plant et al., 2007).

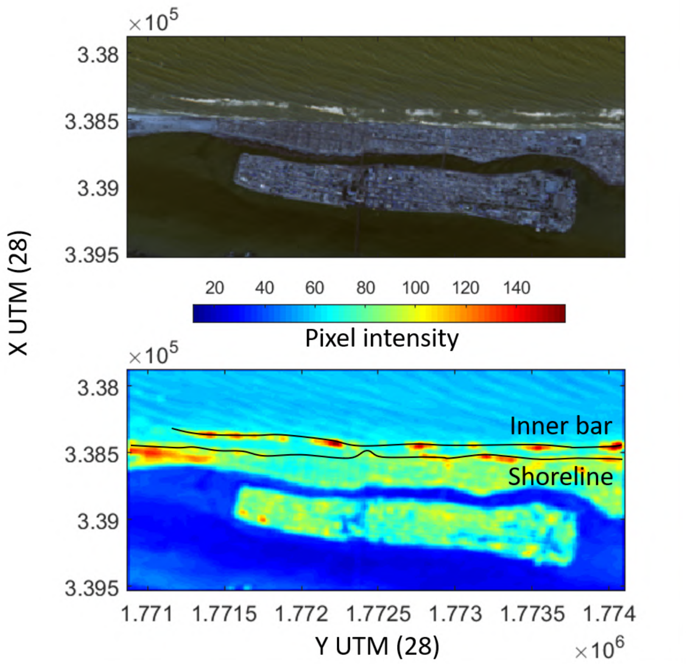

Figure 4.10: **(Top)** Raw Sentinel-2 satellite image 03-04-2018. **(Bottom)** Pixel intensity map and location of the inner sand bar and shoreline.

While it is generally applied to time-averaged imagery, here satellites provide an instant of wave breaking and cannot smooth out individual waves. This results in an inherent uncertainty of the order of a wavelength and swash excursion for the sandbar location and coastline respectively (Vos et al., 2019). The wave data were obtained from the ERA 5 global reanalysis database, which uses a coupled wind-wave-atmosphere model that has been widely used and validated (Hersbach et al., 2020). The data are produced by the European Centre for Medium-Range Weather Forecasts (`https://www.ecmwf.int`).

No additional corrections have been applied to the satellite images as they are orthorectified by the data provider.

4.3.2 Seasonal sand bar dynamics at Saint Louis

Because of its low latitude, Senegal has a seasonal system with two distinct periods: the dry season (from November to May) and the rainy season (from June to October) (Sadio et al., 2017). It is also influenced by distant swells in the North Atlantic, with the summer calm and the winter energetic storms (Almar et al., 2019b). This contrasting two-phase seasonal cycle has a significant impact on the wave and sea climate (i.e. water colour, sediment in suspension) and hence on the coastal morphology. The time series of the wave parameters (Figure 4.6.a) show that the Senegalese coasts are subject to a very energetic wave climate (on average for the period 2016-2022 the significant wave height $H_S = 1.68m$ and the period $T_P = 8.32s$). Considering the wave spectra, the differences between the two seasons are very pronounced: during the dry season, the waves are more energetic and come mainly from the NNW direction, whereas during the wet season the wave direction is more diverse.

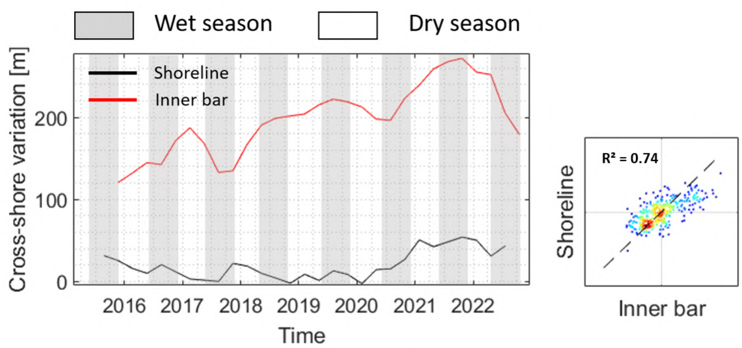

Figure 4.11: Every 3-months longshore averaged time series of the shoreline (black) and sand bar (red). The correlation between the inner bar and shoreline position is presented on the right panel. The grayed areas indicate the wet season periods, the white ones the dry season periods.

This seasonal wave cycle has a profound effect on the dynamics of the shoreline, but also on the nearshore sand bar system. It should be noted that, despite its importance, the description of the nearshore sand bar system in Saint Louis is lacking in the literature. This study aims to characterise this system and the relationship between the sandbars and shoreline dynamics. With its medium sediment size (0.21 mm) and its energetic wave forcing (Garlan et al., 2020), the Saint Louis coastline exhibits a double bar system (Figure 4.13.d.f.2.3.), which can be detected on satellite images by the foam generated during wave breaking. It is composed of a very dynamic inner bar - the one closest to the shore - and an outer bar whose dynamics are slower as it is deeper. The time series of both the coastline (black) and the inner bar (red) show interdependent dynamics (Figure 4.11): the correlation between them is high (anticorrelated, with explained variance $R^2 = 0.74$). The dry and wet seasons have a strong influence on the dynamics of the shoreline and the inner bar. For the coastline, the beach erodes during the dry season and expands during the wet season (Figure 4.11; black line). The inner bar shows a more complex situation: during the dry season the bar is strongly three-dimensional, while it is more linear when the wave climate is less energetic (Figure 4.13). Its migration amplitude is much larger than that of the coastline (Figure 4.11; red line): the inner bar is very dynamic and rapidly cycling. The uncertainties – inherent to the satellite resolution and the swash excursion – are estimated to be ±50 m for the sandbars and ±15 m for the shoreline position.

4.3.3 Shoreward accretion wave event

As we expected a gradual erosion of the shore based on previous trends (Ndour et al., 2018; Bergsma et al., 2020; Taveneau et al., 2021), a massive and rapid beach accretion of about +50 m between 2020 and 2021 challenged our scientific reasoning. To investigate this sudden accretion phenomenon further, and as the wave climate during this period did not show any anomaly (Figure 4.6), three satellite images were chosen Figure 4.13: one before the accretion (1), one during the accretion (2) and one after (3). The inner bar during the wet season - which represents less energetic conditions - has progressively migrated landward and is completely welded to the shore, contributing to its massive widening. Seaward migrating sand bars are the most commonly observed in the literature. However, four different modes of landward migration of a sand bar have been identified for swell-dominated beaches: sand bar welding (SW ; mode I) occurring during low-energy conditions after a moderately energetic winter, a large sand bar becoming a terrace bar (STT ; mode II) during a subsequent very low-energy period, a terrace bar becoming a sand bar (TST ; mode III) during moderately energetic conditions, and finally sand bar splitting (SS ; mode IV) (Vidal-Ruiz and de Alegría-Arzaburu, 2020). This last mode occurs during low energy conditions: the outer bar flattens and follows a net offshore migration (NOM) cycle, while the remaining inner part migrates landward. Mode IV corresponds to what has been observed at Saint Louis using satellite imagery: during the wet season in 2019, the sandbar splits. The inner bar then migrated progressively landward to finally weld to the shore in 2020 during the wet season (less energetic wave conditions), resulting in this sudden and massive beach accretion.

The inner bar migrated landward throughout the year 2020, and we now want to understand whether this accretion is local and only related to the welding of the inner bar to the coast, or whether it is a phenomenon with a larger spatial extent. To this end, the position of the coast, averaged over a distance of three kilometres on the longitudinal axis, is studied at two different locations in non-urbanised areas: 2 km north of the city, called *upstream*, and 2 km south of the city, called *downstream*. From the observed evolution of the per-area trends (Figure 4.12), it is clear that the +50 m accretion anomaly is only found around the city of Saint Louis. While the *city* area clearly shows an accretive pattern in 2020, the other two seem to be dominated by an erosive trend over the period 2016-2022.

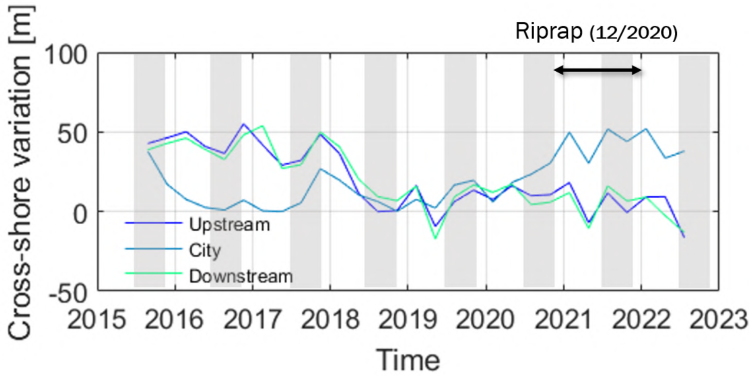

Figure 4.12: Longshore 3 km-averaged shoreline over the entire acquisition period of Sentinel-2 on the upstream of Saint Louis **(Top)**, the urban area **(Centre)**, and downdrift area **(Bottom)**. The grayed areas indicate the wet season periods, the white ones the dry season periods.

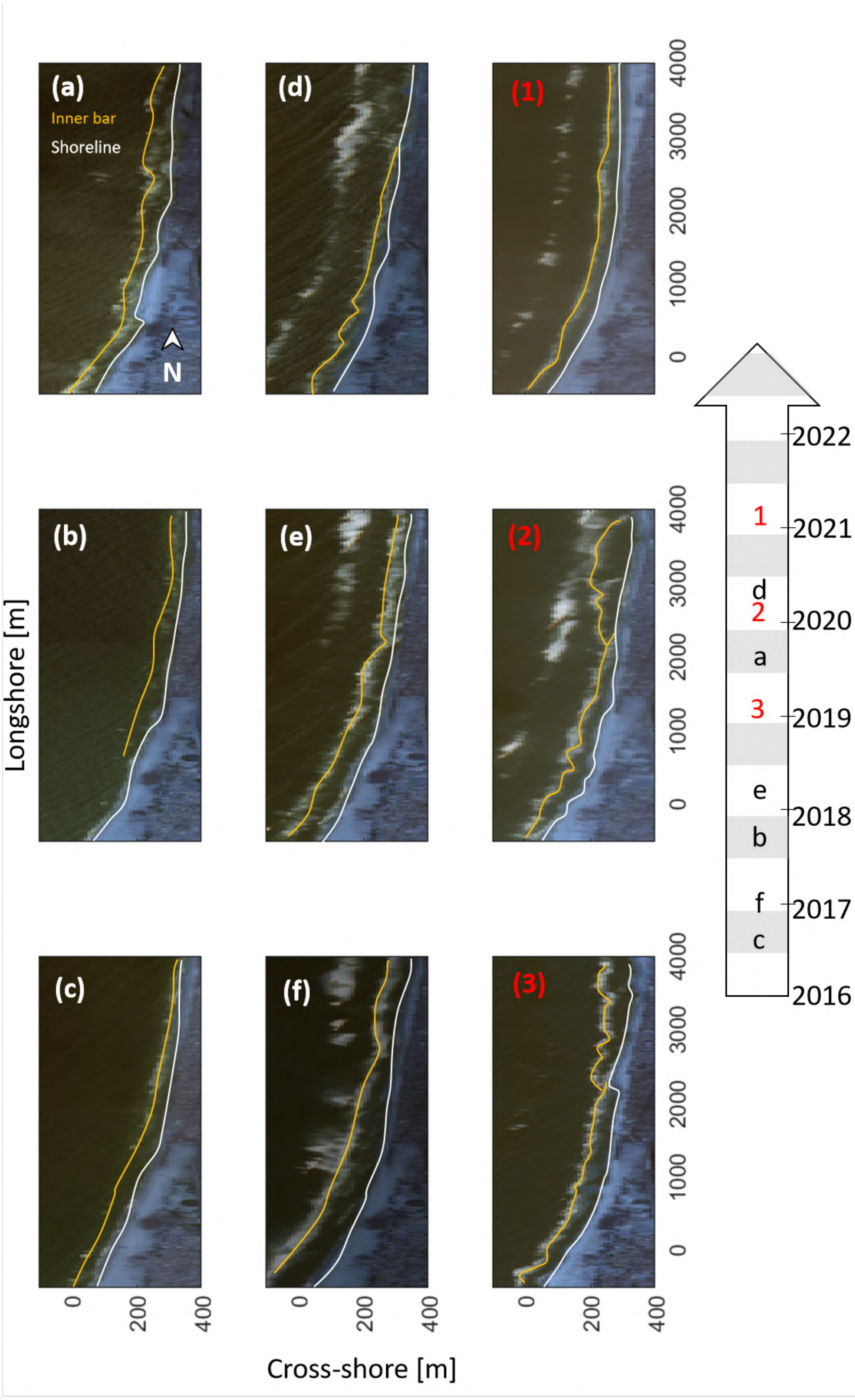

Figure 4.13: S2 images of the study area located around Saint Louis city, images chosen during the wet (gray) and dry (white) seasons. For better visibility the shoreline is shown as a white line and the inner sand bar as a yellow one. The 1, 2, 3 images show the shoreline / sand bar system before (1), during (2) and after (3) the beach accretion trend.

4.3.4 Discussion on sand bar dynamics

Regarding the driving mechanisms responsible for this sudden accretion on the beach, several causes have been considered: a change in the wave climate (ruled out by our results because no rapid evolution is observed in 2021), an evolution related to the sand spit (but this is much less frequent, with a period of 35 years), a positive effect of the rip-rap (but it was completed after 2020), and sand waves from the Saharan desert coast. Indeed, these regional features, generated by shoreline instabilities (Ashton et al., 2001) or other anomaly-causing mechanisms, propagate under wave-induced drift. However, examination of the shoreline anomaly a few kilometres north and south of the city shows no such feature that would precede the accretion observed at Saint Louis. Finally, an oil terminal with a 1km breakwater was built 10km off the coast in 2021, which could also affect the coastline. Is it responsible for attenuating the wave energy so that the wave conditions are sufficient to control the bar and its splitting?

The construction of the sea wall, which began at the end of 2020, was the strategy chosen to protect the population from the dangers of the sea as quickly and urgently as possible. The rate of erosion recorded in Saint Louis, triggered by the rupture of the coastal spit in 2003, was rapid (around -4.2 m/year (Ndour et al., 2018)) and endangered the population living on the *Langue de Barbarie* sand spit, with the collapse of buildings and the implementation of a resettlement plan. Faced with such a catastrophic situation, rockfill became the obvious choice: a protective measure had to be put in place as a matter of urgency. However, the observed accumulation anomaly occurred during the construction of the protective structure. As the aim of the study was to understand the reason(s) for such a widening of the beach, it is clear that the protection structure is in no way responsible. The natural dynamics of the sand bar system explains this sudden accretion and once again highlights the need to understand the morphodynamics of a beach. In fact, the inner bar split during low-energy conditions (probably around the 2019 rainy season, according to satellite imagery). According to the landward migration mechanisms of the bar described in (Vidal-Ruiz and de Alegría-Arzaburu, 2020), the remaining inner bar had slowly migrated towards the coastline and finally, during the wet season of 2020, gradually and completely welded to the beach, resulting in the accretion of about 50 m. In (Almar et al., 2010), the welding of a bar horn to the beach resulted in an accretion of approximately 100,000 m3 for a cross-shore accretion feature of over 100 m along the same length of shoreline. Several other bar bursts were detected in the time series along the *Langue de Barbarie* coastline, far from the riprap influence zone, proving that beach nourishment by the sand bar is the phenomenon responsible for beach accretion.

This study highlights the benefits of using satellite tools to monitor sandbars and coastal morphology. The splitting of sandbars is difficult to detect at the local scale (a few tens of metres), or almost impossible to detect if the splitting phenomenon does not occur in the field of view of the camera, as is the case with Shoreward Propagative Accretive Waves (Price et al., 2013; Almar et al., 2010; Price et al., 2017; Wijnberg and Holman, 2007), or with in situ surveys, which are less frequent and miss some of the high-frequency coastal events and variability (Bergsma et al., 2022). This makes a clear case for including satellite monitoring in coastal monitoring strategies (Benveniste et al., 2019; Melet et al., 2020a) as a complement to high-frequency video monitoring and in-situ measurements. This is the only way forward if we are to understand the relationship between 1) the foreshore and the air beach (Anthony and Aagaard, 2020) and 2) between local and regional scales, both of which are crucial for science-based decision making and effective management strategies (Alves et al., 2020). With ground-based observations generally lacking in Africa, these open-access satellite data are a game changer (Almar et al., 2022a; Vitousek et al., 2022).

4.4 Chapter conclusion

The study of the bathymetry of a coastline to understand the exchange of sand volume between the subaqueous zone and the aerial beach was necessary to fully understand the dynamics of the sandbars and the associated response of the coastline. Due to the inherent limitations of the Pleiades-derived offshore bathymetry (acquisition of pseudo video with large dt $=\sim$ T), the repeatability of the Sentinel-2 mission was preferred to observe the nearshore area. It has provided a better understanding of the dynamics of submerged sand bars and the correlation between these sand bars and the shoreline dynamics, highlighting the strong control of the sand bar on the large shoreward accretion wave observed in late 2021 on the urban beach of Saint Louis.

Sand volume exchange is not limited to the sand bar/shoreline dynamics alone. It has been shown in chapter 3, thanks to the Pleiades images, that a large volume of sand is continuously captured at the tip of the spit. One might wonder whether or not this elongation has an effect on the surrounding coastline. The following chapter will present the mechanism of the *Langue de Barbarie* sand spit, and the results will be extended to other sites around the world.

Chapter 5

On the cyclic nature of wave-dominated sand spits

Contents

5.1 Introduction

As mentioned in chapter 3, the hypothesis that the southward elongation of the *Langue de Barbarie* is not only determined by climatic control of the wave regime but as an intrinsic dynamic has been raised and highlighted with the every 6 months Pleiades data set. This mechanism strongly influences the upwelling of the spit, leading to erosion trends, while part of the sediment accumulates at the tip of the spit (Davis Jr and Hayes, 1984; Aubrey and Gaines, 1982). It is essential to better anticipate beach erosion and the closure of river mouths, which would have a major impact on the population as the risk of flooding will increase in the coming years (Cisse et al., 2022). In this chapter, a climate-forceless conceptual model of *Langue de Barbarie* elongation is proposed and tested. This result is then extended to three other wave-dominated spits around the world: in Chile, Benin and Mozambique.

The first part of this chapter is based on the results of (Taveneau et al., 2021), the second part on a recently submitted paper.

5.2 Methods

5.2.1 Sand spit data extraction

Here, shorelines are used as a proxy to assess the morphodynamics of our selected deltas and estuaries, in particular to track the evolution of their spits and barriers. To do this we use the open source Python toolkit *CoastSat* (Vos et al., 2019). Within the *CoastSat* set of routines, publicly available optical satellite imagery can be downloaded, starting with Landsat 5 data acquired by NASA in 1984. Earlier versions of Landsat are not used due to inconsistencies in pixel resolution and coverage. Landsat 6 never reached orbit, but from 1999 the Landsat dataset includes Landsat 7 (1999), Landsat 8 (2013) and soon Landsat 9 (2021). The ground sampling distance, the pixel size, is constant over this period at a maximum of 30 m for the colour bands and 15 m resolution for the panchromatic band. Note that the multispectral bands are pansharpened to 15 m within the *CoastSat* tool (although this has no resolution improvement on pixel ratios such as the NDWI). The revisit interval at the same location is typically every 16 days. In addition to Landsat data, Sentinel 2 data is also available. The European Copernicus programme initially launched two satellites with optical sensors, S2A (2015) and S2B (2017) - S2C and D are planned for the coming years. Sentinel 2A and B provide optical imagery at 10 m resolution with a revisit interval depending on the latitude, but at worst every 5 days at the equator, enabling high-frequency coastal studies (Bergsma and Almar, 2020).

For Landsat and Sentinel satellite optical imagery, the *CoastSat* tool provides a trained machine learning model to classify sea, land, white water and beach on a pixel-by-pixel basis. The pixel classification is used to optimise the use of the Modified Normalised Difference Water Index (MNDWI), excluding pixels related to white water and land, and focusing on the interface between water and sand pixels. An optimal shoreline position is then found using an Otsu procedure by minimising the variance between the MNDW indices. Shoreline vectors are the output, which we then use in this paper as a proxy to evaluate the morphodynamics of our selected deltas and estuaries. The procedure is rather summarised here, for all details we refer to (Vos et al., 2019).

The *CoastSat* tool is globally applicable for any region of interest. For a particular study area, the satellite optical imagery is sub-sampled. In this case, we only sample the satellite optical imagery around the sand spits up to their maximum observed length.

5.2.2 Spectral analysis of the coastline

Cyclical behaviour is generally well captured by Fourier analysis. The amplitude of the Fourier transform allows us to assess the importance of a range of time scales. A Discrete Fourier Transform (DFT) is the numerical solution to the Fourier transform (Sevgi, 2007). Although the Fast Fourier Transform exists, here we choose to analyse a set of preset time scales (annual) and their associated amplitudes and therefore use the DFT directly.

$$\tilde{H}(k) = \sum_{n=0}^{N-1} h_n(x) e^{-2\pi i f n/N} \tag{5.1}$$

Where $\tilde{H}(k)$ is the discrete Fourier approximation of a continuous Fourier transform, $h_n(x)$ is the input signal – in this case the cross-shore position in time for a given point along the shoreline, f is the frequency in time, n is the current sample, and N is the total number of samples. For spectral analysis, it is important to ensure that the input signal $(h_n(x))$ is sampled equidistantly. This is often not the case for satellite-derived products: depending on the location, the revisit interval varies due to satellite orbits, but also the visibility (Bergsma and Almar, 2020).

5.3 Saint Louis sand spit "Langue de Barbarie" evolution

The *Langue de Barbarie* developed downdrift in conjunction with the diversion of the river mouth and its southward migration (Anthony, 2015). Energetic waves - as in the case of Saint Louis - cause massive sand accumulation and are prone to rapid spit elongation, much more so than less energetic waves which are responsible for small sand accumulations and spit curvature (Allard et al., 2008). The 2003 rupture had dramatic consequences for the *Langue de Barbarie*: the sand spit further downdrift was recycled into estuarine bars, while the rest was transported southwards by longshore currents, severely impacting infrastructure in the *Langue de Barbarie* (Anthony, 2015; Ndour et al., 2018; Bergsma et al., 2020). Nowadays, the northern spit of the *Langue de Barbarie* is still elongating (Figure 5.1), explained by the lower bypass and the strong increase of the LST as it happened from 2012 to 2013, generating the ensuing exceptionally rapid elongation of the *Langue de Barbarie* spit between June 2013 and May 2015 ($\simeq 2km$) (Sadio et al., 2017). The results of shoreline tracking by (Bergsma et al., 2020) with a longer observation period of regular revisit satellite missions (Landsat and Sentinel-2) confirmed that the spit is migrating southwards at an average rate of 590 m/year after 2012. The modelling of the morphological evolution of the *Langue de Barbarie* was drawn as an equation 5.2. This simple deterministic spit growth equation provides a useful first-pass model of spit evolution independent of climate forcing, demonstrating that changes in the wave regime are not the main driving factor. Interactions between sediment transport and fluid flow create morphological feedback and lead to self-organised patterns (Coco and Murray, 2007), which explains the differences found in table 3.2 (satellite measured spit growth rate versus "forced" spit growth rates (Duc Anh et al., 2020)) and why these "forced" spit growth rates are much lower than the satellite derived measurements. Other parameters such as human interactions, sediment availability and sea level rise also play an important role in the longer term (Pradhan et al., 2015; Tribe, 2008; Stancheva et al., 2011).

Based on this assumption, the spit tip positions from 2015 to 2020 (collected with Sentinel-2 satellites) and the median LST ($Q = 530 \times 10^3 m^3/year$), a parametric model of the *Langue de Barbarie* spit's intrinsic stochastic growth over time t can be expressed as:

$$\frac{x}{L} = 1.85 \times 10^{-6} Q (\frac{t}{T})^{4.46 \times 10^{-6} Q} \tag{5.2}$$

With $p_{value} \leq 0.01$, where x is the position of the tip of the spit from the northern end, and L is the maximum spit extension value ($L = 32$ km). The T value represents a cycle duration (here $T = 35$ years, derived from extrapolation of the fitted data Figure 5.1.a). Here we define a spit cycle as the moment when the elongation of the *Langue de Barbarie* reached its maximum, causing the closure of the mouth of the Senegal River when $\frac{x}{L} \longrightarrow 1$. According to our model, the migration rates of the spits increase with time, which is consistent with the migration rates derived from CoastSat (Table 3.2). Similarly, the spit width W averaged over a distance of 1 km along the coast at transect Y - located 1 km south of the defined urban area and shown in Figure 2.1 - can be expressed as:

$$\frac{W}{W_{max}} = \frac{t}{T}^2 - \frac{t}{T} + 1 \tag{5.3}$$

With $p_{value} \leq 0.01$ and $W_{max} = 354$ m is the maximum width at transect Y. We can first observe a phase of rapid decrease in spit width since 2008 - this decrease correlates with the southern extension of the *Langue de Barbarie* (Figure 5.1) - and a second phase of width accretion. Taking into account the equation 5.3, the erosion trend of the beach located under the urban area will decrease after 2030, and the accretion will be reversed (Figure 5.1.b).

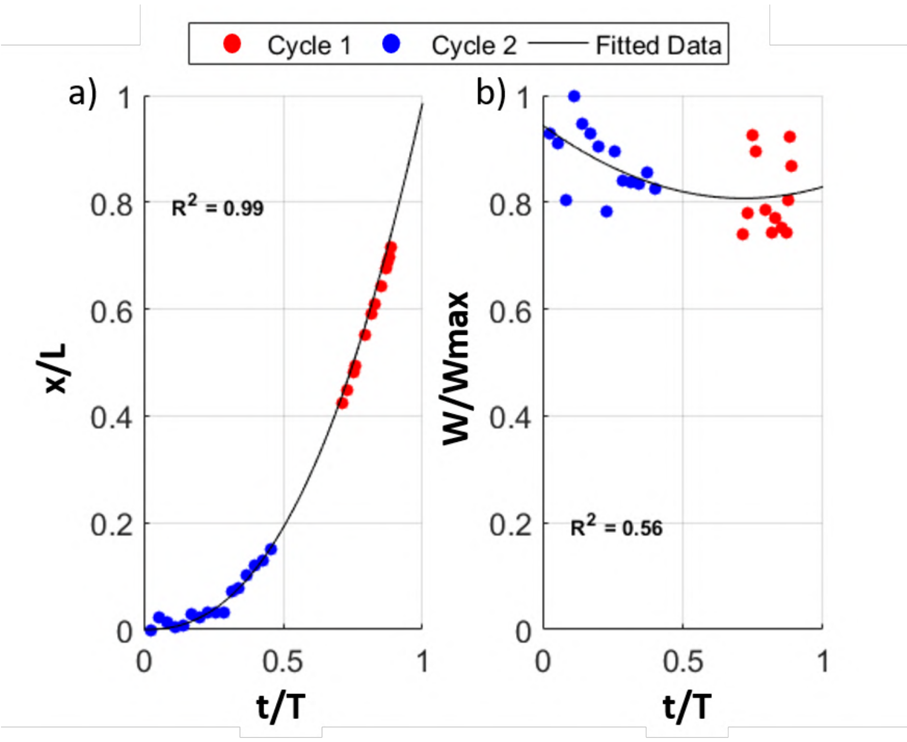

Figure 5.1: (**a**) Sand spit tip positions for cycle 1 (1984-2003 ; red) and cycle 2 (2003-2020 ; blue) derived from CoastSat tool (Vos et al., 2019) and fitted data expressed as Equation 5.2. (**b**) Sand spit averaged width evolution between transect $Y = 1.7705 \times 10^6$ Y UTM (28) and 1 km South with its fitted data expressed as Equation 5.3 (Right)

Cycle 1 is defined from the start of Landsat data acquisition in 1984 to 2003, the date of the artificial break, as shown in Figure 5.1. Cycle 2 is the new sand spit cycle initiated after the spit breach. Given our modelling, we can estimate that the mouth is likely to close around 2040. Studying the cyclicity of the Senegalese sand spit raises another question: is this cyclicity specific to this site, or can these results be extended to other sand spits with similar environmental characteristics?

5.4 Similar study sites worldwide

5.4.1 The cases of Chile, Mozambique and Benin

River deltas, and the type of ebb/flood deltas, spits and barrier islands they form, are generally classified according to the relative dominance of tidal versus wave energy (Davies, 1980). There are five classes; tidal dominated (high/low), mixed energy (tidal/wave dominated) and wave dominated. For our study we are interested in ebb deltas that contain sand spits and therefore focus on a relatively high importance of incident waves rather than tides. Here we are looking for deltas with sand spits that are located in a similar environment: a wave-dominated micro-tidal environment with a strong oblique wave regime, which leads to strong alongshore sediment transport and thus lengthening of the sand spit down-drift. However, to avoid concentration in a single area and still be globally representative, the four selected sites are distributed around the world (Figure 5.2): *El Peñon* Mataquito river delta in Chile (Figure 5.3.3), the *Langue de Barbarie* on the Senegal river delta in Senegal (Figure 5.3. 2), the *Bouche du Roi* at the Mono river delta in Benin (Figure 5.3.1) and the Pomene estuary in Mozambique (Figure 5.3.4).

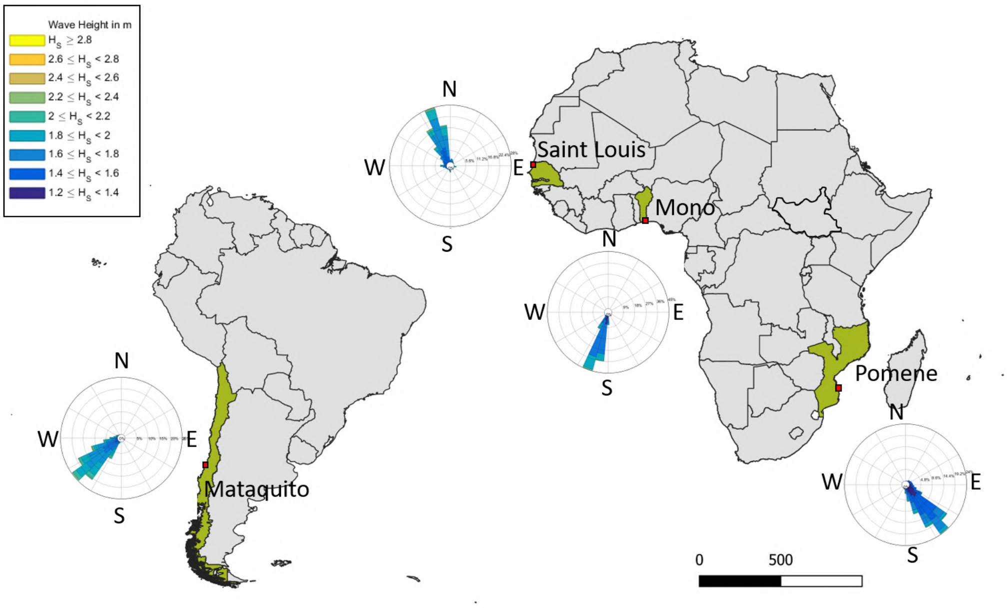

Figure 5.2: Location on the world map with their associated wave roses (Pereira) of **(a)** *El Peñon* sand spit on Mataquito estuary in Chile, **(b)** the *Langue de Barbarie* in Senegal, **(c)** the *Bouche du Roi* in Benin, **(d)** the Pomene estuary in Mozambique. The intensity on the wave roses represents the frequency of the significative wave height H_S over the time period 1979-2016 (ERA5 data (Hersbach et al., 2018))

The *El Peñon* delta is located in Chile (western South America, western central Chile ; Figure 5.2.a). Where the
textitMataquito River meets the Pacific Ocean. With a mean wave height of $H_S = 2.7$ m and a peak period of $T_P = 11.7$ s (from National Oceanic and Atmospheric Administration nearest mode) (Villagran et al., 2011) and a semi-diurnal tidal regime with a mean tidal range of 0.9 m, the *El Peñon* delta is strongly dominated by waves. The delta is exposed to a predominantly southwesterly incident wave climate, which results in the formation of sand spits associated with sediment accumulation (Cienfuegos et al., 2014) induced by wave-driven alongshore currents and sediment transport. The *El Peñon* delta was exposed to the 2010 Chilean tsunami, resulting in the complete disappearance of the sand spit. Interestingly, the initial recovery was rapid and a sand spit formed in the following year (Villagran et al., 2011).

The *Bouche du Roi* sand spit in the *Mono* estuary is located in Benin (West Africa, Southern Benin ; Figure 5.2.c) where the passage from Lake Aheme to the coast runs into the Atlantic Ocean. The Mono estuary is dominated by waves with a mean wave height varying between H_S = 0.5-1.5 m and a peak period between T_P = 10-15s (Blivi et al., 2002). The semi-diurnal tidal regime has a mean tidal range of 1.05 m. This area is also subject to strong oblique waves leading to an eastward drift along the coast (about 1 $\times 10^6 m^3/year$) (Anthony and A.B.Blivi, 1999; Davies, 1980; Blivi et al., 2002; Abessolo et al., 2021; Lawson et al., 2021; Almar et al., 2015). Until the construction of the deep-water ports at Cotonou (1962) and Lomé (1967), the estuary seemed to be in equilibrium between hydrodynamic forcing, geological configuration and sediment supply and transport. After the introduction of the harbours, a significant unidirectional drift in the upstream direction was observed, leading to a large erosion of the downstream sand spit (Blivi et al., 2002). In addition to the deep-water harbours, which altered the geological configuration and sediment transport, the construction of the *Nangbéto* river dam – built between 1984 and 1987 – altered the sediment supply. In response, the sand spit periodically reached its maximum length and closed the mouth of the river (Laïbi et al., 2012), thus reducing the cyclic life span. The *Mono* estuary closed in 1987, leading to a breach, either artificial or natural. The most likely cause of the breach is natural; the river forced its way over the sand spit and created an opening. Similar to the situation at Saint Louis in Senegal, two other artificial breaches, in 1999 and 2009 respectively, were initiated to avoid flooding and breaching processes and to prevent the destruction of the village of *Djondji* (Laïbi et al., 2012). The growth rate of this sand spit is about 700 m/year (Lawson et al., 2021).

The *Pomene* estuary (East Africa, Southern Mozambique; Figure 5.2.d) is slightly different as it is more of a bay with a barrier island and is the most exposed to tidal energy of the sand spit systems considered here. The *Pomene* estuary is in a mixed energy regime / wave/tide dominated considering a mean wave height of H_S = 1.35 m and a peak period of T_P = 9.3 s (from the (Hersbach et al., 2018) dataset). The semi-diurnal tidal regime has a mean tidal range of 3 m. The bay faces the Indian Ocean, and the sand spit develops northwards in response to the prevailing south-easterly swell and associated alongshore sediment transport. It has been suggested that the bay is threatened by coastal erosion due to climate change (Chemane et al., 1997). The extension of the spit towards the NNW is explained by sediment deposition associated with alongshore sediment transport (Massuanganhe and Arnberg, 2008). Satellite imagery has shown a long-term erosion trend on the eastern side of the spit and a north-northwest extension.

The *Langue de Barbarie* sand spit in Senegal is not described further as this work has been done previously (see chapter 2).

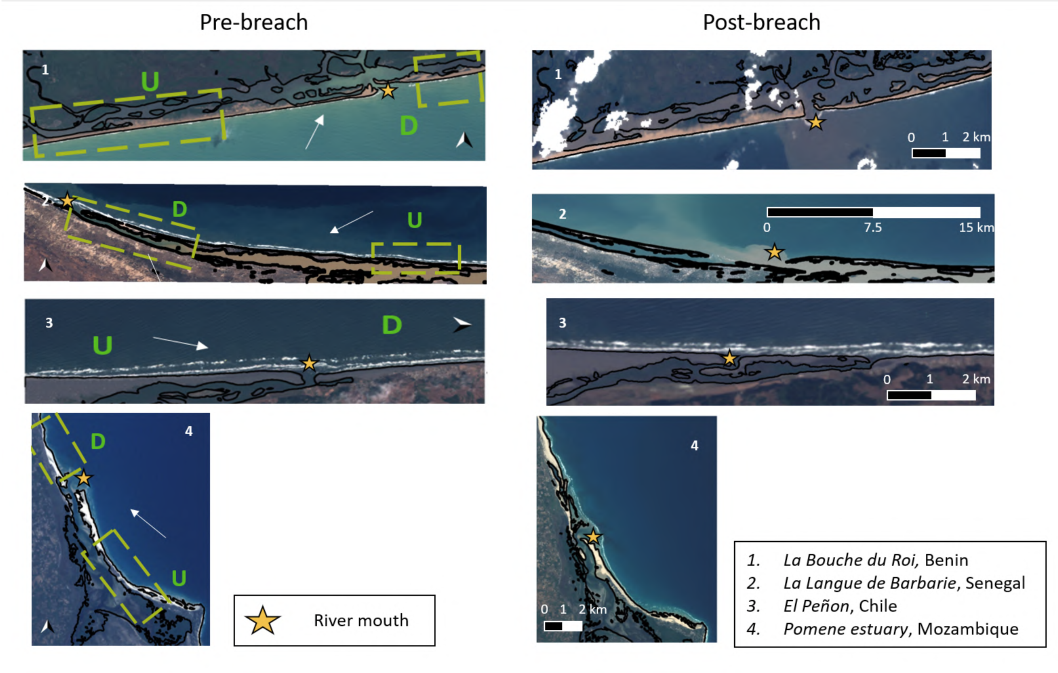

Figure 5.3: Satellite images (S2) of the spits shape before and after a breach. The white arrows represent the LST direction and the green squares on the are the delimitation of the *up-drift* (U) and *down-drift* (D) areas that are further studied. The river mouth is indicated with a yellow star for a better visibility.

5.4.2 Conceptual model improvement

Based on the work done and presented in section 5.3, the same conceptual model equation is applied there to the three other wave-dominated spits: Chile, Benin and Mozambique. As pointed out by e.g. (Oertel, 1977; FitzGerald et al., 2001), sand spits follow a cyclic pattern in which newly formed spits mature and when they reach their "old age" breaching occurs, eventually resetting the cycle. This cyclic perception in terms of spit development and extension can be conceptually represented as a function of time as shown in (Taveneau et al., 2021). According to this conceptual model, a cycle runs from $0 < \frac{x}{L} < 1$ and $\frac{x}{L} \longrightarrow 1$ represents the moment when the elongation of the sand spit reaches its maximum, leading to a closure of the river mouth and/or a new breach. In particular, this approach neglects wave driven effects. Here, we propose to include a wave-driven alongshore sediment transport component Q according to the equation 5.4.

$$\frac{x}{L} = aQ(\frac{t}{T})^b \tag{5.4}$$

where x = the length of the sand spit
L = the maximum length of the sand spit
t = time

T = the period of a spit cycle
Q = longshore sediment transport $[m^3/year]$
a, b = scalar coefficients

For each sand spit, the length and time characteristics were normalized with the system characteristic length and period.

5.4.3 Results

5.4.3.1 Intrinsic versus forced dynamics

The conceptual sand spit model presented above allows us to identify the relative contribution of intrinsic cyclic behaviour (effectively deactivating the temporal variability of Q) and forced sand spit behaviour by wave dynamics. In order to apply the conceptual spit model to the four selected sites, a measured spit length and cyclic period are required. For each of the sites, these two characteristics are derived from satellite optical imagery collected since 1984 by manually tracing the spit tip over time. This resulted in the following characteristics:

Sites	Length [km]	Period [years]
Chile	7.4	42
Benin	11.3	10
Senegal	32	35
Mozambique	12.9	24

Table 5.1: Sand spits characteristics: the maximum length of the sand spit (measured with observations) and the duration of a cycle (estimated with the conceptual model).

During the period analysed, at least 2 (partial) cycles are observed per site: 2 cycles for *Senegal*, 2 cycles for *Chile*, 3 cycles for *Mozambique* and 4 cycles for *Benin*, indicated by the squares, diamonds, asterisks and circles respectively in Figure 5.4. Together with the basic parameters (Table 5.1), we can now fit the observations to the conceptual model, represented by equation 5.4. One might expect the exponential component in the equation 5.4, b, to be greater than 1, allowing for increased migration rates as the tip moves away from its origin, as observed early in (Taveneau et al., 2021). However, when fitted to the observations, the coefficient b tends towards 1, indicated by the black line (Figure 5.4). A $R^2 = 0.75$ for the different sites combined shows that the conceptual model performs quite well. In particular, the conceptual formulation depends on an average LST and should be considered as representative for the intrinsic spit development part over the study period from 1984 to 2021. This also means that external forcings such as climate regimes, irregular sediment supply (from varying river discharge or directional variations that alter the LST), sea level rise are not taken into account in this conceptual model.

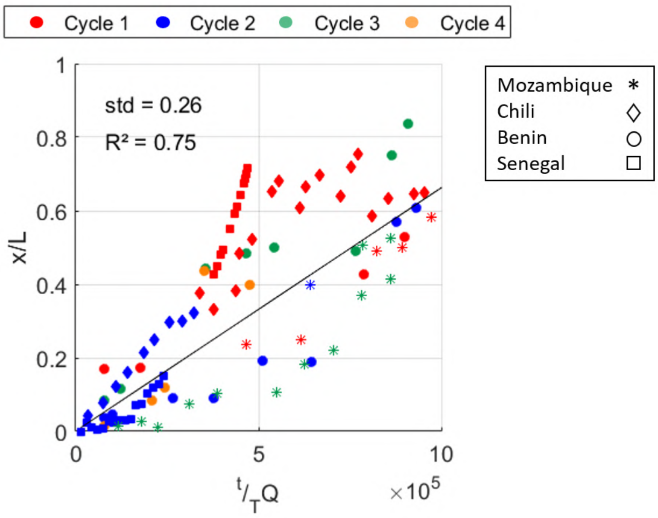

Figure 5.4: Evolution of the sand spits length as a function of time per study sites (markers) derived from the CoastSat tool (Vos et al., 2019) with their associated cycles (colours), and fitted equation expressed as equation 5.4 (black line).

Forced behaviour is seen here as sand spit behaviour driven by temporally varying wave conditions. We can account for this by (re-)activating the temporal variability of Q in equation 5.4. Measured wave conditions, e.g. from wave buoys, are not available in most of the selected areas, so we use aggregated ERA-5 wave conditions products distributed through the Copernicus Climate Data Store as part of the Copernicus Climate Change Service (C3S)(Hersbach et al., 2018). By including time-varying wave conditions, we add a contributing component and expect to explain more of the observed variability. Figure 5.5.a shows the sand spit length time series (from top to bottom) at *Mataquito*, *Mono*, *Pomene* and *Saint Louis*. The vertical lines in the individual sub-plots per site indicate cycle resets (break or event such as at *Mataquito*). From Figure 5.5.a it is clear that the conceptual spit model, which covers only the cyclical behaviour, is broadly in phase with the observations. However, the amplitude - the actual length of the sand spit - is more accurately captured when the cyclic and forced components are combined (yellow). This can be explained by the fact that the cyclic model is linear ($b \approx 1$) with no time-varying component. The estimation of the spit length diverges when the position of the spit tip oscillates (evident for *Mataquito* and *Saint Louis*) due to the variability of the wave conditions. Consequently, adding the wave forcing improves the estimation of the spit length, as indicated by the improvement in the RMS error in Table 5.2. For Benin in particular, we note that the inclusion of wave variability also reduces the phase shift between observations and model, as indicated by the high R^2 coefficient in Table 5.2.

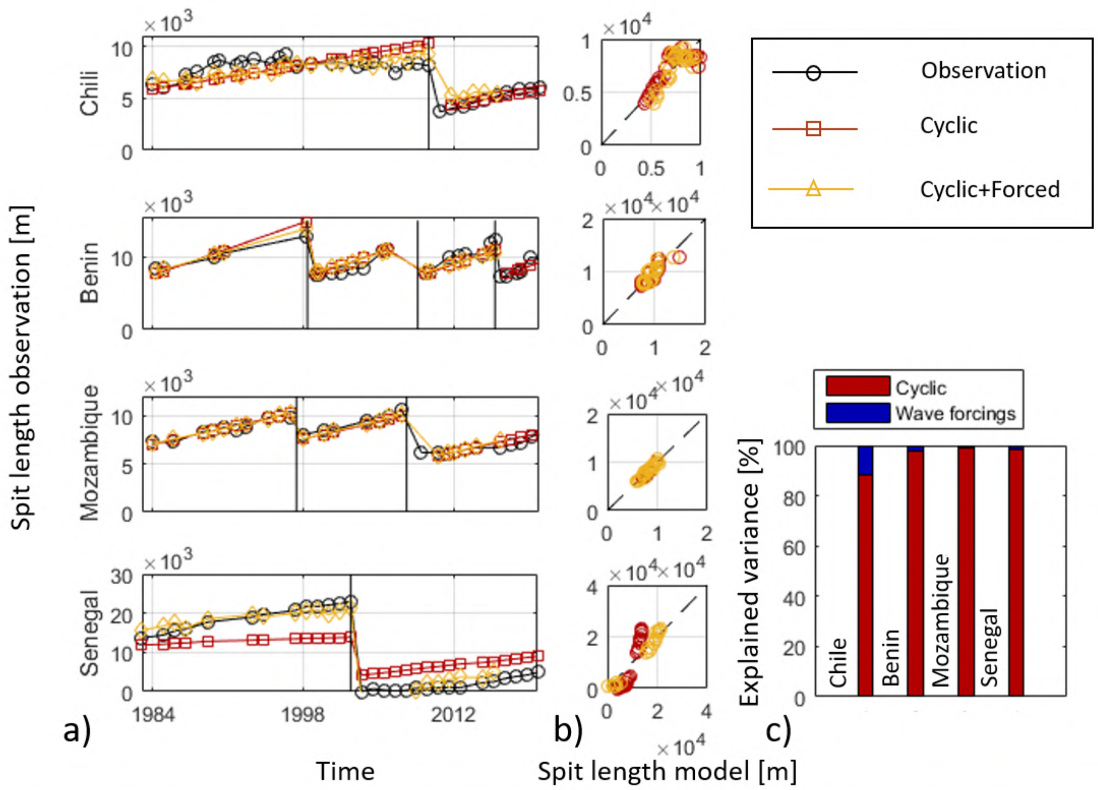

Figure 5.5: **(a)** Evolution of the sand spits length as a function of time between 1984 and 2021 – satellite data (black), projected data with the conceptual model (red), projected data with both the cyclic hypothesis and the wave forcing (yellow) – for the four study sites with position of the breaches (horizontal lines). **(b)** Linear regressions of the sand spits length between the observed data with the model-estimated ones, and the model-estimated ones with the wave forcing. **(c)** The explained variance with the observed data for the cyclic development of the spit length (red), the development of the spit length through wave forcing only (blue).

Site	R^2 Cyclic	R^2 Cyclic+Forced	RMSE Cyclic	RMSE Cyclic+Forced
Chile	0.67	0.70	1.03 km	0.82 km
Benin	0.75	0.82	0.83 km	0.68 km
Mozambique	0.93	0.95	0.34 km	0.33 km
Senegal	0.94	0.97	5.66 km	1.56 km

Table 5.2: Correlation coefficients per study site between the observed data and the conceptual model estimated ones with and without the wave forcings along with the associated RMS errors.

Similarly, the two applications of the conceptual sand spit model, cyclic and cyclic+forced, allow analysis of the relative contribution in terms of variance explained, as shown in Figure 5.5.c and Table 5.2. At all different sites, the vast majority of the variance is explained by the intrinsic cyclic sand spit behaviour. The average gain in explained variance is 4% when wave conditions are included. This tells us that resetting or breaching is predominantly a matter of time. However, where the spit tip is located, the actual position in time, is only weakly dependent on the wave variability to which it is exposed.

5.4.3.2 Vicinity imprints of sand spit signature

Having developed a simple cyclic model for the spit tip in time, we now investigate how these dynamics affect its surroundings. To do this, a DFT procedure is applied to shoreline time series along the coast, *up-drift*, *sand spit* where the entrance to the open ocean is from $x = 0$ to $\frac{x}{L} \longrightarrow 1$ and the third zone is *down-drift*. For Benin, Mozambique and Senegal, time series are shown with their spatial boundaries in Figure 5.2. The sand spit at *Mataquito*, Chile, is excluded from this analysis because the cyclic period is longer than the available coastal time series. As the present study focuses on inter-annual to decadal evolution, the cross-shore positions are aggregated annually and linearly interpolated for missing years at the beginning of the sampling period (early Landsat images). This ensures a consistent data set, even with temporally sparse clear-sky imagery during rainy periods. The analysed time series are shown in Figure 5.6 (middle panel) per site, together with the annually averaged wave time series (top panel). In this data set and for the three study sites, sudden changes in time on the longshore axis (red), immediately followed by locally important cross-shore variations in the down-drift area (blue dashed line), are due to a breach occurring in the same down-drift area. These down-drift cross-shore variations physically correspond to the collapse or retreat of the down-drift part of the sand spit caused by the breaching mechanism, this phenomenon being particularly visible for the Senegal and Benin sites. On the other hand, the up-drift time series (continuous blue line) are quite stable in time and therefore their cross-shore variation in time is less affected by the breaches occurring in the spit.

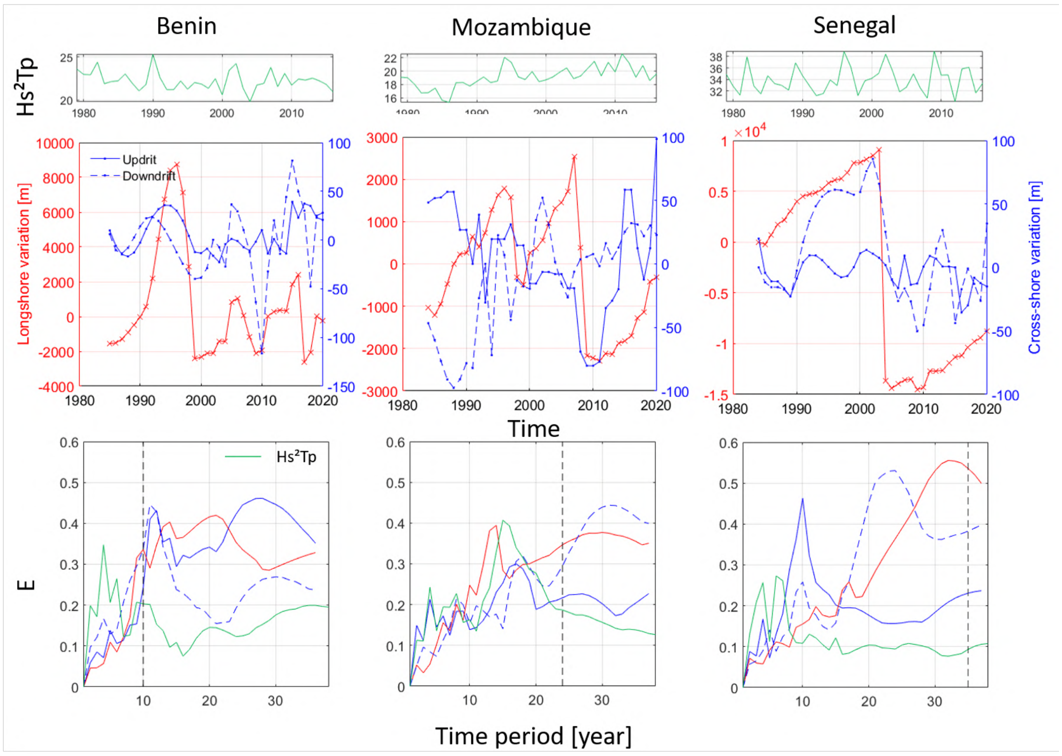

Figure 5.6: **(Top)** Wave time series (1979-2016) annually averaged per site. **(Middle)** Spectral analysis of the cross-shore coastline variation up-drift and down-drift, and alongshore variation on the sand spit over the years for the four study sites. The vertical red dashed line represents the cycle duration estimated with the conceptual model. The vertical dashed black line corresponds to the sand spit cycle period (T_{cycle}) as found in section 5.4.3.1 (i.e. maximum of sand-spit alongshore position variance). **(Bottom)** Studied time series per zones: averaged cross-shore evolution of the up-drift and down-drift areas in blue and longshore evolution of the spits length in red. For better visibility, the median of each signal is subtracted.

In terms of dominant timescales, in Figure 5.6 the spectra in the bottom panels are calculated from the time series shown in the middle panels. An energy peak in the spectra indicates a certain dominance of these frequencies in the time series. In the case of the *Bouche du Roi* spit in Benin, the observed spit tip cycle period corresponds well to an energy peak in the up- and downdrift shoreline spectra, although the energy peak is more pronounced in the downdrift. For *Saint Louis*, the up- and down-drift shoreline spectra have a significantly shorter time scale than the found spit tip cycle period, more or less a third compared to the spit itself. For *Pomene* in Mozambique, the spectral analysis suggests a cyclic period of the order of 15 years and appears to be driven more by wave variability.

Of the three sites, the *Bouche du Roi* spit in Benin has the shortest cycle and thus the largest number of cycles occurring during the study period. Therefore, the *Bouche du Roi* is given special attention in the analysis to determine the influence of the cyclical spit mechanism on the surrounding coastline. Figure 5.7, shows that there is a weak correlation between the cyclicity of the sand spit and the up-drift, while both the sand spit area and the down-drift have a clear influence on the coastal cyclicity. Waves drive the cross-shore variability of the shoreline on the whole spit at high (8 years) and low frequency (23 years), but the elongation of the spit seems to be mostly driven by high-frequency phenomena, and mostly by its cyclicity (darker red area around the T_{cycle}).

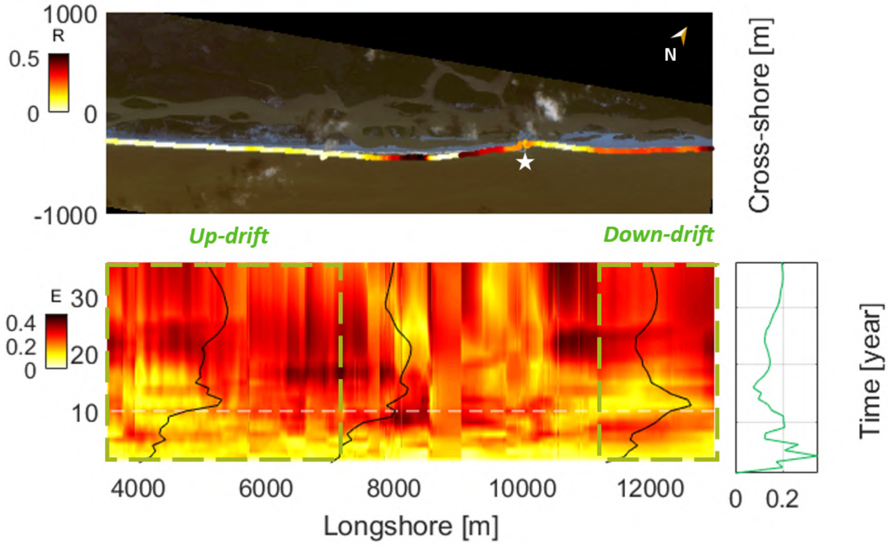

Figure 5.7: Benin sand spit (Mono river, Grand Popo): **(Top)** Correlation between the model output and the cross-shore variation over time map-projected onto a Sentinel-2 image. The white star indicates the position of the breach on the satellite image. **(Bottom)** Energy distribution over the shoreline cross-shore positions in time – the white horizontal dashed line corresponds to the spit cycle, the black lines represent the zone-by-zone DFT. The wave parameters spectrum over time ($H_S^2 T_P$) is presented on the right in green as a point of comparison. To avoid the pixel to pixel noise, the time series are averaged every 100 m. The cycle period is shown as a white dashed line for a better visualization. The found correlation maxima are also visible as energy maxima (red shades) at the T_{cycle} position.

5.5 Discussion

5.5.1 Sand spits as a major source of coastal variability

Sand spit elongation models through literature is mainly based on the LST-variation being the most impacting factor for spit lengthening (Kraus, 1999; Palalane et al., 2014; Duc Anh et al., 2020) and suggests that the elongation is directly proportional to the LST rate and dependent on fundamental geometric parameters and time. In this study we can also emphasize through the investigation on the *Bouche du Roi* sand spit that LST variability only has a limited impact on a sand spit morphology. However, our results indicate that the overall sand spit behaviour is under the combined influence of climate and cyclic forcing.

5.5.2 A prediction tool for coastal management around sand spits

Our model results show a better agreement between spit lengthening and the cyclic model than with wave climate variability: the explained variance (Figure 5.5.c) shows that, on average over the four spits, 83% of the spit lengthening process is due to its natural cyclicity. In contrast, Figure 5.6 shows that waves definitely have an impact when comparing wave variability with cross-shore shoreline evolution. This observation raises an important question: are cross-shore and longshore variations on wave-dominated spits driven by different forcings? The case of *Bouche du Roi* in Benin is an illustration of this: in the longshore direction, one can see the distribution of factors that influence the cross-shore variation of the shoreline. The up-drift is in no way influenced by the cyclical development of the spit, only by high and low frequency wave forcing (a residual). However, the tip of the spit - where the breaches occurred - and therefore its length, is influenced by waves and its intrinsic evolution, with cyclicity as the dominant driver. Finally, the down-drift area is modulated by both drivers. It should be noted that the timescales observed in the down-drift also have higher frequencies than the spit itself. This has been observed elsewhere and can be attributed to the LST entering the inlet through sandbars that break away from the up-drift side, migrate across the mouth of the river and weld to the down-drift side(Burvingt et al., 2022; Kraus, 1999; Kraus and Galgano, 2001).

Spits are attractive (for trade and tourism due to their natural diversity) and therefore densely populated areas (Pradhan et al., 2015). As the length of the spit has a major impact on its inhabitants, a tool for predicting the length of the spit is key for decision making to preserve the local population and their activities. Breaches - referred to in this study as the beginning of a spit cycle - are responsible for extreme shoreline retreat of the up-drift area on the cross-shore axis, endangering communities and compromising infrastructure. Knowledge of the following wave-dominated spit parameters: longshore sediment transport, maximum length of the spit and its growth rate, allows a rough prediction of the date of mouth closure. This estimation could be used to anticipate the decision to open artificial breaches in order to avoid a disaster like that of Saint Louis City (Senegal) in 2003 (Sadio et al., 2017; Bergsma et al., 2020).

To reinforce our conclusions on the applicability of our cyclic model, a blind application of our model on a well-documented sand spit is proposed here to discuss its relevance. The Cap Ferret is a very dynamic and wave dominated spit (Stive et al., 2002a; Nahon et al., 2019). To test our cyclical conceptual model for sand spits, this section applies the equation 5.4 to the Cap Ferret to see if the observed T_{cycle} can be predicted from the spit parameters given in Table 5.3.

Length	28 km
Q_{mean}	$0.63\times10^6 m^3/year$
Growth rate	100-250 $m/year$

Table 5.3: The cap Ferret sand spit characteristics based on literature (Stive et al., 2002a; Nahon et al., 2019)

Over the last few decades, this spit has migrated southwards, which is also the direction of the LST, sometimes reaching the southern edge of the inlet and merging with it. The hypothesis of autocyclicity of this landform was raised and estimated with a period of about 80 years (Michel and Howa, 1997). Two T_{cycle} were calculated based on the minimum and maximum values of spit growth, and the average of these two values is taken as the final estimate of T_{cycle} with our conceptual model. Here we find $T_{cycle} \simeq 84$ years. The literature, which our prediction based on the conceptual model, shows a high degree of agreement here. While our model still needs to be confronted with other spits in different environments, our hypothesis of a cyclic nature of spits seems to be valid and should be further investigated.

5.5.3 Inherent limitations of the data

The satellite imagery used in this study provides a regional spatial understanding, with pixel resolution varying between 10m and 30m depending on the satellite mission from which the data originates. The derived coastlines are accurate to within an error of ±10 m (or ±30 m). We consider this error to be due to the kilometric scale of the sand spit.

The quality of our model regression with the data and spectral analysis is affected by the lack of data over time. Changes in spit morphology on a regional scale are extremely long processes - several decades - as shown in this study. As open access satellite data start in 1984, it is only possible to study the morphodynamics of sand spits over a period of 38 years, when there are not too many gaps in the data. Considering the estimated cycle duration - which varies between 10 and 42 years in our study - the lack of data on a temporal scale has a particular impact on the Discrete Fourier Transform analysis. Our conceptual model relies only on the hypothesis that spit elongation is free of climatic forcing; the elongation process does not depend on the temporal variability of the LST.

For example, in section 5.4.3.2 one may wonder why the cycle period peak is not the one that prevails for the Senegalese spit, as it seems to match in the case of Benin and Mozambique. This spit cycle duration is about 35 years, while we have access to 37 years of data (where there is no gap in the data) with the open access satellite imagery.

5.5.4 Discussion on our cyclic model parameters

The type of model chosen (equation 5.4 ; section 5.4.3.1) can also be discussed. In this study, the case $b = 1$ was taken because the first evaluated b was very, which also simplifies as a linear equation. Physically, $b = 1$ means that the same amount of sand is captured by the spit each year. Since our model is based on the hypothesis that spit elongation is LST dependent, but that LST variability does not affect the elongation process, $b = 1$ implies that the sediment bypass varies with the LST: as the LST increases, the sediment bypass increases and vice versa. $b < 1$ would mean that the farther the tip of the spit is from the mouth of the river, the slower the rate of migration. Assuming that $t \longrightarrow \infty$, the length of the spit will tend to stabilise around a certain value. Looking back at Figure 5.4, this seems to have been the case for the *El Peñon* spit in Chile (red diamonds) before the tsunami destroyed the spit in 2010, initiating the start of a new cycle. In contrast, $b > 1$ would mean that the further away the spit is from the mouth of the river, the higher its migration rate. In the study (Taveneau et al., 2021), the same methodology was applied to the *Langue de Barbarie* sand spit alone, with the difference that the b parameter is LST dependent. It was found that the further away the tip of the spit is from the mouth of the river, the greater the migration rate. In this study the total power coefficient was greater than 1 and can be discussed here. Since the width of the spit is inversely proportional to its length (Kraus, 1999; Duc Anh et al., 2020), some of the sediment material that comes from the up-drift part of the erosion and the sediment bypass partially accumulates at the tip of the spit (Aubrey and Gaines, 1982). In the case of the Senegalese spit, it has been estimated that the spit can trap up to 35% of this sand volume (Taveneau et al., 2021).

One could ask if there is a stable position of the spit, where the tip of the spit is far enough away from the up-drift part that there is no negative feedback on the beach width (erosion pattern), and at the same time close enough not to block commercial activities (fishing) with a river mouth too far away from inhabited areas (see for example Senegal). Such a position could be evaluated, assessing the pros and cons of both the economic impact and the local impact on beach width.

5.6 Chapter conclusion

In this study, a cyclic climate-free conceptual model is proposed for the wave-dominated lengthening process of sand spits. Satellite imagery over a long acquisition period (37 years) allowed the monitoring of sand spit evolution at a regional scale. Shorelines were derived from four spits around the world (Chile, Senegal, Mozambique and Benin) that share similar environmental conditions with oblique waves, large LST and micro-tidal conditions. The overall results show that 83% of a wave-dominated spit elongation process is self-evolving, cyclical, and affects shoreline downdrift. Our model was applied to a spit that was not part of the sample used to build it, Cap Ferret (France), to assess its reliability. The main cycle period was correctly captured, giving confidence in the prevailing cyclical nature of sand spit observations and our proposed model. However, the morphology of sand spits depends on many influences, not all of which have been taken into account here, in particular the primary influence of human activity. Nevertheless, such a physically reduced predictive model can be easily applied to other wave-dominated sand spits to support coastal protection strategies (artificial breaching, down-drift beach management).

Conclusions and perspectives

5.7 Conclusions

As mentioned in the conclusion of the chapter 1, this thesis aims to answer three main questions. These questions have been presented and answered in the different chapters developed throughout this manuscript: What are the links between local and regional scales? What is the sediment exchange between the submerged and the exposed parts of the beach? And finally, can satellites answer the previous questions and support coastal engineering issues? We summarise the results here in a conclusion that generalises the answer and points the way forward.

5.7.1 What are the links between the local and regional scales?

At Saint Louis, satellite remote sensing with large spatial coverage, a video camera installed locally on the beach, and in-situ surveys form the data set available for the study of beach morphodynamics. Currently, the understanding of coastal morphodynamics faces an observational gap from local to regional scales. Combining tools to unravel the links between these two scales was an objective of the PhD. Originally, this PhD project was set up in response to marine damage in the city of Saint Louis due to a beach that has been eroding over the last few years. As the wave climate is very energetic (Sadio et al., 2017; Almar et al., 2019b), the waves broke on and in the houses, taking entire buildings with them. Many people had to be resettled and the decision to build a longitudinal seawall was taken as a matter of urgency in the face of this catastrophic situation. In fact, the erosion trend was a direct cause of the 2003 breach (Rodríguez et al., 2014; Bergsma et al., 2020; Taveneau et al., 2021) (see chapter 5): as the *Langue de Barbarie* stretched southwards, the up-drift part eroded as a direct effect (Figure 5.8). This post-breach coastal retreat, developed in chapter 3, was primarily due to the spit elongation process: sediments progressively accumulate at the tip of the spit (south), while the northern part (the urban area in our case) provides part of the material supply that is transported south by the LST (Aubrey and Gaines, 1982; Dean and Dalrymple, 2001). As the tip of the spit was only a few kilometres south of the city in the post-breach period, the negative feedback on the coast further north was more intense, resulting in significant erosion rates. As the spit lengthened, this feedback, which put pressure on the integrity of the city, gradually diminished, reducing the erosion rate (see conceptual model chapter 5). The availability of satellite imagery with such spatial coverage made it possible to construct a conceptual model of the spit's lengthening process, anticipating both its lengthening and narrowing. According to the model, this erosion trend is expected to decrease when the tip of the spit is far enough away from the city. In this case, the local and regional scales complement each other well: to measure erosion rates (local) and to understand the phenomenon at its origin (regional). This work illustrates the importance of studying local phenomena at larger spatial scales, and thus the usefulness of satellites in coastal monitoring.

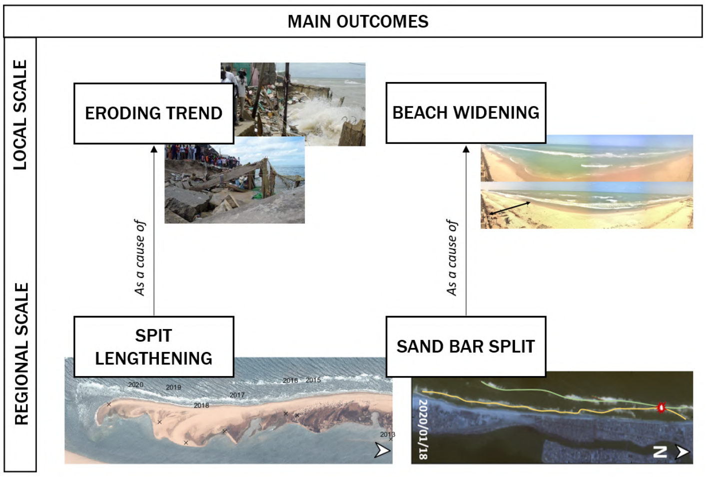

Figure 5.8: Links between local and regional scales to observe coastal morphodynamics.

5.7.2 What are the sedimentary exchanges between the submerged and emerged part of the beach?

The sediment exchange in an open sandy beach is complex and depends on several met-ocean drivers: tides, wind, waves, sea level, human interactions (Komar, 2018), to name but a few. At the main study site, Saint Louis (Senegal), it is essential to understand the mechanism(s) that drive the sediment exchange, since the protection of the population against the risk of erosion is at stake. In chapter 2, an erosion pattern around the urban area was recorded (Ndour et al., 2018; Bergsma et al., 2020; Taveneau et al., 2021). This massive erosion, triggered by the 2003 eruption (Sadio et al., 2017), caused major damage to the town and a relocation plan was drawn up for the most vulnerable population. A sea wall was also considered as a short-term solution to compensate for the significant shoreline retreat, and construction began in late 2020. The most recent accretion of the beach in 2020 (see chapter 4) also highlighted the complementarity between the local and regional scales: high-frequency Sentinel-2 imagery allowed the landward migration of the submarine sandbar to be detected, which gradually and completely welded to the shore, widening the beach locally and massively. The inner splitting of the bar, which caused its landward migration (Vidal-Ruiz and de Alegría-Arzaburu, 2020) and eventual welding to the shore, could not have been detected at the local scale alone (Figure 5.8).

However, during the whole year 2020, an accretion anomaly of +50 m was recorded (cf. chapter 4) at the level of the neighbourhood previously defined as most vulnerable (where the protective rip-rap is under construction). This accretion anomaly has raised several questions/hypotheses as to its origin: is it due to the dynamics of the nearshore sandbars, to the rip-rap under construction, to a larger phenomenon, sand waves from the Saharan desert coast, to the development associated with the sand spit, or to a change in waves? We have shown in chapter 4 that the inner bar, which split during low-energy wave conditions, had progressively migrated landwards to fuse with the shore, resulting in a massive and local (a few kilometres longshore) accretion on the emerging beach. This accretion is then gradually smoothed out along the coast by the strong southward littoral drift.

5.7.3 Can the satellites answer the previous questions to support coastal engineering issues?

As part of the objectives of the PhD, several parameters have been studied and are listed below (an overview of Figure 5.9). However, the satellite missions used to derive these parameters from the imagery were not always successful. Let's list, parameter by parameter, the satellite mission used, the success or failure of its study, and what were the limiting factors or what allowed the study to succeed. As a reminder, three satellite missions were used: Pleiades with a low frequency acquisition but with a very high spatial resolution, Sentinel-2 and Landsat constellations with a high frequency acquisition but with a less good ground pixel resolution (see chapter 3). As the main objective of this thesis was to understand the mechanisms and the dynamics of the Saint Louis littoral, adaptations were necessary to answer the concrete problems of the PPCS project.

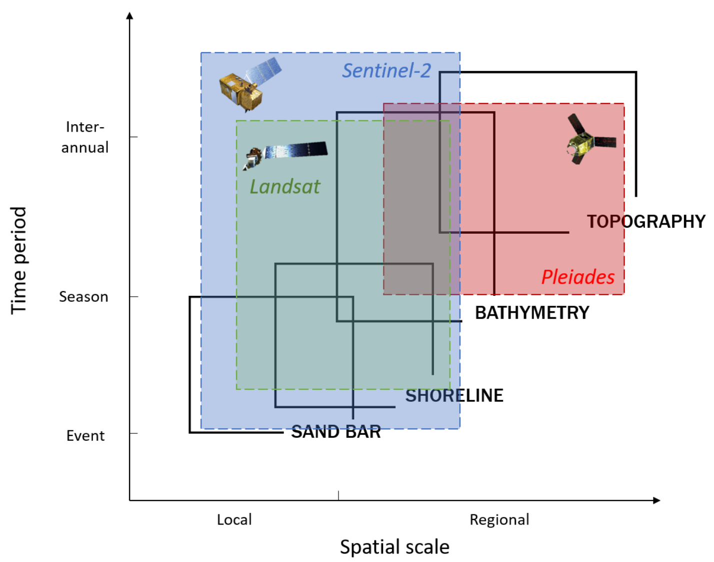

Figure 5.9: Spatial coverage of the different satellite missions used during the PhD along with the analysed processes through their imagery.

– Topography

The topography is derived from the Pleiades constellation and is better described in chapter 3. The results obtained were obtained with a metric error, which is less good than the study carried out by (Almeida et al., 2019). However, the profile of the beach is well captured by the satellite, allowing the slope of the beach to be assessed as $\beta \simeq 4$ %. However, there are limitations to the method: the land/water interface remains difficult for the satellite to estimate (Loghin et al., 2020), as the methodology used is based on the correlation of fixed points between three successive images. As the swash zone is highly dynamic, it is impossible for the tri-stereogrammetric method to derive this land/sea interface correctly as there are no fixed points in this area - this unassessable distance is about ± 10-30 m (cf. chapter 3), which represents a large part of the beach. The topography in the urban area (local scale) was not in line with the project objectives. On a regional scale, however, it has allowed the study of north-south sediment exchange by simultaneously recording the narrowing around the urban area and the southward extension of the *Langue de Barbarie*.

– Shoreline

  For shoreline dynamics, a high-frequency approach was chosen using the optical satellite missions Landsat and Sentinel-2 (see chapter 2). The study of shoreline change allowed the development of a conceptual model for the extension of the spit (chapter 5) and the understanding of the sudden accretion of beaches around the urban area of Saint Louis (chapter 4). This tool was perfectly suited to answer the questions of the PPCS (ADM/AFD) project, as it allowed the understanding of beach morphodynamics on a regional spatial scale.

– Bathymetry

  The bathymetry was also derived primarily from the Pleiades constellation (see chapter 4). The offshore area is correctly estimated by depth inversion techniques, but the estimation of the nearshore area is a failure. The position of the sandbar can, however, be detected by a depth anomaly - the bathymetry becomes locally close to zero around its location - but a sandbar position every 6 months is largely insufficient to determine its dynamics. The use of Pleiades images with a δT of about 9 seconds between them is a severe limitation for estimating wave parameters for a site whose mean wave period is $T_P = 9.23$ s (Sadio et al., 2017). Bathymetric estimates from Pleiades imagery are insufficient to meet the objectives of the project, so a regional high-frequency optical approach has been implemented to understand sandbar dynamics.

– Sand bars

  The sandbars, whose position is derived from Sentinel-2 optical imagery, can be detected by the induced foam generated when a wave breaks on these submarine structures. The high-frequency acquisition of the Sentinel-2 satellite allows the morphodynamics of these features to be studied (see chapter 4). The sandbars are very dynamic features, and the 10 m ground/pixel resolution of the S2 satellite and its regular revisit make it a perfectly suited tool for tracking their position.

In summary, satellites can support coastal engineering issues, depending on the mechanisms (and their spatio-temporal scales) one wishes to study. To achieve the objectives of the PPCS project, high precision is not required, but high frequency acquisition is. In fact, as explained above, the swash induces an error of a few tens of metres in the shoreline detection: there is no need for high precision data in this case. In addition, the S2 satellites were able to detect the splitting and welding of the sandbars that caused the massive accretion in front of the most threatened neighbourhood, a phenomenon that could easily have been missed if the sandbars had been studied at a local scale. To conclude on the satellite tool, it is necessary to choose the appropriate mission according to the coastal process to be studied.

5.8 Perspectives

Sandy beaches have a very complex dynamic, depending on several parameters acting at different spatio-temporal scales. The implementation of a strategy to protect these vulnerable areas requires a good understanding of their intrinsic dynamics, which cannot be neglected. This manuscript raises two important questions:

- What should be done in Saint Louis with the new knowledge generated by this thesis?
- What are the requirements for satellites in coastal monitoring?

5.8.1 Saint Louis beach dynamics

We can see how complex and dynamic the Saint Louis coastal system is, and how difficult it is to anticipate all the mechanisms (sand spit, sand bar, anthropisation) that ultimately affect the local population. Here we explore the possibilities of better protecting the coastline and anticipating catastrophic events on the basis of the research carried out. It should be emphasised that this manuscript has shown that the dynamics of the Saint Louis beach are dominated by intrinsic phenomena rather than climatic ones. The sea wall built in front of the most endangered part of Saint Louis was designed as a short-term solution (fifteen years at most) to protect the population as quickly as possible. Ultimately, it is essential to understand the morphodynamics of the Langue de Barbarie, because in a few years' time another protection system will have to be put in place. With climate change, the accentuation of phenomena such as coastal erosion and marine submergence will increase (Gornitz, 1991; Small et al., 2000; Melet et al., 2018, 2020a), jeopardising the integrity of the city of Saint Louis. Evidence suggests that sea-level rise is having a major impact on the socio-economic activities of the city, and a recent study shows that sea-level rise is the factor that most influences its occurrence (Cisse et al., 2022). As the *Langue de Barbarie* has a very low topography ($\simeq$ 2 m above sea level; chapter 3), more than half of this land could be flooded under extreme wave conditions, making it a highly vulnerable site to climate change (Vousdoukas et al., 2022).

A sustainable protection at Saint Louis?

The sea wall was built with the idea that it would protect the coast for about fifteen years. The aim of this thesis was to determine the natural morphodynamics of the *Langue de Barbarie* on a regional and local scale in order to assess its effectiveness and sustainability. On the basis of the observations made, several lines of action can be explored for the implementation of a long-term protection solution:

- Controlling the sand bar dynamics.

  It has been seen in chapter 4 that the recent accretion of the beach is due to sand bar dynamics. A way to control the sand bar dynamics could be explored (e.g. submerged breakwaters). If such a solution were to be adopted, it should also be borne in mind that the longshore drift along the Senegalese coasts is one of the strongest in the world (Almar et al., 2019b), and that the wave climate (especially during the dry season) is highly energetic (Sadio et al., 2017). These are limiting factors for any type of submerged structure. A study, from numerical modelling for example (Marchesiello et al., 2022), to understand and anticipate the location of the bar split phenomenon could be carried out to better anticipate the location of the accretive phases of the coastline.

- Managing the sand spit length to minimize the erosive feedback on the *up-drift*.

  In chapter 5 it was shown that the length of the spit has a direct effect on the up-drift erosion: the headland provides part of the sediment supply that accumulates at the tip (Dean and Dalrymple, 2001). But the area affected changes with the length of the spit: in the case of the urban beach of Saint Louis, the longer the spit, the more southerly the eroded area. When the spit is long enough, the natural dynamics of the urban area are free from the influence of the spit. Managing the length of the spit by controlling the position of the river mouth could limit the erosion trend towards the city. However, alongshore drift is again a limiting coastal engineering factor at Saint Louis, despite the regular and costly dredging currently undertaken to better control the navigation channel at the mouth of the river.

However, a recent study (Dada et al., 2021) has shown that a project like the one in Saint Louis rarely succeeds if the local population does not feel threatened and/or invested in protecting their environment. This is why communication is a facet that will be discussed below.

Communication and social engineering: an indicator for both scientists and local populations

Soft skills such as communication and transfer were key elements of the PPCS project. If scientists develop strategies to protect the coast, but the authorities and/or the population do not feel the urgency to protect their environment (and vice versa), the action is useless. One of the two parties will not be invested in the project and its action will be diminished. Therefore, during the project period, different axes were set up. Based on the social survey carried out in West African coastal systems (Dada et al., 2021), Olusegun Dada (IRD) and Baba Sy (UGB) carried out a social survey in Saint Louis (March 2022) to find out if the local people are worried about sea hazards, erosion, salinity issues, impact on fishing activities and the global context of the management and extension of the *Langue de Barbarie* sand spit/breaching (see similar survey results in Ghana (Dada et al., 2022)). A specific and detailed questionnaire was designed for the occasion, and a precise mapping of the houses to be surveyed by district was made.

Meetings between the AFD, local authorities and communities were also an important part of the project to monitor progress. On the occasion of the Franco-African summit, the IRD produced a video explaining the situation in Saint Louis and the reasons for such a financial and social investment.

Scientific exchanges and inter-institutional training sessions have been organised. The first took place in Senegal, where IRD/LEGOS and CNES partners organised a training session on the extraction of coastal indicators by video camera using Matlab, the use of Pleiades satellites, and the management of the CoastSat tool for coastal monitoring using Python. The second was in Toulouse in June 2022, where Amadou Diouf, Cheikh Omar Tidjani Cissé and Jean-Paul Youm came to work with satellite DEM products and extract data from the Saint Louis camera. As a result of this collaboration, several papers have been submitted or are in preparation. One recently published paper (Cisse et al., 2022) is based on the DEM generated in chapter 3 and presented in 5.10.2.

5.8.2 The future of satellite tools in coastal engineering

To illustrate satellite performances

The performance of satellites for coastal monitoring has been discussed in the conclusion above and each mission used with its strengths and weaknesses has been listed in Figure 5.9 and discussed in Chapter 2. A wealth of satellite tools are being developed to better serve the needs of coastal engineering issues, such as ASP (Shean et al.) used chapter 3, MicMac (Rupnik et al., 2017, 2018) or CARS (Youssefi et al., 2020; Michel et al., 2020) (a CNES product) to reconstruct the 3D of a terrain. As well as for topography, many works now use satellite imagery to derive bathymetry such as (Traganos et al., 2018; Sagawa et al., 2019; Ashphaq et al., 2021; Taveneau et al., 2022; Almar et al., 2022b; Bergsma et al., 2021; Gawehn et al., 2022) using wave parameter detection (used chapter 4) or bathymetric inversion by water colour (McKinna et al., 2015).

Sentinel-2, Landsat and Pleiades were the missions chosen to address the problems, highlighting the weaknesses of using Pleiades in particular, whose δt is too large to correctly estimate usable near-shore bathymetry. Other satellites such as Jilin (Almar et al., 2022b) or Venµs (Bergsma et al., 2021) showed promising results on the use of satellites for bathymetry estimation with RMS errors of 0.5 m and 1.07 m respectively. However, to answer coastal engineering questions, a satellite with a very high acquisition frequency is preferred to one with high resolution (see section 5.7). Finally, new satellite missions such as CO3D (Constellation Optique en 3D) or Pleiades Neo will be used for coastal engineering purposes.

Earth observation in Africa

Africa has a large proportion of the world's sandy beaches (Figure 5.10 ; (Luijendijk et al., 2018)) and is therefore exposed to a wide range of marine hazards such as coastal erosion and flooding. However, it is difficult to quantify and predict these phenomena and to monitor coastlines because of the lack of available data on the African continent. Recent advances in remote sensing techniques for coastal monitoring have made it possible to access - free of charge - a large dataset that meets the needs of studies to improve decision-making on the implementation of sustainable protection of coastal environments and their resilience to climate change (Alves et al., 2020; Taveneau et al., 2021; Almar et al., 2022c).

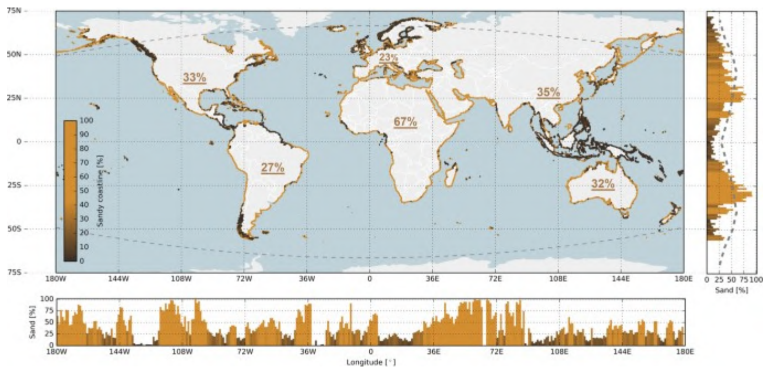

Figure 5.10: World distribution of sandy beaches from (Luijendijk et al., 2018).

Several programs, such as the PPCS project to which this doctoral work sought to respond, have been designed to bring together different countries to improve coastal areas research. Here is a non-exhaustive list of such programs:

- WACA (West Africa Coastal Areas Management Program, 2015).
- WARCO (West African Regional Coastal Observation).
- SCO (Space for Climate Observatory) aiming at bringing together the scientific community, public authorities and businesses around solutions for mitigating and adapting to the impacts of climate change.
- EO AFRICA with the European Space Agency (ESA) that stands for African framework for research, innovation, communities and applications. (`https://eo4society.esa.int/eo-africa/`).
- Copernicus programme (with ESA) that provides free access to satellite data.

Access to free data makes it possible to monitor and study coastal issues in countries where data is lacking. This further emphasises the need to open up the means of good practice in research and reinforces the commitment of scientists to community coding practices with shared platforms such as GitHub (free access to scientific tools ; `https://github.com`), data mapping - webGIS (free map coverage; e.g. `http://www.webgis.com`), data format - FAIR (Findable, Accessible, Interoperable, Reusable) data, accessible cloud computing power - GEE (Google Earth Engine) data, global reanalyses - such as ECMWF's ERA5. These shared sciences enable international collaborations and provide easy access to good quality data for developing countries. However, even when such platforms exist, it is not always obvious how to communicate their content or make use of these data. For example, an initiative is currently underway to develop and improve the global use of data from the Copernicus Marine Service. Space agencies are also very active with several programmes to promote Earth observation data (e.g. SCO, EO4Africa) in support of coastal management programmes (WACA, World Bank) in Africa. Because of their relevance, a list of available open access data and tools by discipline, such as coastal dynamics, could be created and disseminated to the international scientific community - especially in developing countries.

Conclusions et Perpectives

5.9 Conclusions

Comme mentionnées dans la conclusion du chapitre 1, ce travail de thèse vise à répondre à trois questions principales. Ces questions ont été présentées et répondues dans les différents chapitres développés tout au long de ce manuscrit. Nous résumons ici les résultats dans une conclusion qui généralise la réponse à ces trois questions qui sont : quels sont les liens entre les échelles locale et régionale ? Quels sont les échanges sédimentaires entre les parties immergées et émergées de la plage ? Et enfin, les satellites peuvent-ils répondre aux questions précédentes et aux problématiques d'ingénierie côtière ?

5.9.1 Quels sont les liens entre l'échelle locale et l'échelle régionale ?

À Saint Louis, des images satellites à grande couverture spatiale, une caméra installée localement sur la plage, et des données in situ constituent l'ensemble des données disponibles pour l'étude de la morphodynamique de la plage. Actuellement, les études de morphodynamique côtière sont confrontées à un manque de compréhension entre les échelles locale et régionale. La combinaison d'outils permettant de comprendre les liens entre ces deux échelles était un des objectifs du doctorat. À l'origine, ce projet de doctorat a été mis en place en réponse aux dommages causés par la mer dans la ville de Saint Louis, en raison d'une plage qui s'est érodée et est devenue inexistante au fil des ans. Le climat de vagues y étant très énergétique (Sadio et al., 2017; Almar et al., 2019b), les vagues se brisaient sur les maisons emportant avec elles des bâtiments entiers. Au fil du temps, la plage s'est progressivement élargie devant l'enrochement de protection mis en place. Si l'on considère uniquement l'échelle locale (la caméra et les mesures in situ), cette soudaine accrétion aurait pu être attribuée à la structure de protection, ou à la dynamique des barres sableuses qui sont – localement – dans le champ de vision de la caméra. Il n'est donc pas possible de voir que ce système d'érosion/accrétion est une conséquence de la dynamique de structures à plus grande échelle spatiale. En effet, la tendance à l'érosion a été une cause directe de la brèche de 2003 (Rodríguez et al., 2014; Bergsma et al., 2020; Taveneau et al., 2021) (cf. chapitre 5) : alors que la *Langue de Barbarie* s'étirait vers le sud, la partie urbanisée s'érodait peu à peu (Figure 5.8). Ce recul du trait de côte post-brèche (développé au chapitre 3) est en effet principalement dû au processus d'allongement de la flèche : les sédiments s'accumulent progressivement à l'extrémité de la flèche sableuse (au sud) tandis que la partie nord (la zone urbaine dans notre cas) fournit une partie des sédiments qui sont transportés vers le sud par la dérive littorale (Dean and Dalrymple, 2001; Aubrey and Gaines, 1982). Comme la pointe de la flèche sableuse (après 2003) n'était que quelques kilomètres au sud de la ville, la rétroaction négative sur la côte plus au nord était plus intense et induisait des taux d'érosion importants. Avec son allongement progressif, cette rétroaction qui compromettait l'intégrité de la ville de Saint Louis a peu à peu diminué, réduisant avec elle les taux d'érosion (cf. modèle conceptuel 5). Le fait de disposer d'images satellites avec une telle couverture spatiale a permis de construire un modèle conceptuel pour le processus d'allongement de la flèche sableuse afin d'anticiper à la fois son allongement et son rétrécissement en largeur. Selon le modèle, cette tendance à l'érosion doit diminuer lorsque l'extrémité de la flèche est suffisamment éloignée de la ville. Dans ce cas, les échelles locale et régionale se complètent bien : pour mesurer les taux d'érosion (locaux), et pour comprendre quel phénomène est à son origine (régional). Ces travaux illustrent donc l'importance d'étudier les phénomènes locaux à une plus grande échelle spatiale, et donc l'utilité des satellites en matière de suivi des côtes.

5.9.2 Quels sont les échanges sédimentaires entre les parties immergées et émergées de la plage ?

Les échanges sédimentaires d'une plage sableuse ouverte sont complexes et dépendent de plusieurs facteurs : la marée, le vent, les vagues, le niveau de la mer, les interactions humaines (Komar, 2018) pour ne citer que ces exemples. Sur notre principal site d'étude, Saint Louis (Sénégal), il est primordial de comprendre le ou les mécanismes qui pilotent les échanges sédimentaires, car il en va de la protection de la population face au risque d'érosion. Dans le chapitre 2, la tendance à l'érosion autour de la zone urbaine a été mise en évidence (Ndour et al., 2018; Bergsma et al., 2020; Taveneau et al., 2021). Cette érosion massive, initiée par la brèche de 2003, a causé de gros dégâts dans la ville, et un plan de relocalisation des populations les plus menacées a été mis en place. Un enrochement de protection a également été envisagé comme solution à court terme pour compenser l'important recul du littoral (sa construction a commencé fin 2020). La récente accrétion de la plage en 2020 (cf. chapitre 4) a également mis en avant la complémentarité entre les échelles locale et régionale : les données Sentinel-2 haute fréquence permettent d'observer la migration vers la côte de la barre sableuse qui s'est, de manière progressive, complètement soudée au rivage provoquant un élargissement massif et local de la plage. La brèche dans la barre interne, à l'origine du processus de sa migration et puis de sa soudure à la côte (Vidal-Ruiz and de Alegría-Arzaburu, 2020), n'aurait pas pu être détectée avec une étude à l'échelle locale (Figure 5.8).

Cependant, sur l'ensemble de l'année 2020, une anomalie d'accrétion de + 50 m a été enregistrée (cf. chapitre 4) au niveau du quartier précédemment défini comme le plus à risque (où l'enrochement de protection est en cours de construction). Cette anomalie d'accrétion a soulevé plusieurs questions/hypothèses quant à son origine : est-elle due à la dynamique des barres sableuses, à l'enrochement de protection en cours de construction, aux vagues de sable provenant de la côte désertique du Sahara, à l'évolution liée à la flèche sableuse, ou à un changement du régime de vagues ? Nous avons démontré au chapitre 4 que la barre interne, qui s'est rompue lors de conditions de vagues peu énergétiques, a progressivement migré vers la terre pour se souder au rivage, entraînant une accrétion massive et locale (quelques kilomètres longshore) de la plage émergée. Cette accrétion s'est progressivement lissée le long de la côte sous l'influence de la forte dérive littorale.

5.9.3 Les satellites peuvent-ils répondre aux questions précédentes et aux problématiques d'ingénierie côtière ?

Dans le cadre des objectifs du doctorat, plusieurs paramètres ont été étudiés et énumérés ci-dessous (aperçu Figure 5.9). Cependant, les missions satellites utilisées pour calculer ces paramètres à partir d'images à grande couverture spatiale n'ont pas toujours été couronnées de succès. Listons paramètre par paramètre la mission satellite utilisée, le succès ou non de son étude, et quels ont été les facteurs limitants ou qui ont permis la réussite de l'étude. Pour rappel, trois missions satellites ont été utilisées : Pleiades avec une acquisition basse fréquence mais une très haute résolution spatiale, Sentinel-2 et les constellations Landsat avec une acquisition haute fréquence mais une moins bonne résolution spatiale (cf. chapitre 3). Les enjeux de ce doctorat étant avant tout de comprendre les mécanismes et la dynamique du littoral de Saint Louis, des ajustements ont été nécessaires afin de répondre aux problématiques concrètes du projet PPCS.

– Topographie

  La topographie est dérivée de la constellation Pleiades et mieux décrite dans le chapitre 3. Les résultats obtenus viennent avec une erreur métrique qui est moins bonne que ceux de l'étude menée par (Almeida et al., 2019). Cependant, le profil de la plage est bien estimé par le satellite, ce qui permet d'évaluer la pente de la plage comme étant de $\beta \simeq 4$ %. La méthode a malgré tout rencontré quelques limites : l'interface terre/mer est difficile (Loghin et al., 2020) à estimer par le satellite, car la méthode d'estimation de la topographie est basée sur la corrélation de points fixes entre trois images successives dans le temps. Comme la zone de swash est très dynamique, il est impossible avec la méthode de tri-stéréogrammétrie de correctement estimer cette interface terre/mer puisqu'il n'existe pas de points fixes entre ces images – cette distance non évaluable est estimée à environ $\pm$ 10-30 m (cf. chapitre 3), ce qui est une erreur très grande considérant la largeur de la plage étudiée. Le paramètre topographie dans la zone urbaine (échelle locale) n'était donc pas conforme à ce qui était recherché pour les objectifs du projet. À l'échelle régionale, elle a cependant permis d'étudier les échanges sédimentaires nord-sud en captant à la fois le rétrécissement en largeur de la flèche sableuse autour de la zone urbaine, et l'étirement vers le sud de la cette dernière.

– Trait de côte

  Pour la dynamique du littoral, une approche haute fréquence a été choisie en utilisant les missions satellitaires optiques Landsat et Sentinel-2 (cf. chapitre 2). L'étude des variations du trait de côte a permis d'établir un modèle conceptuel de l'allongement de la flèche sableuse (chapitre 5), et de visualiser l'accrétion soudaine de la plage vers la zone urbaine de Saint Louis (chapitre 4). Cet outil était en parfait accord pour répondre aux problématiques du projet PPCS, car il a permis de débloquer la compréhension de la morphodynamique de la plage de Saint Louis à une échelle spatiale régionale.

– Bathymetrie

Dans un premier temps, la bathymétrie a également été dérivée de la constellation Pleiades (cf. chapitre 4). La zone au large est correctement estimée avec la technique d'inversion de la profondeur, mais l'estimation de la zone proche du rivage s'avère être est un échec. La position de la barre sableuse peut cependant être détectée par une anomalie de profondeur – la bathymétrie devient localement proche de zéro vers sa position – mais avoir des données de position de barre tous les 6 mois est largement insuffisant pour déterminer sa dynamique. L'utilisation d'images Pleiades avec un écart δT d'environ 9 secondes entre celles-ci est une énorme limitation, pour estimer les paramètres de vague, pour un site dont la période de vague moyenne est de $T_P = 9.23$ s. L'estimation de la bathymétrie par utilisation des images Pleiades est donc insuffisante pour répondre aux objectifs du projet, c'est pourquoi une approche optique régionale à haute fréquence a été mise en place pour comprendre la dynamique des barres sableuses.

– Barres sableuses

  Les barres sableuses, dont la position est dérivée de l'imagerie optique Sentinel-2, peuvent être détectées grâce à l'écume induite qui est générée lorsqu'une vague se brise sur ces structures sous-marines. L'acquisition à haute fréquence du satellite Sentinel-2 permet d'étudier la morphodynamique de ces éléments (cf. chapitre 4). Les barres sableuses sont des éléments très dynamiques et la résolution sol/pixel de 10 m du satellite S2, ainsi que sa revisite régulière en font un outil parfaitement adapté pour en suivre leur position.

En résumé, les satellites peuvent répondre aux problématiques de l'ingénierie côtière selon les mécanismes que l'on souhaite étudier. Pour répondre aux objectifs du projet PPCS, une haute précision n'est pas nécessaire, mais une acquisition à haute fréquence l'est. En effet, et comme expliqué ci-dessus, le swash induit une erreur de quelques dizaines de mètres dans la détection du trait de côte : il n'y a pas besoin de données de haute précision dans ce cas puisque l'erreur restera grande dans tous les cas. De plus, les satellites S2 ont pu détecter la brèche puis la soudure de la barre sableuse qui est responsable de l'accrétion massive devant le quartier le plus menacé. Ce phénomène aurait facilement pu être manqué si les barres sableuses étaient étudiées à une échelle locale uniquement. Pour conclure sur l'outil satellitaire, il est nécessaire de choisir la mission appropriée en fonction du processus côtier que l'on veut étudier.

5.10 Perspectives

Les plages sableuses ont une dynamique très complexe qui dépend de plusieurs paramètres ayant un impact à différentes échelles spatio-temporelles. La mise en place d'une stratégie de protection de ces zones vulnérables nécessite une bonne compréhension de leur dynamique intrinsèque, qui ne peut pas être négligée. Au travers de ce manuscrit, deux questions importantes ont été soulevées :

- Que faire à Saint Louis avec les nouvelles connaissances apportées par ce travail de doctorat ?
- Quels sont les besoins des satellites en matière de suivi des côtes ?

5.10.1 La dynamique de la plage à Saint Louis

On peut constater à quel point le système côtier de Saint Louis est complexe et dynamique, et combien il est difficile d'anticiper tous les mécanismes côtiers (flèche sableuse, barre sableuse, anthropisation) qui peuvent avoir un impact sur les populations locales. Nous explorons ici les possibilités de mieux protéger le littoral et de mieux anticiper les événements catastrophiques sur la base des recherches qui ont été menées. En effet, l'enrochement construit devant le quartier le plus à risque de Saint Louis est une solution court terme (une quinzaine d'années tout au plus) dont le rôle était de protéger le plus rapidement possible les populations. In fine, il est essentiel de comprendre la morphodynamique de la Langue de Barbarie, car un autre moyen de protection devra être mis en place d'ici quelques années. Avec le changement climatique, l'accentuation des phénomènes tels que l'érosion côtière et les submersions marines vont croître (Gornitz, 1991; Small et al., 2000; Melet et al., 2018, 2020a), mettant en péril l'intégrité de la ville de Saint Louis. Des témoignages rapportent que les submersions marines affectent grandement les activités socio-économiques de la ville, et une étude récente montre que la hausse du niveau de la mer est le facteur qui impacte le plus leur occurrence (Cisse et al., 2022). La Langue de Barbarie ayant une topographie très basse ($\simeq$ 2 m au-dessus du niveau de la mer ; chapitre 3), plus de la moitié de ces terres pourrait être inondée lors de conditions de vagues extrêmes, ce qui en fait un site hautement vulnérable au changement climatique (Vousdoukas et al., 2022).

Un moyen de protection pérenne

L'enrochement de protection a été construit avec l'idée qu'il protégerait la côte pendant une quinzaine d'années. Ce travail de thèse avait pour but de déterminer à l'échelle régionale et locale la morphodynamique naturelle du littoral de la Langue de Barbarie. Sur la base des observations de ce travail, plusieurs pistes peuvent être explorées quant à la mise en place d'une solution de protection longue durée :

– Contrôler la dynamique des barres sableuses.

  Il a été vu au chapitre4 que l'accrétion récente de la plage est due à la dynamique des barres sableuses. Une façon de contrôler la dynamique des barres sableuses pourrait être explorée au travers d'une étude renforcée (atténuateur de houle par exemple). Si une telle solution devait être employée, il faudrait également garder à l'esprit que la dérive littorale le long des côtes sénégalaises fait partie des plus puissantes dérives au monde (Almar et al., 2019b), et que le climat des vagues (surtout pendant la saison sèche) est très énergétique (Sadio et al., 2017). Ce sont des facteurs limitants pour tout type de structure immergée. Une étude, à partir de modélisations numériques par exemple (Marchesiello et al., 2022), permettant de comprendre et d'anticiper la localisation du phénomène de brèche dans la barre interne pourrait être menée afin de mieux anticiper la localisation des phases d'accrétives du trait de côte.

– Gérer la longueur de la flèche sableuse pour minimiser la rétroaction érosive sur la zone *amont.*

  Il a été montré chapitre 5 que la longueur de la flèche sableuse a un impact direct sur la tendance à l'érosion ou non de la partie amont de celle-ci. Une partie de l'apport sédimentaire s'accumulant au bout de la flèche vient directement de la zone amont (Dean and Dalrymple, 2001). Mais la zone impactée change avec l'allongement de la flèche : dans le cas de Saint Louis, plus la flèche s'allonge, plus la zone d'érosion migre dans la même direction que celle du phénomène d'allongement. Lorsque la flèche est suffisamment longue, la dynamique naturelle de la zone urbaine s'affranchit de la zone d'influence de la flèche sableuse. La gestion de la longueur de la Langue de Barbarie par le contrôle de la position de l'embouchure de la rivière pourrait limiter la tendance à l'érosion de la ville.

Cependant, une étude récente (Dada et al., 2021) a prouvé que si la population locale ne se sent pas menacée et/ou investie dans la protection de son environnement, un projet tel que celui mis en place à Saint Louis ne réussit que rarement. C'est pourquoi la communication est une facette qui est abordée ci-dessous.

La communication : un indicateur pour les scientifiques et les populations locales

Les *soft skills* comme la communication et la transmission ont été des éléments clés du projet PPCS. En effet, si les scientifiques mettent en place des stratégies pour protéger le littoral alors que les autorités locales et/ou la population ne ressentent pas l'urgence de protéger leur environnement (et inversement), l'action est inutile. L'une des deux parties ne sera pas investie dans le projet et son action s'en trouvera diminuée. C'est pourquoi, durant la période du projet, différents axes ont été mis en place. Sur la base de l'enquête sociale menée dans les systèmes côtiers d'Afrique de l'Ouest (Dada et al., 2021), Olusegun Dada (IRD) et Baba Sy (UGB) ont réalisé une enquête sociale à Saint Louis (mars 2022) pour voir si les habitants se sentent concernés par les risques marins, l'érosion, les problèmes de salinité dans les réserves d'eau douce, les impacts sur les activités de pêche, et le contexte global de la gestion et de l'allongement de la Langue de Barbarie (voir étude similaire au Ghana (Dada et al., 2022)). Un questionnaire spécifique et détaillé a été créé pour l'occasion, et une cartographie précise des habitations à interroger par quartier a été établie.

Des réunions entre l'AFD et les autorités locales ont également constitué une part importante du projet pour suivre l'avancement des travaux. À l'occasion du sommet France-Afrique, un clip vidéo a été réalisé par l'IRD pour expliquer la situation à Saint Louis et pourquoi un tel investissement financier et social a été déployé.

Des sessions d'échanges scientifiques et de formation inter instituts ont été organisées. La première a eu lieu au Sénégal où Rafael Almar, Erwin Bergsma et moi-même avons réalisé une session d'enseignement sur l'extraction d'indicateurs côtiers par caméra avec Matlab, l'utilisation des satellites Pléiades, et la gestion de l'outil CoastSat (Vos et al., 2019) pour la surveillance du littoral respectivement. La seconde s'est déroulée à Toulouse en juin 2022, où Amadou Diouf, Cheikh Omar Tidjani Cissé et Jean-Paul Youm sont venus travailler sur des produits DEMs satellitaires et continuer à extraire des données de la caméra de Saint Louis. Suite à cette collaboration, plusieurs articles sont à soumettre, ou ont été soumis. Un travail récemment publié (Cisse et al., 2022) et basé sur le chapitre DEM généré 3 est présenté 5.10.2.

5.10.2 Le futur des outils satellitaires en ingénierie côtière

Illustration des performances satellites

La performance des satellites pour le suivi des côtes, les missions utilisées, et la mise en avant de ses forces et ses faiblesses a été listée et discutée dans la conclusion ci-dessus (Figure 5.9 et chapitre 2). Beaucoup d'outils exploitant des images satellitaires sont en cours de développement pour mieux répondre aux besoins de l'ingénierie côtière, comme ASP (Shean et al.) utilisé au chapitre 3, MicMac (Rupnik et al., 2017, 2018), ou CARS (Youssefi et al., 2020; Michel et al., 2020) (outil du CNES) qui permettent de reconstruire la 3D d'un terrain. De même que pour la topographie, de nombreux travaux utilisent maintenant des images satellites pour calculer des bathymétries à grande échelle spatiale comme (Traganos et al., 2018; Sagawa et al., 2019; Ashphaq et al., 2021; Taveneau et al., 2022; Almar et al., 2022b; Bergsma et al., 2021; Gawehn et al., 2022) utilisant comme méthode la détection des paramètres de vague (utilisée chapitre 4), ou encore l'inversion bathymétrique par couleur de l'eau (McKinna et al., 2015).

Sentinel-2, Landsat et Pleiades sont les missions qui ont été choisies pour répondre à nos problématiques, en gardant cependant en tête les faiblesses de l'utilisation de Pleiades décrites plus tôt dont le δT est trop grand pour estimer correctement une bathymétrie exploitable, ou une interface terre/mer précise. D'autres satellites comme Jilin (Almar et al., 2022b) ou Venµs (Bergsma et al., 2021) ont montré des résultats prometteurs sur l'utilisation des satellites pour l'estimation de la bathymétrie avec des erreurs RMS respectives de 0.5 m et 1.07 m. Cependant, pour répondre à des problématiques de génie côtier, un satellite à très haute fréquence d'acquisition est préféré à un satellite à haute résolution (cf. section 5.7). De nouvelles missions satellitaires telles que CO3D (Constellation Optique en 3D), ou Pleiades Neo sont encore à explorer pour des fins de génie côtier.

Observation de la terre en Afrique

L'Afrique contient une grande proportion des plages sableuses du monde (Figure 5.10 ; (Luijendijk et al., 2018)), et est donc très exposée à une multitude de risques marins tels que l'érosion côtière et les submersions marines. Cependant, il est difficile de quantifier et d'anticiper ces phénomènes et de surveiller les rivages, car la banque de données disponible sur le continent africain est limitée. Les progrès récents des techniques de télédétection pour la surveillance des côtes ont permis l'accès - gratuit - à un large ensemble de données qui répond aux besoins d'études pour améliorer la prise de décision concernant la mise en œuvre de protections durables des environnements côtiers et leur résilience au changement climatique (Alves et al., 2020; Taveneau et al., 2021; Almar et al., 2022c).

Plusieurs programmes, comme le projet PPCS auquel ce travail de doctorat a cherché à répondre, ont été conçus pour rassembler différents pays afin d'améliorer la recherche sur les zones côtières. Voici une liste non exhaustive de ces programmes :

- WACA (West Africa Coastal Areas Management Program, 2015).
- WARCO (West African Regional Coastal Observation).
- SCO (Space for Climate Observatory) avisant à rassembler la communauté scientifique, les autorités publiques et les entreprises autour de solutions pour atténuer les effets du changement climatique et s'y adapter.
- EO AFRICA avec l'Agence spatiale européenne (ESA), qui représente le cadre africain pour la recherche, l'innovation, les communautés et les applications (`https://eo4society.esa.int/eo-africa/`).
- Copernicus programme (ESA) qui permet l'accès gratuit à des données satellites.

L'accès à des données gratuites permet de surveiller et d'étudier les problèmes côtiers dans les pays où les données font défaut. Cela souligne la nécessité d'ouvrir les moyens de recherche et renforce l'engagement des scientifiques dans les plateformes partagées telles que GitHub (accès gratuit aux outils scientifiques ; `https://github.com`), webGIS (couverture cartographique gratuite ; `http://www.webgis.com`), les données FAIR (Findable, Accessible, Interoperable, Reusable), les données GEE (Google Earth Engine), les données ERA5... L'ouverture et le partage de la science permettent de générer des collaborations internationales et de faciliter l'accès à des données de bonne qualité pour les pays en développement. Cependant, même si ces plateformes existent, la communication de leur contenu, ou l'exploitation de ces données n'est pas toujours évidente. Par exemple, il y existe actuellement une initiative sur le développement et une meilleure utilisation des données du service maritime de Copernicus dans le monde entier. Les agences spatiales sont également très actives avec plusieurs programmes de promotion des données d'observation de la Terre (entre autres, SCO, EO4Africa) en soutien aux programmes de gestion côtière (WACA, de la banque mondiale) en Afrique. En raison de leur pertinence, la liste de données et d'outils disponibles en accès libre par discipline, comme celle de la dynamique côtière, pourrait être créée et diffusée à la communauté scientifique internationale – notamment dans les pays en développement.

Appendix A

List of articles in collaboration published, or to be published:

- Observing and predicting coastal erosion at the Langue de Barbarie sand spit around Saint Louis (Senegal, West Africa) through satellite-derived digital elevation model and shoreline (2021) ; Remote Sensing ; Taveneau A., Almar R., Bergsma E., Sy B.A., Ndour A., Sadio M, Garlan T. ; `https://doi.org/10.3390/rs13132454`.
- Satellite-Based Land/sea Continuum: An Application to Monitor the Saint Louis Coast (senegal, West Africa) (2022) ; The International Archives of Photogrammetry, Remote Sensing and Spatial Information Sciences ; Taveneau A., Almar R., Bergsma E.W.J., Sy B., Ndour A.
- On the cyclic nature of wave-dominated sand spits with implications for coastal zone management ; Taveneau A., Almar R., Bergsma E.W.J. ; *(submitted)*.
- Video monitoring of Saint Louis urban beach (Senegal): documenting a rapid accretive sand wave: Diouf, A., Almar, R., Cisse, C.O., Sy, B., Sy, B., Taveneau, A., Sakho, I., Sow, B., Abesselo, G., Ndour, A., Ba, K., Montano, J., Bersgma, E.W., Camara, I. (*draft*).
- Sand bar and shoreline monitoring through Sentinel-2 and Landsat regular-revisit satellites at Saint Louis (Senegal, West Africa) : Taveneau A., Almar R., Bergsma, E. ; (*draft*).
- Extreme coastal water levels with potential flooding risk at the low-lying Saint Louis historic city, Senegal (West Africa) (2022) ; Front. Mar. Sci. (Coastal Ocean Processes) ; Cissé C.O.T., Brempong E., Taveneau A., Almar R., Sy B.A., Angnuureng D.B. ;`https://doi.org/10.3389/fmars.2022.993644`.
- Suivi par satellite de l'évolution du trait de côte de plages aménagées sur la Petite côte (Sénégal, Afrique de l'Ouest) : cas de Rufisque, Ndayane et Saly ; Cissé C.O.T., Taveneau A.
- Extreme coastal water levels evolution at Dakar (Senegal, West Africa) ; Cissé C.O.T., Youm J.P.M., Jolicoeur S., Almar, R., Taveneau A., Sy B.A. ; (*submitted*).

remote sensing

Article

Observing and Predicting Coastal Erosion at the Langue de Barbarie Sand Spit around Saint Louis (Senegal, West Africa) through Satellite-Derived Digital Elevation Model and Shoreline

Adélaïde Taveneau [1,*,†], Rafaël Almar [1,†], Erwin W. J. Bergsma [2,†], Boubou Aldiouma Sy [3], Abdoulaye Ndour [4], Mamadou Sadio [4] and Thierry Garlan [5]

[1] Institut de Recherche pour le Développement, LEGOS (IRD/CNRS/CNES/Université de Toulouse), 31400 Toulouse, France; rafael.almar@ird.fr
[2] Centre National d'Etudes Spatiales (CNES), 31400 Toulouse, France; erwin.bergsma@cnes.fr
[3] Leidi Laboratory, Department of Geography, Territorial Dynamics and Development, Gaston Berger University (UGB), SN-SL, Saint Louis 46024, Senegal; boubou-aldiouma@ugb.edu.sn
[4] Laboratory of Sedimentology, Department of Geology, Faculty of Sciences and Technics, Cheikh Anta Diop University (UCAD), SN-DK, Dakar 12500, Senegal; abdoulaye17.ndour@ucad.edu.sn (A.N.); sadiomamadou@yahoo.fr (M.S.)
[5] Service Hydrographique et Océanographique de la Marine (SHOM), 29240 Brest, France; thierry.garlan@shom.fr
* Correspondence: adelaide.taveneau@ird.fr
† These authors contributed equally to this work.

check for updates

Citation: Taveneau, A.; Almar, R.; Bergsma, E.W.J.; Sy, B.A.; Ndour, A.; Sadio, M.; Garlan, T. Observing and Predicting Coastal Erosion at the Langue de Barbarie Sand Spit around Saint Louis (Senegal, West Africa) through Satellite-Derived Digital Elevation Model and Shoreline. *Remote Sens.* **2021**, *13*, 2454. https://doi.org/10.3390/rs13132454

Academic Editor: Dimitris Poursanidis

Received: 3 May 2021
Accepted: 20 June 2021
Published: 23 June 2021

Abstract: Coastal erosion at Saint Louis in Senegal is affecting the local population that consists of primarily fishermen communities in their housing and their access to the sea. This paper aims at quantifying urban beach erosion at Saint Louis, Senegal, West Africa which is located on the northern end of the 13 km long *Langue de Barbarie* sand spit. The coastal evolution is examined quantitatively over a yearly period using Pleiades sub-metric satellite imagery that allows for stereogrammetry to derive Digital Elevation Models (DEMs). The comparison with ground truth data shows sub-metric differences to the satellite DEMs. Despite its interest in remote areas and developing countries that cannot count on regular surveys, the accuracy of the satellite-derived topography is in the same order as the coastal change itself, which emphasizes its current limitations. These 3D data are combined with decades-long regular Landsat and Sentinel-2 imagery derived shorelines. These observations reveal that the sand spit is stretching, narrowing at its Northern part while it is lengthening downdrift Southward, independently from climatological changes in the wave regime. A parametric model based on a stochastic cyclic sand spit behaviour allows for predicting the next northern opening of a breach and the urban erosion at Saint Louis.

Keywords: earth observations; Pleiades; satellites; topography; sand spit; morphodynamics; coastal engineering; coastal vulnerability; modeling

1. Introduction

The African continent contains the largest percentage of dynamic sandy coasts worldwide (66% [1]). Hence, it makes the African continent particularly exposed to sea-level rise and coastal erosion. Given this, and the fact that the majority of the population lives close to the coastline [2,3], it is paramount to understand and act upon identified threats to ensure the sustainability of these coastal environments. This is, even more, highlighted given that 80% of the West African population lives at the coast coinciding with the presence of major mega-cities and infrastructures which need increased protection against increasing hazards [4–6]. At the same time, climate change will exacerbate sea level rise and sea hazards, and will compound the current problems [7–9]. Coastal management is traditionally carried out by implementing "stabilization" of the cross-shore position and shape of the shoreline. However, this approach has been proven not always effective due to the lack of consideration of the integrated complexity of coastal dynamics [10]. Alternatively, an increasing interest in adaptable, sustainable and effective coastal protection measures to preserve these highly variable sandy coastlines can be observed recently. For example, dynamic cobble revetment and protection that mimic natural beach profiles (see a review [11]), or nature-based solution to anticipate coastal vulnerability due to sea hazards and climate change [12]. These solutions stabilise the upper beach and provide over-topping protection. Before such a solution can be implemented, it is necessary to quantify the morphodynamics of the beach such as the natural trend and variability. In coastal engineering, access to detailed coastal topography is, therefore, crucial [13,14] for the implementation of concrete solutions, planning and risk mitigation [15]. Besides local conventional topography measurements with, e.g., GPS, high-resolution digital elevation models (DEMs) derived from space are emerging as an efficient alternative, covering large regional as sand spits (inaccessible) areas to quantify the evolution of beaches [16–22].

Sand spits are particularly dynamic areas and their morphological evolution relies on many parameters such as sediment availability, human interactions, or sea-level rise [23–25]. The understanding of a sand spit evolution represents a major challenge due to their socio-economic and ecological matters [26–28]. This is why the satellite monitoring of sand spits provides the following interests: obtaining data merely with a regional coverage [29], and offering an effective and accurate methodology for monitoring their morphological evolution as it was done on the Douro estuary [30].

Conventional coastal monitoring in situ measurements collected with Real Time Kinematic GPS (RTK-GPS) systems, or newer approaches with drones or video-based techniques [31–34] are reliable, but limited to the local scale. Yet, to accurately estimate erosional coastal processes, it is essential to fully understand beach morphodynamics at a regional scale. DEMs derived from remote sensing techniques such as airborne LiDAR (Light Detection and Ranging) are among one of the solutions to obtain these data accurately [16] at a larger spatial scale however airborne LiDAR acquisitions remain costly. Alternatively, on-demand optical satellites such as Pleiades (CNES/Airbus) or WorldView-3 deliver images with decimetric resolution and worldwide coverage. These types of satellites embody an interest in the monitoring of rapid evolution such as the impact of a storm on beach erosion at regional scale [19,20,35]. These agile satellites also offer the novel opportunity to derive topography and bathymetry DEMs from a single overpass, [17,36,37], with a vertical accuracy and precision for topography that is similar to state-of-the-art survey methodologies for coastal monitoring (0.35 m $\leq RMSE \leq$ 0.48 m [37]).

This work aims to improve our understanding of the observed severe erosion of the urbanized area of Saint Louis (Senegal, West Africa), a UNESCO world heritage historical city, built on the dynamic *Langue de Barbarie* sand spit [38,39]. We analyze the local and regional beach dynamics related to the Southwards extension and narrowing of the *Langue de Barbarie* where a breach was artificially conducted in 2003, leading to morphological lengthening of the sand spit and increased erosion at the Saint Louis urban area. This work also offers a pioneering opportunity to combine regular revisit and long term Landsat and Sentinel-2 missions with new possibilities offered by the sub-metric very high-resolution satellite-derived DEMs in a coastal engineering study with a new detailed regional vision of the topography evolution over time.

2. Materials

2.1. Study Site: Saint Louis (Senegal)

The *Langue de Barbarie* (Northern Senegal, Figure 1) is located between Saint Louis and the mouth of the Senegal River and the Atlantic ocean. Due to a strong hydro-sedimentary environment—dominated by strong oblique waves (mainly in the northwest direction) which results in one of the most powerful littoral sediment transports (LST) in the world—the sand spit is very dynamic [38,39]. Thus, the coastline around Saint Louis and the

Langue de Barbarie is subject to a large Southwards sediment transport, leading to significant morphological changes and ultimately erosion [38,40]. The tidal regime is semi-diurnal and micro-tidal: 0.5 m at neap tides and 1.6 m at spring tides. Over the last century, the length of the sand spit fluctuated between 10 km and 30 km and primarily migrated Southwards. A major flood in Saint Louis in October 2003 required an urgent decision—an artificial breach was initiated in the barrier island to alleviate extreme water levels on the Senegal River at the city of Saint Louis. The breach which was initially 4 m wide, rapidly widened to function as the new river mouth. The width of the river mouth increased to nearly 2 km in October 2006 and the former river mouth further downstream closed [38,40]. During the post-breach (after 2003) period, the width of the new river entrance stabilized between 0.5 km and 1 km. This stabilisation is linked to a balance between the hydraulic efficiency of the river, including tidal flow, and the energy of the incident waves and sediment bypass [38,41]. From 2003 to 2011, the length of the sand spit, and the position of the river mouth have been stable, while from 2012 onward the sand spit has migrated Southward with a migration rate of about 600 m/year [42]. Simultaneously (after the post-2003 breach), the sand spit has shown cross-shore erosion trends, at a rate of −4.2 m/year [4], which seems to be directly linked to the artificial breach in 2003 [40,42].

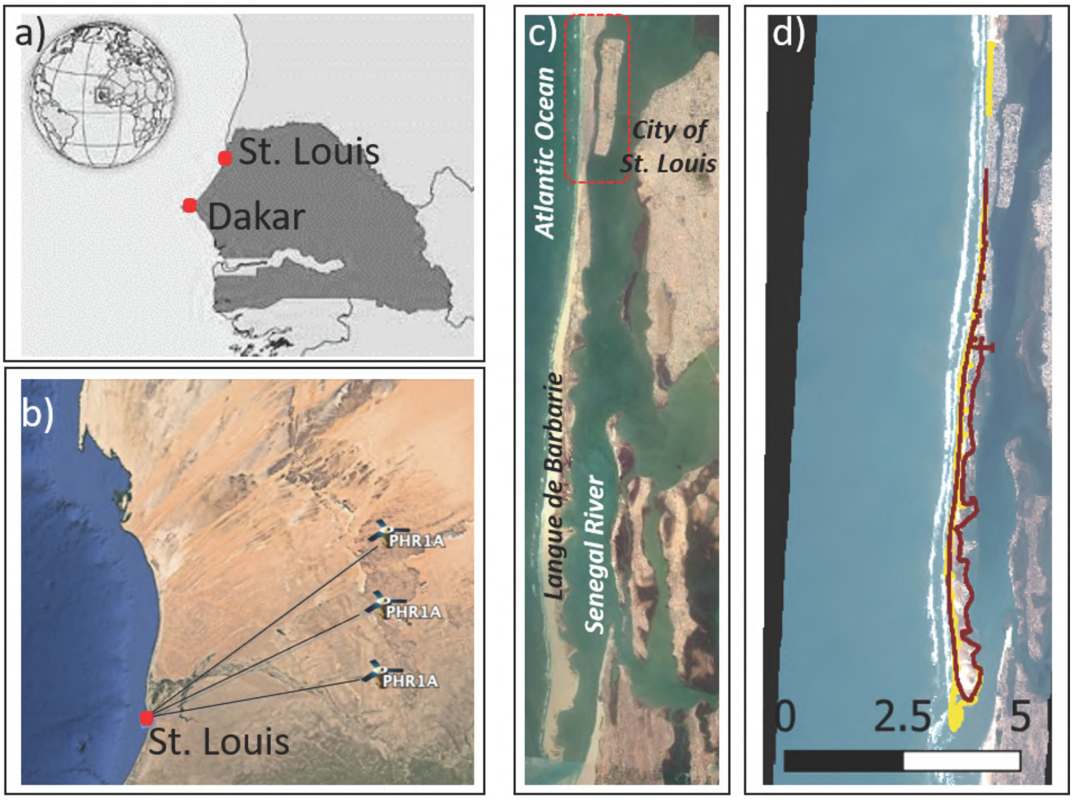

Figure 1. (**a**) Localisation of the city of Saint Louis (Senegal). (**b**) Data acquisition by Pleiades satellite. (**c**) Overview of the *Langue de Barbarie* and localisation of the urban area in red. (**d**) localisation of the in situ data—March 2019 in red and March 2020 in yellow with a km scale.

2.2. Satellite Images

2.2.1. On-Demand Very High Resolution Pleiades Images

The Pleiades satellites, 1A and 1B—respectively launched in 2011 and 2012—orbit out-of-phase at an altitude of 694 km. In addition to single or (tri)stereo images, the Pleiades constellation has the capability to acquire a burst of up to 12 images during a single pass. At Saint Louis, such burst and tri-stereo images (>3 to 12 images) are collected bi-yearly (Figure 1b). In this work, we use the satellite data collected on the 2 March 2019 and the 11 March 2020. The meteorological conditions for the two satellite acquisitions are given further down. Panchromatic and multi-spectral images were collected with a respective ground pixel-resolution of 0.5 m and 2 m.

The tri-stereo Pleiades images were collected at the across-orbit angle 25°, and −17°, for March 2019 and March 2020, respectively, resulting in a difference of 42° between the two acquisitions. For each of the two acquisitions, the time difference between the individual images is set to $dT \simeq 6$ s. This gives a base to height ratio for the two data sets of $B/H = 0.12$. In general, for flat areas a low B/H value gives a better height accuracy of the stereoscopy [43]. The Pleiades images were acquired at an approximately equal tidal elevation of +0.8 m.

Around the same time of the satellite acquisitions (from 2 to 5 March 2019 and 7–10 March 2020), field campaigns were carried out to obtain ground-truth data-sets over a distance 13 km along the *Langue de Barbarie* (Figure 1c), at low tide conditions (0.8 m). An RTK-GPS system was used to carry out topographic surveys, that serve as the ground-truth to validate satellite-derived topography (Figure 1d).

2.2.2. Regular-Revisit Long Term Landsat and Sentinel-2 Images

Landsat optical satellites were launched by the National Aeronautics and Space Administration (NASA) in 1984 for Landsat 5 (L5), 1999 for Landsat 7 (L7) and 2013 for Landsat 8 (L8). They orbit at an altitude of 705 km and have a cycle of about 16 days. They provide multi-spectral imagery with a 30 m resolution.

Sentinel-2A and 2B were launched in 2013 and 2015, respectively, and are part of the European program Copernicus. They orbit at an altitude of 786 km, the resolution of their imagery is 10 m, and they can revisit the same location every 5 days. Landsat and Sentinel imagery is freely available, and regular visits to the same location provide a wealth of data [29,44]. This allows to monitor a specific area with a good resolution on a regional scale and to follow fast events such as storms.

3. Methods

3.1. Pleiades-Derived Topography

The coastal DEMs (Digital Elevation Models) are derived from the sensor-level Pleiades panchromatic images (0.5 m resolution) using a tri-stereogrammetry method with the AMES Stereo Pipeline (ASP) software [45] to produce a 2 m resolution DEM. Another robust open-access tool—the CNES Algorithms to Reconstruct Surface (CARS)—was also used to produce DEMs of the study site [46,47]. For the tri-stereo methodology—both ASP and CARS—three panchromatic images are taken as input (0.5 m resolution), are correlated pair by pair, and then a final correlation between the two correlated pairs gives the output DEM. Both methods use the Rational Polynomial Coefficient (RPC)—which is provided with the imagery—and gives a relationship between the satellite image coordinates and the ground coordinates. The planimetric coordinates were referenced to the ellipse and the resulting DEM was subsequently orthorectified.

Then a co-registration algorithm that removes DEM offsets, checks for altitude-dependent biases, checks for sensor-specific and higher-order altitude-related biases [48] is applied. This algorithm. [49] is developed based on the method of Nuth and Kääb [48], and is a robust analytical solution based on the residuals of the pairwise elevation difference, and the aspect and slope of the study site to correct for bias and errors between the DEMs. Finally, all the resulting DEMs were vertically fixed using a set of ground control points (GCPs) collected during the in situ acquisitions of March 2019. It is only after this post-processing sequence that the DEMs [50] of March 2019 and March 2020 are compared to infer a Spatio-temporal evolution of the *Langue de Barbarie*.

The AMES Stereo Pipeline software has a feature that ortho-rectifies a sensor-level satellite image using its geometry by the accompanied RPC file, and in the process creates a DEM at a set resolution [45]. The method is as follows: a DEM is calculated from three raw satellite images (panchromatic or multispectral) using the tri-stereogrammetry method described above. This DEM is automatically ortho-rectified, after which the satellite images at the sensor are projected onto the DEM [45], so that the output images are fully ortho-rectified.

To validate the satellite-based topography method, an inter-comparison between in situ data and Pleiades-derived topographies has been realized Section 4.1. DEMs were individually median-filtered in two dimensions (over 10 m longshore, and 5 m cross-shore). The obtained beach profiles were averaged and the vertical offset between the Pleiades data and the in situ data has been removed from the Pleiades data.

The uncertainty of the method at the lower beach related to high-frequency unresolved hydrodynamics is estimated using the swash excursion length, computed as follows:

$$swash = \frac{1.1}{2}\left(1.56T^2 H_S(0.5625\beta^2 + 0.004)\right)^{\frac{1}{2}} \tag{1}$$

wherein T is the wave period, H_S the significant wave height and β the beach slope derived from Pleiades imagery. This equation is the up-to-date reference formulation relevant for a wide range of conditions [51,52].

3.2. Multi-Sensor Shorelines

Waterlines are detected from the ortho-rectified satellite imagery using the Normalized Difference Water (NDW) index in Section 4.2. The NDWI is a fraction between the green and near infra-red bands.

$$NDWI = \frac{Green_{band} - InfraRed_{band}}{Green_{band} + InfraRed_{band}} \tag{2}$$

As water bodies largely absorb light in the visible to the infrared electromagnetic spectrum domain, NDWI uses green and near-infrared bands, respectively, $Green_{band}$ and $InfraRed_{band}$ parameters in Equation (2) to identify water bodies [53]. Once waterbodies are distinguished, the shoreline is determined as the intersect between these bodies. The calculated NDWI ranges values $\in [-1;0]$ representing bright surfaces with no vegetation or water content. The shorelines mapped Figure 5 are derived from Landsat and Sentinel-2 satellite imagery using the open-access tool CoastSat [44]. This python toolkit uses Landsat 5-7-8 for 2003 to 2014, and Sentinel-2 for 2015 to 2020 data from Google Earth Engine, and provides multi-year time series of any sandy coast in the world. Cropping those images around our study site enabled the easy retrieval of the *Langue de Barbarie* shorelines and tip positions. To be consistent with the Pleiades data, the shorelines have been mapped around March for each year. Sentinel-2 imagery allows coastal monitoring of fast events as it can revisit the same location within few days (approximately every 5 days for our study site) [29].

The volume of beach sand was calculated by multiplying the area of the sand spit tip obtained from the coastlines (CoastSat [44]) and the mean land height obtained from Pleiades DEMs. To properly understand the magnitudes obtained on the sand volumes of the tip of the *Langue de Barbarie*, the annual LST was calculated from the ERA5 data by annually averaging the results from Kaczmarek [54], Kamphuis [55], and Bayram's formula [56]. The spit growth rates, derived from that LST estimates, has been computed as follows:

$$R_S = \frac{Q}{B_S(D_B + D_C)} \tag{3}$$

wherein Q is the LST, B_S the constant spit width, D_B the berm height and D_C the depth of closure [27].

4. Results

4.1. Comparison with Ground Truth

Three cross-shore transects (TA, TB and TC; Figure 2a) have been selected on the *Langue de Barbarie* sand spit to illustrate the performance of the satellite-derived topography in comparison to the field data. These cross-shore transects are at the same location for the

2019 and 2020 data sets. For the inter-comparison, the DEMs used are the ones produced with ASP [45], as the RMSE is higher than 3 m for the DEMs produced with CARS [46,47].

The beach profiles are generally well captured by the Pleiades derived topography (Figure 2a) considering a root mean squared error between 0.71 m $\leq RMSE \leq$ 1.19 m in March 2019, and 0.97 m $\leq RMSE \leq$ 1.07 m in March 2020 (Table 1). The overall RMS errors for 2019 and 2020 are $RMSE_{2019} = 1.31$ m and $RMSE_{2020} = 1.15$ m, respectively. Considering that the in situ surveys and Pleiades acquisitions were few days apart, small morphological changes may have occurred at the lower-beach zone within this period resulting in minor differences. It is also apparent that the stereoscopy method underperforms in 2019 at the lower beach face as for 0 m to 30 m cross-shore no topography could be derived (Figure 2b).

Table 1. Difference between satellite-based DEM and RTK-GPS survey (RMS error) for each cross-shore transect.

Transects	RMSE (m) 03/19	RMSE (m) 03/20
T1	1.19	0.92
T2	1.01	0.97
T3	0.72	1.07

The annual change in topography can be observed on the beach cross-shore transects (Figure 2b). An accretion is observed at the Northern transect, which is closer to the urban area according to Figure 1c, and the beach seems relatively stable for the other two (TB and TC ; Figure 2b). TA shows a greater discrepancy with in situ measurements than the other two transects. This can be explained by the particularly energetic wave climate during the 2019 survey (Table 2)which can impact the lower beach [57].

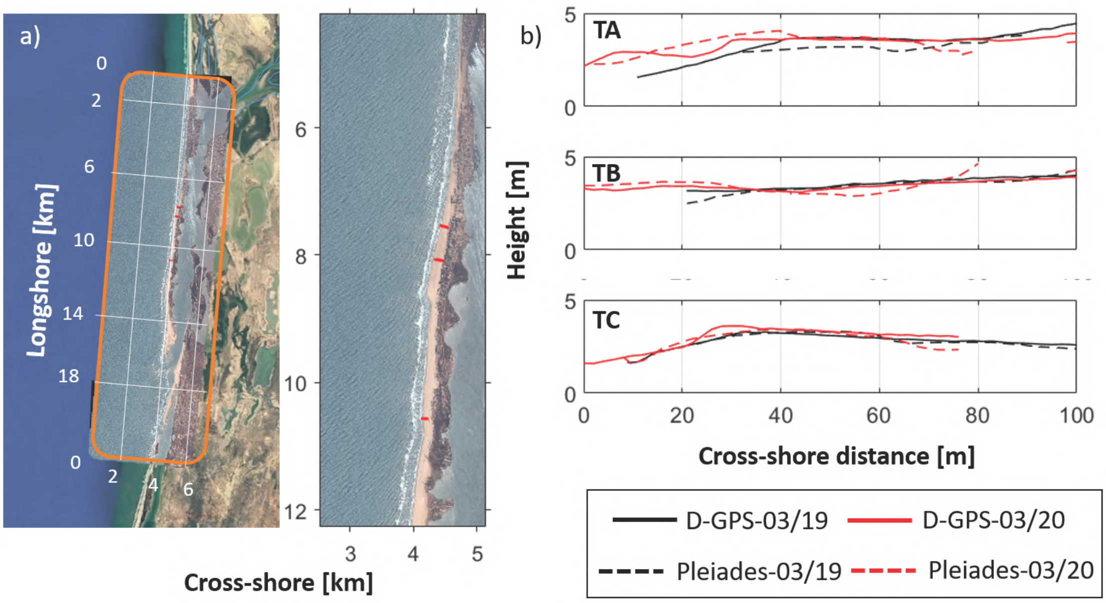

Figure 2. (**a**) Satellite image superposed from March 2019 with chosen transects for inter-comparison and zoom onto the chosen transects. (**b**) Inter-comparison (Pleiades—dashed lines, and D-GPS—continuous lines) over the chosen transects in March 2019 and March 2020 [45].

To estimate the extent of the lower beach swash zone related uncertainty, the horizontal swash excursion has been calculated using an empirical parametrization Equation (1) and ocean forcing (Table 2) with a constant beach slope $\beta \simeq 4\%$ (value estimated in Section 4.2). For 2019, the horizontal swash excursion is estimated at $\simeq$31 m and $\simeq$12.9 m in 2020. The projected horizontal tidal excursion for both acquisitions is $\simeq$20 m. This width seems to correspond to the 2019 Pleiades lack of data, as emphasized in Figure 2b.

4.2. Erosion within the Urban Area

Figure 3a, the shoreline changes were calculated from the difference between the 2019 and 2020 waterline position. Two cross-shore transects that experience the largest rates of shoreline change were selected (100 m $\leq$ *Distance* $\leq$ 400 m corresponding to T3, and 1400 m $\leq$ *Distance* $\leq$ 1500 m corresponding to T1, Figure 3a).

The iso-topographies position (Figure 3b) allows an estimate of the average slope of the beach at $\simeq$4%, and shows a beach-narrowing that is also visible on the zoomed satellite images (Figure 3b). This narrowing is particularly noticeable for transects T1 and T3, where the rates of shoreline change are the highest: $\simeq -20$ m/year for both (Figure 3a). The beach at T2 seems stable and its rate of shoreline change is lower ($\simeq -5$ m). However wave conditions were different between the two Pleiades acquisitions: as the tide was the same (0.8 m—low tide conditions; Table 2), the swell was more energetic in 2019 resulting in a more expressed beach run-up.

A previous study explained the observed erosion trends in the urban area from 2004 to 2020 (North side of Saint Louis—corresponding to transect T1 ; Figure 3b) as a response to the 2003 *Langue de Barbarie* breach [42]. Not only an erosion trend was identified, but the erosion rate has also accelerated over the last two decades (from 2000 to 2020) in the vicinity of the fish market [42]. The erosion trend is still observable from the Pleiades satellite imagery in the urban area (Figure 3).

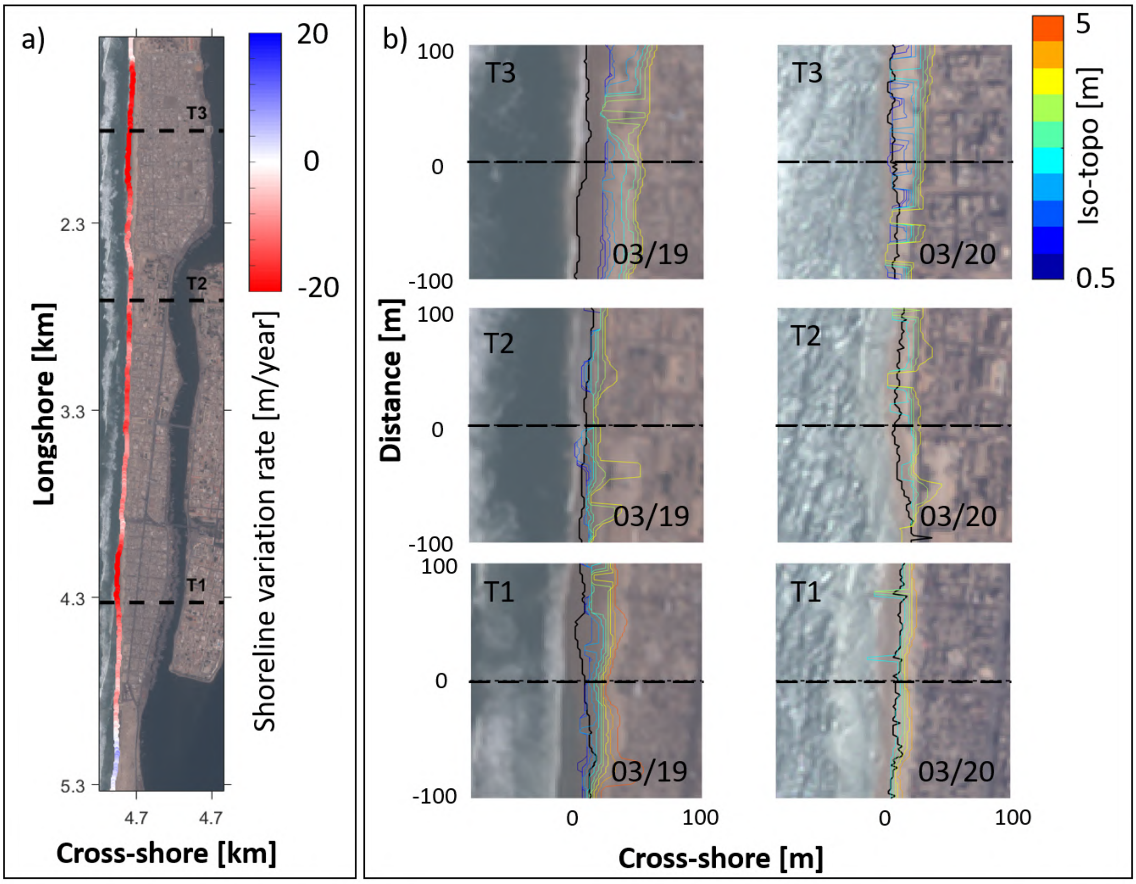

Figure 3. (**a**) Erosion rate within a year derived from Pleiades images in the urban area—calculated from the difference between the waterlines position of 2019 and 2020. (**b**) Iso-topographies derived from Pleiades onto the chosen transects which height ranging from 0.5 m to 5 m (color lines), and associated waterline position (black lines).

Table 2. Waves and wind parameters during the Pleiades acquisitions.

Date	Wind Speed (kt)	Wind Dir (°)	Hs (m)	Wave Dir (°)	T (s)	Tide (m)
2 March 2019	11	80	2.3	290	17	0.8
17 March 2020	14	360	1.8	350	8	0.8

4.3. Sand Spit Extension

Figure 4a,c shows that from 2019 to 2020, the length of the sand spit increased and the *Langue de Barbarie* stretched southward at an average migration rate of 740 m/year. The inland sand spit remained stable, and the Southern part of the spit gained a large volume within a year (Figure 4b). The spots that lost volume on the Atlantic ocean side (Figure 4b) are immediately followed by spots that gained volume in the Southern direction, which is also the direction of the LST.

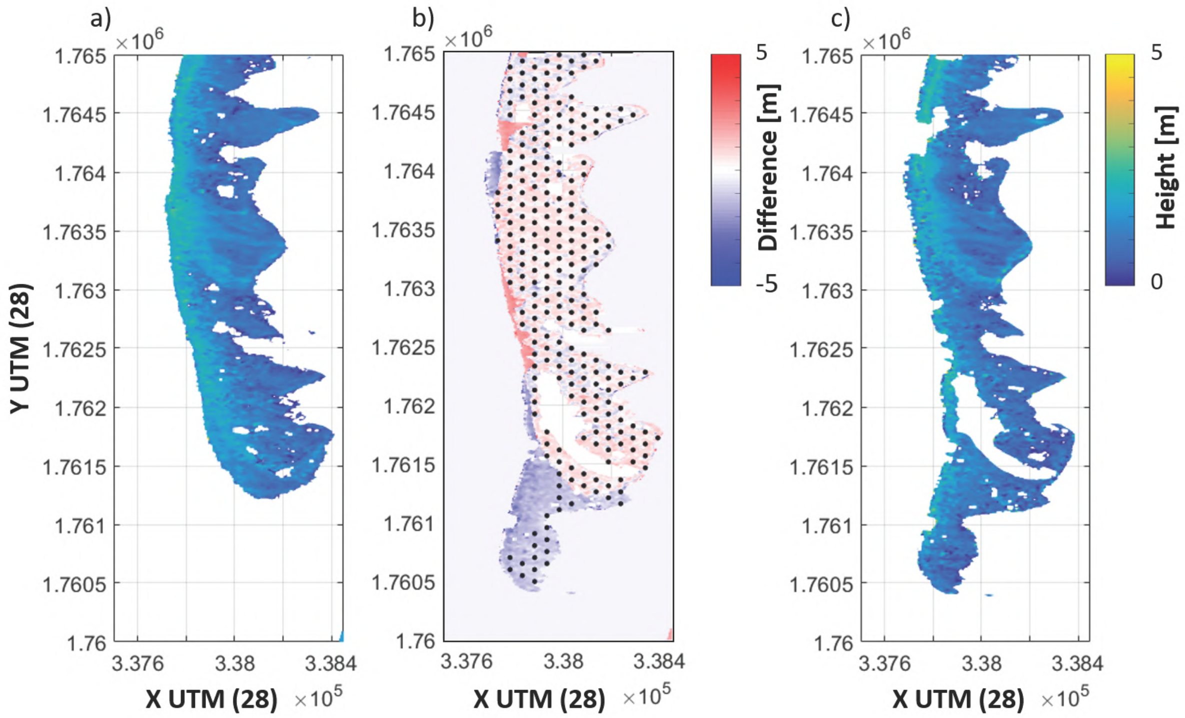

Figure 4. (**a**) Sand spit natural area morphology derived from Pleiades—March 2019. (**b**) DEMs difference (2020–2019) with stippled area represents the vertical change (<1 m). (**c**) Sand spit natural area morphology derived from Pleiades—March 2020.

The longshore sediment transport rates, provided by the SOGREAH firm (1994) [38,42,58], give a drift volume from North to South which ranged between 600 to 700 × 10^3 m^3/year, and appears to be the direct cause of the southward stretching and narrowing of the sand spit in the northern part (Figure 4a,c). The accretion at the Southern tip of the sand spit is particularly noticeable in Figure 4b represented by the red colours. A large portion of the inland sand spit remained stable with a vertical change inferior to 1 m—stippled area Figure 4b—between 2019 and 2020. One can notice that the major morphological changes occurred at the Southern tip of the *Langue de Barbarie*, and several spots along the Atlantic face of the sand-spit.

Over the region of interest determined Figure 5a, the average topography elevation was estimated to be $H_{average} = 1.07$ m with the 2019 and 2020 Pleiades DEMs. Migration rates tremendously vary over the past 5 years (Table 3), as does sand volume dragged from North to South by the LST and captured by the sand spit which shows great variability (Figure 5b). From 2015 to 2020, the alongshore migration of the sand spit is averaged to be approximately 230 × 10^3 m^3/year. This represents 35% of the North to South drift volume ([38,39]), meaning that the sand spit extension has the potential to capture a large quantity of the alongshore sand drift.

Table 3. Migration rates over the years derived from satellite measurements and Equation (3).

Date	Migration Rate CoastSat [44] (m/Year)	Migration Rate Estimates (Equation (3)) (m/Year)
2015/2016	160	210
2016/2017	870	250
2017/2018	550	280
2018/2019	460	350
2019/2020	740	270

The coastlines shown in Figure 5a are derived from Sentinel-2 satellite imagery with the CoastSat tool [44] highlight the southward accretion trend of the *Langue de Barbarie* over the last 5 years. Since 2015, the position of the tip of the sand spit has shifted increasingly southward, with migration rates ranging from 160 m/year to 870 m/year (Table 3).

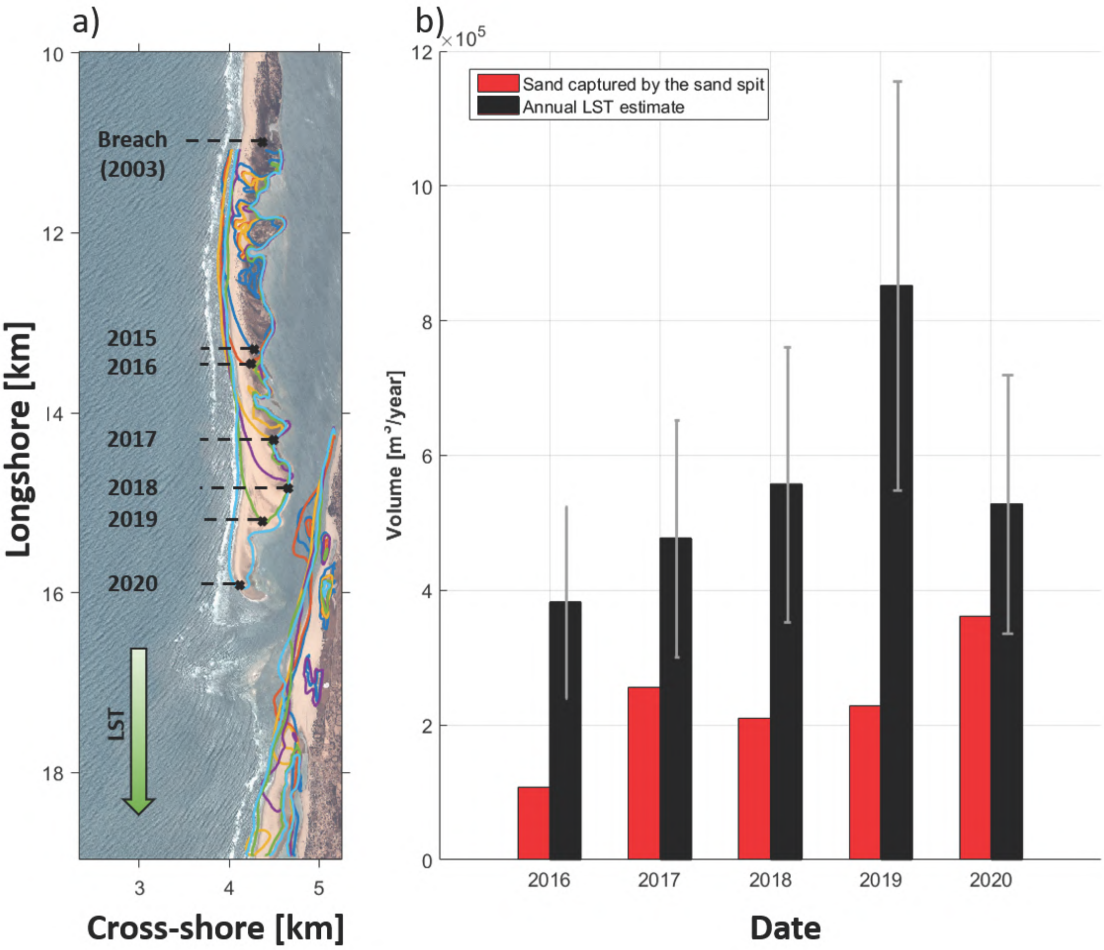

Figure 5. (**a**) Sand spit tip' position and shorelines derived from S2-satellite over time using Coastsat Open-Access tool [44]. (**b**) Volume of sand annually captured by the sand spit (red) compared to the annual LST estimates obtained from ERA5 data (black) with its standard deviation (gray).

The calculated migration rates based on a sand conservation Equation [27], and thus the LST (Table 3), show here a large difference with the satellite-derived observations, proving that the southward sand spit growth is not only ruled by climate control on wave regime but has an intrinsic dynamics. Based on the sand spit tip positions from 2015 to

2020, and the median LST ($Q = 530 \times 10^3$ m^3/year), a parametric model of the *Langue de Barbarie* sand spit intrinsic stochastic growth over time t can be expressed as:

$$\frac{x}{L} = 1.85 \times 10^{-6} Q (\frac{t}{T})^{4.46 \times 10^{-6} Q} \quad (4)$$

With $p_{value} \leq 0.01$, x being the position of the tip of the spit from the northern end, and L representing the maximum spit extension value ($L = 32$ km). The T value represents a cycle duration (here $T = 35$ year, derived from the extrapolation of the fitted data Figure 6a). Here we define a spit cycle as the moment when the elongation of the *Langue de Barbarie* reached its maximum, causing the closure of the mouth of the Senegal River when $\frac{x}{L} \longrightarrow 1$. According to our model, the sand spit migration rates increase with time, which is consistent with the Coastsat-derived migration rates (Table 3). Similarly, the spit width W averaged over an alongshore distance of 1 km at transect Y—which is located at 1 km South of the defined urban area and represented Figure 2a—can be expressed as:

$$\frac{W}{W_{max}} = \frac{t}{T}^2 - \frac{t}{T} + 1 \quad (5)$$

With $p_{value} \leq 0.01$, and $W_{max} = 354$ m the maximum width at transect Y. We can first observe a phase of rapid decrease of the sand spit width since 2008—that decrease being correlated with the southwards lengthening of the *Langue de Barbarie* (Figure 6)—and a second phase of a width accretion. Considering Equation (5), the erosion trend of the beach located under the urban area will reduce and inverse to accretion after 2030 (Figure 6b).

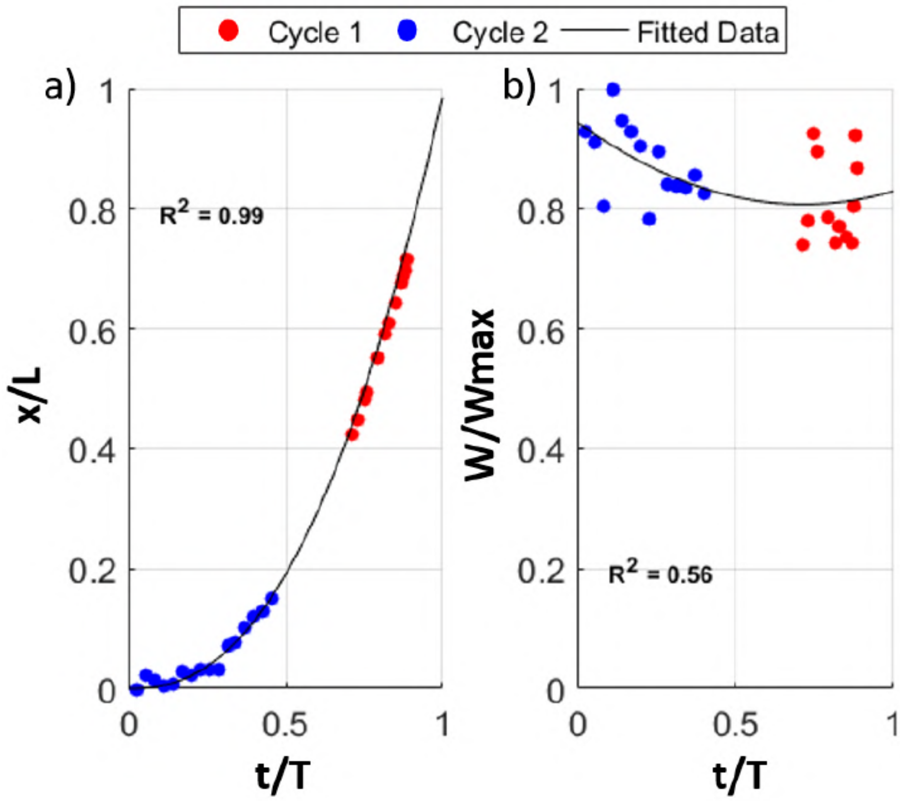

Figure 6. (**a**) Sand spit tip' positions for cycle 1 (1984–2003; red) and cycle 2 (2003–2020; blue) derived from CoastSat tool [44] and fitted data expressed as Equation (4). (**b**) Sand spit averaged width evolution between transect $Y = 1.7705 \times 10^6$ Y UTM (28) and 1 km South with its fitted data expressed as Equation (5) (Right).

Cycle 1 is defined from the start of Landsat data acquisitions in 1984, to 2003 which is the date of the artificial breach, as shown in Figure 6. Cycle 2 is the new sand-spit cycle initiated after the spit breaching. Considering our modeling, we can estimate that the river mouth will probably close around 2040.

5. Discussion

5.1. Satellite-Based Coastal Monitoring for Coastal Engineering: Potential Strengths

This work shows the potential of very high-resolution satellites use for coastal monitoring, and in particular, the monitoring of sediment dynamics (review in [18]) and quantifying spatial and temporal volumetric beach evolution [22,59]. Satellites cover larger regions than classical surveys methods, allow an overall understanding of beach morphodynamics, enable the accessibility of remote data sources and open the possibility of forthcoming precision improvements. Satellites make it possible to have a large bank of data available over a long time period in developing countries. The erosion rate and shoreline position derived from Pleiades and Sentinel-2 time series allows to identify of the most vulnerable hot-spots along this coastal stretch (Section 4.2), and emphasizes the role of large-scale dynamics to study small scale beach dynamics. This is highlighted by the erosion trend in the urban area (Northern *Langue de Barbarie*), and the stretching of the sand spit towards the South while the Northern part is narrowing (Section 4.3). This erosion is probably a joint result of sequestering of part of the sand load transported by the LST in the post-2003 breach—which is now the new river-mouth—and a reinforced tidal prism through this new mouth [40,60].

The potential of very high-resolution satellites, such as Pleiades, for coastal monitoring, has been highlighted in our study, and the investigation on the Saint Louis coastline changes will continue. A protection structure is to be built from December 2020 to protect the urban area in the North part of the sand spit [61], and to protect the most threatened inhabitants. After assessing pre-construction beach variability to design the structure, the satellite monitoring will continue to monitor the efficiency of that protection, and its impact downstream.

5.2. The Langue de Barbarie Sand Spit Stochastic Cyclic Evolution: Predicting Next Breaching and Erosion in Saint Louis

Pleiades data allows monitoring the short-term morphological changes of the *Langue de Barbarie* sand spit. From 1984 to 2020, the Northern spit elongation, calculated from various observations (CORONA, LANDSAT, SPOT, aerial photographs and field measurements, Sentinel-2, Pleiades; [38,42]) has tremendously fluctuated from low values (<170 m/year), to highest values (>1200 m/year). The use of remote-sensing methods allows the coverage of regional areas, such as the *Langue de Barbarie* which is 10 to 20 km long, and allows long-term monitoring of sand spits morphological changes [24,27,30,38,42]. Sentinel-2 data represents an even greater interest in that field as an every 8 day image is collected for our study site [29], enabling the monitoring of fast-events—such a tool would have permitted the monitoring of the post-2003 artificial breach period in our case with the dramatic widening of the breach.

The *Langue de Barbarie* developed downdrift in conjunction with the river-mouth diversion and its southwards migration [40]. Energetic swells—as is the case in Saint Louis—cause a massive sand accumulation and is prone to a rapid spit elongation, much more than less energetic waves that are responsible for small sand accumulation, and spit curvature [24]. The 2003 breach had dramatic consequences onto the *Langue de Barbarie*: the spit sand further downdrift was recycled into river-mouth bars, while the rest was transported southwards by longshore currents, strongly impacting the infrastructures into the *Langue de Barbarie* [4,40,42]. Nowadays, the Northern spit of the *Langue de Barbarie* is still lengthening (Figure 6), explained by the lower bypassing and sharp increase of the LST as it happened from 2012 to 2013, generating the ensuing exceptionally rapid elongation of the *Langue de Barbarie* spit between June 2013 and May 2015 ($\simeq$2 km) [38]. The results with shoreline tracking by [42] with a longer period of observation of regular revisit satellite missions (Landsat and Sentinel-2) confirmed that after 2012, the sand spit migrates Southwards with an average rate of 590 m/year. The results found in Section 4.3 are part of the sand spit extension trend, and modelling of the *Langue de Barbarie* morphological evolution was drawn as Equation (4). This simple deterministic spit growth equation provides a first-pass useful model of a sand spit development independent of climate forcing, proving that the changes in wave regime are not the main driving factor. Interactions between sediment transport and fluid flow create morphological feedbacks and lead to self-organized patterns [62], that explains the differences found Table 3 (satellite-measured spit growth rate versus "forced" spit growth rate [27]) and why those "forced" spit growth rates are much lower than the satellite-derived measurements. Other parameters such as human interactions, sediment availability, and sea-level rise also play a substantial role in the longer-term [25,26,63].

As the *Langue de Barbarie* extents Southwards in a 35 years cycle, the sand spit width is decreasing (Figure 6) [64]. From 2008, our results indicate an acceleration in the spit-narrowing process south of the defined urban area, and thus an erosion acceleration in that zone. Considering our model (Equation (5)), the erosion trend on the *Langue de Barbarie* is temporary: by 2030, this trend will reverse and the beach will start accreting again as this urban area will be located far from the river mouth and thus be free from its influence. Our model (Equation (4)) also predicts that by 2040, the spit length will reach its maximum and will likely cause the river mouth closure at the southern end: a new breach will potentially naturally or artificially have to be made to prevent Saint Louis city from flooding.

Our cyclic model relies on the LST, and enables a long term (decades) description and forecast of the *Langue de Barbarie* morphodynamics. The stretching (Figure 5) and narrowing seem to be the direct cause of the erosion found at Saint Louis, especially around urbanized areas (Northern *Langue de Barbarie*) where sediment availability is limited (Section 4.2). Pradhan et al. (2015) [26] demonstrated a similar evolution on a sand spit in India: a continuous elongation of the sand spit caused the erosion of the upstream beaches. With the topography only, one sees just the emerged tip of the "iceberg" ([14]). Nearshore bathymetry in addition to the satellite topographies, a coastal continuum, could improve the volumetric calculations and the understanding of the observed sand spit dynamics in support of our observations ([21]).

To generalize its applicability to other sand-spits, this model could be extended and calibrated using other sand-spit with similar environmental conditions and which morphology is wave-dominated.

5.3. Limitations

DEMs derived from tri-stereogrammetry methods to obtain topography estimation present promising results and constitute a new way to estimate morphological changes of a coastal area. However, it comports limits that are to take into account [65] like the difficulties encountered by Pleiades when analyzing water surfaces, and areas with no texture [66]. The global RMSE between in situ measurements and Pleiades estimations is 1.15 m $\leq RMSE \leq$ 1.31 m (Section 4.2) and those results are not as good as what was found in Almeida et al. (2019) [37] study. The difference between the two studies can be explained by the flatness of the *Langue de Barbarie* topography ($\simeq$2.56 m above sea level). The flatness of a site has an indirect impact on the DEM accuracy [67]—low reflectance and texture of the raw optical satellite image result from specific ground characteristics, altering the calculation of the disparity that is converted into ground elevation. The signal-metric changes induced by a storm or at seasonal scale—is about the same order as the noise: this study show the potential of the method but highlight the need for more accuracy and further developments. However, as the slopes at our beach/dune system are weak ($\simeq$4%, Section 4.2), the tri-stereo method does not produce large errors and dependency on the view monitoring as it is the case for cliffs 3D-reconstitution [68]. Our study site has a limited set of GCPs. Increasing the number of GCPs would improve the correction of DEMs, and decrease the overall RMSE.

A large uncertainty arises from the satellite-derived DEM. Other open-access tools can generate a surface model with a stereo-method, such as MicMac [69]. In previous studies the vertical mean error of the surface models ranged as follows: 0.35 m $\leq$ ASP $\leq$ 0.48 m [37], and 0.17 m $\leq$ MicMac $\leq$ 0.34 m [70]. In our work, we used ASP and CARS to perform a tri-stereo, but the RMSE between in situ data and the CARS produced-DEMs were not satisfying enough to use them in our beach morphology study. Those values compete with the centimetric-errors obtained with the LiDAR method for the assessment of coastal processes [71–73] which vertical accuracy ranged from 0.05 m to 0.15 m [74].

The most dynamic part of the beach is the lower beach, which is the most challenging section for stereoscopy due to hydrodynamics (swash) between images, tide level at the moment of the acquisition (time of acquisition not flexible) and the lack of texture (Section 4.2). The DEMs are validated punctually at control points to estimate the uncertainty/error in the waterline estimations (horizontal displacement of an iso-level)—impacting the calculated erosion rate Figure 3—and volume change (vertical evolution), so the validation of those parameters apply for the two latter and no assessment can be drawn from the Pleiades DEMs. It is also to observe that the transect TA shows a greater difference between the D-GPS transects and the Pleiades estimations than TB and TC: the beach profile trend is yet found by the satellite, but despite the correction applied on the DEMs data, the lower beach relief morphology (0 m $\simeq$ *Cross-shore* $\simeq$ 40 m ; Figure 2b) does not match between the in situ data, and the satellite-derived topography. It is especially notable in the 2019 data that there is no estimation of the topography for cross-shore values $\in [0, 30]$ m (Figure 2b). That is to link to the fact that the waves conditions during the Pleiades acquisition in March 2019 were particularly energetic ($H_S = 2.3$ m, and $T = 17$ s ; Table 2), which induces an important run-up on the beach. As the tri-stereo method is not the most suitable for the topography of the lower beach, the study of the bathymetry of the near-shore and intertidal zone would provide more accurate results.

5.4. The Impact of Satellite Acquisition Geometry on DEM Accuracy

The DEMs obtained from stereo methods have their accuracy relying on several parameters that are to determine before ordering a Pleiades image set [43,68,75]. In March 2019, a set of 10 images is available, allowing to study the impact of two input parameters on the DEM reliability. The RMSE between the DEMs and the in situ data set has been calculated for two regions of interest: over the whole Pleiades DEM and the urban area emphasized Figure 1c.

Over the 2019 Pleiades sequence, the RMSE standard deviation for the B/H ratio is 0.08 on the whole satellite image, and 0.05 in the urban area. That emphasizes the fact that the Base to Height (B/H) ratio does have a strong impact on the DEM accuracy. However, as the along-orbit Angle parameter does not highlight a trend when the whole DEM is considered, it shows a greater variability within the urban area with a 0.27 standard deviation value. The DEMs accuracy is better in two cases: when the stereo-estimation is built from very close to Nadir along-orbit angle, or when the stereo-estimation is built from large alongshore angles $\in [-18°, -12°, 11°, 16°]$.

When the terrain presents more irregularities in the topography—like in the urban area with the presence of buildings—the stereo method works better and the provided DEM is more accurate when using high along-orbit angles in between the used satellite-pair images [66,68]. However, as the topography-study site is very low over the largest inland part, the conclusion is that neither the B/H ratio nor the along angle parameter have a huge impact on our method-accuracy. However, considering the results and the method limitations, the ideal conditions for a Pleiades acquisition would be at low tide, and during the summer to avoid heavy swells conditions.

6. Conclusions

In this article, 2m Digital Elevation Models (DEMs) derived from sub-metric Pleiades optical satellites were used to monitor coastal changes around Saint Louis (Senegal, West

Africa) along the *Langue de Barbarie* sand spit over a year (March 2019–March 2020). The tri-stereo method used here to calculate the DEMs gives a metric root mean squared differences when compared to RTK-GPS surveys. By bringing together the local erosion at the urban area with the larger scale extension of the *Langue de Barbarie* sand spit, this work offers a new vision of regional morphodynamics and how the scales are tangled. Even if a standalone use for coastal studies is not yet conceivable at this stage considering the encountered accuracy limitations, satellite-based topography monitoring appears as a breakthrough in decade-old technological barriers of linking coastal spatio-temporal scales, which is crucial to understand coastal behaviour, and for coastal engineering.

Using available long term satellite monitoring, a stochastic model for the morphological evolution of the *Langue de Barbarie* sand spit-free from climate forcing—has also been proposed and offers the possibility to anticipate its behaviour and erosion trends over time. This will allow the implementation of efficient and sustainable infrastructures to combat the erosion in Saint Louis [76].

Author Contributions: A.T. did the analyses and wrote the manuscript, R.A. and E.W.J.B. supervised and validated ; B.A.S., A.N., M.S., T.G. collected in situ-measurements used in the analyses; R.A. and E.W.J.B. revised the manuscript at different stages and collaborated on the ideas. All authors have read and agreed to the published version of the manuscript.

Funding: This research was funded by AFD (Agence Française de Développement—France), ADM (Agence de Développement Municipal—Senegal), and IRD (Institut de Recherche et de Développement); Surveys were funded under the PEA MEPELS. Erwin Bergsma was funded through a Postdoctoral fellowship of the French Space Agency (CNES).

Data Availability Statement: Not applicable.

Acknowledgments: The authors would like to thank the SHOM for the topograpic in situ measurements, UCAD and UGB for their time and help in Saint Louis.

Conflicts of Interest: The authors declare no conflict of interest.

Abbreviations

The following abbreviations are used in this manuscript:

DEM	Digital Elevation Model
RTK	Real Time Kinematic
ASP	Ames Setero Pipelines
RPC	Rational Polynomial Coefficient
NDWI	Normalized Difference Water Index
RMSE	Root Mean Squared Error
LST	Longshore Sediment Transport

References

1. Luijendijk, A.; Hagenaars, G.; Ranasinghe, R.; Baart, F.; Donchyts, G.; Aarninkhof, S. The state of world's beaches. *Sci. Rep.* **2018**, *8*, 6641. [CrossRef] [PubMed]
2. Small, C.; Nicholls, R. A global analysis of human settlement in coastal zones. *J. Coast. Res.* **2003**, *19*, 584–599.
3. Nicholls, R.; Small, C. Improved estimates of coastal population and exposure to hazards released. *Eos Trans. Am. Geophys. Union* **2011**, *83*, 301–305. [CrossRef]
4. Ndour, A.; Laïbi, R.A.; Sadio, M.; Degbe, C.G.; Diaw, A.T.; Oyédé, L.M.; Anthony, E.J.; Dussouillez, P.; Sambou, H.; hadji Balla Dièye, E. Management strategies for coastal erosion problems in west Africa: Analysis, issues, and constraints drawn from the examples of Senegal and Benin. *Ocean. Coast. Manag.* **2018**, *156*, 92–106. [CrossRef]
5. Alves, B.; Angnuureng, D.B.; Morand, P.; Almar, R. A review on coastal erosion and flooding risks and best management practices in West Africa: What has been done and should be done. *J. Coast. Conserv.* **2020**, *24*, 1–22. [CrossRef]
6. Dada, O.; Almar, R.; Morand, P.; Menard, F. Towards West African coastal social-ecosystems sustainability: Interdisciplinary approaches. *Ocean. Coast. Manag.* **2021**, *211*, 105746. [CrossRef]
7. Jongman, B. Effective adaptation to rising flood risk. *Nat. Commun.* **2018**, *9*. [CrossRef]
8. Sinay, L.; Carter, R.W.B. Climate Change Adaptation Options for Coastal Communities and Local Governments. *Climate* **2020**, *8*, 7. [CrossRef]

9. Temmerman, S.; Meire, P.; Bouma, T.J.; Herman, P.M.J.; Ysebaert, T.; Vriend, H.J.D. Ecosystem-based coastal defence in the face of global change. *Nature* **2013**, *504*, 79–83. [CrossRef] [PubMed]
10. Marzougui, W.; Oueslati, A. Les plages de la côte d'Ejjehmi-Soliman (golfe de Tunis, Tunisie): Exemple d'accélération de l'érosion marine dans une cellule sédimentaire artificiellement tronçonnée. *Physio-Geo* **2017**, *11*, 21–41. [CrossRef]
11. Bayle, P.M.; Blenkinsopp, C.E.; Conley, D.; Masselink, G.; Beuzen, T.; Almar, R. Performance of a dynamic cobble berm revetment for coastal protection, under increasing water level. *Coast. Eng.* **2020**, *159*, 103712. [CrossRef]
12. Maiolo, M.; Mel, R.A.; Sinopoli, S. A Stepwise Approach to Beach Restoration at Calabaia Beach. *Water* **2020**, *12*, 2677. [CrossRef]
13. Gesch, D.; Brock, J.; Parrish, C.; Rogers, J.; Wright, C. Introduction: Special issue on advances in topobathymetric mapping, models, and applications. *J. Coast. Res.* **2016**, *76*, 1–3. [CrossRef]
14. Anthony, E.J. Wave influence in the construction, shaping and destruction of river deltas: A review. *Mar. Geol.* **2015**, *361*, 53–78. [CrossRef]
15. McBride, R.; Taylor, M.; Byrnes, M. Coastal morphodynamics and Chenier-Plain evolution in southwestern Louisiana, USA: A geomorphic model. *Geomorphology* **2007**, *88*, 367–422. [CrossRef]
16. Le Mauff, B.; Juigner, M.; Ba, A.; Robin, M.; Launeau, P.; Fattal, P. Coastal monitoring solutions of the geomorphological response of beach-dune systems using multi-temporal LiDAR datasets (Vendée coast, France). *Geomorphology* **2018**, *304*, 121–140. [CrossRef]
17. Collin, A.; Hench, J.L.; Pastol, Y.; Planes, S.; Thiault, L.; Schmitt, R.J.; Holbrook, S.J.; Davies, N.; Troyer, M. High resolution topobathymetry using a Pleiades-1 triplet: Moorea Island in 3D. *Remote Sens. Environ.* **2018**, *208*, 109–119. [CrossRef]
18. Salameh, E.; Frappart, F.; Almar, R.; Baptista, P.; Heygster, G.; Lubac, B.; Raucoules, D.; Almeida, L.P.; Bergsma, E.W.J.; Capo, S.; et al. Monitoring Beach Topography and Nearshore Bathymetry Using Spaceborne Remote Sensing: A Review. *Remote Sens.* **2019**, *11*, 2212. [CrossRef]
19. Benveniste, J.; Cazenave, A.; Vignudelli, S.; Fenoglio-Marc, L.; Shah, R.; Almar, R.; Andersen, O.; Birol, F.; Bonnefond, P.; Bouffard, J.; et al. Requirements for a Coastal Hazards Observing System. *Front. Mar. Sci.* **2019**, *6*, 348. [CrossRef]
20. Melet, A.; Teatini, P.; Le Cozannet, G.; Jamet, C.; Conversi, A.; Benveniste, J.; Almar, R. Earth Observations for Monitoring Marine Coastal Hazards and Their Drivers. *Surv. Geophys.* **2020**, *41*, 1489–1534. [CrossRef]
21. Bergsma, E.W.J.; Almar, R.; Rolland, A.; Binet, R.; Brodie, K.L.; Bak, A.S. Coastal morphology from space: A showcase of monitoring the topography-bathymetry continuum. *Remote Sens. Environ.* **2021**, *261*, 112469. [CrossRef]
22. Turner, I.L.; Harley, M.D.; Almar, R.; Bergsma, E.W. Satellite optical imagery in Coastal Engineering. *Coast. Eng.* **2021**, *167*, 103919. [CrossRef]
23. Aubrey, D.; Gaines, A. Rapid formation and degradation of barrier spits in areas with low rates of littoral drift. *Mar. Geol.* **1982**, *49*, 257–277. [CrossRef]
24. Allard, J.; Bertin, X.; Chaumillon, E.; Pouget, F. Sand spit rhythmic development: A potential record of wave climate variations? Arçay Spit, western coast of France. *Mar. Geol.* **2008**, *253*, 107–131. [CrossRef]
25. Stancheva, M.; Ratas, U.; Orviku, K.; Palazov, A. Sand Dune Destruction Due to Increased Human Impacts along the Bulgarian Black Sea and Estonian Baltic Sea Coasts. *J. Coast. Res.* **2011**, *64*, 324–328.
26. Pradhan, U.; Mishra, P.; Mohanty, P.K.; Behera, B. Formation, Growth and Variability of Sand Spit at Rushikulya River Mouth, South Odisha Coast, India. *Procedia Eng.* **2015**, *116*, 963–970. [CrossRef]
27. Duc Anh, N.Q.; Tanaka, H.; Tam, H.S.; Tinh, N.X.; Tung, T.T.; Viet, N.T. Comprehensive Study of the Sand Spit Evolution at Tidal Inlets in the Central Coast of Vietnam. *J. Mar. Sci. Eng.* **2020**, *8*, 722. [CrossRef]
28. Nahon, A.; Idier, D.; Sénéchal, N.; Féniès, H.; Mallet, C.; Mugica, J. Imprints of wave climate and mean sea level variations in the dynamics of a coastal spit over the last 250 years: Cap Ferret, SW France. *Earth Surf. Process. Landf.* **2019**, *44*, 2112–2126. [CrossRef]
29. Bergsma, E.W.; Almar, R. Coastal coverage of ESA' Sentinel 2 mission. *Adv. Space Res.* **2020**, *65*, 2636–2644. [CrossRef]
30. Teodoro, A.; Pais-Barbosa, J.; Gonçalves, H.; Veloso-Gomes, F.; Taveira-Pinto, F. Extraction of Cabedelo sand spit area (Douro estuary) from satellite images through image processing techniques. *J. Coast. Res.* **2011**, *SI 64*, 1740–1744.
31. Holman, R.; Plant, N.; Holland, T. cBathy: A robust algorithm for estimating nearshore bathymetry. *JGR Oceans* **2013**, *118*, 2595–2609. [CrossRef]
32. Bergsma, E.W.J.; Conley, D.C.; Davidson, M.A.; O'Hare, T.J.; Almar, R. Storm Event to Seasonal Evolution of Nearshore Bathymetry Derived from Shore-Based Video Imagery. *Remote Sens.* **2019**, *11*, 519. [CrossRef]
33. Bergsma, E.; Almar, R. Video-based depth inversion techniques, a method comparison with synthetic cases. *Coast. Eng.* **2018**, *138*, 199–209. [CrossRef]
34. Angnuureng, D.B.; Jayson-Quashigah, P.N.; Almar, R.; Stieglitz, T.C.; Anthony, E.J.; Aheto, D.W.; Appeaning Addo, K. Application of Shore-Based Video and Unmanned Aerial Vehicles (Drones): Complementary Tools for Beach Studies. *Remote Sens.* **2020**, *12*, 394. [CrossRef]
35. Eustáquio Amaro, V.; Santana Gomes, L.R.; Ferreira de Lima, F.G.; Scudelari, A.C.; Freitas Neves, C.; Vieira Busman, D.; Silva Santos, A.L. Multitemporal Analysis of Coastal Erosion Based on Multisource Satellite Images, Ponta Negra Beach, Natal City, Northeastern Brazil. *Mar. Geod.* **2015**, *38*, 1–25. [CrossRef]
36. Almar, R.; Bergsma, E.W.J.; Maisongrande, P.; de Almeida, L.P.M. Wave-derived coastal bathymetry from satellite video imagery: A showcase with Pleiades persistent mode. *Remote Sens. Environ.* **2019**, *231*, 111263. [CrossRef]

37. Almeida, L.; Almar, R.; Bergsma, E.; Berthier, E.; Baptista, P.; Garel, E.; Dada, O.; Alves, B. Deriving High Spatial-Resolution Coastal Topography From Sub-meter Statellite Stereo Imagery. *Remote Sens.* **2019**, *11*, 590. [CrossRef]
38. Sadio, M.; Anthony, E.J.; Diaw, A.T.; Dussouillez, P.; Fleury, J.T.; Kane, A.; Almar, R.; Kestenare, E. Shoreline Changes on the Wave-Influenced Senegal River Delta, West Africa: The Roles of Natural Processes and Human Interventions. *Water* **2017**, *9*, 357. [CrossRef]
39. Almar, R.; Kestenare, E.; Boucharel, J. On the key influence of remote climate variability from Tropical Cyclones, North and South Atlantic mid-latitude storms on the Senegalese coast (West Africa). *Environ. Res. Commun.* **2019**, *1*, 071001. [CrossRef]
40. Anthony, E.J. Patterns of Sand Spit Development and Their Management Implications on Deltaic, Drift-Aligned Coasts: The Cases of the Senegal and Volta River Delta Spits, West Africa. In *Sand and Gravel Spits*; Randazzo G., Jackson D., Cooper J., Eds.; Coastal Research Library; Springer: Cham, Switzerland, 2015; pp. 21–36.
41. Anthony, E.J.; Aagaard, T. The lower shoreface: Morphodynamics and sediment connectivity with the upper shoreface and beach. *Earth-Sci. Rev.* **2020**, *210*, 103334. [CrossRef]
42. Bergsma, E.; Sadio, M.; Sakho, I.; Almar, R.; Garlan, T.; Gosselin, M.; Gauduin, H. Sand-spit evolution and inlet dynamics derived from space-borne optical imagery: Is the Senegal-river inlet closing? *J. Coast. Res.* **2020**, *95*, 372–376. [CrossRef]
43. Jacobsen, K.; Topan, H. Corrigendum to "DEM generation with short base length Pleiades triplet". *Int. Arch. Photogramm. Remote Sens. Spat. Inf. Sci.* **2015**, *XL-3/W2*, 297. [CrossRef]
44. Vos, K.; Splinter, K.D.; Harley, M.D.; Simmons, J.A.; Turner, I.L. CoastSat: A Google Earth Engine-enabled Python toolkit to extract shorelines from publicly available satellite imagery. *Environ. Model. Softw.* **2019**, *122*, 104528. [CrossRef]
45. Shean, D.; Alexandrov, O.; Moratto, Z.; Smith, B.; Joughin, I.; Porter, C.; Morin, P. An automated,open-source pipeline for mass production of digital elevation models (DEMs) from very-high-resolutioncommercial stereo satellite imagery. *ISPRS J. Photogramm. Remote Sens.* **2016**, *116*, 101–117. [CrossRef]
46. Youssefi, D.; Michel, J.; Sarrazin, E.; Buffe, F.; Cournet, M.; Delvit, J.M.; L'Helguen, C.; Melet, O.; Emilien, A.; Bosman, J. CARS: A Photogrammetry Pipeline Using Dask Graphs to Construct A Global 3D Model. In Proceedings of the IGARSS 2020—2020 IEEE International Geoscience and Remote Sensing Symposium, Waikoloa, HI, USA, 26 September–2 October 2020; pp. 453–456. [CrossRef]
47. Michel, J.; Sarrazin, E.; Youssefi, D.; Cournet, M.; Buffe, F.; Delvit, J.; Emilien, A.; Bosman, J.; Melet, O.; L'Helguen, C. A new satellite imagery stereo pipeline designed for scalability, robustness and performance. *ISPRS Int. Arch. Photogramm. Remote Sens. Spat. Inf. Sci.* **2020**, *2*, 171–178. [CrossRef]
48. Nuth, C.; Kääb, A. Co-registration and bias corrections of satellite elevation data sets for quantifying glacier thickness change. *Cryosphere* **2011**, *5*, 271–290. [CrossRef]
49. McNabb, R. *PyBob: A Python Package of Geospatial Toolsand Version 0.25*; Github: San Francisco, CA, USA, 2019.
50. M., T.; A., E.R.S.; R., R.; A.E., H. Co-registration of Satellite Images Based on Invariant Local Features. *Intell. Syst.* **2015**, *323*, 653–660.
51. Stockdon, H.F.; Holman, R.A.; Howd, P.A.; Sallenger, A.H. Empirical parameterization of setup, swash, and runup. *Coast. Eng.* **2006**, *53*, 573–588. [CrossRef]
52. Melet, A.; Meyssignac, B.; Almar, R.; Le Cozannet, G. Under-estimated wave contribution to coastal sea-level rise. *Nat. Clim. Chang.* **2018**, *8*, 234–239. [CrossRef]
53. McFeeters, S. The use of the Normalized Difference Water Index (NDWI) in the delineation of open water features. *Int. J. Remote Sens.* **1996**, *17*, 1425–1432. [CrossRef]
54. Kaczmarek, L.M.; Ostrowski, R.; Pruszak, Z.; Rozynski, G. Selected problems of sediment transport and morphodynamics of a multi-bar nearshore zone. *Estuar. Coast. Shelf Sci.* **2005**, *62*, 415–425. [CrossRef]
55. Kamphuis, W. Alongshore Sediment Transport Rate. *J. Waterw. Port Coast. Ocean. Eng.* **1991**, *117*, 622–640. [CrossRef]
56. Bayram, A.; Larson, M.; Hanson, H. A new formula for the total longshore sediment transport rate. *Coast. Eng.* **2007**, *54*, 700–710. [CrossRef]
57. Dail, H.J.; Merrifield, M.A.; Bevis, M. Steep beach morphology changes due to energetic wave forcing. *Mar. Geol.* **2000**, *162*, 443–458. [CrossRef]
58. SOGREAH. *Etudes De Faisabilité Et D'avant Projet Sommaire De L'émissaire Deltaand Rapport Final: Grenoble, France*; Technical Report; SOGREAH: Grenoble, France, 1994.
59. Eamer, J.B.; Walker, I.J. Quantifying spatial and temporal trends in beach–dune volumetric changes using spatial statistics. *Geomorphology* **2013**, *191*, 94–108. [CrossRef]
60. Niang, A.; Kane, A. Morphological and Hydrodynamic Changes in the Lower Estuary of the Senegal River: Effects on the Environment of the Breach of the 'Langue De Barbarie' Sand Spit in 2003. In *The Land/Ocean Interactions in the Coastal Zone of West and Central Africa; Estuaries of the World*; Diop, S., Barusseau, J.P., Descamps, C., Eds.; Springer: Cham, Switzerland, 2014; pp. 23–40.
61. Ndour, A.; Ba, K.; Almar, A.; Almeida, P.; Sall, M.; Diedhiou, P.M.; Floc'h, F.; Daly, C.; Grandjean, P.; Boivin, J.-P.; et al. On the Natural and Anthropogenic Drivers of the Senegalses (West Africa) Low Coast Evolution: Saint Louis Beach 2016 COASVAR Experiment and 3D Modeling of Short Term Coastal Protection Measures. *J. Coast. Res.* **2016**, *95*, 583–587. [CrossRef]
62. Coco, G.; Murray, A.B. Patterns in the sand: From forcing templates to self-organization. *Geomorphology* **2007**, *91*, 271–290. [CrossRef]

63. Tribe, H. The Geomorphology of Farewell Spit and Its Sensitivity to Sea-Level Rise. Master's Thesis, School of Geography, Environment and Earth Sciences, Victoria University of Wellington, Wellington, New Zealand, 2008.
64. Dean, R.; Dalrymple, R. Long-term processes. In *Coastal Processes with Engineering Applications*; Cambridge University Press: Cambridge, UK, 2001; pp. 35–70.
65. Amante, C. Estimating Coastal Digital Elevation Model Uncertainty. *J. Coast. Res.* **2018**, *34*, 1382–1397. [CrossRef]
66. Loghin, A.M.; Otepka-Schremmer, J.; Pfeifer, N. Potential of Pléiades and WorldView-3 Tri-Stereo DSMs to Represent Heights of Small Isolated Objects. *Sensors* **2020**, *20*, 2695. [CrossRef] [PubMed]
67. Yamazaki, D.; Ikeshima, D.; Tawatari, R.; Yamaguchi, T.; O'Loughlin, F.; Neal, J.; Sampson, C.; Kanae, S.; Bates, P. A high-accuracy map of global terrain elevations. *Geophys. Res. Lett.* **2017**, *44*, 5844–5853. [CrossRef]
68. Letortu, P.; Jaud, M.; Théry, C.; Nabucet, J.; Taouki, R.; Passot, S.; Augereau, E. The potential of Pléiades images with high angle of incidence for reconstructing the coastal cliff face in Normandy (France). *Int. J. Appl. Earth Obs. Geoinf.* **2020**, *84*, 101976. [CrossRef]
69. Rupnik, E.; Daakir, M.; Pierrot Deseilligny, M. MicMac—A free, open-source solution for photogrammetry. *Open Geospat. Data Softw. Stand* **2017**, *2*, 1–9. [CrossRef]
70. Rupnik, E.; Pierrot-Deseilligny, M.; Delorme, A. 3D reconstruction from multi-view VHR-satellite images in MicMac. *ISPRS J. Photogramm. Remote Sens.* **2018**, *139*, 201–211. [CrossRef]
71. Sallenger, A.H., Jr.; Krabill, W.; Swift, R.; Brock, J.; List, J.; Hansen, M.; Holman, R.; Manizade, S.; Sontag, J.; Meredith, A.; et al. Evaluation of airborne topographic lidar for quantifying beach changes. *J. Coast. Res.* **2003**, *19*, 125–133.
72. Chen, B.; Yang, Y.; Wen, H.; Ruan, H.; Zhou, Z.; Luo, K.; Zhong, F. High-resolution monitoring of beach topography and its change using unmanned aerial vehicle imagery. *Ocean. Coast. Manag.* **2018**, *160*, 103–116. [CrossRef]
73. Rotnicka, J.; Dłużewski, M.; Dąbski, M.; Rodzewicz, M.; Włodarski, W.; Zmarz, A. Accuracy of the UAV-Based DEM of Beach–Foredune Topography in Relation to Selected Morphometric Variables, Land Cover, and Multitemporal Sediment Budget. *Estuaries Coasts* **2020**, *43*, 1939–1955. [CrossRef]
74. Nelson, A.; Reuter, H.; Gessler, P. Chapter 3 DEM Production Methods and Sources. *Dev. Soil Sci.* **2009**, *33*, 65–85. [CrossRef]
75. Hasegawa, H.; Matsuo, K.; Koarai, N.; Watanabe, N.; Masaharu, H.; Fukushima, Y. DEM accuracy and the base to height (B/H) ratio of stereo images. *Int. Arch. Photogramm. Remote Sens.* **2000**, *33*, 356–359.
76. Morris, R.; Boxshall, A.; Swearer, S. Climate-resilient coasts require diverse defence solutions. *Nat. Clim. Chang.* **2020**, *10*, 485–487. [CrossRef]

frontiers | Frontiers in Marine Science

TYPE Original Research
PUBLISHED 01 December 2022
DOI 10.3389/fmars.2022.993644

Check for updates

OPEN ACCESS

EDITED BY
Javier Benavente,
University of Cádiz, Spain

REVIEWED BY
Papa Ibnou Ndiaye,
Cheikh Anta Diop University, Senegal
William James Pringle,
Argonne National Laboratory (DOE),
United States

*CORRESPONDENCE
Cheikh Omar Tidjani Cisse
cheikhomartidjaniciss@yahoo.fr

SPECIALTY SECTION
This article was submitted to Coastal Ocean Processes, a section of the journal Frontiers in Marine Science

RECEIVED 13 July 2022
ACCEPTED 15 November 2022
PUBLISHED 01 December 2022

CITATION
Cisse COT, Brempong EK, Taveneau A, Almar R, Sy BA and Angnuureng DB (2022) Extreme coastal water levels with potential flooding risk at the low-lying Saint Louis historic city, Senegal (West Africa). *Front. Mar. Sci.* 9:993644. doi: 10.3389/fmars.2022.993644

Extreme coastal water levels with potential flooding risk at the low-lying Saint Louis historic city, Senegal (West Africa)

Cheikh Omar Tidjani Cisse[1*], Emmanuel K. Brempong[2,3,4], Adélaïde Taveneau[4], Rafael Almar[4], Boubou Aldiouma Sy[1] and Donatus Bapentire Angnuureng[2]

[1]Laboratory Leïdi "Dynamics of the Territories and Development" Department of Geography, University Gaston Berger, Saint-Louis, Senegal, [2]Africa Centre of Excellence in Coastal Resilience, Centre for Coastal Management, School of Biological Sciences (SBS), University of Cape Coast, Cape Coast, Ghana, [3]Department of Fisheries and Aquatic Sciences (DFAS), University of Cape Coast, Cape Coast, Ghana, [4]Laboratory of Geophysical and Oceanographic Spatial Studies (LEGOS), University of Toulouse/CNRS/IRD/CNES), Toulouse, France

In a context of global warming characterized by a mean sea level rise and extreme meteorological events, the study of the causes for coastal flooding is essential to protect communities and ecosystems. Densely urbanized, and rather unprotected cities in developing countries such as the historic Saint Louis city in Senegal are particularly vulnerable to coastal flooding and sea hazards. From satellite-derived high resolution DEM and global ocean reanalyses, here we quantify the extreme coastal water level in order to identify the neighborhoods and places of particular socio-economical interest of Saint-Louis potentially vulnerable to flooding. The results reveal that the most severe levels have the potential to flood up to almost half of this low-lying river mouth plain. Social, economic and heritage stakes are exposed, and the artisanal fisherman district of Gueth Ndar, is particularly vulnerable to coastal flooding because of its low elevation and situation on the sand barrier. The co-occurrence of high tides and wave-induced runup contributes most to ECWL but they do not present a significant trend over the study period. The results show that over the period 1994-2015, potential flood risk increased by nearly one day per year, primarily due to sea level rise, sounding a warning signal to take countermeasures to protect communities and infrastructure.

KEYWORDS

coastal flooding, extreme coastal water level, satellite-derived DEM, heritages issues, sea level rise, wave runup

Introduction

In a global context marked by global warming leading to an increasing rise in sea level, coastal areas are increasingly threatened by the risks of erosion and coastal flooding (Woodruff and Stults, 2016; Kulp and Strauss, 2019; Almar et al., 2021; Kirezci et al., 2020). Coastal areas are among the most vulnerable ecosystems and will be gradually exposed to the effects of climate change over the course of the century (IPCC report, Oppenheimer et al., 2019). According to recent studies, for instance in Almar et al. (2021), the IPCC RCP8.5 scenario would give 50x increase in coastal overtopping by 2100, worldwide. These hazards occur when strong winds and low atmospheric pressure act on the sea surface to cause a temporary rise in sea level (Wells, 2011; Prime et al., 2016), becoming a real environmental concern for anthropized coastlines (e.g. Le Roy et al., 2015). Knowing that more than 600 million people reside in the low elevation coastal zone (<10 m, Ganguli and Merz, 2020), that the coastal activities expose the population to floods and storms (Dupuis, 2016) and that 3/4 of the world's largest cities are located on those vulnerable areas (Melet et al., 2018), the combination of current massive urban growth and climate change impacts exposes coastal cities to increased and unprecedented coastal risks and environmental issues (Cain et al., 2015; Bongarts Lebbe et al., 2021). Whether riverine or coastal, flooding is one of the most devastating coastal hazards in the world, causing numerous deaths and significant socio-economic consequences each year (Kupfer et al., 2022). According to Vousdoukas et al. (2016), coastal flooding will increase in the context of future storm variability and sea level rise. Nowadays, flooding represent one of the most important issues facing coastal communities (Woodruff et al., 2013).

On the Atlantic coast of Central and West Africa, coastal flooding is one of the greatest threats to the socio-economic and environmental balances of countries south of the Sahara (Tchindjang et al., 2019; Alves et al., 2020; Dada et al., 2021; Vousdoukas et al., 2022). Most West African major cities are exposed to flooding there, and current forecasts show that sub-Saharan Africa and the low elevation, flat deltaic and island coastal regions are among the most affected areas by climate change (Gemenne et al., 2017; Giardino et al., 2018). Extreme Coastal Water Level (ECWL) at the coast results from the combination of several different coastal processes (Eq. 1); the regional sea level anomaly (here referred to as SLA) due to the steric effect, ocean circulation and transfer of mass from the continents (ice sheets, glaciers, land water) to the ocean, storm surge or "Dynamic Atmospheric Correction" (DAC) due to atmospheric pressure and winds, astronomical tide (T) and wave effects here referred to as runup (R) which includes a time-averaged component (setup) and an oscillatory component (swash) (see Melet et al., 2018; Dodet et al., 2019; Almar et al., 2021).

The West Africa coast is generally considered a storm-free environment, dominated by North Atlantic distant swells (Sadio, 2017; Almar et al., 2019; Ndour et al., 2020). The evolution of the sandy coast is controlled by strong longshore sediment drift resulting from oblique waves (Laïbi et al., 2014; Almar et al., 2015; Giardino et al., 2018; Almar et al., 2019; Anthony et al., 2019). Tidal amplitude is typically micro to meso at open stretches of coasts, with the highest amplitudes recorded in deltas and estuaries of Guinea, Guinea-Bissau and Sierra Leone (2.8 - 4.7 m; Diop et al., 2014). Senegalese urban coastal areas, which are low elevated and made of loose or low-strength materials (Weissenberger et al., 2016; Ndour et al., 2018; Ndour et al., 2020) often lying on barrier and at delta, are particularly exposed to marine flooding, which has severe consequences on coastal development (Quiroga et al., 2021). Located at the mouth of the Senegal River, Saint-Louis has a mixed environmental problem with respect to flooding, affected by both coastal flooding and river flooding (Sall, 2006; Wade et al., 2008; Ndour et al., 2018). Although this situation is well known in the history of this city, the situation recently worsened (Durand et al., 2010; Sadio, 2017; Bergsma et al., 2020) due to the rising sea level together with the increase in ocean influence induced by a breach made in the Langue de Barbarie in 2003, a coastal spit that previously protected the city from the Atlantic. When large storm surges occur during rainy periods, when the agitation of the sea hinders the evacuation of river water (Sadio et al. 2017), large-scale events can occur, including those of August 2017 and February 2018, which caused the destruction of 100 houses and the displacement of 2600 people (Diagne, 2020).

In the context of ongoing climate change and the prediction of an increase in climatic instability, the extension of flood-prone areas, in relation to a given climatic hazard, is a scientific concern with strong societal implications (Breilh et al., 2012), but in Senegal, there is almost non- existent work on marine flooding and the anticipation of their impact and mitigation/adaptation (Cisse et al., 2022). In addition, given the gradual artificialization of Saint-Louis coastline, which is reflected in the emergence of numerous coastal protection projects (Alves et al., 2020) such as a riprap built between 2020 and 2022 it is of the essence to study coastal flooding. According to Tebaldi et al. (2012) understanding coastal flooding vulnerability is essential to the decision-making logic and to the protection policies of coastal communities and assets.

Using satellite-derived data and model hindcast data, this paper aims to evidence the vulnerability of the historic Saint-Louis city to potential coastal flooding where it endangers property and people, economic activities, and cultural and religious heritage.

Study area

The city of Saint-Louis is located in northern Senegal (Figure 1). It has the characteristics of an amphibious city, as it is built partly on the mainland, partly on an island in the Senegal River and partly on the Langue de Barbarie (Sall, 2006).

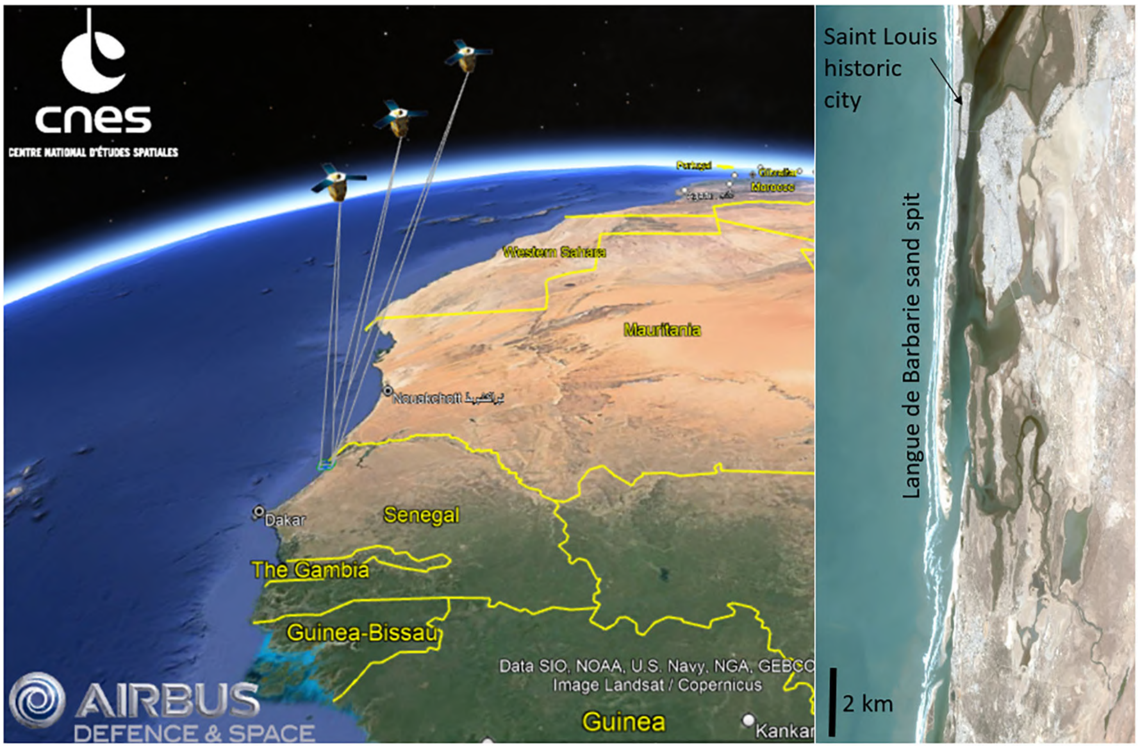

FIGURE 1
Location of the study area and satellite images acquisition. (Left) Pleiades satellite (CNES/Airbus) tri-stereo acquisition (made using Google Earth). (Right) North-oriented Pleiades satellite image of Saint Louis city.

The latter is a sandy coastal spit that extends for 40 km and has a variable width of about 100 m. Bounded by the Atlantic Ocean to the west and the Senegal River to the east, the Langue de Barbarie forms an elongated peninsula running north-south (Kante and Fall, 2019; Brüning, 2022). It is a highly urbanized site with the presence of human settlements, artisanal landing ports, tourist facilities, and a national park of high environmental value. Indeed, like other sections of the Senegalese coastline, the Saint-Louis coastline is among the most vulnerable to flooding and erosion risks. It has a flat topography (most neighborhoods are built less than 2 m above sea level), sandy soil, and a site dominated by water, which exposes the population to many natural hazards, the most recurrent of which are floods (Durand et al., 2010; Sy et al., 2011).

Materials and methods

Topographic data

The Digital Elevation Model (DEM) used in this study is derived from the very high- resolution optical imagery from Pleiades satellite (CNES/Airbus) - see Figure 1. Using Pleiades panchromatic image (0.5 m ground pixel resolution), a tri-stereogrammetry method is performed using the NASA software ASP (Ames Stereo Pipeline; Shean et al., 2016) to extract the topography of the Langue de Barbarie (Almeida et al., 2019; Salameh et al., 2019; Taveneau et al., 2021). The use of tri-stereo method (three images) is preferred over stereo one (two images) as it significantly improves the derived-topography (Almeida et al., 2018; Collin et al., 2018; Taveneau et al., 2021; James et al., 2022). The images selected for this work are 3 acquired in March 2019, and further processed using the method further described by Taveneau et al., 2021. The obtained DEM has a 2 m ground pixel resolution and is map-projected into the UTM 28 coordinates system thanks to the RPC (Rational Polynomial Coefficient) geometric file provided with each Pleiades product.

This satellite-derived DEM-generation method allows a good relative map-projection of the data, but the vertical values "float" in absolute as no elevation information is provided within ASP. Ground control points are essential to give reference points to the DEM and correct the offset. With ground surveys carried out few days apart from the satellite acquisition using a RTK-GPS (Real Time Kinematic - Global Positioning System) with a centimetric-precision (performed by the SHOM, the French Navy Hydrographic and Oceanographic Service) over 13 km of the Langue de Barbarie), the DEM elevation is vertically-corrected (Garlan et al., 2020) thanks to the collected ground control points. Overall, although it depends on the nature of the ground (e.g., buildings, flat terrain, vegetation), sub-metric to metric accuracy is obtained from Pleaides mission-derived DEMs after offset correction (Almeida et al., 2019; Taveneau et al., 2021).

Hydrodynamic data

Quantification of extreme coastal water levels requires the availability of hydrodynamic, meteorological and tidal parameters. Tide data are extracted from the global tide FES2014 model (Finite Element Solution, Carrere et al., 2016) at hourly resolution and gridded worldwide at a 1/16° resolution and produced by Laboratory of Geophysical and Oceanographic Spatial Studies of Toulouse (LEGOS). Atmospheric pressure and winds component (DAC) is produced by the Collecte Localisation Satellites (CLS) Space Oceanography Division using the MOG2D model from LEGOS and distributed by AVISO (Archiving, Validation and Interpretation of Satellite Oceanographic data), with support from Centre National d'Etudes Spatiales (CNES) (http://www.aviso.altimetry.fr/). Altimetric-derived SLA, including global mean level rise, is extracted at the closest altimetry gridded data point from AVISO and it corresponds to offshore regional sea level (Marti et al., 2021). ERA-Interim reanalysis data (global climate and weather data available from 1979 onward) at a 0.5° x 0.5° resolution developed by the European Center for Medium-Range Weather Forecasting (ECMWF) model are used for waves data at a 6-hour resolution over the 1994-2015 period. Wave runup R is computed following the dissipative beach form of Stockdon et al., 2006 (see Almar et al., 2021):

$$R = 0.043\sqrt{H_s L_o}$$

Where H_s and L_o are offshore significant wave height and wavelength. All the above-mentioned parameters are resampled on an hourly basis over the 2013-2015 period. All the hydrodynamic data used in this study are global dataset available worldwide are all extracted at the nearest point from Saint Louis city (latitude 16.23°, longitude -16.21°) in the corresponding grids, which ensures here a maximum distance of 50 km from the coarsest grid. They correspond to off the coast forcing and does not reflect local coastal complex processes that might occur (i.e. interactions between drivers, waves refraction, morphology changes – see Idier et al., 2019; Bergsma et al., 2022).

Quantification of the extreme coastal water level

To quantify the extreme coastal water level at Saint-Louis, we use the formula of Almar et al. (2021) (Eq. 1):

$$\mathbf{ECWL} = \mathbf{SLA} + \mathbf{DAC} + \mathbf{T} + \mathbf{R} \tag{1}$$

The extreme levels are generated following the combination of several parameters, this model incorporates the sea level anomaly (SLA), the height of the storm surge (DAC) due to atmospheric pressure and winds, the level of the astronomical tide (T) and the height of wave breaking (R). In order to physically determine the impact of extreme water level reached by the sea in Saint-Louis, we define the severe water levels corresponding to the top 2%, thus the 98th percentile (following a common definition of extreme storms). The cumulative annual occurrence of the of the time spent over this threshold is computed over the study period.

To compute overtopping and flooding potential, the topographic data in this work are set to a geoidal coordinate system (vertical datum). Here, the ECWL are converted to geodetic data using the vertical datum value (0.981m) of Wöppelmann et al. (2008), so that they can be superimposed with the topographic data. It should be recalled that the vertical datum used is that of the tide gauge in Dakar, because there is no one in Saint-Louis.

To study the trend of evolution of the extremes in Saint-Louis on the basis of annualized data, the regress function of the Matlab software (linear regression) is used. In addition, the statistical test p-value is calculated to determine the level of significance of the trend.

Flood zone and mapping and risk for infrastructures

The methodological approach to flood mapping adopted in this work is based on the calculation of the percentage of potentially floodable surface through the satellite-derived DEM and the raster calculator tool of the Arc Gis software. Then, from the OSM (Open Street Map) databases, the properties (buildings, parcels, etc.) are vectorized in Arc Gis. To identify the infrastructures potentially exposed to flooding, spatial queries similar to the selection by location are made in order to extract the properties that are under the spatial extension of a certain ECWL threshold.

Results

Evolution of extreme coastal level occurrences

The thresholds representing the percentiles of low (30%), moderate (60%) and severe (98%) ECWL correspond to -0.05 m, 0.78 m and 1.98 m, respectively (Figure 2A). Figure 2B shows the evolution of the most severe threshold that presents a strong interannual variability. The maximum temporal occurrence of the 1.98 m level was 180 hours between 1995 and 2000, but since 2005, there are 3 years out of 5 where it does not exceed 100 h, with a minimum value of 54h. By extension, the occurrence of floods has weakened over the sequence 2005-2010. On the other hand, from 2010, there is an increase in the frequency of flooding, with a maximum value of 220h, which reflects an increase in the total annual duration of extreme sea levels, and probably the frequency of coastal flooding in Saint-Louis. Overall, the increasing trend in occurrence (significant at 95% level) is 1h per year which correspond to almost a day spent with flooding over this 23 years period.

Flood-prone areas and associated impacts

To show the potential of extension of the coastal flooding in Saint-Louis, a mapping of flood-prone areas is performed based on the two highest percentiles, 60th and 98th, combined with satellite-based DEM (Figure 3). This because the 30th (-0.05 m) percentile does not generate any risk of flooding in Saint-Louis.

Figure 3 shows a significant variation in the extent of flooding between the 60th and 98th percentiles and highlights a spatial contrast of the Saint-Louis coastline sections submerged by extreme water-levels. The used-approach reveals that 10% of the Saint Louis area would be potentially flooded under the 60th ECWL threshold, in this low-lying river mouth alluvial plain. This surface potentially submerged under the severe 98th ECWL threshold reaches 45% of the area is floodable, reaching key urbanized areas.

The results reveal that some neighborhoods of Saint-Louis are potentially exposed to extreme coastal water levels. Indeed, much of the area covered by the Langue de Barbarie is submersible. Figure 4 shows that the district of Gueth Ndar (the most densely populated of Saint Louis and Senegal; Diop, 2017) is the most exposed to coastal flooding, followed by Ndar Toute and Goxxu Mbacc. On the other hand, important governmental infrastructures located on the island of Saint-Louis appears to be preserved: the spatial extent of the severe water level (98th percentile) does not affect this part of Saint-Louis (north and south island). Moreover, the spatial disparity of the flood extension observed on the Langue de Barbarie is similar to that observed in the Sor suburb. In this part of Saint-Louis, only the neighborhoods located in front of the Senegal River are subject to flooding and the Pikine neighborhood located inside the Sor suburb. From the 10 sites (Goxxu Mbacc, Ndiollofène, Gueth Ndar, North and South Islands, Corniche, Balacos, Diamaguene, Léona and Pikine), Gueth Ndar remains the most vulnerable to coastal flooding. This is explained by its elevation characteristics largely below the hydrodynamic extreme levels (i.e. 1.98 m). In terms of infrastructure, the spatial queries performed reveal that 140 of the 24588 buildings and 452 plots of land (or parcels) on 13796 can be flooded. This means that many social, economic, cultural and religious assets are potentially endangered if not protection is deployed.

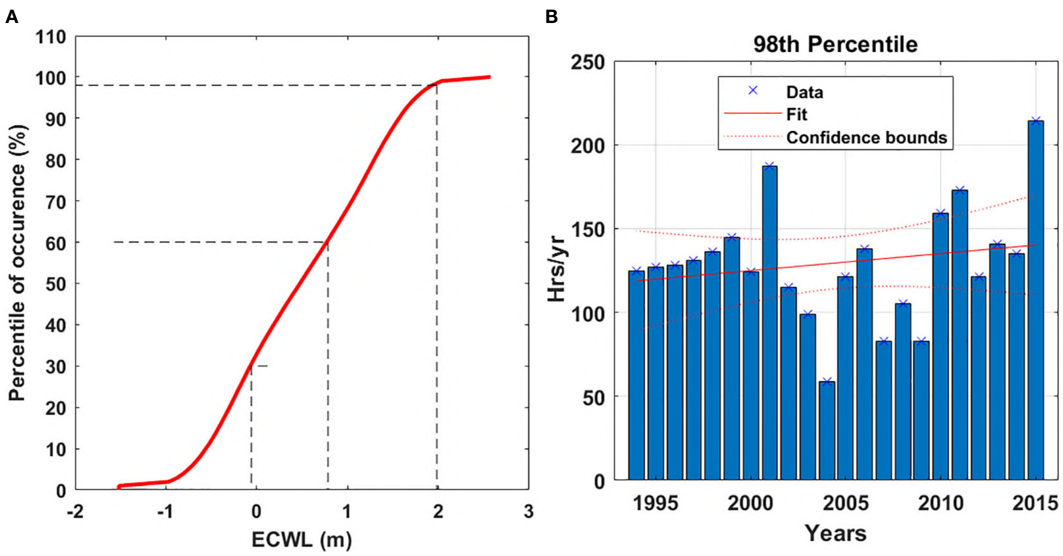

FIGURE 2
(A) Distribution of different percentiles of extreme coastal water level (ECWL), from 1994 to 2015. **(B)** Number of hours per year that coastal sea level at Saint-Louis reaches the 98th percentile (1.98 m).

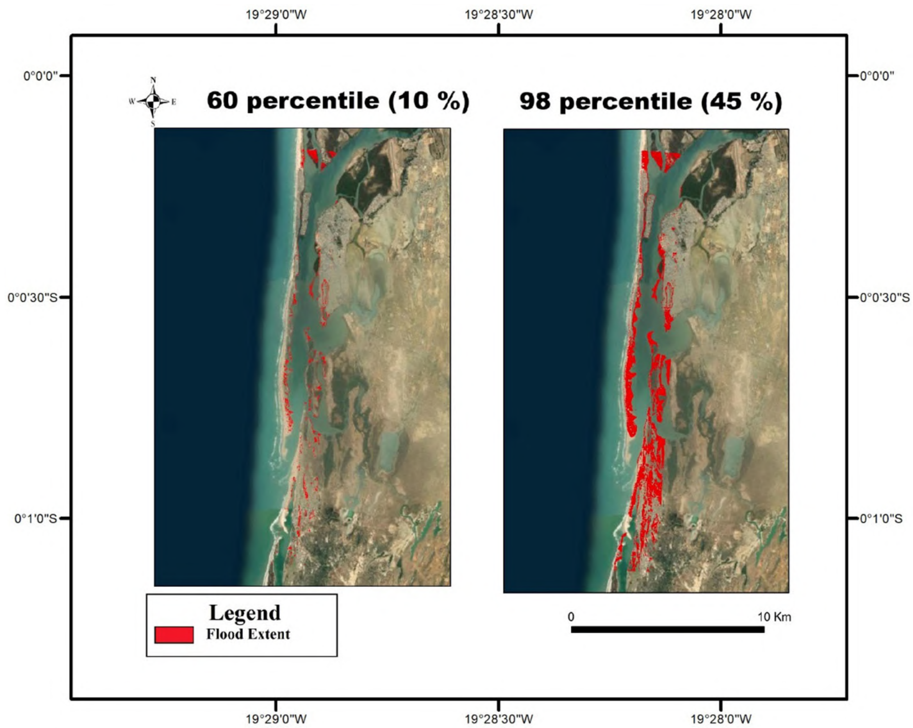

FIGURE 3
Spatial extent (red) of potential flooding for the moderate and severe ECWL scenarios, i.e. the 60th and 98th percentile.

Hydrodynamic factors contributing to coastal flooding

Since the estimation of EWCL from the Almar et al. (2021) model involves four parameters, we estimate here the relative weight of each of them in the 98th percentile for the period 1994-2015. Figures 5A–E shows hourly overall timeseries and annual means of each component. Figure 5F shows the aggregated annual conditions that produced a level above the 98th percentile. The tide (T) contributes the most with 71%, followed by wave run-up (R) with 25%, sea level anomaly (SLA) drives 3%, with a negligible contribution (<1%) of storm surge height due to atmospheric pressure and winds (DAC) in this storm free environment. Noteworthy, while SLA and DAC are dominated by interannual low varying evolutions (i.e. season to years), waves and particularly tide have rapid changes (i.e. hours to days).

The analysis of the evolution of the extreme level of coastal waters in Saint-Louis reveals that despite his minor influence on ECWL events, only SLA shows a significant 3.5 mm/yr trend at the 95% level (pvalue less than 0.05), which contributes to the increase in potential flooding. However, the large variability of wave runup T and R during the events prevent a robust overall trend assessment of ECWL on the study period and is a clear source of uncertainty for coastal flooding risk prediction in Saint Louis and elsewhere. This is due to the combined effect of their large amplitude with high frequency signal with a random phasing: waves randomly reach the coast during neap or spring tides, low or high tides.

Discussion

The estimation of the extreme coastal water level in Saint-Louis reveals that this section of the Senegalese coastline is extremely vulnerable to ocean-induced flooding. Being a highly urbanized site with an urban growth of 5% (Sidibe, 2013), there is no doubt that the shores are highly exposed to coastal flooding. Therefore we cannot talk about risk or vulnerability without the existence of stakes (Pont, 2015): socio-economic or environmental. The potential flood events of the Langue de Barbarie are likely to affect social, cultural, economic, heritage and cultural matters. Flooding in Saint-Louis causes a wide range of impacts (Sall, 2006). From a spatial point of view, the potential impacts manifest themselves in variable geometry. Of the 10 sites (Goxxu Mbacc, Ndiollofène, Gueth Ndar, North and

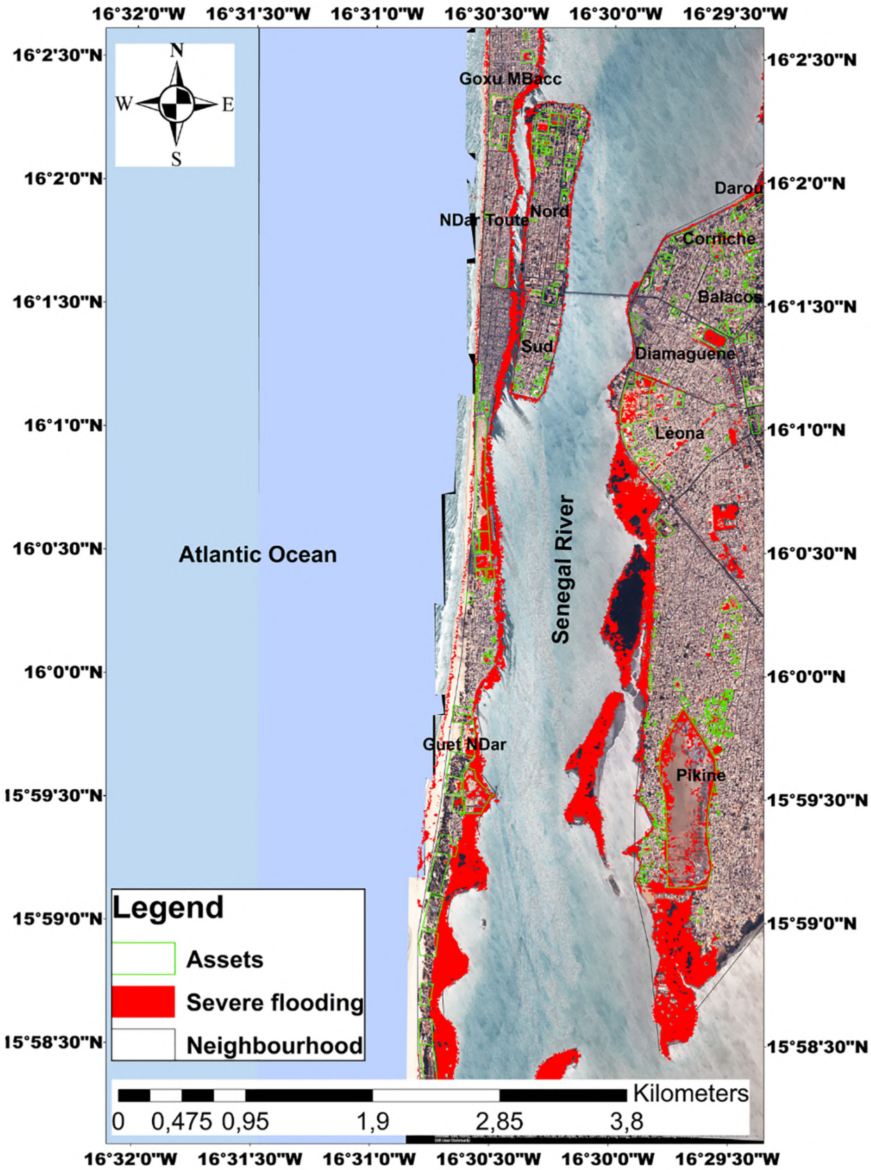

FIGURE 4
Map of infrastructures and assets of Saint Louis likely to be potentially flooded under the 98th ECWL percentile (i.e. 1.98 m).

South Islands, Corniche, Balacos, Diamaguene, Léona and Pikine), the site of Gueth Ndar remains the most vulnerable to coastal flooding. The district of Gueth Ndar is the most exposed to flooding likely to be induced by the 1.98m water level. Given its high human density, it is the most populated neighborhood of the Saint Louis, but also of Senegal and West Africa (Diop, 2017; Brüning, 2022). This high human concentration combined with its sensitivity to flooding, makes it particularly vulnerable. Many of the social assets (including historical cemetery) present in this part of the Langue de Barbarie would be impacted by flooding, which would also have consequences for the population as well as for socio-economic activities, particularly fishing, which is the dominant activity. This situation of vulnerability should incite decision makers and coastal managers to consider the protection of this section of the Saint-Louis coastline. Efforts concerning the protection of coastal communities of the Langue de Barbarie have been made through the construction of a protective dyke of 3m height in 2022. However, beyond the hard methods of coastal protection, other alternatives of protection should be adopted such as soft and nature based solutions (Alves et al.,

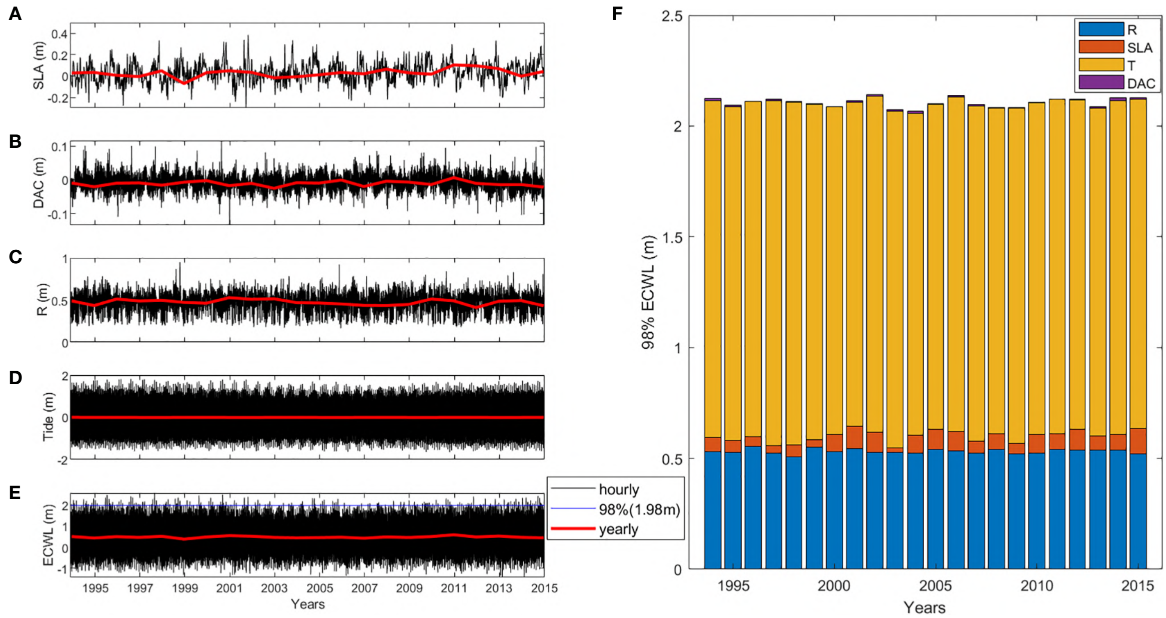

FIGURE 5
(A–E) ECWL components hourly (black) and yearly (red) timeseries and **(F)** contribution of each ECWL component passing the 98 percentile and potentially causing severe flooding in Saint-Louis between 1994 and 2015. In **(F)** the components are aggregated yearly during the moments overpassing the 98 percentile. Blue line in **(E)** stands for the 98th percentile of the ECWL timeseries, and referred to as "severe" value.

2020). Indeed, our results show that more and more extreme coastal water levels are expected and could overtop and overflow the protective dike. To this end, the use of soft development measures would be an effective solution. Soft solutions are less damaging to the environment than hard solutions (Schoones et al., 2019). Moreover, Baldé et al. (2021) showed that beach nourishment in the Langue de Barbarie, in this case the beaches of Pilote Bar, played an important role in that it contributed to beach widening. This method can also be efficient in dealing with coastal flooding. A wide, fattened beach provides good protection against erosion and overwash by decreasing runup propagation, as well as the probability of crossing (Duvat, 2001; Balouin et al., 2012; Itzkin et al., 2021). Moreover, it is likely to encounter the phenomena of land subsidence of this densely populated Gueth Ndar neighborhood. Continued subsidence catalyzes sea level rise, which in turn increases water levels, which exacerbates coastal flooding (Moller et al., 2014). According to Woodruff et al. (2013), the impacts of coastal flooding can be mitigated in part through the implementation of adaptation strategies using conservative sediment management and human-induced subsidence reduction. The protection of this sandy strip (Langue de Barbarie) is of paramount importance, as its disappearance could have significant impacts on the city of Saint-Louis and the Sor suburb. In fine, the relocation of populations may be a possible solution to protect people. Moreover, a relocation project to offer long-term protection to the populations of the Langue of Barbarie in Saint-Louis is underway. A 14-hectare relocation site located in Diougop outside the city of Saint-Louis is being developed. On this site, 600 housing units will be built to accommodate 10,000 people (Brüning, 2022). This relocation project is currently encountering a number of pitfalls related to the issue of social acceptability. The populations of Gueth Ndar, who are mostly fishermen, feel that this policy of relocation inland would take them away from their place of work, the sea. However, a participatory approach should be adopted to facilitate acceptance of the project if their cultural and socio-economic contribution to the identity of Saint-Louis is to be maintained.

Given that the drivers of coastal flooding are varied (Prime et al., 2016), we attempted to separately analyze the factors contributing to coastal flooding in Saint-Louis. Our results show that the tide is the dominant driver of coastal flooding in Saint-Louis. This observation is also made by Durand et al. (2010) on the Langue de Barbarie. This finding is consistent with Almeida et al. (2018) and Dada et al. (2019) works showing at other low-lying coasts exposed to energetic waves that coastal flooding in Nha Trang (Vietnam) and low-lying mud coast in Nigeria Delta (Gulf of Guinea) are due to the interaction between waves and tide. Durand et al. (2010) also points out that the tidal range has significantly increased after the opening in 2003 of a breach in the sandspit and water levels in Saint-Louis lagoon are increasingly aligned with the rhythm of the tides. However, due to the lack of long-term tide gauges in Saint Louis, more generally along the African coast (Abessolo Ondoa et al., 2019; Marti et al., 2021; Almar et al., 2022), our current study is limited by the use of the FES2014 tide data which are harmonic-based, off-shore, and do not reflect change over time (Figure 5D); any trends or changes in local tides in could not be determined. Our results also show interannual variability in the temporal occurrence of extreme water levels at Saint-Louis. Especially since our results reveal that the tide is the main factor contributing to coastal flooding in Saint- Louis, and that in a global context of global warming the sea level is expected to increase. Thus, the impact of flooding in Saint-Louis will strongly impact coastal communities. Due to the presence of the river, the study area is at great risk of flooding as the sea level rises gradually. Sea level rise by 2100 will strengthen coastal flooding in Saint-Louis (Sall, 2006). Our data reveal that waves have a significant impact on the occurrence of ECWL events at Saint-Louis. As a difference with tides, the action of waves on extreme events is likely to take significant proportions especially in a context of climate and climate variability change, it should be remembered. In particular, waves have a strong interannual fluctuation controlled by the North Atlantic Oscillation (Almar et al., 2019). Climate change, - which is reflected in the sea level rise, has the effect of strengthening the action of waves (Costa, 1995; Wang et al., 2003; Melet et al., 2018), and will influence the generation of swells of high intensity at the coast (Sergent et al., 2010; Vitousek et al., 2017). This concern is confirmed by the global simulations of Vitousek et al. (2017) that identify the inter-tropical zone as particularly exposed to future increase in coastal flooding.

In St. Louis, we find that this increase in potentially inundated area with ECWL is rather linear (Table 1). Interestingly, while there is considerable climate-induced variability in waves, model predictions do not indicate clear long-term trends (Melet et al., 2020a), nor does the R runup. While current ECWL maxima are about 2 m, with a 1 m sea level rise offset, as predicted (Oppenheimer et al., 2019) for the late 21st century, the inundated area can be expected to increase by 25% if no protective measures are taken.

TABLE 1 Potential flooded area (%) at Saint Louis for ECWL thresholds.

ECWL (m)	Potential flooded area (%)
0,05	0,29
0,5	4,5
1	15,20
1,5	30,13
2	45,42
2,5	58,30
3	67,43

Lastly, it should be noted that when interpreting the consequences of overtopping on coastal flooding, the occurrence of overtopping does not necessarily imply that the entire low elevation coastal zone is flooded. Rather, overtopping drives localized coastal flooding, immediately adjacent to areas of overtopping, which would likely be both temporally and spatially variable due to the combined effects of temporal and alongshore gradients in breaking wave heights, and alongshore variations in coastal elevation maxima (Almar et al., 2021). Even if a standalone use for coastal studies (e.g. without ground control point) is not yet conceivable at this stage with operational accuracy (Taveneau et al., 2021; Turner et al., 2021), considering the encountered accuracy limitations, satellite-based topography monitoring appears as a breakthrough in decade-old monitoring technological barriers (Benveniste et al., 2019; Melet et al., 2020b), in support of coastal engineering.

Conclusion

By combining satellite-derived DEM with reanalyzes and satellite observations of sea level components, this paper assessed the vulnerability of the Saint-Louis coastline to the potential risk of coastal flooding. Testimonies already reported various impacts on economic, cultural, patrimonial and infrastructural. Our results confirm that this site is extremely vulnerable to coastal flooding potential almost half of this low lying river mouth plain flooded under severe water levels. Spatially, the different neighborhoods of Saint-Louis are unequally affected with the most exposed one, also one of the poorest with vulnerable communities, being located on the Langue of Barbarie sandspit. Sea level rise is the main factor for the trend. However, the fact that on top of rising sea, that the compound influence of waves and tide that is predominant responsible for the events induce a large uncertainty on the prediction of coastal risk. This study documents coastal risk flooding potential and its drivers which is not sufficiently quantified and understood on the Senegalese coasts and West Africa, and whose knowledge is an essential element in the elaboration of coastal development schemes and protection of coastal communities.

Data availability statement

The original contributions presented in the study are included in the article/supplementary material. Further inquiries can be directed to the corresponding author.

Author contributions

All authors contributed to the article and approved the submitted version.

Funding

This article was produced with the support of coastal protection project in Saint-Louis (PPCS) co-financed by French Agency for Development/Municipal Development Agency. Convention n°CSN156102.

Acknowledgments

The authors would want to thank the Senegalese Agence of Development Municipal (ADM), the French Agency Development (AFD) for funding this research and the program DINAMIS for making the satellite Pleiades data available.

Conflict of interest

The authors declare that the research was conducted in the absence of any commercial or financial relationships that could be construed as a potential conflict of interest.

Publisher's note

All claims expressed in this article are solely those of the authors and do not necessarily represent those of their affiliated organizations, or those of the publisher, the editors and the reviewers. Any product that may be evaluated in this article, or claim that may be made by its manufacturer, is not guaranteed or endorsed by the publisher.

References

Abessolo Ondoa, G., Almar, R., Castelle, B., Testut, L., Léger, F., Sohou, Z., et al. (2019). Sea Level at the coast from video-sensed waves: Comparison to tidal gauges and satellite altimetry. *J. Atmospheric Oceanic Technol.* 36 (8), 1591–1603. doi: 10.1175/JTECH-D-18-0203.1

Almar, R., Kestenare, E., Reyns, J., Jouanno, J., Anthony, E. J., Laibi, R., et al. (2015). Response of the bight of Benin (Gulf of Guinea, West Africa) coastline to anthropogenic and natural forcing, Part1: Wave climate variability and impacts on the longshore sediment transport. *Continental Shelf Res.* 110, 48–59.

Almar, R., Kestenare, E., and Boucharel, J. (2019). On the key influence of remote climate variability from tropical cyclones, north and south Atlantic mid-latitude storms on the Senegalese coast (West Africa). *Environ. Res. Commun.* 1 (7), 071001. doi: 10.1088/2515-7620/ab2ec6

Almar, R., Ranasinghe, R., Bergsma, E. ,. W. J., Diaz, H., Melet, A., Papa, F., et al. (2021). A global analysis of extreme coastal water levels with implications for potential coastal overtopping. *Nat. communication* 12, 3775. doi: 10.1038/s41467-021-24008-9

Almar, R., Stieglitz, T., Addo, K. A., Ba, K., Ondoa, G. A., Bergsma, E. W., et al. (2022). Coastal zone changes in West Africa: challenges and opportunities for satellite earth observations. *Surveys Geophysics*, 1–27. doi: 10.1007/s10712-022-09721-4

Almeida, L. P., Almar, R., Bergsma, E. W., Berthier, E., Baptista, P., Garel, E., et al. (2019). Deriving high spatial-resolution coastal topography from sub-meter satellite stereo imagery. *Remote Sens.* 11 (5), 590. doi: 10.3390/rs11050590

Almeida, L. P., Almar, R., Meyssignac, B., and Viet, N. T. (2018). Contributions to coastal flooding events in southeast of Vietnam and their link with global mean sea level rise. *Geosciences* 8, 437. doi: 10.3390/geosciences8120437

Alves, B., Angnuureng, D. B., Morand, P., and Almar, R. (2020). A review on coastal erosion and flooding risks and best management practices in West Africa: what has been done and should be done. *J. Coast. Conserv.* 24 (3), 1–22. doi: 10.1007/s11852-020-00755-7

Anthony, E. J., Besset, M., Dussouillez, P., Goichot, M., and Loisel, H. (2019). Overview of the moonsoon-influenced ayeyarwady river delta, and delta shoreline mobility in response to changing fluvial sediment supply. *Mar. Geology* 417, 106038. doi: 10.1016/j.margeo.2019.106038

Baldé, O., Sakho, I., Diouf, M. ,. B., Bop, M., Tine, D., and Ibouroi, W. (2021). Effectiveness of pilote bar (St. Louis) beach nourishment after a decade of erosion. *Eur. Sci. J.* 1710, 207–231.

Balouin, Y., Belon, R., Stépanian, A., and Bodéré, G. (2012). General study for the protection of the coastline of the eastern plain of Corsica: management recommendations. *Rapport BRGM/ RP 61650-FR*, 52.

Benveniste, J., Cazenave, A., Vignudelli, S., Fenoglio-Marc, L., Shah, R., Almar, R., et al. (2019). Requirements for a coastal hazards observing system. *Front. Mar. Sci.* 6, 348. doi: 10.3389/fmars.2019.00348

Bergsma, E. W., Almar, R., Anthony, E. J., Garlan, T., and Kestenare, E. (2022). Wave variability along the world's continental shelves and coasts: Monitoring opportunities from satellite earth observation. *Adv. Space Res.* 69 (9), 3236–3244. doi: 10.1016/j.asr.2022.02.047

Bergsma, E. W., Sadio, M., Sakho, I., Almar, R., Garlan, T., Gosselin, M., et al. (2020). Sand-spit evolution and inlet dynamics derived from space-borne optical imagery: Is the Senegal-river inlet closing? *J. Coast. Res.* 95 (SI), 372–376. doi: 10.2112/SI95-072.1

Bongarts Lebbe, T., Rey-Valette, H., Chaumillon, É., Camus, G., Almar, R., Cazenave, A., et al. (2021). Designing coastal adaptation strategies to tackle sea level rise. *Front. Mar. Sci.* 1640.

Breilh, J. F., Chaumillon, E., and Bertin, J. (2012). "Improve of a static flooding method and application to the case of the xynthia storm," in *XIIth National Conference on Coastal Engineering*, Cherbourg (Nantes, France: Paralia). doi: 10.5150/jngcgc.2012.100-B

Brüning, L. (2022). *Erosion côtière au nord du sénégal: migrations et stratégies d'adaptation* (these de géographie, instiut: Institut de Géographie, Université de Neuchâtel).

Cain, A., Cisse, O., Abdrabo, M., and Sah Akwen, N. (2015). Climate-responsive planning for angola's coastal cities. *Dev. Workshop*, 4.

Carrere, L., Lyard, F. H., Cancet, M., and Guillot, A. (2016). "Finite element solution FES2014, a new tidal model – validation results and perspectives for improvements," in *ESA Living Planet Conference* (Paris, France: European Space Agency).

Cisse, C. O. T., Sagne, P., Ba, K., Fall, B., Sy, B. A., and Marone, A. (2022). Modelling of extreme water levels on Malibu, gadaye and malika sandy beaches (Dakar, Senegal) following the 19 November. *Eur. Sci. J.* 18 (3), 80–100. doi: 10.19044/esj.2022.v18n3p79

Collin, A., Hench, J. L., Pastol, Y., Planes, S., Thiault, L., Schmitt, R. J., et al. (2018). High resolution topobathymetry using a Pleiades-1 triplet: Moorea island in 3D. *Remote Sens. Environ.* 208, 109–119. doi: 10.1016/j.rse.2018.02.015

Costa, S. (1995). "Sea Level rise and response strategies: the case of the Normandy-picardy coastline," in *Annales de géographie* 107, n°600edition, 179–200.

Dada, O., Almar, R., Morand, P., and Ménard, F. (2021). Towards West African coastal social- ecosystems sustainability: Interdisciplinary approaches. *Ocean Coast. Manage.* 211, 105746. doi: 10.1016/j.ocecoaman.2021.105746

Dada, O. A., Almar, R., and Oladapo, M. I. (2019). Recent coastal sea level variations and flooding events in the Nigerian transgressive mud coast of gulf of Guinea. *J. Afr. Earth Sci.* 161, 103668. doi: 10.1016/j.jafrearsci.2019.103668

Diagne, M. K. (2020). Coastal erosion: The hydra that keeps engulfing the Senegalese coasts, what's green? *Sustain. Dev. bimonthly* 13.

Diop, C. (2017). Water and sanitation in the neighborhood of guet ndar-Senegal cheikh DIOP. *Int. J. Eng. Works* 4 (5), 93–100.

Diop, S., Fabres, J., Pravettoni, R., Barusseau, J. P., Descamps, C., and Ducrotoy, J. P. (2014). The western and central africa land–sea interface: a vulnerable, threatened, and important coastal zone within a changing environment. *land/ocean Interact. Coast. zone west Cent. Afr.*, 1–8.

Dodet, G., Melet, A., Ardhuin, F., Bertin, X., Idier, D., and Almar, R. (2019). The contribution of wind-generated waves to coastal sea-level changes. *Surveys Geophysics* 40 (6), 1563–1601. doi: 10.1007/s10712-019-09557-5

Dupuis, L. (2016). *The erosion of the coves of the city of schoelcher: determination of the dynamics and processes involved* (University of the Antilles), 151.

Durand, P., Anselme, B., and Thomas, Y. F. (2010). The impact of the opening of the breach in the langue de barbarie in saint-Louis, Senegal in 2003: a change in the nature of the flood hazard? *Cybergeo: Eur. J. Geography Environment Nature Landscape* 496. doi: 10.4000/cybergeo.23017

Duvat, C. V. (2001). Evaluation of beach vulnerability to erosion: application to the Seychelles archipelago. *Geomorphology* 7 (1), 31–40.

Ganguli, P., and Merz, B. (2020). *Compounding effects of riverine and coastal floods and its implications for coastal urban flood residence* (EGU General Assembly 2020). doi: 10.5194/egusphere-egu2020-6439

Garlan, T., Almar, R., Gauduin, H., Gosselin, M., Morio, O., and Labarthe, C. (2020). 3D variability of sediment granulometry in two tropical environments: Nha trang (Vietnam) and saint-Louis (Senegal). *J. Coast. Res.* 95 (SI), 495–499. doi: 10.2112/SI95-096.1

Gemenne, F., Blocher, J., De Longueville, F., Telenti, S. V. D., Zickraf, C., Gharbaoui, D., et al. (2017). Climate change, natural disasters and population displacement in West Africa. *Geo-Eco-Trop: Int. J. Trop. Geology* 41 (3).

Giardino, A., Schrijvershof, R., Nederhoff, C. M., De Vroeg, H., Briere, C., Tonnon, P. K., et al. (2018). A quantitative assessment of human interventions and climate change on the West African sediment budget. *Ocean Coast. Manage.* 156, 249–265. doi: 10.1016/j.ocecoaman.2017.11.008

Idier, D., Bertin, X., Thompson, P., and Pickering, M. D. (2019). Interactions between mean sea level, tide, surge, waves and flooding: mechanisms and contributions to sea level variations at the coast. *Surveys Geophysics* 40 (6), 1603–1630. doi: 10.1007/s10712-019-09549-5

Itzkin, M., Moore, L. J., Ruggiero, P., Hacker, S. D., and Biel, R. G. (2021). The relative influence of dune aspect ratio and beach width on dune erosion as a function of storm duration and surge level. *Earth Surf. Dynam.* 9, 12231237.

James, D., Collin, A., Muty, A., and Qin, R. (2022). Satellite–derived topography and morphometry for VHR coastal habitat mapping: The Pleiades–1 tri–stereo enhancement. *Remote Sens.* 14 (1), 219. doi: 10.3390/rs14010219

Kante, F., and Fall, N. A. (2019). 3.3 Érosion côtière et déplacement de populations. Étude de cas du site de recasement des sinistrés de la langue de barbarie dans la ville de saint-Louis du sénégal. *Edité publié avec l'aimable soutien* 51, 51–53.

Kirezci, E., Young, I. R., Ranasinghe, R., Muis, S., Nicholls, R. J., Lincke, D., et al. (2020). Projections of global-scale extreme sea levels and resulting episodic coastal flooding over the 21st century. *Sci. Rep.* 10 (1), 1–12.

Kulp, S. A., and Strauss, B. H. (2019). New elevation data triple estimates of global vulnerability to sea-level rise and coastal flooding. *Nat. Commun.* 10 (1), 1–12.

Kupfer, S., Aguilar, S. S., Niekerk, L. V., Luck-Voger, M., and Vafeidis, A. T. (2022). Investigating the interaction of waves and river discharge during compound flooding at breede estuary, south Africa. *Nat.Hazards Earth Syst.Sci* 22, 187–205. doi: 10.5194/nhess-22-187-2022

Laïbi, R. A., Anthony, E. J., Almar, R., Castelle, B., Senechal, N., and Kestenare, E. (2014). Longshore drift cell development on the human-impacted bight of Benin sand barrier coast, West Africa. *J. Coast. Res.* 70 (10070), 78–83.

Le Roy, S., Pedreros, R., André, C., Paris, F., Lecacheux, S., Marche, F., et al. (2015). Coastal flooding of urban areas by overtopping: Dynamic modelling application to the Johanna storm, (2008) in gâvres (France). *Nat. Hazards Earth Syst. Sci.* 15 (11), 2497–2510. doi: 10.5194/nhess-15-2497-2015

Marti, F., Cazenave, A., Birol, F., Passaro, M., Léger, F., Niño, F., et al. (2021). Altimetry-based sea level trends along the coasts of western Africa. *Adv. Space Res.* 68 (2), 504–522. doi: 10.1016/j.asr.2019.05.033

Melet, A., Almar, R., Hemer, M., Le Cozannet, G., Meyssignac, B., and Ruggiero, P. (2020a). Contribution of wave setup to projected coastal sea level changes. *J. Geophysical Research: Oceans* 125 (8), e2020JC016078. doi: 10.1029/2020JC016078

Melet, A., Meyssignac, B., Almar, R., and Le Gozannet, G. (2018). Under estimate wave contribution to coastal sea-level rise. *Nat. Climate Change* 8, 234–239. doi: 10.1038/s41558-018-0088-y

Melet, A., Teatini, P., Le Cozannet, G., Jamet, C., Conversi, A., Benveniste, J., et al. (2020b). Earth observations for monitoring marine coastal hazards and their drivers. *Surveys Geophysics* 41 (6), 1489–1534. doi: 10.1007/s10712-020-09594-5

Möller, I., Kudella, M., Rupprecht, F., Spencer, T., Paul, M., Wesenbeeck, B. K. V., et al. (2014). Wave attenuation over coastal saltmarshes under storm surge conditions. *Nat. Geosci.* 7. doi: 10.1038/NGEO2251

Ndour, A., Ba, K., Almar, A., Almeida, P., Sall, M., Diedhiou, P. M., et al. (2020). On the natural and anthropogenic drivers of the Senegalese (West Africa) low coast evolution: Saint Louis beach 2016 COASTVAR experiment and 3D modeling of short term coastal protection measures. *J. Coast. Res.* 95 (SI), 583–587. doi: 10.2112/SI95-114.1

Ndour, A., Laïbi, R. A., Sadio, M., Degbe, C. G., Diaw, A. T., Oyédé, L. M., et al. (2018). Management strategies for coastal erosion problems in West Africa: analysis, issues, and constraints drawn from the examples of Senegal and Benin. *Ocean Coast. Manage.* 156, 92–106. doi: 10.1016/j.ocecoaman.2017.09.001

Oppenheimer, M., Glavovic, B., Hinkel, J., van de Wal, R., Magnan, A. K., Abd-Elgawad, A., et al. (2019). Sea Level rise and implications for low lying islands, coasts and communities. *IPCC Spec. Rep. Ocean Cryosph. Change Clim* 355, 126–129.

Pont, C. (2015). *Addressing and characterizing the risk of on Mediterranean sandy coasts: the example of Mediterranean sandy coasts: the example of the commune of leucate, master 1 risks and environment* Vol. 150 (Paris, France: Institute of Geography University of Paris 1 Pantheon-Sorbonne).

Prime, T., Brown, J. M., and Plater, A. J. (2016). Flood inundation uncertainty: the case of a 0.5% annual probablity flood event. *Environ. science&policy* 59, 1–9.

Quiroga, I. A., Elisa Sainz de Murieta, E. S., Losada, I., Toimil, A., Torres, S., Markanday., A., et al. (2021). Coastal flooding and erosion under climate change : risk assessment risk in Dakar. *BC3 Policy Briefs Rep. Res. carried*, 9.

Sadio, M. (2017). Morphodynamics and development of the coastal spits of the Senegal coast. *Journal of Coastal Research* (university Cheikh Anta Diop of Dakar and Aix-Marseille University), 403. thesis in physical geography, speciality: geomorphology.

Sadio, M., Anthony, E. J., Diaw, A. T., Dussouillez, P., Fleury, J. T., Kane, A., Almar, R., and Kestenare, E. (2017). Shoreline changes on the wave-influenced senegal river delta, west africa: The roles of natural processes and human interventions. Water. 9(5):357, 2017.

Salameh, E., Frappart, F., Almar, R., Baptista, P., Heygster, G., Lubac, B., et al. (2019). Monitoring beach topography and nearshore bathymetry using spaceborne remote sensing: A review. *Remote Sens.* 11 (19), 2212.

Sergent, P., Prevot, G., and Trmal, C. (2010). Reinforcement of shallow structures with respect to of the sea level rise, collection of the acts of the days. *impacts Climate Change Coast. risks* (Orleans, France), 147–151.

Sall, M. (2006). *Flooding and sea level rise in saint-Louis of Senegal: potential impacts and adaptation measures* (university of Le Mans), 332. Thesis of geography.

Shean, D., Alexandrov, O., Moratto, Z., Smith, B., Joughin, I., Porter, C., et al. (2016). An automated, open-source pipeline for mass production of digital elevation models (DEMs) from very-high-resolution commercial stereo satellite imagery. *ISPRS J. Photogramm. Remote Sens.* 116, 101–117.

Schoonees, T., Gijón Mancheño, A., Scheres, B., Bouma, T. J., Silva, R., Schlurmann, T., et al. (2019). Hard structures for coastal protection, towards greener designs. *Estuaries Coasts* 42 (7), 1709–1729.

Sidibe, I. (2013). A coastal territory in a political, economic and religious space in Senegal: the case of ouakam bay (Dakar). *spaces populations societies*, 159–176.

Stockdon, H. F., Holman, R. A., Howd, P. A., and Sallenger, A. H.Jr. (2006). Empirical parameterization of setup, swash, and runup. *Coast. Eng.* 53 (7), 573–588. doi: 10.1016/j.coastaleng.2005.12.005

Sy, B. A., Alonso Bilbao, I., Sy, A. A., Perez, I. S., and Valido, S. R. (2011). Results of the 2010-2012 monitoring of the evolution of the open gap on the Langue de Barbarie in Senegal and its consequences. *Physio-Geo* 7, 136. doi: 10.4000/physio-geo.3569

Taveneau, A., Almar, R., Bergsma, E. W., Sy, B. A., Ndour, A., Sadio, M., et al. (2021). Observing and predicting coastal erosion at the langue de barbarie sand spit around saint-Louis (Senegal, West Africa) through satellite-derived digital elevation model and shoreline. *Remote Sens.* 13 (13), 2454. doi: 10.3390/rs13132454

Tchindjang, M., Mbevo, F., and Bodpa, ,. A. (2019). *Building the port city of tomorrow in Atlantic Africa* edition ecm, 30p.

Tebaldi, C., Strass, B. H., and Zervas., C. E. (2012). Modelling sea level rise impacts on storm surges along us coasts. *Envr.Res.Lett* 7, 014032. doi: 10.1088/1748-9326/7/1/014032

Turner, I. L., Harley, M. D., Almar, R., and Bergsma, E. W. (2021). Satellite optical imagery in coastal engineering. *Coast. Eng.* 167, 103919. doi: 10.1016/j.coastaleng.2021.103919

Vitousek, S., Barnard, P. L., Fletcher, C. H., Frazer, N., Erikson., L., and Storlazzi, C. D. (2017). Doubling of coastal flooding frequency within decades due to sea-level rise. *Sci. Rep.* 7, 1399. doi: 10.1038/s41598-017-01362-7

Vousdoukas, M. I, Voukouvalas, E., Mentaschi, L., Dottori, F., Giardino, A., Bouziotas, D., et al. (2016). Developments in large-scale coastal flood hazard mapping. *Nat. Hazards Earth Syst. Sci.* 16, 1841–1853. doi: 10.5194/nhess-16-1841-2016

Vousdoukas, M. I., Clarke, J., Ranasinghe, R., Reimann, L., Khalaf, N., Duong, T. M., et al. (2022). African Heritage sites threatened as sea-level rise accelerates. *Nat. Climate Change* 12 (3), 256–262. doi: 10.1038/s41558-022-01280-1

Wade, S., Rudant, J. P., Ba, K., and Ndoye, B. (2008). Remote sensing and management of natural disasters :application to the study of urban flooding of saint-Louis and gulling due to water erosion in nioro du Rip(Senegal). *Rev. teledetection*, 203–210.

Wang, X. L., Zwiers, F. W., and Swail, V. R. (2003). North Atlantic ocean wave cliamte change scenarios for the twebty first century. *J. Climate* 17, 2368–2383. doi: 10.1175/1520-0442(2004)017<2368:NAOWCC>2.0.CO;2

Weissenberger, S., Noblet, M., Plante, S., Chouinard, O., Guillemot, J., Aube, M., et al. (2016). Climate change, coastal development and vulnerability: a comparison of French, Canadian and Senegalese territories. *VertigO - electronic J. Environ. sciences Volume 16 Issue 3 Environ. vulnerabilities: historical Perspect.*, 2–33. doi: 10.4000/vertigo.18050

Wells, N. C. (2011). "The atmosphere and ocean: a physical introduction," (John Wiley & Sons).

Woodruff, J. D., Irish, J. L., and Camargo, S. J. (2013). Coastal flooding by tropical cyclones and sea-level rise. *Nature* 504, 44–51. doi: 10.1038/nature12855

Woodruff, S. C., and Stults, M. (2016). Numerous strategies but limited implementation guidance in US local adaptation plans. *Nat. Climate Change* 6 (8), 796–802.

Wöppelmann, G., Miguez, B. L., and et Creach, R. (2008). Tide gauge records at Dakar, Senegal (Africa): Towards a 100-years consistent sea-level time series. (Vienna, Austria: European Geophysical Union, General Assambly).

Bibliography

Aagaard, T., 1988. Nearshore bar morphology on the low-energy coast of northern zealand, denmark. Geografiska Annaler: Series A, Physical Geography 70, 59–67.

Abessolo, G., Almar, R., Angnuureng, D., Bonou, F., Sohou, Z., Camara, I., Diouf, A., Alory, G., Onguéné, R., Mama, A., et al., 2022. African coastal camera network: Monitoring ocean, climate, and human impacts .

Abessolo, G.O., Larson, M., Almar, R., et al., 2021. Modeling the bight of benin (gulf of guinea, west africa) coastline response to natural and anthropogenic forcing. Regional Studies in Marine Science 48, 101995.

Adams, P.N., Keough, K.M., Olabarrieta, M., 2016. Beach morphodynamics influenced by an ebb-tidal delta on the north florida atlantic coast. Earth Surface Processes and Landforms 41, 936–950.

AFD, 2018. Lutter contre l'érosion côtière du littoral de Saint Louis. Technical Report. AFD.

Airy, G., 1841. Tides and waves. Trigonometry, On the Figure of the Earth , 396.

Aleman, N., Certain, R., Robin, N., Barusseau, J.P., 2017. Morphodynamics of slightly oblique nearshore bars and their relationship with the cycle of net offshore migration. Marine Geology 392, 41–52.

Allard, J., Bertin, X., Chaumillon, E., Pouget, F., 2008. Sand spit rhythmic development: A potential record of wave climate variations? arçay spit, western coast of france. Marine Geology 253, 107–131. doi:https://doi.org/10.1016/j.margeo.2008.05.009.

Almar, R., Bergsma, E.W., Brodie, K.L., Bak, A.S., Artigues, S., Lemai-Chenevier, S., Cesbron, G., Delvit, J.M., 2022a. Coastal topo-bathymetry from a single-pass satellite video: insights in space-videos for coastal monitoring at duck beach (nc, usa). Remote Sensing 14, 1529.

Almar, R., Bergsma, E.W., Brodie, K.L., Bak, A.S., Artigues, S., Lemai-Chenevier, S., Cesbron, G., Delvit, J.M., 2022b. Coastal topo-bathymetry from a single-pass satellite video: insights in space-videos for coastal monitoring at duck beach (nc, usa). Remote Sensing 14, 1529.

Almar, R., Bergsma, E.W., Catalan, P.A., Cienfuegos, R., Suarez, L., Lucero, F., Lerma, A.N., Desmazes, F., Perugini, E., Palmsten, M.L., et al., 2021a. Sea state from single optical images: A methodology to derive wind-generated ocean waves from cameras, drones and satellites. Remote Sensing 13, 679.

Almar, R., Bergsma, E.W., Maisongrande, P., de Almeida, L.P.M., 2019a. Wave-derived coastal bathymetry from satellite video imagery: A showcase with pleiades persistent mode. Remote Sensing of Environment 231, 111263.

Almar, R., Bergsma, E.W., Thoumyre, G., Baba, M.W., Cesbron, G., Daly, C., Garlan, T., Lifermann, A., 2021b. Global satellite-based coastal bathymetry from waves. Remote Sensing 13, 4628.

Almar, R., Bonneton, P., Senechal, N., Roelvink, D., 2009. Wave celerity from video imaging: A new method, in: Coastal Engineering 2008: (In 5 Volumes). World Scientific, pp. 661–673.

Almar, R., Castelle, B., Ruessink, B., Sénéchal, N., Bonneton, P., Marieu, V., 2010. Two- and three-dimensional double-sandbar system behaviour under intense wave forcing and a meso–macro tidal range. Continental Shelf Research 30, 781–792.

Almar, R., Kestenare, E., Boucharel, J., 2019b. On the key influence of remote climate variability from tropical cyclones, north and south atlantic mid-latitude storms on the senegalese coast (west africa). Environmental Research Communications 1(7).

Almar, R., Kestenare, E., Reyns, J., Jouanno, J., Anthony, E., Laibi, R., Hemer, M., Du Penhoat, Y., Ranasinghe, R., 2015. Response of the bight of benin (gulf of guinea, west africa) coastline to anthropogenic and natural forcing, part1: Wave climate variability and impacts on the longshore sediment transport. Continental Shelf Research 110, 48–59.

Almar, R., Ranasinghe, R., Sénéchal, N., Bonneton, P., Roelvink, D., Bryan, K.R., Marieu, V., Parisot, J.P., 2012. Video-based detection of shorelines at complex meso–macro tidal beaches. Journal of Coastal Research 28, 1040–1048.

Almar, R., Stieglitz, T., Addo, K.A., Ba, K., Ondoa, G.A., Bergsma, E.W., Bonou, F., Dada, O., Angnuureng, D., Arino, O., 2022c. Coastal zone changes in west africa: challenges and opportunities for satellite earth observations. Surveys in Geophysics , 1–27.

Almeida, L., Almar, R., Bergsma, E., Berthier, E., Baptista, P., Garel, E., Dada, O., Alves, B., 2019. Deriving high spatial-resolution coastal topography from sub-meter statellite stereo imagery. Remote Sens. 11, 590.

Alves, B., Angnuureng, D.B., Morand, P., Almar, R., 2020. A review on coastal erosion and flooding risks and best management practices in west africa: what has been done and should be done. Journal of Coastal Conservation 24, 1–22.

Alves, R.B., Bapentire, A.D., Almar, R., Louarn, A., Rossi, P.L., Corsini, L., Morand, P., 2022. Compendium: Coastal management practices in west africa: existing and potential solutions to control coastal erosion, prevent flooding and mitigate damage to society .

Amante, C., 2018. Estimating coastal digital elevation model uncertainty. Journal of Coastal Research 34(6), 1382–1397.

ANCORIM, 2017. Panorama des solutions douces de protection des côtes. Technical Report. ANCORIM.

Angnuureng, D., Brempong, K., Jayson-Quashigah, P., Dada, O., Akuoko, S., Frimpomaa, J., Mattah, P., Almar, R., 2022. Satellite, drone and video camera multi-platform monitoring of coastal erosion at an engineered pocket beach: A showcase for coastal management at elmina bay, ghana (west africa). Regional Studies in Marine Science , 102437.

Angnuureng, D.B., Jayson-Quashigah, P.N., Almar, R., Stieglitz, T.C., Anthony, E.J., Aheto, D.W., Appeaning Addo, K., 2020a. Application of shore-based video and unmanned aerial vehicles (drones): Complementary tools for beach studies. Remote Sensing 12. doi:10.3390/rs12030394.

Angnuureng, D.B., Jayson-Quashigah, P.N., Almar, R., Stieglitz, T.C., Anthony, E.J., Aheto, D.W., Appeaning Addo, K., 2020b. Application of shore-based video and unmanned aerial vehicles (drones): complementary tools for beach studies. Remote Sensing 12, 394.

Anthony, E., 2015. Patterns of sand spit development and their management implications on deltaic, drift-aligned coasts: The cases of the senegal and volta river delta spits, west africa, in: Springer, C. (Ed.), Randazzo G., Jackson D., Cooper J. (eds) Sand and Gravel Spits. Coastal Research Library, pp. pp. 21–36.

Anthony, E., A.B.Blivi, 1999. Morphosedimentary evolution of a delta-sourced, drift-aligned sandbarrier–lagoon complex, western bight of benin. Marine Geology 158, 161–176. doi:10.1016/S0025-3227(98)00170-4.

Anthony, E.J., Aagaard, T., 2020. The lower shoreface: Morphodynamics and sediment connectivity with the upper shoreface and beach. Earth-Science Reviews 210, 103334. doi:https://doi.org/10.1016/j.earscirev.2020.103334.

Ashphaq, M., Srivastava, P.K., Mitra, D., 2021. Review of near-shore satellite derived bathymetry: Classification and account of five decades of coastal bathymetry research. Journal of Ocean Engineering and Science 6, 340–359.

Ashton, A., Murray, A.B., Arnoult, O., 2001. Formation of coastline features by large-scale instabilities induced by high-angle waves. Nature 414, 296–300.

Ashton, A., Nienhuis, J., Ells, K., 2016. On a neck, on a spit: controls on the shape of free spits. Earth Surface Dynamics 4, 193–210.

Aubrey, D., Gaines, A., 1982. Rapid formation and degradation of barrier spits in areas with low rates of littoral drift. Marine Geology 49, 257–277. URL: https://www.sciencedirect.com/science/article/pii/0025322782900433, doi:https://doi.org/10.1016/0025-3227(82)90043-3.

Baily, B., Nowell, D., 1996. Techniques for monitoring coastal change: a review and case study. Ocean & coastal management 32, 85–95.

Bayram, A., Larson, M., Hanson, H., 2007. A new formula for the total longshore sediment transport rate. Coastal Engineering 54, 700–710. URL: https://www.sciencedirect.com/science/article/pii/S0378383907000464, doi:https://doi.org/10.1016/j.coastaleng.2007.04.001.

Benavente, J., Río, L.D., Anfuso, G., Gracia, F., Reyes, J., 2002. Utility of morphodynamic characterisation in the prediction of beach damage by storms. Journal of Coastal Research 36(10036), 56–64. doi:10.2112/1551-5036-36.sp1.56.

Benveniste, J., Cazenave, A., Vignudelli, S., Fenoglio-Marc, L., Shah, R., Almar, R., Andersen, O., Birol, F., Bonnefond, P., Bouffard, J., Calafat, F., Cardellach, E., Cipollini, P., Le Cozannet, G., Dufau, C., Fernandes, M.J., Frappart, F., Garrison, J., Gommenginger, C., Han, G., Høyer, J.L., Kourafalou, V., Leuliette, E., Li, Z., Loisel, H., Madsen, K.S., Marcos, M., Melet, A., Meyssignac, B., Pascual, A., Passaro, M., Ribó, S., Scharroo, R., Song, Y.T., Speich, S., Wilkin, J., Woodworth, P., Wöppelmann, G., 2019. Requirements for a coastal hazards observing system. Frontiers in Marine Science 6, 348. URL: https://www.frontiersin.org/article/10.3389/fmars.2019.00348, doi:10.3389/fmars.2019.00348.

Bergsma, E., Almar, R., 2018a. Video-based depth inversion techniques, a method comparison with synthetic cases. Coastal Engineering 138, 199–209.

Bergsma, E., Sadio, M., Sakho, I., Almar, R., Garlan, T., Gosselin, M., Gauduin, H., 2020. Sand-spit evolution and inlet dynamics derived from space-borne optical imagery: Is the senegal-river inlet closing? Journal of Coastal Research, Special Issue No. 95 , 372–376.

Bergsma, E.W., Almar, R., 2018b. Video-based depth inversion techniques, a method comparison with synthetic cases. Coastal Engineering 138, 199–209.

Bergsma, E.W., Almar, R., 2020. Coastal coverage of esa' sentinel 2 mission. Advances in Space Research 65, 2636–2644. doi:https://doi.org/10.1016/j.asr.2020.03.001.

Bergsma, E.W., Almar, R., de Almeida, L.P.M., Sall, M., 2019a. On the operational use of uavs for video-derived bathymetry. Coastal Engineering 152, 103527.

Bergsma, E.W., Almar, R., Anthony, E.J., Garlan, T., Kestenare, E., 2022. Wave variability along the world's continental shelves and coasts: Monitoring opportunities from satellite earth observation. Advances in Space Research 69, 3236–3244.

Bergsma, E.W., Almar, R., Maisongrande, P., 2019b. Radon-augmented sentinel-2 satellite imagery to derive wave-patterns and regional bathymetry. Remote Sensing 11, 1918.

Bergsma, E.W., Almar, R., Rolland, A., Binet, R., Brodie, K.L., Bak, A.S., 2021. Coastal morphology from space: A showcase of monitoring the topography-bathymetry continuum. Remote Sensing of Environment 261, 112469.

Bergsma, E.W.J., Almar, R., Maisongrande, P., 2019c. Radon-augmented sentinel-2 satellite imagery to derive wave-patterns and regional bathymetry. Remote Sensing 11. URL: https://www.mdpi.com/2072-4292/11/16/1918, doi:10.3390/rs11161918.

Bergsma, E.W.J., Conley, D.C., Davidson, M.A., O'Hare, T.J., Almar, R., 2019d. Storm event to seasonal evolution of nearshore bathymetry derived from shore-based video imagery. Remote Sensing 11(5), 519. doi:519.10.3390/rs11050519.

Bergsma, E.W.J., Conley, D.C., Davidson, M.A., O'Hare, T.J., Almar, R., 2019e. Storm event to seasonal evolution of nearshore bathymetry derived from shore-based video imagery. Remote Sensing 11(5), 519. doi:519.10.3390/rs11050519.

Birrien, F., Castelle, B., Marieu, V., Dubarbier, B., 2013. On a data-model assimilation method to inverse wave-dominated beach bathymetry using heterogeneous video-derived observations. Ocean engineering 73, 126–138.

Black, K., Mead, S., 2001. Design of the gold coast reef for surfing, public amenity and coastal protection: surfing aspects. Journal of Coastal Research , 115–130.

Blivi, A., Anthony, E.J., Oyédé, L.M., 2002. Sand barrier development in the bight ofbenin, west africa. Ocean and Coastal Management 45, 185–200.

Boothroyd, J.C., 1985. Tidal inlets and tidal deltas, in: Coastal sedimentary environments. Springer, pp. 445–532.

Bouvier, C., Balouin, Y., Castelle, B., 2017. Video monitoring of sandbar-shoreline response to an offshore submerged structure at a microtidal beach. Geomorphology 295, 297–305.

Bouvier, C., Balouin, Y., Castelle, B., Valentini, N., 2020. Video depth inversion at a microtidal site exposed to prevailing low-energy short-period waves and episodic severe storms. Journal of Coastal Research 95, 1021–1026.

Bouvier, C., Castelle, B., Balouin, Y., 2019. Modeling the impact of the implementation of a submerged structure on surf zone sandbar dynamics. Journal of Marine Science and Engineering 7, 117.

Brière, C., Janssen, S.K., Oost, A.P., Taal, M., Tonnon, P.K., 2018. Usability of the climate-resilient nature-based sand motor pilot, the netherlands. Journal of coastal conservation 22, 491–502.

Brodie, K.L., Palmsten, M.L., Hesser, T.J., Dickhudt, P.J., Raubenheimer, B., Ladner, H., Elgar, S., 2018. Evaluation of video-based linear depth inversion performance and applications using altimeters and hydrographic surveys in a wide range of environmental conditions. Coastal Engineering 136, 147–160.

Bruun, P., 1988. The bruun rule of erosion by sea-level rise: A discussion on large-scale two- and three-dimensional usages. Journal of Coastal Research 4, 627–648. URL: http://www.jstor.org/stable/4297466.

Burvingt, O., Lerma, A.N., Lubac, B., Mallet, C., Senechal, N., 2022. Geomorphological control of sandy beaches by a mixed-energy tidal inlet. Marine Geology 450, 106863.

Caballero, I., Stumpf, R.P., 2019. Retrieval of nearshore bathymetry from sentinel-2a and 2b satellites in south florida coastal waters. Estuarine, Coastal and Shelf Science 226, 106277.

Castelle, B., Bonneton, P., Senechal, N., Dupuis, H., Butel, R., Michel, D., 2006. Dynamics of wave-induced currents over an alongshore non-uniform multiple-barred sandy beach on the aquitanian coast, france. Continental shelf research 26, 113–131.

Castelle, B., Bourget, J., Molnar, N., Strauss, D., Deschamps, S., Tomlinson, R., 2007. Dynamics of a wave-dominated tidal inlet and influence on adjacent beaches, currumbin creek, gold coast, australia. Coastal Engineering 54, 77–90. doi:https://doi.org/10.1016/j.coastaleng.2006.08.007.

Castelle, B., Ruessink, B., Bonneton, P., Marieu, V., Bruneau, N., Price, T.D., 2010. Coupling mechanisms in double sandbar systems. part 1: Patterns and physical explanation. Earth Surface Processes and Landforms 35, 476–486.

Castelle, B., Scott, T., Brander, R., McCarroll, R., 2016. Rip current types, circulation and hazard. Earth-Science Reviews 163, 1–21.

Cazenave, A., Cozannet, G.L., Benveniste, J., Woodworth, P.L., Champollion, N., 2017. Monitoring coastal zone changes from space. Eos 98 doi:https://doi.org/10.1029/2017EO085581.

Cesbron, G., Melet, A., Almar, R., Lifermann, A., Tullot, D., Crosnier, L., 2021. Pan-european satellite-derived coastal bathymetry-review, user needs and future services. Frontiers in Marine Science , 1591.

Charlier, R.H., Chaineux, M.C.P., Morcos, S., 2005. Panorama of the history of coastal protection. Journal of Coastal Research 21, 79–111.

Chaumillon, E., Ozenne, F., Bertin, X., Long, N., Ganthy, F., 2014. Wave climate and inlet channel meander bend control spit breaching and migration of a new inlet: La coubre sandspit. Journal of Coastal Research 70, 109–114.

Chemane, D., Motta, H., Achimo, M., 1997. Vulnerability of coastal resources to climate changes in mozambique: a call for integrated coastal zone management. Ocean and Coastal Management 37, 63–83.

Chen, B., Yang, Y., Wen, H., Ruan, H., Zhou, Z., Luo, K., Zhong, F., 2018. High-resolution monitoring of beach topography and its change using unmanned aerial vehicle imagery. Ocean and Coastal Management 160, 103–116. doi:https://doi.org/10.1016/j.ocecoaman.2018.04.007.

Christie, P., 2005. Is integrated coastal management sustainable? Ocean & Coastal Management 48, 208–232. URL: https://www.sciencedirect.com/science/article/pii/S0964569105000542, doi:https://doi.org/10.1016/j.ocecoaman.2005.04.002. sustainability of Integrated Coastal Management.

Cienfuegos, R., Villagran, M., Aguilera, J.C., Catalán, P., Castelle, B., Almar, R., 2014. Video monitoring and field measurements of a rapidly evolving coastal system: the river mouth and sand spit of the mataquito river in chile. Journal of Coastal Research .

Cisse, C.O.T., Brempong, E., Taveneau, A., Almar, R., Sy, B.A., Angnuureng, D.B., 2022. Extreme coastal water levels with potential flooding risk at the low-lying saint louis historic city, senegal (west africa). Frontiers in Marine Science , 2480.

Coco, G., Murray, A.B., 2007. Patterns in the sand: From forcing templates to self-organization. Geomorphology 91, 271–290. URL: `https://www.sciencedirect.com/science/article/pii/S0169555X07003819`, doi:`https://doi.org/10.1016/j.geomorph.2007.04.023`. 38th Binghamton Geomorphology Symposium: Complexity in Geomorphology.

Collin, A., Hench, J.L., Pastol, Y., Planes, S., Thiault, L., Schmitt, R.J., Holbrook, S.J., Davies, N., Troyer, M., 2018. High resolution topobathymetry using a pleiades-1 triplet: Moorea island in 3d. Remote Sensing of Environment 208, 109–119. URL: `https://www.sciencedirect.com/science/article/pii/S003442571830021X`, doi:`https://doi.org/10.1016/j.rse.2018.02.015`.

Cooper, J., 2001. Geomorphological variability among microtidal estuaries from the wave-dominated south african coast. Geomorphology 40, 99–122.

Corral, L.R., Schling, M., 2017. The impact of shoreline stabilization on economic growth in small island developing states. Journal of Environmental Economics and Management 86, 210–228. URL: `https://www.sciencedirect.com/science/article/pii/S0095069617303662`, doi:`https://doi.org/10.1016/j.jeem.2017.06.001`. special issue on environmental economics in developing countries.

Cox, C., Munk, W., 1954. Measurement of the roughness of the sea surface from photographs of the sun's glitter. Josa 44, 838–850.

Dada, O., Almar, R., Morand, P., Ménard, F., 2021. Towards west african coastal social-ecosystems sustainability: Interdisciplinary approaches. Ocean & Coastal Management 211, 105746.

Dada, O.A., Angnuureng, D.B., Almar, R., Dzantor, S., Morand, P., 2022. Social perceptions of coastal hazards in the anlo beach community in the western region of ghana. Journal of Coastal Conservation 26, 1–13.

Dail, H.J., Merrifield, M.A., Bevis, M., 2000. Steep beach morphology changes due to energetic wave forcing. Marine Geology 162, 443–458. doi:`https://doi.org/10.1016/S0025-3227(99)00072-9`.

Daly, C., Baba, W., Bergsma, E., Thoumyre, G., Almar, R., Garlan, T., 2022. The new era of regional coastal bathymetry from space: A showcase for west africa using optical sentinel-2 imagery. Remote Sensing of Environment 278, 113084.

Davidson, M., Van Koningsveld, M., de Kruif, A., Rawson, J., Holman, R., Lamberti, A., Medina, R., Kroon, A., Aarninkhof, S., 2007. The coastview project: Developing video-derived coastal state indicators in support of coastal zone management. Coastal Engineering 54, 463–475.

Davies, J., 1980. in: 2nd ed. London: Longman (Ed.), Geographical variation in coastal development, p. 212.

Davis Jr, R.A., Hayes, M.O., 1984. What is a wave-dominated coast?, in: Developments in Sedimentology. Elsevier. volume 39, pp. 313–329.

De Vriend, H.J., 1991. Mathematical modelling and large-scale coastal behaviour: Part 2: Predictive models. Journal of hydraulic research 29, 741–753.

Dean, R., Dalrymple, R., 2001. Long-term processes, in: Cambridge: Cambridge University Press, . (Ed.), Coastal Processes with Engineering Applications, pp. pp. 35–70.

Dean, R.G., 2002. Beach nourishment: theory and practice. volume 18. World scientific.

Dean, R.G., 2018. Principles of beach nourishment. CRC handbook of coastal processes and erosion , 217–232.

Dean, R.G., Dalrymple, R.A., 2004. Coastal processes with engineering applications. Cambridge University Press.

Dolan, R., Hayden, B., Heywood, J., 1978. A new photogrammetric method for determining shoreline erosion. Coastal Engineering 2, 21–39.

Dubarbier, B., 2014. Modélisation numérique de l'évolution des profils de plages sableuses dominées par l'action de la houle. Ph.D. thesis. Université de Bordeaux.

Dubarbier, B., Castelle, B., Marieu, V., Ruessink, G., 2015. Process-based modeling of cross-shore sandbar behavior. Coastal Engineering 95, 35–50.

Dubarbier, B., Castelle, B., Ruessink, G., Marieu, V., 2017. Mechanisms controlling the complete accretionary beach state sequence. Geophysical Research Letters 44, 5645–5654.

Duc Anh, N.Q., Tanaka, H., Tam, H.S., Tinh, N.X., Tung, T.T., Viet, N.T., 2020. Comprehensive study of the sand spit evolution at tidal inlets in the central coast of vietnam. Journal of Marine Science and Engineering 8. doi:10.3390/jmse8090722.

Duhamel, P., Knafou, R., 2003. Tourisme et littoral: intérêts et limites d'une mise en relation/tourism and coastline: interests and limits about a relationship, in: Annales de géographie, JSTOR. pp. 47–67.

Dulou, C., Belzons, M., Rey, V., 2000. Laboratory study of wave bottom interaction in the bar formation on an erodible sloping bed. Journal of Geophysical Research: Oceans 105, 19745–19762.

Eamer, J.B., Walker, I.J., 2013. Quantifying spatial and temporal trends in beach–dune volumetric changes using spatial statistics. Geomorphology 191, 94–108. URL: https://www.sciencedirect.com/science/article/pii/S0169555X13001359, doi:https://doi.org/10.1016/j.geomorph.2013.03.005.

Elgar, S., Guza, R., 1985. Shoaling gravity waves: Comparisons between field observations, linear theory, and a nonlinear model. Journal of fluid mechanics 158, 47–70.

Eustáquio Amaro, V., Santana Gomes, L., R., Ferreira de Lima, F., G., Scudelari, A., C., Freitas Neves, C., Vieira Busman, D., Silva Santos, A., L., 2015. Multitemporal analysis of coastal erosion based on multisource satellite images, ponta negra beach, natal city, northeastern brazil. Marine Geodesy 38, 1–25.

Evans, O., 1942. The origin of spits, bars, and related structures. Journal of Geology 50. doi:https://doi.org/10.1086/625087.

Faria, A.G., Thornton, E., Lippmann, T., Stanton, T., 2000. Undertow over a barred beach. Journal of Geophysical Research: Oceans 105, 16999–17010.

Feagin, R.A., Sherman, D.J., Grant, W.E., 2005. Coastal erosion, global sea-level rise, and the loss of sand dune plant habitats. Frontiers in Ecology and the Environment 3, 359–364.

Fenster, M., Dolan, R., 1996. Assessing the impact of tidal inlets on adjacent barrier island shorelines. Journal of Coastal Research , 294–310.

FitzGerald, D.M., Buynevich, I.V., Rosen, P.S., 2001. Geological evidence of former tidal inlets along a retrograding barrier: Duxbury beach, massachusetts, usa. Journal of Coastal Research , 437–448.

Fitzgerald, D.M., Penland, S., Nummedal, D., 1984. Control of barrier island shape by inlet sediment bypassing: East frisian islands, west germany. Marine Geology 60, 355–376.

Fredsoe, J., Deigaard, R., 1992. Mechanics of coastal sediment transport. volume 3. World scientific publishing company.

Frihy, O.E., 2001. The necessity of environmental impact assessment (eia) in implementing coastal projects: lessons learned from the egyptian mediterranean coast. Ocean and Coastal Management 44, 489–516. URL: https://www.sciencedirect.com/science/article/pii/S096456910100062X, doi:https://doi.org/10.1016/S0964-5691(01)00062-X.

Garlan, T., Almar, R., Gauduin, H., Gosselin, M., Morio, O., Labarthe, C., 2020. 3d variability of sediment granulometry in two tropical environments: Nha trang (vietnam) and saint-louis (senegal). Journal of Coastal Research 95, 495–499.

Garnier, R., Falqués, A., Calvete, D., Thiebot, J., Ribas, F., 2013. A mechanism for sandbar straightening by oblique wave incidence. Geophysical Research Letters 40, 2726–2730.

Gawehn, M., Almar, R., Bergsma, E.W., de Vries, S., Aarninkhof, S., 2022. Depth inversion from wave frequencies in temporally augmented satellite video. Remote Sensing 14, 1847.

Gesch, D., Brock, J., Parrish, C., Rogers, J., Wright, C., 2016. Introduction: Special issue on advances in topobathymetric mapping, models, and applications. Journal of Coastal Research 76(10076), 1–3. doi:10.2112/SI76-001.

Gornitz, V., 1991. Global coastal hazards from future sea level rise. Palaeogeography, Palaeoclimatology, Palaeoecology 89, 379–398.

Goussard, J., 2014. Présentation du plan régional de prévention des risques côtiers en afrique de l'ouest et de la mission d'observation du littoral ouest africain, in: Actes du Colloque international Connaissances et compréhension des risques côtiers. Aléas enjeux, représentations, gestion, pp. 154–162.

Grasso, F., Castelle, B., Ruessink, B., 2012. Turbulence dissipation under breaking waves and bores in a natural surf zone. Continental Shelf Research 43, 133–141.

Hallegatte, S., Green, C., Nicholls, R.J., Corfee-Morlot, J., 2013. Future flood losses in major coastal cities. Nature climate change 3, 802–806.

Hancock, M.J., 2005. Generation of sand bars under surface waves. Ph.D. thesis. Massachusetts Institute of Technology.

Hasegawa, H., Matsuo, K., Koarai, N., Watanabe, N., Masaharu, H., Fukushima, Y., 2000. Dem accuracy and the base to height (b/h) ratio of stereo images. International Archives of Photogrammetry and Remote Sensing XXXIII, Part 84.

Hequette, A., Ruz, M.H., 1991. Spit and barrier island migration in the southeastern canadian beaufort sea. Journal of Coastal Research , 677–698.

Hersbach, H., Bell, B., Berrisford, P., Biavati, G., Horányi, A., Muñoz Sabater, J., Nicolas, J., Peubey, C., Radu, R., Rozum, I., Schepers, D., Simmons, A., Soci, C., Dee, D., Thépaut, J.N., 2018. Era5 hourly data on single levels from 1979 to present. copernicus climate change service (c3s) climate data store (cds). (accessed on < dd-mmm-yyyy >). doi:`10.24381/cds.adbb2d47`.

Hersbach, H., Bell, B., Berrisford, P., Hirahara, S., Horányi, A., Muñoz-Sabater, J., Nicolas, J., Peubey, C., Radu, R., Schepers, D., et al., 2020. The era5 global reanalysis. Quarterly Journal of the Royal Meteorological Society 146, 1999–2049.

Hicks, D.M., Hume, T.M., Swales, A., Green, M.O., 1999. Magnitudes, spatial extent, time scales and causes of shoreline change adjacent to an ebb tidal delta, katikati inlet, new zealand. Journal of Coastal Research , 220–240.

Hinkel, J., Nicholls, R.J., Tol, R.S., Wang, Z.B., Hamilton, J.M., Boot, G., Vafeidis, A.T., McFadden, L., Ganopolski, A., Klein, R.J., 2013. A global analysis of erosion of sandy beaches and sea-level rise: An application of diva. Global and Planetary change 111, 150–158.

Hoefel, F., Elgar, S., 2003. Wave-induced sediment transport and sandbar migration. Science 299, 1885–1887.

Holman, R., Bergsma, E.W., 2021. Updates to and performance of the cbathy algorithm for estimating nearshore bathymetry from remote sensing imagery. Remote Sensing 13, 3996.

Holman, R., Plant, N., Holland, T., 2013. cbathy: A robust algorithm for estimating nearshore bathymetry. JGR Oceans 118, 2595–2609.

Holman, R.A., Brodie, K.L., Spore, N.J., 2017. Surf zone characterization using a small quadcopter: Technical issues and procedures. IEEE Transactions on geoscience and remote sensing 55.

Inman, D.L., Brush, B.M., 1973. The coastal challenge: Fragile ribbons which border our land require more understanding, new technology, and resolute planning. Science 181, 20–32.

IRD-UCAD-UGB, C., 2019. Proposition technique MISE EN ŒUVRE D'UN SUIVI SCIENTIFIQUE DE LONG TERME DU LITTORAL ET DES IMPACTS DE L'OUVRAGE DE PROTECTION COTIERE DE LA LANGUE DE BARBARIE. Technical Report. IRD, UCAD, UGB.

Iribarren, R., Nogales, C., 1954. Other verifications of the formula for calculating breakwater embankments. Permanent International Association of Navigation Congresses 39, 119–139.

Jackson, L.A., Tomlinson, R., McGrath, J., Turner, I., 2003. Monitoring of a multi functional submerged geotextile reef breakwater, in: Coastal Engineering 2002: Solving Coastal Conundrums. World Scientific, pp. 1923–1935.

Jacobsen, K., Topan, H., 2015. Corrigendum to "dem generation with short base length pleiades triplet". Int. Arch. Photogramm. Remote Sens. Spatial Inf. Sci. XL-3/W2, 297–297. doi:10.5194/isprsarchives-XL-3-W2-81-2015.

James, D., Collin, A., Mury, A., Qin, R., 2022. Satellite-derived topography and morphometry for vhr coastal habitat mapping: The pleiades-1 tri-stereo enhancement. Remote Sensing 14. URL: https://www.mdpi.com/2072-4292/14/1/219, doi:10.3390/rs14010219.

Kaczmarek, L.M., Ostrowski, R., Pruszak, Z., Rozynski, G., 2005. Selected problems of sediment transport and morphodynamics of a multi-bar nearshore zone. Estuarine, Coastal and Shelf Science 62, 415–425. URL: https://www.sciencedirect.com/science/article/pii/S0272771404002367, doi:https://doi.org/10.1016/j.ecss.2004.09.006. the European contribution to global coastal zone research: An ELOISE (European Land-Ocean Interaction Studies) project.

Kamphuis, W., 1991. Alongshore sediment transport rate. Journal of Waterway, Port, Coastal, and Ocean Engineering 117(6), 622–640.

Keulegan, G.H., 1951. Wind tides in small closed channels. National Bureau of Standards.

Kidner, D., Thomas, M., Leigh, C., Oliver, J., Morgan, C., 2004. Coastal monitoring with lidar: Challenges, problems and pitfalls. Proceedings of SPIE - The International Society for Optical Engineering 5574. doi:10.1117/12.565648.

Komar, P.D., 2018. Beach processes and erosion–an introduction. Handbook of coastal processes and erosion , 1–20.

Kraus, N.C., 1999. Analytical model of spit evolution at inlets. Technical Report. ARMY ENGINEER WATERWAYS EXPERIMENT STATION VICKSBURG MS COASTAL AND . . . .

Kraus, N.C., Galgano, F.A., 2001. Beach erosional hot spots: types, causes, and solutions. Technical Report. ENGINEER RESEARCH AND DEVELOPMENT CENTER VICKSBURG MS COASTAL AND HYDRAULICS LAB.

Kudryavtsev, V., Yurovskaya, M., Chapron, B., Collard, F., Donlon, C., 2017. Sun glitter imagery of ocean surface waves. part 1: Directional spectrum retrieval and validation. Journal of Geophysical Research: Oceans 122, 1369–1383.

Kupfer, S., Santamaria-Aguilar, S., van Niekerk, L., Lück-Vogel, M., Vafeidis, A.T., 2022. Investigating the interaction of waves and river discharge during compound flooding at breede estuary, south africa. Natural Hazards and Earth System Sciences 22, 187–205.

Lacroix, D., Mora, O., De Menthière, N., Béthinger, A., 2019. La montée du niveau de la mer: conséquences et anticipations d'ici 2100, l'éclairage de la prospective. Rapport d'étude , 172.

Lafon, V., Apoluceno, D.D.M., Dupuis, H., Michel, D., Howa, H., Froidefond, J.M., 2004. Morphodynamics of nearshore rhythmic sandbars in a mixed-energy environment (sw france): I. mapping beach changes using visible satellite imagery. Estuarine, Coastal and Shelf Science 61, 289–299.

Laïbi, R.A., Anthony, E.J., Almar, R., Castelle, B., Senechal, N., Kestenare, E., 2014. Longshore drift cell development on the human-impacted bight of benin sand barrier coast, west africa. Journal of Coastal Research , 78–83.

Lawson, S.K., Tanaka, H., Udo, K., Hiep, N.T., Tinh, N.X., 2021. Evaluation of sandspit growth and longshore sediment transport rates at the "bouche du roi" inlet, benin, using remotely sensed images. Journal of Japan Society of Civil Engineers, Ser. B1 (Hydraulic Engineering) 77, I_667–I_672.

Laïbi, R., Antoine, G., Anthony, E.J., Lucien-Marc, O., 2012. Apport des sÉries d'images landsat dans l'Étude de la dynamique spatio-temporelle de l'embouchure de l'estuaire des fleuves mono et couffo au bÉnin, avant et aprÈs la construction du barrage de nangbÉto sur le mono. Teledetection, Editions des Archives Contemporaines , 179–198.

Le Mauff, B., Juigner, M., Ba, A., Robin, M., Launeau, P., Fattal, P., 2018. Coastal monitoring solutions of the geomorphological response of beach-dune systems using multi-temporal lidar datasets (vendée coast, france). Geomorphology 304, 121–140. URL: `https://www.sciencedirect.com/science/article/pii/S0169555X17305457`, doi:`https://doi.org/10.1016/j.geomorph.2017.12.037`.

Le Xuan, T., Ba, H.T., Thanh, V.Q., Wright, D.P., Hasan Tanim, A., Tran Anh, D., 2022. Evaluation of coastal protection strategies and proposing multiple lines of defense under climate change in the mekong delta for sustainable shoreline protection. Ocean & Coastal Management 228, 106301. URL: `https://www.sciencedirect.com/science/article/pii/S0964569122002770`, doi:`https://doi.org/10.1016/j.ocecoaman.2022.106301`.

Leatherman, S.P., 1979. Migration of assateague island, maryland, by inlet and overwash processes. Geology 7, 104–107.

Letortu, P., Jaud, M., Théry, C., Nabucet, J., Taouki, R., Passot, S., Augereau, E., 2020. The potential of pléiades images with high angle of incidence for reconstructing the coastal cliff face in normandy (france). International Journal of Applied Earth Observation and Geoinformation 84, 101976. doi:`https://doi.org/10.1016/j.jag.2019.101976`.

Lippmann, T., Holman, R., 1990. The spatial and temporal variability of sand bar morphology. Journal of Geophysical Research: Oceans 95, 11575–11590.

Lippmann, T.C., Holman, R.A., 1989. Quantification of sand bar morphology: A video technique based on wave dissipation. Journal of Geophysical Research: Oceans 94, 995–1011.

Lippmann, T.C., Smith, G.M., 2009. Shallow surveying in hazardous waters, pp. 1–12.

Loghin, A.M., Otepka-Schremmer, J., Pfeifer, N., 2020. Potential of pléiades and worldview-3 tri-stereo dsms to represent heights of small isolated objects. Sensors 20. URL: `https://www.mdpi.com/1424-8220/20/9/2695`, doi:`10.3390/s20092695`.

Lorenzo, F., Alonso, A., Pagés, J., 2007. Erosion and accretion of beach and spit systems in northwest spain: a response to human activity. Journal of Coastal Research 23, 834–845.

Loureiro, C., Ferreira, Ó., Cooper, J.A.G., 2012. Extreme erosion on high-energy embayed beaches: influence of megarips and storm grouping. Geomorphology 139, 155–171.

Luijendijk, A., Hagenaars, G., Ranasinghe, R., Baart, F., Donchyts, G., Aarninkhof, S., 2018. The state of the world's beaches. Scientific reports 8, 1–11.

Lyzenga, D.R., Malinas, N.P., Tanis, F.J., 2006. Multispectral bathymetry using a simple physically based algorithm. IEEE Transactions on Geoscience and Remote Sensing 44, 2251–2259.

Marchesiello, P., Chauchat, J., Shafiei, H., Almar, R., Benshila, R., Dumas, F., Debreu, L., 2022. 3d wave-resolving simulation of sandbar migration. Ocean Modelling , 102127.

Marzougui, W., Oueslati, A., 2017. Les plages de la côte d'ejjehmi-soliman (golfe de tunis, tunisie): exemple d'accélération de l'érosion marine dans une cellule sédimentaire artificiellement tronçonnée. Physio-Geo 11, 21–41.

Masselink, G., Black, K.P., 1995. Magnitude and cross-shore distribution of bed return flow measured on natural beaches. Coastal Engineering 25, 165–190.

Masselink, G., van Heteren, S., 2014. Response of wave-dominated and mixed-energy barriers to storms. Marine Geology 352, 321–347.

Masselink, G., Kroon, A., 2009. Morphology and morphodynamics of sandy beaches. Coastal Zones and Estuaries. Encyclopedia of Life Support Systems , 221–243.

Massuanganhe, E.A., Arnberg, W., 2008. Monitoring spit development in pomene, southern mozambique, using landsat data. Geo-Environment and Landscape Evolution 100, 119–127. doi:`10.2495/GEO080121`.

McFeeters, S., 1996. The use of the normalized difference water index (ndwi) in the delineation of open water features. International Journal of Remote Sensing 17, 1425–1432.

McKinna, L.I., Fearns, P.R., Weeks, S.J., Werdell, P.J., Reichstetter, M., Franz, B.A., Shea, D.M., Feldman, G.C., 2015. A semianalytical ocean color inversion algorithm with explicit water column depth and substrate reflectance parameterization. Journal of Geophysical Research: Oceans 120, 1741–1770.

McNabb, R., . Pybob: A python package of geospatial toolsand version 0.25and github: San francisco, ca, usa, 2019. URL: `https://github.com/iamdonovan/pybob`.

Melet, A., Meyssignac, B., Almar, R., Le Cozannet, G., 2018. Under-estimated wave contribution to coastal sea-level rise. Nature Climate Change 8, 234–239. doi:`10.1038/s41558-018-0088-y`.

Melet, A., Teatini, P., Le Cozannet, G., Jamet, C., Conversi, A., Benveniste, J., Almar, R., 2020a. Earth observations for monitoring marine coastal hazards and their drivers. Surveys in Geophysics .

Melet, A., Teatini, P., Le Cozannet, G., Jamet, C., Conversi, A., Benveniste, J., Almar, R., 2020b. Earth observations for monitoring marine coastal hazards and their drivers. Surveys in Geophysics 41, 1489–1534.

Michel, D., Howa, H., 1997. Morphodynamic behaviour of a tidal inlet system in a mixed-energy environment. Physics and Chemistry of the Earth 22, 339–343.

Michel, J., Sarrazin, E., Youssefi, D., Cournet, M., Buffe, F., Delvit, J., Emilien, A., Bosman, J., Melet, O., L'Helguen, C., 2020. A new satellite imagery stereo pipeline designed for scalability, robustness and performance. ISPRS - International Archives of the Photogrammetry, Remote Sensing and Spatial Information Sciences .

Moulton, M., Elgar, S., Raubenheimer, B., 2014. Improving the time resolution of surfzone bathymetry using in situ altimeters. Ocean Dynamics 64, 755–770.

Nahon, A., Idier, D., Sénéchal, N., Fénièes, H., Mallet, C., Mugica, J., 2019. Imprints of wave climate and mean sea level variations in the dynamics of a coastal spit over the last 250 years: Cap ferret, sw france. Earth Surface Processes and Landforms 44, 2112–2126.

Ndour, A., Ba, K., Almar, A., Almeida, P., Sall, M., Diedhiou, P., Floc'h, F., Daly, C., Grandjean, P., Boivin, J.P., et al., 2020. On the natural and anthropogenic drivers of the senegalese (west africa) low coast evolution: Saint louis beach 2016 coastvar experiment and 3d modeling of short term coastal protection measures. Journal of Coastal Research 95, 583–587.

Ndour, A., Ba, Kand Almar, R., Almeida, P., Sall, M., Diedhiou, P., Floc'h, F., Daly, C., P., G., Boivin, J.P., Castelle, B., Biausque, M., Detandt, G., Tomety Folly, S., Capet, X., Garlan, T., Marchesiello, P., Beshila, R., Diaz, H., Bergsma, E., Sadio, M., Sakho, I., Sy, B., 2016. On the natural and anthropogenic drivers of the senegalses (west africa) low coast evolution: Saint louis beach 2016 coasvar experiment and 3d modeling of short term coastal protection measures. Journal of Coastal Research 95, 583–587.

Ndour, A., Laïbi, R.A., Sadio, M., Degbe, C.G., Diaw, A.T., Oyédé, L.M., Anthony, E.J., Dussouillez, P., Sambou, H., hadji Balla Dièye, E., 2018. Management strategies for coastal erosion problems in west africa: Analysis, issues, and constraints drawn from the examples of senegal and benin. Ocean and Coastal Management 156, 92–106. URL: `https://www.sciencedirect.com/science/article/pii/S0964569117300728`, doi:`https://doi.org/10.1016/j.ocecoaman.2017.09.001`. sI: MSforCEP.

Nelson, A., Reuter, H., Gessler, P., 2009. Chapter 3 dem production methods and sources, in: Hengl, T., Reuter, H.I. (Eds.), Geomorphometry. Elsevier. volume 33 of *Developments in Soil Science*, pp. 65–85. URL: `https://www.sciencedirect.com/science/article/pii/S0166248108000032`, doi:`https://doi.org/10.1016/S0166-2481(08)00003-2`.

Niang, A., Kane, A., 2014. Morphological and hydrodynamic changes in the lower estuary of the senegal river: Effects on the environment of the breach of the 'langue de barbarie' sand spit in 2003, in: Estuaries of the World. Springer, C. (Ed.), Diop S., Barusseau JP., Descamps C. (eds) The Land/Ocean Interactions in the Coastal Zone of West and Central Africa, pp. pp. 23–40.

Nuth, C., Kääb, A., 2011. Co-registration and bias corrections of satellite elevation data sets for quantifying glacier thickness change. The Cryosphere 5, 271–290.

Oertel, G.F., 1977. Geomorphic cycles in ebb deltas and related patterns of shore erosion and accretion. Journal of Sedimentary Research 47, 1121–1131.

O'Hare, T.J., Davies, A., 1993. Sand bar evolution beneath partially-standing waves: laboratory experiments and model simulations. Continental Shelf Research 13, 1149–1181.

Pachauri, R.K., Allen, M.R., Barros, V.R., Broome, J., Cramer, W., Christ, R., Church, J.A., Clarke, L., Dahe, Q., Dasgupta, P., et al., 2014. Climate change 2014: synthesis report. Contribution of Working Groups I, II and III to the fifth assessment report of the Intergovernmental Panel on Climate Change. Ipcc.

Palalane, J., Larson, M., Hanson, H., 2014. Analytical model of sand spit evolution, in: Proceedings of 34th International Conference on Coastal Engineering.

Pereira, D., . Wind rose: Matlab central file exchange. retrieved november 23, 2021. URL: `https://www.mathworks.com/matlabcentral/fileexchange/47248-wind-rose`.

Pernetta, J.C., Milliman, J.D., 1995. Land-ocean interactions in the coastal zone: implementation plan. Oceanographic Literature Review 9, 801.

Peterson, C.H., Bishop, M.J., 2005. Assessing the environmental impacts of beach nourishment. Bioscience 55, 887–896.

Pierce, J., 1969. Sediment budget along a barrier island chain. Sedimentary Geology 3, 5–16.

Pilkey, O.H., Neal, W.J., Bush, D.M., 2009. Coastal erosion. Coastal Zones and Estuaries , 32–42.

Plant, N.G., Aarninkhof, S.G., Turner, I.L., Kingston, K.S., 2007. The performance of shoreline detection models applied to video imagery. Journal of Coastal Research 23, 658–670.

Powell, M.A., Thieke, R.J., Mehta, A.J., 2006. Morphodynamic relationships for ebb and flood delta volumes at florida's tidal entrances. Ocean Dynamics 56, 295–307.

Pradhan, U., Mishra, P., Mohanty, P.K., Behera, B., 2015. Formation, growth and variability of sand spit at rushikulya river mouth, south odisha coast, india. Procedia Engineering 116, 963–970. URL: `https://www.sciencedirect.com/science/article/pii/S1877705815020421`, doi:`https://doi.org/10.1016/j.proeng.2015.08.387`. 8th International Conference on Asian and Pacific Coasts (APAC 2015).

Prasad, D.H., Kumar, N.D., 2014. Coastal erosion studies—a review. International Journal of Geosciences 2014.

Previmer, . URL: `https://www.previmer.org/`.

Price, T., van Kuik, N., de Wit, L., Dionísio António, S., Ruessink, B., et al., 2017. Shoreward propagating accretionary waves (spaws): observations from a multiple sandbar system. Proceedings Coastal Dynamics 2017 , 1081–1089.

Price, T., Ruessink, B., 2011. State dynamics of a double sandbar system. Continental Shelf Research 31, 659–674.

Price, T., Rutten, J., Ruessink, B., 2011. Coupled behaviour within a double sandbar system. Journal of Coastal Research , 125–129.

Price, T.D., et al., 2013. Morphological coupling in a double sandbar system. Utrecht University.

Radon, J., 1917. On the determination of functions from their integrals along certain manifolds. Ber. Verh, Sachs Akad Wiss. 69, 262–277.

Ranasinghe, R., Larson, M., Savioli, J., 2010. Shoreline response to a single shore-parallel submerged breakwater. Coastal Engineering 57, 1006–1017.

Ranasinghe, R., Turner, I.L., Symonds, G., 2006. Shoreline response to multi-functional artificial surfing reefs: A numerical and physical modelling study. Coastal Engineering 53, 589–611.

Ribas, F., Falqués, A., Garnier, R., 2017. Nearshore sand bars, in: Atlas of Bedforms in the Western Mediterranean. Springer, pp. 73–79.

Rice, M.P., 1974. Closure conditions mouth of the russian river. Shore and Beach 42, 15–20.

Robin, N., Levoy, F., Monfort, O., 2007. Bar morphodynamic behaviour on the ebb delta of a macrotidal inlet (normandy, france). Journal of Coastal Research 23, 1370–1378.

Rodríguez, S., Alonso Bilbao, I., Sánchez García, M.J., Casamayor Font, M., García Weil, L.F., Sy, B., Sy, A., Faye, C., 2014. Morphodynamic study of an artificial inlet in langue de barbarie (senegal) from 2003 to 2014 using landsat images .

Rotnicka, J., Dłużewski, M., Dąbski, M., Rodzewicz, M., Włodarski, W., Zmarz, A., 2020. Accuracy of the uav-based dem of beach–foredune topography in relation to selected morphometric variables, land cover, and multitemporal sediment budget. Estuaries and Coasts 43, 1939—-1955.

Ruessink, B., Kuriyama, Y., Reniers, A., Roelvink, J., Walstra, D., 2007. Modeling cross-shore sandbar behavior on the timescale of weeks. Journal of Geophysical Research: Earth Surface 112.

Ruessink, B., Pape, L., Turner, I., 2009. Daily to interannual cross-shore sandbar migration: Observations from a multiple sandbar system. Continental Shelf Research 29, 1663–1677.

Ruggiero, P., Voigt, B., Kaminsky, G., 2000. Beach monitoring for enhanced decision-making, in: Coastal Society 17th Conference Coasts at the Millennium-Portland, Oregon, pp. 516–524.

Rupnik, E., Daakir, M., Pierrot Deseilligny, M., 2017. Micmac – a free, open-source solution for photogrammetry. Open geospatial data, softw. stand 2.

Rupnik, E., Pierrot-Deseilligny, M., Delorme, A., 2018. 3d reconstruction from multi-view vhr-satellite images in micmac. ISPRS Journal of Photogrammetry and Remote Sensing 139, 201–211. doi:https://doi.org/10.1016/j.isprsjprs.2018.03.016.

Sadio, M., Anthony, E.J., Diaw, A.T., Dussouillez, P., Fleury, J.T., Kane, A., Almar, R., Kestenare, E., 2017. Shoreline changes on the wave-influenced senegal river delta, west africa: The roles of natural processes and human interventions. Water 9. doi:10.3390/w9050357.

Sagawa, T., Yamashita, Y., Okumura, T., Yamanokuchi, T., 2019. Satellite derived bathymetry using machine learning and multi-temporal satellite images. Remote Sensing 11, 1155.

Salameh, E., Frappart, F., Almar, R., Baptista, P., Heygster, G., Lubac, B., Raucoules, D., Almeida, L.P., Bergsma, E.W.J., Capo, S., De Michele, M., Idier, D., Li, Z., Marieu, V., Poupardin, A., Silva, P.A., Turki, I., Laignel, B., 2019. Monitoring beach topography and nearshore bathymetry using spaceborne remote sensing: A review. Remote Sensing 11. doi:10.3390/rs11192212.

Sallenger, A.H., J., Krabill, W., Swift, R., Brock, J., List, J., Hansen, M., Holman, R., Manizade, S., Sontag, J., Meredith, A., et al., 2003. Evaluation of airborne topographic lidar for quantifying beach changes. J. Coast. Res. 19, 125–133.

Santos, D., Abreu, T., Silva, P.A., Santos, F., Baptista, P., 2022. Nearshore bathymetry retrieval from wave-based inversion for video imagery. Remote Sensing 14, 2155.

Schmeltz, E., Sorensen, R., McCarthy, M., Nersesian, G., 1982. Breach/inlet interaction at moriches inlet, in: Coastal Engineering 1982, pp. 1062–1077.

Schoonees, J., Lenhoff, L., Raw, A., 1999. Preventing natural breaching of the major sand spit protecting the port of walvis bay, in: Coastal Engineering 1998, pp. 1475–1488.

Schwartz, M.L., 1982. The encyclopedia of beaches and coastal environments .

Seiji, M., Uda, T., Tanaka, S., 1987. Statistical study on the effect and stability of detached breakwaters. Coastal Engineering in Japan 30, 131–141.

Sénéchal, N., Bonneton, P., Dupuis, H., 2002. Generation of secondary waves due to wave propagation over a bar: A field investigation, in: Ocean Wave Measurement and Analysis (2001), pp. 764–772.

Sevgi, L., 2007. Numerical fourier transforms: Dft and fft. IEEE Antennas and Propagation Magazine 49, 238–243.

Shand, R.D., 2003. Relationships between episodes of bar switching, cross-shore bar migration and outer bar degeneration at wanganui, new zealand. Journal of Coastal Research , 157–170.

Shean, D., Alexandrov, O., Moratto, Z., Smith, B., Joughin, I., Porter, C., Morin, P., . An automated,open-source pipeline for mass production of digital elevation models (dems) from very-high-resolutioncommercial stereo satellite imagery.isprs j. Remote Sens. 116, 101–117.

Small, C., Gornitz, V., Cohen, J.E., 2000. Coastal hazards and the global distribution of human population. Environmental Geosciences 7, 3–12.

Small, C., Nicholls, R.J., 2003. A global analysis of human settlement in coastal zones. Journal of coastal research , 584–599.

SOGREAH, 1994. Etudes de Faisabilité et d'avant projet sommaire de l'émissaire Deltaand Rapport final: Grenoble, France. Technical Report. SOGREAH.

Splinter, K.D., Harley, M.D., Turner, I.L., 2018. Remote sensing is changing our view of the coast: Insights from 40 years of monitoring at narrabeen-collaroy, australia. Remote Sensing 10, 1744.

Splinter, K.D., Holman, R.A., Plant, N.G., 2011. A behavior-oriented dynamic model for sandbar migration and 2dh evolution. Journal of Geophysical Research: Oceans 116.

Splinter, K.D., Turner, I.L., Davidson, M.A., Barnard, P., Castelle, B., Oltman-Shay, J., 2014. A generalized equilibrium model for predicting daily to interannual shoreline response. Journal of Geophysical Research: Earth Surface 119, 1936–1958.

Stancheva, M., Ratas, U., Orviku, K., Palazov, A., 2011. Sand dune destruction due to increased human impacts along the bulgarian black sea and estonian baltic sea coasts. Journal of Coastal Research 64, 324–328.

Stilwell Jr, D., 1969. Directional energy spectra of the sea from photographs. Journal of Geophysical Research 74, 1974–1986.

Stive, M.J., Aarninkhof, S.G., Hamm, L., Hanson, H., Larson, M., Wijnberg, K.M., Nicholls, R.J., Capobianco, M., 2002a. Variability of shore and shoreline evolution. Coastal engineering 47, 211–235.

Stive, M.J., Aarninkhof, S.G., Hamm, L., Hanson, H., Larson, M., Wijnberg, K.M., Nicholls, R.J., Capobianco, M., 2002b. Variability of shore and shoreline evolution. Coastal engineering 47, 211–235.

Stockdon, H.F., Holman, R.A., 2000. Estimation of wave phase speed and nearshore bathymetry from video imagery. Journal of Geophysical Research: Oceans 105, 22015–22033.

Stockdon, H.F., Holman, R.A., Howd, P.A., Sallenger, A.H., 2006. Empirical parameterization of setup, swash, and runup. Coastal Engineering 53, 573–588. doi:`https://doi.org/10.1016/j.coastaleng.2005.12.005`.

Sunamura, T., 1988. Beach morphologies and there change. Nearshore Dynamics and Caostal Processes , 136–161.

Tahoun, M., El Rahman Shabayek, A., Reulke, R., Hassanien, A., 2015. Co-registration of satellite images based on invariant local features. Intelligent Systems'2014 323, 653–660.

Taveneau, A., Almar, R., Bergsma, E., Ndour, A., Sy, B., Lemain-Chenevier, S., Liffermann, A., Giros, A., Gosselin, M., Garlan, T., 2020. Topographie 3d satellite (pléïades) : Application à l'évolution côtière de la langue de barbarie. Journées Nationales Génie Côtier - Génie Civil 16, 297–302. doi:`10.5150/jngcgc.2020.034`.

Taveneau, A., Almar, R., Bergsma, E., Sy, B., Ndour, A., 2022. Satellite-based land/sea continuum: An application to monitor the saint louis coast (senegal, west africa). The International Archives of the Photogrammetry, Remote Sensing and Spatial Information Sciences XLIII-B3-2022, 1005–1010. doi:`10.5194/isprs-archives-XLIII-B3-2022-1005-2022`.

Taveneau, A., Almar, R., Bergsma, E.W.J., Sy, B.A., Ndour, A., Sadio, M., Garlan, T., 2021. Observing and predicting coastal erosion at the langue de barbarie sand spit around saint louis (senegal, west africa) through satellite-derived digital elevation model and shoreline. Remote Sensing 13. URL: `https://www.mdpi.com/2072-4292/13/13/2454`, doi:`10.3390/rs13132454`.

Thornton, E., Humiston, R., Birkemeier, W., 1996. Bar/trough generation on a natural beach. Journal of Geophysical Research: Oceans 101, 12097–12110.

Thornton, E.B., Guza, R., 1983. Transformation of wave height distribution. Journal of Geophysical Research: Oceans 88, 5925–5938.

Thornton, E.B., MacMahan, J., Sallenger Jr, A., 2007. Rip currents, mega-cusps, and eroding dunes. Marine geology 240, 151–167.

Tissier, M., Bonneton, P., Almar, R., Castelle, B., Bonneton, N., Nahon, A., 2011. Field measurements and non-linear prediction of wave celerity in the surf zone. European Journal of Mechanics-B/Fluids 30, 635–641.

Toimil, A., Álvarez-Cuesta, M., Losada, I., 2022. Neglecting the effect of long-and short-term erosion can lead to spurious coastal flood risk projections and maladaptation. Coastal Engineering , 104248.

De la Torre, Y., Belon, R., Balouin, Y., Stephanian, A., 2014. Inventaire et analyse des solutions douces de gestion de l'erosion cotiere et applicabilite au littoral corse. BRGM/RP-63034-FR , 59.

Traganos, D., Poursanidis, D., Aggarwal, B., Chrysoulakis, N., Reinartz, P., 2018. Estimating satellite-derived bathymetry (sdb) with the google earth engine and sentinel-2. Remote Sensing 10, 859.

Tribe, H., 2008. The Geomorphology of Farewell Spit and Its Sensitivity to Sea-level Rise. Master 's Thesis, School of Geography, Environment and Earth Sciences, Victoria University of Wellington, Wellington, New Zealand. Ph.D. thesis. Victoria University of Wellington.

Tsukada, F., Shimozono, T., Matsuba, Y., 2020. Uav-based mapping of nearshore bathymetry over broad areas. Coastal Engineering Journal 62, 285–298.

Tung, T.T., Walstra, D.J.R., van de Graaff, J., Stive, M.J., 2009. Morphological modeling of tidal inlet migration and closure. Journal of Coastal Research , 1080–1084.

Turner, I.L., Harley, M.D., Almar, R., Bergsma, E.W.J., 2021. Satellite optical imagery in Coastal Engineering. Coastal Engineering 167, 103919. doi:`10.1016/j.coastaleng.2021.103919`.

Turner, R.K., Subak, S., Adger, W.N., 1996. Pressures, trends, and impacts in coastal zones: interactions between socioeconomic and natural systems. Environmental management 20, 159–173.

Valentini, N., Saponieri, A., Damiani, L., 2017. A new video monitoring system in support of coastal zone management at apulia region, italy. Ocean & coastal management 142, 122–135.

Van Enckevort, I., Ruessink, B., 2003. Video observations of nearshore bar behaviour. part 1: alongshore uniform variability. Continental Shelf Research 23, 501–512.

Van Enckevort, I., Ruessink, B., Coco, G., Suzuki, K., Turner, I., Plant, N.G., Holman, R.A., 2004. Observations of nearshore crescentic sandbars. Journal of Geophysical Research: Oceans 109.

Vidal-Ruiz, J.A., de Alegría-Arzaburu, A.R., 2020. Modes of onshore sandbar migration at a single-barred and swell-dominated beach. Marine Geology 426, 106222.

Villagran, M., Cienfuegos, R., Almar, R., Catalán, P., Camaño, A., 2011. Natural post-tsunami recovery of the mataquito river mouth, after the 2010 chilean tsunami, in: AGU Fall Meeting Abstracts, pp. OS44B–05.

Vitousek, S., Buscombe, D.D., Vos, K., Barnard, P., Ritchie, A., Warrick, J., 2022. The future of coastal monitoring through satellite remote sensing .

Vos, K., Splinter, K.D., Harley, M.D., Simmons, J.A., Turner, I.L., 2019. Coastsat: A google earth engine-enabled python toolkit to extract shorelines from publicly available satellite imagery. Environmental Modelling and Software 122, 104528. doi:https://doi.org/10.1016/j.envsoft.2019.104528.

Vousdoukas, M.I., Clarke, J., Ranasinghe, R., Reimann, L., Khalaf, N., Duong, T.M., Ouweneel, B., Sabour, S., Iles, C.E., Trisos, C.H., et al., 2022. African heritage sites threatened as sea-level rise accelerates. Nature climate change 12, 256–262.

de Vriend, H.J., Capobianco, M., Chesher, T., De Swart, H.d., Latteux, B., Stive, M., 1993. Approaches to long-term modelling of coastal morphology: a review. Coastal engineering 21, 225–269.

Wamsley, T.V., Kraus, N.C., 2005. Coastal barrier island breaching, Part 2: Mechanical breaching and breach closure. Technical Report. ENGINEER RESEARCH AND DEVELOPMENT CENTER VICKSBURG MS COASTAL AND HYDRAULICSLAB.

Weissenberger, S., Noblet, M., Plante, S., Chouinard, O., Guillemot, J., Aubé, M., Meur-Ferec, C., Michel-Guillou, E., Gaye, N., Kane, A., Kane, C., Niang, A., Seck, A., 2016. Changments climatiques, changements du littoral et évolution de la vulnerabilité côtiere au fil du temps: comparaison deterritoire francais, canadien et sénégalais. Vertigo, la revue électronique en sciences de l'environnement 16, 2–33. doi:https://doi.org/10.4000/vertigo.18050.

Wijnberg, K.M., Holman, R., 2007. Video-observations of shoreward propagating accretionary waves. Proceedings of the RCEM 2007, 737–743.

Wright, L.D., Short, A.D., 1984. Morphodynamic variability of surf zones and beaches: a synthesis. Marine geology 56, 93–118.

Xu, H., 2006. Modification of normalised difference water index (ndwi) to enhance open water features in remotely sensed imagery. International journal of remote sensing 27, 3025–3033.

Yamazaki, D., Ikeshima, D., Tawatari, R., Yamaguchi, T., O'Loughlin, F., Neal, J., Sampson, C., Kanae, S., Bates, P., 2017. A high-accuracy map of global terrain elevations. Geophysical research Letters 44, 5844–5853.

Yates, M., Guza, R., O'reilly, W., 2009. Equilibrium shoreline response: Observations and modeling. Journal of Geophysical Research: Oceans 114.

Youssefi, D., Michel, J., Sarrazin, E., Buffe, F., Cournet, M., Delvit, J.M., L'Helguen, C., Melet, O., Emilien, A., Bosman, J., 2020. Cars: A photogrammetry pipeline using dask graphs to construct a global 3d model, in: IGARSS 2020 - 2020 IEEE International Geoscience and Remote Sensing Symposium, pp. 453–456. doi:10.1109/IGARSS39084.2020.9324020.

Yurovskaya, M., Kudryavtsev, V., Chapron, B., Collard, F., 2019. Ocean surface current retrieval from space: The sentinel-2 multispectral capabilities. Remote sensing of Environment 234, 111468.

Zăinescu, F.I., Vespremeanu-Stroe, A., Tătui, F., 2019. The formation and closure of the big breach of sacalin spit associated with extreme shoreline retreat and shoreface erosion. Earth Surface Processes and Landforms 44, 2268–2284.

Zaremba, R.E., Leatherman, S.P., 1984. Overwash Processes and Foredune Ecology, Nauset Spit, Massachusetts. Technical Report. ARMY ENGINEER WATERWAYS EXPERIMENT STATION VICKSBURG MS ENVIRONMENTAL LAB.